(19)日本国特許庁(JP)　(12)公表特許公報(A)　(11)特許出願公表番号
特表2004-510515
(P2004-510515A)
(43)公表日　平成16年4月8日(2004.4.8)

(51)Int.Cl.[7]	F I			テーマコード（参考）
A61B 6/03	A61B	6/03	360G	4C093
A61B 5/055	A61M	29/00		4C096
A61M 29/00	G06T	15/00	200	4C167
G01R 33/54	G06T	17/40	E	5B050
G06T 15/00	A61B	5/05	380	5B080

審査請求 未請求　予備審査請求 有　（全 247 頁）　最終頁に続く

(21)出願番号　特願2002-533259(P2002-533259)
(86)(22)出願日　平成13年10月1日(2001.10.1)
(85)翻訳文提出日　平成15年4月3日(2003.4.3)
(86)国際出願番号　PCT/US2001/030704
(87)国際公開番号　WO2002/029764
(87)国際公開日　平成14年4月11日(2002.4.11)
(31)優先権主張番号　60/237,665
(32)優先日　平成12年10月3日(2000.10.3)
(33)優先権主張国　米国(US)
(31)優先権主張番号　09/777,120
(32)優先日　平成13年2月5日(2001.2.5)
(33)優先権主張国　米国(US)

(71)出願人　500149094
ザ　リサーチ　ファウンデーション　オブ　ステイト　ユニヴァーシティ　オブ　ニューヨーク
アメリカ合衆国　ニューヨーク州　１１７９４　ストーニー　ブルーク　ステイト　ユニヴァーシティ　オブ　ニューヨーク　アット　ストーニー　ブルーク　オフィス　オブ　テクノロジー　ライセンシング
(74)代理人　100072051
弁理士　杉村　興作
(72)発明者　アリー　イー　コーフマン
アメリカ合衆国　ニューヨーク州　１１８０３　プレーンヴュー　シダー　ドライヴ　ウエスト　９４

最終頁に続く

(54)【発明の名称】器官のような物体の３次元仮想検査を行うシステムおよび方法

(57)【要約】
内臓のような物体の３次元視覚化画像を、体積視覚化技術を使用して発生する方法を提供する。この技術は、多走査画像化方法と、多解像度画像化方法と、複雑な３次元物体のスケルトンを発生する方法とを含む。用途は、仮想膀胱鏡検査と、仮想喉頭鏡検査と、仮想血管造影検査とをとりわけ含む。

【特許請求の範囲】
【請求項１】
物体の仮想調査を行う方法において、
コントラスト剤の存在によって膨張させた物体の少なくとも１回の走査を行うステップと、
前記コントラスト剤を除去した前記物体の少なくとも１回の走査を行うステップと、
前記走査を、複数のボクセルを具える対応する体積データセットに変換するステップと、
画像分割を行い、各々の走査のボクセルを複数のカテゴリに分類するステップと、
各々の走査の体積データセットを共通座標系に登録するステップと、
前記体積データセットの少なくとも２つを本質的に同時に表示するステップと、
前記体積データセットの一方において仮想ナビゲーション動作を行い、対応するナビゲーション動作を少なくとも１つの他の体積データセットにおいて生じさせるステップとを含むことを特徴とする、仮想調査を行う方法。
【請求項２】
請求項１に記載の仮想調査を行う方法において、前記膨張させた物体の少なくとも１回の走査が、前記物体の横走査および冠状走査を含むことを特徴とする、仮想調査を行う方法。
【請求項３】
請求項２に記載の仮想調査を行う方法において、前記コントラスト剤を除去した前記物体の少なくとも１回の走査が、前記物体の横走査および冠状走査を含むことを特徴とする、仮想調査を行う方法。
【請求項４】
請求項３に記載の仮想調査を行う方法において、前記物体を膀胱としたことを特徴とする、仮想調査を行う方法。
【請求項５】
請求項４に記載の仮想調査を行う方法において、前記走査をコンピュータ断層撮影走査としたことを特徴とする、仮想調査を行う方法。
【請求項６】
請求項４に記載の仮想調査を行う方法において、前記走査を超音波画像走査としたことを特徴とする、仮想調査を行う方法。
【請求項７】
請求項４に記載の仮想調査を行う方法において、前記走査を磁気共鳴画像走査としたことを特徴とする、仮想調査を行う方法。
【請求項８】
請求項７に記載の仮想調査を行う方法において、前記コントラスト剤を尿としたことを特徴とする、仮想調査を行う方法。
【請求項９】
請求項１に記載の仮想調査を行う方法において、前記コントラスト剤を除去した前記物体の少なくとも１回の走査が、前記物体の横走査および冠状走査を含むことを特徴とする、仮想調査を行う方法。
【請求項１０】
請求項１に記載の仮想調査を行う方法において、前記物体を膀胱としたことを特徴とする、仮想調査を行う方法。
【請求項１１】
請求項１０に記載の仮想調査を行う方法において、前記走査をコンピュータ断層撮影走査としたことを特徴とする、仮想調査を行う方法。
【請求項１２】
請求項１０に記載の仮想調査を行う方法において、前記走査を超音波画像走査としたことを特徴とする、仮想調査を行う方法。
【請求項１３】

請求項１０に記載の仮想調査を行う方法において、前記走査を磁気共鳴画像走査としたことを特徴とする、仮想調査を行う方法。
【請求項１４】
請求項１３に記載の仮想調査を行う方法において、前記コントラスト剤を尿としたことを特徴とする、仮想調査を行う方法。
【請求項１５】
請求項１に記載の仮想調査を行う方法において、前記膨張させた物体の少なくとも１回の走査と、前記コントラスト剤を除去した前記物体の少なくとも１回の走査とを評価し、前記走査の一方においてコントラストがより可視である領域を識別するステップと、興味ある領域においてより高いコントラストを有する前記走査を評価し、前記物体の生理学的特長を決定するステップとをさらに含むことを特徴とする、仮想調査を行う方法。
【請求項１６】
請求項１５に記載の仮想調査を行う方法において、前記画像分割のステップが、ボクセルを前記ボクセルの局所強度ベクトルに基づいて分類するステップを含むことを特徴とする、仮想調査を行う方法。
【請求項１７】
請求項１６に記載の仮想調査を行う方法において、前記画像分割のステップが、領域成長アルゴリズムを使用し、前記分類されたボクセルに基づいて前記物体の領域を識別するステップをさらに含むことを特徴とする、仮想調査を行う方法。
【請求項１８】
請求項１に記載の仮想調査を行う方法において、前記体積画像データセットを、前記座標系に関する複数の領域に分割するステップをさらに含むことを特徴とする、仮想調査を行う方法。
【請求項１９】
請求項１８に記載の仮想調査を行う方法において、前記複数の領域が、３次元座標系において規定された８個の領域を含むことを特徴とする、仮想調査を行う方法。
【請求項２０】
物体の仮想調査を行う方法において、
前記物体の画像走査を行い、画像走査データを取得するステップと、
前記取得された画像走査データを複数のボクセルに変換するステップと、
前記ボクセル間を補間し、拡張データセットを発生するステップと、
画像分割を行い、前記ボクセルを複数のカテゴリに分類するステップと、
前記拡張データセットから前記物体内部の体積を抽出するステップと、
前記拡張データセットから減少解像度データセットを発生するステップと、
前記拡張データセットをツリーデータ構造に格納するステップと、
前記拡張データセットおよび減少解像度データセットに関する画像をレンダリングするステップと、
前記減少解像度データセットおよび拡張データセットのうち少なくとも１つを表示に関して選択するステップとを含むことを特徴とする、仮想調査を行う方法。
【請求項２１】
請求項２０に記載の仮想調査を行う方法において、前記選択するステップが、
画像相互作用中前記減少解像度データセットを選択するステップと、
画像相互作用が予め決定された期間中に起こらなかった場合、前記拡張データセットを選択するステップとを含むことを特徴とする、仮想調査を行う方法。
【請求項２２】
請求項２０に記載の仮想調査を行う方法において、前記画像走査をコンピュータ断層撮影走査としたことを特徴とする、仮想調査を行う方法。
【請求項２３】
請求項２０に記載の仮想調査を行う方法において、前記画像走査を磁気共鳴画像走査としたことを特徴とする、仮想調査を行う方法。

【請求項２４】
請求項２０に記載の仮想調査を行う方法において、前記画像走査を超音波画像走査としたことを特徴とする、仮想調査を行う方法。
【請求項２５】
請求項２０に記載の仮想調査を行う方法において、前記物体を喉頭としたことを特徴とする、仮想調査を行う方法。
【請求項２６】
請求項２０に記載の仮想調査を行う方法において、前記ツリー構造をバイナリ空間分割ツリー構造としたことを特徴とする、仮想調査を行う方法。
【請求項２７】
仮想血管造影検査を行う方法において、
大動脈の少なくとも一部を含む画像走査データを取得するステップと、
前記画像走査データを、複数のボクセルを含む体積表現に変換するステップと、
前記体積表現を分割し、前記ボクセルを複数のカテゴリのうち１つに分類するステップと、
前記分割された体積表現を解析し、大動脈壁における動脈瘤の少なくとも一部を表すボクセルを識別するステップと、
動脈瘤の少なくとも一部を表すボクセルの周囲の少なくとも１つの閉表面を発生し、前記動脈瘤の輪郭を評価するステップとを含むことを特徴とする、仮想血管造影検査を行う方法。
【請求項２８】
請求項２７に記載の仮想血管造影検査を行う方法において、前記画像走査をコンピュータ断層撮影走査としたことを特徴とする、仮想血管造影検査を行う方法。
【請求項２９】
請求項２７に記載の仮想血管造影検査を行う方法において、前記画像走査を磁気共鳴画像走査としたことを特徴とする、仮想血管造影検査を行う方法。
【請求項３０】
請求項２７に記載の仮想血管造影検査を行う方法において、前記分割動作が、ボクセルを、少なくとも、血、組織およびカルシウム堆積物のカテゴリに分類することを特徴とする、仮想血管造影検査を行う方法。
【請求項３１】
請求項２７に記載の仮想血管造影検査を行う方法において、前記動脈瘤の体積を、前記発生された閉表面を使用して評価するステップをさらに含むことを特徴とする、仮想血管造影検査を行う方法。
【請求項３２】
請求項２７に記載の仮想血管造影検査を行う方法において、前記大動脈管腔を通るナビゲーション経路を発生するステップをさらに含むことを特徴とする、仮想血管造影検査を行う方法。
【請求項３３】
請求項３２に記載の仮想血管造影検査を行う方法において、前記動脈瘤の長さを、前記ナビゲーション経路に基づいて評価するステップをさらに含むことを特徴とする、仮想血管造影検査を行う方法。
【請求項３４】
血管の仮想内視鏡検査を行う方法において、
前記血管の少なくとも一部を含む画像走査データを取得するステップと、
前記画像走査データを、複数のボクセルを含む体積表現に変換するステップと、
前記体積表現を分割し、前記ボクセルを、血、組織およびカルシウム堆積物のカテゴリを含む複数のカテゴリのうちの１つに分類するステップと、
前記血管を通るナビゲーション経路を発生するステップとを含むことを特徴とする、血管の仮想内視鏡検査を行う方法。

【請求項３５】
請求項３４に記載の血管の仮想内視鏡検査を行う方法において、前記血管を頚動脈としたことを特徴とする、血管の仮想内視鏡検査を行う方法。
【請求項３６】
請求項３４に記載の血管の仮想内視鏡検査を行う方法において、前記ナビゲーション経路に沿って前記頚動脈の直径を決定し、狭窄の領域を識別するステップをさらに含むことを特徴とする、血管の仮想内視鏡検査を行う方法。
【請求項３７】
請求項３４に記載の血管の仮想内視鏡検査を行う方法において、前記画像走査をコンピュータ断層撮影走査としたことを特徴とする、血管の仮想内視鏡検査を行う方法。
【請求項３８】
請求項３４に記載の血管の仮想内視鏡検査を行う方法において、前記画像走査を磁気共鳴画像走査としたことを特徴とする、血管の仮想内視鏡検査を行う方法。
【請求項３９】
仮想血管造影検査を使用してステントグラフトの特性を決定する方法において、
大動脈の少なくとも一部を含む画像走査データを取得するステップと、
前記画像走査データを、複数のボクセルを含む体積表現に変換するステップと、
前記体積表現を分割し、前記ボクセルを複数のカテゴリのうちの１つに分類するステップと、
前記分割された体積表現を解析し、前記大動脈壁における動脈瘤の少なくとも一部を表すボクセルを識別するステップと、
動脈瘤の少なくとも一部を表すボクセルの周囲の少なくとも１つの閉表面を発生し、前記動脈瘤の輪郭を評価するステップと、
前記動脈瘤輪郭の終了点の位置を識別するステップと、
前記動脈瘤輪郭の終了点間の長さを計算し、前記ステントグラフトの長さを決定するステップと、
前記動脈瘤輪郭の終了点における前記大動脈管腔の直径を計算し、前記ステントグラフトの必要な外側直径を決定するステップとを含むことを特徴とする、仮想血管造影検査を使用してステントグラフトの特性を決定する方法。
【請求項４０】
請求項３９に記載の仮想血管造影検査を使用してステントグラフトの特性を決定する方法において、前記動脈瘤と通常の大動脈管腔との界面の角度を決定し、前記ステントグラフトの対応する端の角度方向を決定するステップをさらに含むことを特徴とする、仮想血管造影検査を使用してステントグラフトの特性を決定する方法。
【請求項４１】
請求項３９に記載の仮想血管造影検査を使用してステントグラフトの特性を決定する方法において、前記動脈瘤に最も近い動脈ブランチの位置を突き止め、前記ステントグラフトの最大長を決定するステップをさらに含むことを特徴とする、仮想血管造影検査を使用してステントグラフトの特性を決定する方法。
【請求項４２】
請求項４１に記載の仮想血管造影検査を使用してステントグラフトの特性を決定する方法において、前記動脈瘤に最も近い動脈ブランチが、腎臓および大腿部動脈ブランチの少なくとも一方を含むことを特徴とする、仮想血管造影検査を使用してステントグラフトの特性を決定する方法。
【請求項４３】
請求項３９に記載の仮想血管造影検査を使用してステントグラフトの特性を決定する方法において、前記動脈瘤の端に最も近い大動脈領域の仮想生体組織検査を行い、予測されたグラフトインタフェース位置における前記組織の特性を決定するステップをさらに含むことを特徴とする、仮想血管造影検査を使用してステントグラフトの特性を決定する方法。
【請求項４４】

複数のボクセルで形成された中空物体の３次元画像表現に関するスケルトンを規定する方法において、
前記中空物体内におけるルートボクセルを識別するステップと、
前記中空物体内のすべてのボクセルに関する距離マップを発生するステップであって、前記距離マップが、ユークリッド重み付き距離を有する隣接ボクセルの２６接続立方体プレートを使用して形成される、ステップと、
前記距離マップにおける局所最大値を有するボクセルを、前記中空物体におけるブランチの終了点として識別するステップと、
各々の局所最大値ボクセルに関して、前記ルートボクセルに対する最短接続経路、または、前もって規定された最短経路を決定するステップとを含むことを特徴とする、３次元画像表現に関するスケルトンを規定する方法。

【請求項４５】
請求項４４に記載の３次元画像表現に関するスケルトンを規定する方法において、多解像度データ減少を前記３次元画像表現に行い、前記発生および識別動作に関する減少データセットを発生するステップをさらに含むことを特徴とする、３次元画像表現に関するスケルトンを規定する方法。

【請求項４６】
請求項４４に記載の３次元画像表現に関するスケルトンを規定する方法において、前記最短経路を、前記物体の個々のブランチ内の中心に配置するステップをさらに含むことを特徴とする、３次元画像表現に関するスケルトンを規定する方法。

【請求項４７】
請求項４４に記載の３次元画像表現に関するスケルトンを規定する方法において、前記物体が少なくとも１つの血管を含むことを特徴とする、３次元画像表現に関するスケルトンを規定する方法。

【請求項４８】
請求項４４に記載の３次元画像表現に関するスケルトンを規定する方法において、前記物体が肺の気道を含むことを特徴とする、３次元画像表現に関するスケルトンを規定する方法。

【請求項４９】
請求項４４に記載の３次元画像表現に関するスケルトンを規定する方法において、前記物体が膀胱を含むことを特徴とする、３次元画像表現に関するスケルトンを規定する方法。

【請求項５０】
請求項４４に記載の３次元画像表現に関するスケルトンを規定する方法において、前記物体が脊椎動物の脊髄を含むことを特徴とする、３次元画像表現に関するスケルトンを規定する方法。

【請求項５１】
興味ある領域のコンピュータ支援診断を行う方法において、
前記興味ある領域の少なくとも一部を含む画像走査データを取得するステップと、
前記画像走査データを、複数のボクセルを含む体積表現に変換するステップであって、前記ボクセルの少なくとも一部が前記興味ある領域の表面を表す、ステップと、
表面を表すボクセルの前記部分を、異常を示す幾何学的特長およびテクスチャ特徴の少なくとも一方に関して解析するステップとを含むことを特徴とする、コンピュータ支援診断を行う方法。

【請求項５２】
請求項５１に記載のコンピュータ支援診断を行う方法において、前記テクスチャ特徴を、ボクセルの前記部分の２つのボクセル間の相関を特徴付ける確率密度関数に含めることを特徴とする、コンピュータ支援診断を行う方法。

【請求項５３】
請求項５２に記載のコンピュータ支援診断を行う方法において、前記２つのボクセルを隣接するボクセルとしたことを特徴とする、コンピュータ支援診断を行う方法。

【請求項５４】
請求項５２に記載のコンピュータ支援診断を行う方法において、ボクセルの前記部分の強度を使用し、前記確率密度関数の評価を発生することを特徴とする、コンピュータ支援診断を行う方法。
【請求項５５】
請求項５４に記載のコンピュータ支援診断を行う方法において、複数のボクセル強度を使用し、前記興味ある領域の累積分布関数と、局所累積分布関数とを発生し、前記局所累積分布関数を文脈累積分布関数と比較し、異常な領域を識別することを特徴とする、コンピュータ支援診断を行う方法。
【請求項５６】
請求項５５に記載のコンピュータ支援診断を行う方法において、前記局所累積分布関数と文脈累積分布関数との間の距離を決定し、前記距離が異常の基準を与えることを特徴とする、コンピュータ支援診断を行う方法。
【請求項５７】
請求項５６に記載のコンピュータ支援診断を行う方法において、前記距離を使用し、強度値を、前記興味ある領域の表面を表すボクセルに割り当て、該方法が、強度における変化が異常な領域を表すように前記ボクセルを表示するステップをさらに含むことを特徴とする、コンピュータ支援診断を行う方法。
【請求項５８】
請求項５７に記載のコンピュータ支援診断を行う方法において、前記興味ある領域が結腸を含み、前記異常がポリープを含むことを特徴とする、コンピュータ支援診断を行う方法。
【請求項５９】
請求項５１に記載のコンピュータ支援診断を行う方法において、前記興味ある領域が大動脈を含み、前記異常が腹部の大動脈瘤を含むことを特徴とする、コンピュータ支援診断を行う方法。
【請求項６０】
請求項５１に記載のコンピュータ支援診断を行う方法において、前記表面を二次微分可能な表面として表し、各々の表面体積ユニットが関連するガウス曲率を有し、前記ガウス曲率が結合して、前記幾何学的特長を形成することを特徴とする、コンピュータ支援診断を行う方法。
【請求項６１】
請求項５９に記載のコンピュータ支援診断を行う方法において、複数の予め決定された幾何学的特長テンプレートを規定し、前記表面の幾何学的特長を前記テンプレートと比較し、幾何学的特長分類を決定することを特徴とする、コンピュータ支援診断を行う方法。
【発明の詳細な説明】
【０００１】
【発明の属する技術分野】
本発明は、体積を基礎とする３次元仮想検査を行うシステムおよび方法に関し、より特には、増強された視覚化およびナビゲーション特性を与えるシステムに関する。
【０００２】
【従来の技術】
結腸癌は、世界中で主な死因であり続けている。初期において人間の結腸にポリープとして現れる癌の成長の初期の検出は、患者の回復の可能性を大幅に改善することができる。現在、患者の結腸においてポリープまたは他の塊を検出する２つの慣例的な方法がある。第１の方法は、大腸鏡検査であり、大腸鏡と呼ばれる可撓性光ファイバチューブを使用し、結腸を、前記大腸鏡を直腸に物理的に入れることによって、視覚的に検査する。医師は、前記チューブを操作し、結腸におけるなにか異常な成長を探索することができる。前記大腸鏡検査は、信頼できるが、費用および時間の双方が比較的かかり、患者にとって侵略的で不快な痛い手続きである。

【０００３】
第２の検出技術は、バリウム浣腸および結腸の２次元Ｘ線画像化である。前記バリウム浣腸を使用し、結腸をバリウムで覆い、２次元Ｘ線画像を撮って、結腸の画像を獲得する。しかしながら、バリウム浣腸は、必ずしも結腸全体の図を与えるとは限らず、前記動作を行うときにしばしばオペレータ依存であり、患者を過度の放射線に曝し、大腸鏡ほど感度がよくはない。上述した慣例的な手段における不完全さのため、結腸をポリープに関して検査する、より確実で、それほど侵入的でなく、それほど費用がかからない方法が望ましい。肺のような人間の他の器官を、塊に関して、確実で費用効果的な方法において検査する方法も望ましい。

【０００４】
米国における癌死の別の主要な原因は、膀胱癌である。１９９５年において、５００００の膀胱癌の新しいケースが報告され、この病気の結果として１１０００人の死が報告された。膀胱癌に関する最も一般的な試験は、尿“ディップスティック”または慣例的な尿検査の使用である。しかしながら、これらのような試験は、膀胱癌の検出において、そのより後期の発達段階においてのみ有効であり、癌の成長のサイズまたは位置に関するどのような情報も与えない。現在、膀胱の異常を調べる主な方法である膀胱鏡検査は、正確な結果を与え、任意の以上の関連する細部および位置に関する情報を与えることができる。しかしながら、膀胱鏡検査は、医師に限られた視野しか与えず、サイズの客観的な表示が不足している。加えて、膀胱鏡検査は、厳しい尿道の狭窄あるいは活発な膀胱の出血を有する患者には望ましくない。したがって、特に癌の進行の初期段階において、膀胱癌に関して患者を選別する代わりの手順を開発することが望ましい。

【０００５】
コンピュータ断層撮影およびＭＲＩ（磁気共鳴撮影画像）のような現在利用可能な医療画像化装置を用いる人間の器官の２次元（“２Ｄ”）視覚化は、患者の診断に広く使用されてきた。３次元画像を、操作機械から発生された２次元ピクチャ間に堆積または補間することによって形成することができる。器官の画像化と、３次元空間におけるその体積の視覚化とは、その物理的な侵入がないことと、データ操作の容易さとにより、有利である。しかしながら、３次元体積画像の調査は、内部から器官を仮想的に見る利点を完全に利用するために、正確に行わなければならない。

【０００６】
環境の３次元（“３Ｄ”）体積仮想画像を見るときに、機能的モデルを使用し、仮想空間を調査しなければならない。ある可能なモデルは、ビューワに関して仮想空間を調査する基準点として使用することができる仮想カメラである。一般的な３Ｄ仮想環境内のナビゲーションの文脈におけるカメラ制御は、以前に研究されている。仮想空間のナビゲーションに提案された２つの慣例的な形式のカメラ制御がある。第１のものは、オペレータがカメラを異なった位置および向きにおいて操作し、所望のビューを達成する、カメラのオペレータ完全制御である。オペレータは、前記カメラを実際に操縦する。これは、オペレータが、興味のある特定の区分を調査し、他の区分を無視することを可能にする。しかしながら、大きい領域におけるカメラの完全な制御は、面倒で骨が折れ、オペレータは、調査の開始点と終了点との間のすべての重要な特徴を見るとは限らない。

【０００７】
カメラ制御の第２の技術は、計画ナビゲーション方法であり、この方法は、カメラに、とるべき予め決められた経路を割り当て、オペレータによって変更することができない。これは、予定された“オートパイロット”を有するのと同じである。これは、オペレータが、見ている仮想空間において集中することを可能にし、調査している環境の壁の中に進むことについての心配をする必要がない。しかしながら、この第２の技術は、ビューワに、コースを変更するか、飛行経路に沿って見られた興味ある領域を調査する柔軟性を与えない。

【０００８】
上述した２つのナビゲーション方法を使用し、これらの個々の欠点を最小にしながら双方

の技術の利点を実現することが望ましい。柔軟なナビゲーション技術を、無侵入無痛完全検査を行うために仮想３Ｄ空間において表された人間または動物の器官の調査に用いることが望ましい。望まれるナビゲーション技術は、さらに、滑らかな経路と器官中および周囲の完全な調査とを保証しながら柔軟性を許す、オペレータによる３Ｄ空間における仮想器官の完全な調査を考慮する。加えて、器官を見るのに必要な計算を最小にする技術を使用することによって、実時間設定における器官の調査を表示することができることが望ましい。また、望まれる技術は、任意の仮想物体の調査に等しく適用可能であるべきである。

【０００９】

本発明の他の目的は、見ている物体の一部の視覚化をカスタマイズするために、特定の体積要素を変化する程度に透明または半透明にするために、不透明係数を表現における各々の体積要素に割り当てることである。物体の断面を、前記不透明係数を使用して構成することもできる。

【００１０】

発明の要約

本発明は、人間の器官のような物体の３次元視覚化画像を、体積視覚化技術を使用して発生し、前記仮想画像を、オペレータが、予め規定された飛行経路に沿って移動し、ポリープ、嚢胞、または、器官における他の異常な特徴を識別するために、前記予め規定された経路から離れて、前記画像における興味のある特定の部分に位置および見る角度の双方を調節することを可能にするガイド付きナビゲーションシステムを使用して仮想画像を調査する。

【００１１】

物体の仮想調査を行う方法は、コントラストエージェントの存在によって膨張した物体の少なくとも１つの画像化走査を行うステップを含む。加えて、コントラストエージェントを取り除いた前記物体の少なくとも１つの画像化走査を得る。前記走査を、複数のボクセルで形成された対応する体積データセットに変換する。次に、画像分割を行い、各々の走査のボクセルを複数のカテゴリに分類する。各々の走査の体積データセットを、共通座標系に登録する。次に、表示動作を、前記体積データセットの少なくとも２つにおける対応する画像が実際的に同時に表示される場合、行うことができる。前記体積データセットの１つにおいて行われる仮想ナビゲーション動作の結果、対応するナビゲーション動作が、少なくとも１つの他の体積データセットにおいて起こる。

【００１２】

好適には、前記膨張した物体の少なくとも１つの走査は、前記物体の横走査および冠状走査を含む。同様に、前記コントラストエージェントを取り除いた物体の走査は、前記物体の横走査および冠状走査を含むことが望ましい。この手順は、特に、前記物体が膀胱である場合、仮想膀胱鏡検査を行うのによく適合する。この場合において、前記走査は、一般に、磁気共鳴画像化の形態をとり、前記コントラストエージェントを尿とすることができる。

【００１３】

本発明による他の方法は、物体の仮想調査を行うものである。この方法において、前記物体に画像化走査を行い、画像走査データを得る。得られた画像走査データを、複数の体積ユニットまたはボクセルに変換する。前記ボクセル間を補間することによって、拡張されたデータセットを発生する。次に、画像分割を行い、前記ボクセルを複数のカテゴリに分類することができる。前記物体内の体積を、前記物体の管腔内の種ボクセルからの領域成長アルゴリズムを使用すること等によって、前記拡張されたデータセットから抽出する。次に、解像度が低下したデータセットを、前記拡張されたデータセットから発生する。前記拡張されたデータセットからのデータを効率的に格納し、呼び出すために、このデータを、ツリーデータ構造において格納する。次に、画像を、前記拡張されたデータセットおよび解像度が低下したデータセットの双方に関して描画することができる。次に、これらの画像のうち一方を、見るために選択する。一般に、前記解像度が低下したデータセット

を、ナビゲーションまたは画像相互作用中に選択し、前記拡張されたデータセットを、高解像度静止表示に関して選択する。

【００１４】

仮想血管造影法を行う方法も提供する。この方法において、大動脈の少なくとも一部の画像化走査データを得る。前記画像化走査データを、複数のボクセルを含む体積表現に変換する。前記体積表現を分割し、前記ボクセルを複数のカテゴリのうちの１つに分類する。次に、前記分割された体積表現を解析し、大動脈壁における動脈瘤の少なくとも一部のボクセル表示を識別する。識別された前記動脈瘤の部分から、少なくとも１つの閉鎖表面を、動脈瘤の少なくとも一部のボクセル表示の周囲に発生する。前記閉鎖表面は、前記動脈瘤の輪郭の推定を与える。ナビゲーション経路を、前記大動脈の管腔を通じて確立することができ、長さ、直径、体積および配置のような、前記動脈瘤の特徴を決定することができる。

【００１５】

前記仮想血管造影法を行う方法を使用し、動脈瘤の進行を検出および監視することができ、前記仮想血管造影法を行う方法を、ステントグラフトを配置する必要がある特徴を決定するのに使用することができる。

【００１６】

複数のボクセルで形成された中空物体の３次元画像表現に関するスケルトンを規定する方法も提供する。ルートボクセルを、前記中空物体内で最初に確認する。次に、距離マップを、前記中空物体内のすべてのボクセルに関して発生する。前記距離マップを、重み付きユークリッド距離を有する２６接続キュービックプレートを使用して形成する。前記距離マップにおける局所最大値を有するこれらのボクセルを、前記中空物体におけるブランチの終点として識別する。各々の局所最大値ボクセルに関して、前記ルートボクセルに接続された最も短い経路、または、以前に規定された最短経路を決定する。最短経路の集合を、前記物体の粗いスケルトンとする。この技術は、呼吸器系および心臓血管系のような多ブランチ構造に特に好適である。

【００１７】

【発明の実施の形態】

本願において記載した方法およびシステムを、調査すべき任意の物体に適用することができるが、説明する好適実施形態は、人体における器官、特に結腸の調査である。結腸は、長く、捩れており、患者から金銭と、物理的プローブの不快感および危険性との双方を軽減する仮想調査に特に好適である。制限なく、調査できる器官は、肺、胃、胃腸系の一部、心臓および血管を含む。

【００１８】

図１は、体積視覚化技術を使用する仮想大腸鏡検査を行うのに必要なステップを示す。ステップ１０１は、必要ならば、医師または特定の走査機器のいずれかによって調査のために見るために走査すべき結腸を準備する。この準備は、前記結腸を、口から摂取され、胃を通過した後、前記結腸に入る“カクテル”または液体で洗浄することを含む。前記カクテルは、患者に前記結腸内に存在する排泄物を放出させる。使用する物質の一例は、ゴリテリーである。加えて、結腸の場合において、前記結腸を走査および調査が容易になるように拡張するために、空気またはCO_2を前記結腸内に押し入れることができる。これを、直腸内に配置された小さいチューブによって行い、約１０００ｃｃの空気を前記直腸内に押し入れ、前記直腸を膨張させる。使用するスキャナの形式に応じて、前記結腸における排泄物を前記結腸の壁自身から識別するために、患者にバリウムのような対照物質を飲ませ、なんらかの排出されていない大便を覆う必要があるかもしれない。代わりに、前記結腸を仮想的に調査する方法は、本明細書において後に説明するように、前記仮想調査の前またはその間に、仮想排泄物を除去することができる。ステップ１０１は、図１において点線によって示すように、すべての調査において行う必要があるわけではない。

【００１９】

ステップ１０３は、調査すべき器官を走査する。前記スキャナを、結腸を走査するスパイ

ラルＣＴスキャナ、または、例えばキセノンガスで標識付けされた肺を走査するゼニタＭＲＩ機械のような、当該技術分野においてよく知られた装置とすることができる。前記スキャナは、前記体積視覚化に必要なデータを発生するために、呼吸を止めている間に、ボディの周りの異なった位置から多数の画像を得ることができなければならない。単一ＣＴ画像の一例は、５ｍｍ幅、１：１ないし２：１ピッチのＸ線ビームを使用し、４０ｃｍ視界を、前記結腸の左結腸曲の上部から直腸まで行う。

【００２０】

前記物体の個別のデータ表現を、走査以外の他の方法によって発生することができる。参照によってここに含まれる、１９８８年7月２６日に出願され、１９９１年８月８日に発行された、カウフマンによる“連続的な３次元幾何学的表現を、３次元ボクセルベースシステム内の個別の３次元ボクセルベース表現に変換する方法”というタイトルの米国特許第５０３８３０２号において記載されている技術によって、物体を表現するボクセルデータを幾何学的モデルから得ることができる。加えて、本発明によって３次元ボクセルに変換し、調査することができる画像のコンピュータモデルから、データを発生することができる。この形式のデータの一例は、スペースシャトルを取り巻く乱流のコンピュータシミュレーションである。

【００２１】

ステップ２０４は、前記走査された画像を３次元体積要素（ボクセル）に変換する。結腸を調査する好適実施形態において、前記走査データを、１ｍｍまたは２．５ｍｍの増量において５ｍｍ厚スライスに再フォーマットし、１ｍｍスライスにおいて再構成し、各々のスライスを５１２×５１２画素として表す。こうすることによって、約１ｍｍ^{3}のボクセルを形成する。このようにして、多数の２Ｄスライスを、前記走査の長さに応じて発生する。次に、前記２Ｄスライスの組を、３Ｄボクセルに再構成する。前記スキャナからの２Ｄ画像の３Ｄボクセルへの変換処理を、走査機械それ自身か、コンピュータのような別個の機械のいずれかによって、当該技術分野において既知の技術で行うことができる（例えば、参照によってここに含まれる、１９８８年１１月１１日に出願され、１９９１年１月１５日に発行された、カウフマン他による“ボクセルベースデータを格納し、アクセスし、処理する方法および装置”というタイトルの米国特許第４９８５８５６号を参照）。

【００２２】

ステップ１０５は、オペレータが調査すべき選択された器官の部分を規定することを可能にする。医師は、ポリープが発達しそうな前記結腸の特定の部分に興味を持つかもしれない。見るべき経路の開始点および終了点を、医師／オペレータによって指示することができる。慣例的なコンピュータおよびコンピュータインタフェース（例えば、キーボード、マウスまたはスペースボール）を使用し、調査すべき前記結腸の部分を指定することができる。座標を有するグリッド系をキーボード入力に使用することができ、または、医師／オペレータは、所望の点において“クリック”することができる。前記結腸の全体像も、望むならば見ることができる。

【００２３】

ステップ１０７は、調査している仮想器官の計画されたまたはガイド付きナビゲーション動作を行う。ガイド付きナビゲーション動作を行うことを、任意の時間においてオペレータによって手動で調節することができる、予め規定されたまたは自動的に予め決定された飛行経路に沿って環境を通るナビゲーティングとして規定する。前記走査データを３Ｄボクセルに変換した後、前記器官の内部を、選択された開始点から選択された終了点まで通過しなければならない。前記仮想調査を、前記仮想空間を通って進む、前記終了点をさすレンズを有する小さいカメラを有することにおいてモデル化する。前記ガイド付きナビゲーション技術は、前記カメラとのあるレベルの相互作用を与え、その結果、前記カメラは、オペレータの相互作用がない場合において仮想空間を通って自動的にナビゲートすることができ、同時に、必要な場合、オペレータが前記カメラを操作することを可能にする。ガイド付きナビゲーションを達成する好適な例は、ポテンシャル場を用いて前記カメラの動きを制御する、図２および３において詳細に示す物理的に基づいたカメラモデルを使用

することである。

【００２４】

ステップ１０７と同時に行うことができるステップ１０９は、前記ガイド付きナビゲーション動作の選択された経路の沿った前記カメラの視点から前記器官の内部を表示する。３次元表示を、マーチングキューブ技術のような当該技術分野において既知の技術を使用して発生することができる。しかしながら、前記結腸の実時間表示を発生するために、前記仮想器官の表示に必要な膨大な数のデータの計算を減らす技術が必要である。図９は、この表示ステップをより詳細に示す。

【００２５】

図１に示す方法を、ボディにおける多数の器官を同時に走査することに用いることもできる。例えば、患者を、結腸および肺の双方における癌の成長に関して調査してもよい。図１の方法を、ステップ１０３において興味あるすべての領域を走査し、ステップ１０５において調査すべき現在の器官を選択するように変更する。例えば、医師／オペレータは、最初に結腸を選択して仮想調査し、後に肺を調査してもよい。代わりに、異なった専門の二人の異なった医師が、彼らの個々の専門に関係する、異なった走査された器官を仮想調査してもよい。ステップ１０９に続いて、調査すべき次の器官を選択し、その部分を規定し、調査する。これを、調査が必要なすべての器官が処理されるまで続ける。

【００２６】

図１に関連して説明したステップを、体積要素によって表すことができる任意の物体の調査に用いることもできる。例えば、建築構造物または無生物を同様に表し、調査することができる。

【００２７】

図２は、ステップ１０７におけるガイド付きナビゲーション技術を行う“サブマリン”カメラ制御モデルを示す。ガイド付きナビゲーション中にオペレータ制御がない場合、通常設定ナビゲーションは、前記結腸の一方の選択された端から他方までの飛行経路に沿って前記カメラを自動的に向ける計画されたナビゲーションと同様である。前記計画されたナビゲーション段階中、前記カメラは、前記結腸の表面のより良好な視界を得る、前記結腸の中心においてとどまる。興味ある領域に出合った場合、前記ガイド付きナビゲーションを使用する仮想カメラのオペレータは、前記カメラを相互作用的に特定の領域に近づけ、前記カメラの動きおよび角度を管理し、前記直腸の壁と不本意に衝突することなしに前記興味ある領域を詳細に研究することができる。オペレータは、前記カメラを、キーボードやマウスのような標準的なインタフェース装置、または、スペースボールのような非標準的な装置で制御することができる。カメラを仮想環境において完全に操作するために、前記カメラに関して６自由度が必要である。前記カメラは、水平、垂直およびＺ方向（軸２１７）において移動することができ、他の３自由度（軸２１９）において回転することができ、前記カメラが仮想環境のすべての側面および角度に移動し、操作することができるようにしなければならない。前記ガイド付きナビゲーションに関するカメラモデルは、２つの質点$x_1$２０３および$x_2$２０５を接続する、延びない重さのないロッド２０１を含み、双方の質点はポテンシャル場２１５を受ける。前記ポテンシャル場を、前記カメラを前記器官の壁から押しのけるために、前記器官の壁における高さとして規定する。

【００２８】

前記質点の位置をx_1およびx_2によって与え、これらは同じ質量ｍを有するとする。カメラをサブマリン$x_1$２０３の頭に取り付け、このカメラの見る方向はx_2 x_1と一致する。前記サブマリンは、前記２個の質点が前に規定したポテンシャル場Ｖ（ｘ）からの力と、任意の摩擦力と、任意のシミュレートされた外力とによって影響を受けると、並進運動と、前記モデルの質量ｘの中心の周囲の回転とを行うことができる。x_1、x_2と、ｘとの間の関係は、以下の通りである。

【数１】

$$x = (x,y,z),$$
$$r = (r\sin\theta\cos\varphi, r\sin\theta\sin\varphi, r\cos\theta),$$
$$\mathbf{x}_1 = \mathbf{x} + \mathbf{r},$$
$$\mathbf{x}_2 = \mathbf{x} - \mathbf{r}, \qquad (1)$$

ここで、ｒ、θおよびφは、ベクトルｘｘ$_1$の極座標である。前記モデルの運動エネルギーＴを、ｘ$_1$およびｘ$_2$の運動の運動エネルギーの和として規定する。

【数２】

$$\begin{aligned} T &= \frac{m}{2}(\dot{\mathbf{x}}_1^2 + \dot{\mathbf{x}}_2^2) \\ &= m\dot{\mathbf{x}}^2 + m\dot{\mathbf{r}}^2 \\ &= m(\dot{x}^2 + \dot{y}^2 + \dot{z}^2) + mr^2(\dot{\theta}^2 + \dot{\phi}^2\sin^2\theta). \end{aligned} \qquad (2)$$

【００２９】

次に、前記サブマリンモデルの動きに関する式を、ラグランジュ方程式を使用して得る。

【数３】

$$\frac{d}{dt}\left(\frac{\partial T}{\partial \dot{q}_j}\right) - \frac{\partial T}{\partial q_j} = \sum_{i=1}^{2}\left(\mathbf{F}_i \cdot \frac{\partial \mathbf{x}_i}{\partial q_j}\right), \qquad (3)$$

ここで、ｑ$_j$ｓは、前記モデルの一般化座標であり、これを、時間ｔの変数として考えることができる。

【数４】

$$(q_1, q_2, q_3, q_4, q_5, q_6) = (x, y, z, \theta, \phi, \psi) = \mathbf{q}(t), \qquad (4)$$

ψは我々のカメラシステムのロール角を示し、これを後に説明する。Ｆ$_i$ｓを一般化された力と呼ぶ。前記サブマリンの制御を、シミュレートされた外力をｘ$_1$に用いることによって行う。

【数５】

$$\mathbf{F}_{ext} = (F_x, F_y, F_z),$$

ｘ$_1$およびｘ$_2$の双方は、前記ポテンシャル場からの力と、各々の質点の速度の反対方向において作用する摩擦とによって影響を受けるとする。したがって、発生される力は、以下のように式化される。

【数６】

$$\begin{aligned} \mathbf{F}_1 &= -m\nabla V(\mathbf{x}_1) - k\dot{\mathbf{x}}_1 + \mathbf{F}_{ext}, \\ \mathbf{F}_2 &= -m\nabla V(\mathbf{x}_2) - k\dot{\mathbf{x}}_2, \end{aligned} \qquad (5)$$

ここで、ｋは前記システムの摩擦係数を示す。外力Ｆ$_{ext}$を、図２に示すように、発生された画像における所望の方向２０７におけるマウスボタンの単純なクリックによって、

オペレータによって適用する。このとき、このカメラモデルはその方向において動く。これは、オペレータがマウスボタンの１クリックのみによって前記カメラの少なくとも５自由度を制御することを可能にする。式（２）、（３）および（５）から、我々のサブマリンモデルの５つのパラメータの加速度を以下のように得ることができる。

【数７】

$$
\begin{aligned}
\ddot{x} &= -\frac{1}{2}\left(\frac{\partial V(\mathbf{x}_1)}{\partial x}+\frac{\partial V(\mathbf{x}_2)}{\partial x}\right)-\frac{k\dot{x}}{m}+\frac{F_x}{2m},\\
\ddot{y} &= -\frac{1}{2}\left(\frac{\partial V(\mathbf{x}_1)}{\partial y}+\frac{\partial V(\mathbf{x}_2)}{\partial y}\right)-\frac{k\dot{y}}{m}+\frac{F_y}{2m},\\
\ddot{z} &= -\frac{1}{2}\left(\frac{\partial V(\mathbf{x}_1)}{\partial z}+\frac{\partial V(\mathbf{x}_2)}{\partial z}\right)-\frac{k\dot{z}}{m}+\frac{F_z}{2m},\\
\ddot{\theta} &= \dot{\phi}^2\sin\theta\cos\theta\\
&\quad -\frac{1}{2r}\left[\cos\theta\left\{\cos\phi\left(\frac{\partial V(\mathbf{x}_1)}{\partial x}-\frac{\partial V(\mathbf{x}_2)}{\partial x}\right)+\sin\phi\left(\frac{\partial V(\mathbf{x}_1)}{\partial y}-\frac{\partial V(\mathbf{x}_2)}{\partial y}\right)\right\}\right.\\
&\quad \left.-\sin\theta\left(\frac{\partial V(\mathbf{x}_1)}{\partial z}-\frac{\partial V(\mathbf{x}_2)}{\partial z}\right)\right]\\
&\quad -\frac{k}{m}\dot{\theta}+\frac{1}{2mr}\left(F_x\cos\theta\cos\phi+F_y\cos\theta\sin\phi-F_z\sin\theta\right),\\
\ddot{\phi} &= \frac{1}{\sin\theta}\left[-2\dot{\theta}\dot{\phi}\cos\theta\right.\\
&\quad -\frac{1}{2r}\left\{-\sin\phi\left(\frac{\partial V(\mathbf{x}_1)}{\partial x}-\frac{\partial V(\mathbf{x}_2)}{\partial x}\right)+\cos\phi\left(\frac{\partial V(\mathbf{x}_1)}{\partial y}-\frac{\partial V(\mathbf{x}_2)}{\partial y}\right)\right\}\\
&\quad \left.-\frac{k}{m}\dot{\phi}\sin\theta+\frac{1}{2mr}\left(-F_x\sin\phi+F_y\cos\phi\right)\right], \qquad (6)
\end{aligned}
$$

ここで、

【外１】

$\dot{x}$

および

【外２】

$\ddot{x}$

は、各々、ｘの一次導関数および二次導関数を示し、

【数８】

$$\left(\frac{\partial V(x)}{\partial x},\frac{\partial V(x)}{\partial y},\frac{\partial V(x)}{\partial z}\right)$$

は、点ｘにおけるポテンシャルの勾配を示す。

【外３】

$\ddot{\theta}$

の

【外４】

$\dot{\phi}^2\sin\theta\cos\theta$

および

【外５】

$\ddot{\phi}$

の
【外６】
$$-\frac{2\dot{\theta}\dot{\phi}\cos\theta}{\sin\theta}$$
を、遠心力およびコリオリ力と呼び、これらは、前記サブマリンの角速度の交換に関係がある。前記モデルが、前記サブマリンのロッドに関して規定された慣性モーメントを持たないため、これらの項は、φの数値計算のオーバーフローを生じる傾向にある。幸いにも、これらの項は、前記サブマリンモデルの角速度が重要な場合にのみ重要になり、これは、本質的に、前記カメラが速く動き過ぎることを意味する。器官を適切に見ることができないため、カメラを非常に速く動かせるようにすることは無意味であるため、前記オーバーフロー問題を回避するため、我々のインプリメンテーションにおいてこれらの項を最小にする。
【００３０】
式（６）の最初の３つの式から、以下の条件を満たす場合、前記サブマリンを、前記ポテンシャル場に対する外力によって進ませることはできないことが分かる。
【数９】
$$|\nabla V(\mathbf{x}_1) + \nabla V(\mathbf{x}_2)| > \frac{|\mathbf{F}_{ext}|}{m}.$$
前記サブマリンの速度と、外力
【外７】
$\mathbf{F}_{ext}$
とは、我々のインプリメンテーションにおいて上限を有するため、前記物体の境界において十分高いポテンシャル値を割り当てることによって、前記サブマリンが、前記環境において前記物体または壁に決して衝突しないことを保証することができる。
【００３１】
上述したように、前記カメラシステムのロール角Ψを考える必要がある。可能な１つのオプションは、オペレータに角度の完全な制御を与える。しかしながら、オペレータは、前記カメラを前記モデルのロッドの周りで自由に回転させることができるが、彼または彼女は、容易に方角を見失うかもしれない。好適な技術は、前記カメラの上部の方向を、質量m_2を有する振り子３０１に接続し、この振り子は、図３に示すように前記サブマリンのロッドの周りを自由に回転するとする。振り子の方向r_2を、
$r_2 = \gamma_2$（ｃｏｓθｃｏｓφｓｉｎψ
＋ｓｉｎφｃｏｓψ，ｃｏｓθｓｉｎφｓｉｎψ
－ｃｏｓφｃｏｓψ，－ｓｉｎθｓｉｎψ）
のように表し、この式は、前記サブマリンの運動に伴うこの振り子の正確な運動を計算することができるが、システム方程式を複雑にし過ぎる。したがって、ロール角Ψを除くすべての一般化座標が一定であるとし、したがって、前記振り子システムに関する独立の運動エネルギーを、
【数１０】
$$T_p = \frac{m_2}{2}\dot{\mathbf{r}}_2^2 = \frac{m_2 r_2^2}{2}\dot{\psi}^2.$$
として規定する。これは、前記モデルを前記ロール角に関して簡単にする。このモデルにおいて、重力
【数１１】

$$\mathbf{F}_g = m_2\mathbf{g} = (m_2 g_x, m_2 g_y, m_2 g_z)$$

が質点m_2において作用し、Ψの加速度を、
【数１２】

$$\begin{aligned}\ddot{\psi} = \frac{1}{r_2}\{&g_x(\cos\theta\cos\phi\cos\psi - \sin\phi\sin\psi)\\ &+g_y(\cos\theta\sin\phi\cos\psi + \cos\phi\sin\psi)\\ &+g_z(-\sin\theta\cos\psi)\} - \frac{k_2}{m_2}\dot{\psi}. \qquad (7)\end{aligned}$$

のようなラグランジュ方程式を使用して得ることができる。式（６）および（７）から、一般化座標
【外８】
$\mathbf{q}(t)$
およびこれらの導関数
【外９】
$\dot{\mathbf{q}}(t)$
を、
【数１３】

$$\begin{aligned}\mathbf{q}(t+h) &= \mathbf{q}(t) + h\dot{\mathbf{q}}(t) + \frac{h^2}{2}\ddot{\mathbf{q}}(t) + O(h^3),\\ \dot{\mathbf{q}}(t+h) &= \dot{\mathbf{q}}(t) + h\tilde{\mathbf{q}}(t) + O(h^2),\end{aligned}$$

のようなテイラー級数を使用し、前記サブマリンを自由に動かすことによって、漸近的に計算する。前記サブマリンの動きを滑らかにするために、時間ステップｈを、前記動きを滑らかにするためにできるだけ小さい、しかし、計算コストを減少するのに必要な程度に大きい平衡値として選択する。
【００３２】
ポテンシャル場の定義
図２におけるサブマリンモデルにおけるポテンシャル場は、前記仮想器官における境界（壁または他の物）を、前記サブマリンカメラが前記壁または他の境界と衝突しないことを保証するために、高いポテンシャルを前記境界に割り当てることによって規定する。前記カメラモデルがオペレータによって高いポテンシャル領域に移動するように試みられた場合、前記カメラモデルは、例えばオペレータが前記境界の背後またはポリープの内側の器官を調査することを望まない限り、そうすることが禁止される。仮想大腸鏡検査を行う場合において、ポテンシャル場値を、体積測定結腸データの各々の部分（体積要素）に割り当てる。興味ある特定の領域が図１のステップ１０５において開始点および終了点によって指定された場合、前記走査された結腸の選択された領域内のボクセルを、慣例的なブロッキング操作によって識別する。次に、ポテンシャル値を、前記選択された体積のすべてのボクセルｘに、以下の３つの距離値、すなわち、終了点からの距離ｄｔ（ｘ）と、前記結腸表面からの距離ｄｓ（ｘ）と、前記結腸空間の中心線からの距離ｄｃ（ｘ）とに基づいて割り当てる。ｄｔ（ｘ）を、慣例的な成長戦略によって計算する。前記結腸表面から

の距離ｄｓ（ｘ）を、表面ボクセル内部からの慣例的な成長技術を使用して計算する。ｄｃ（ｘ）を決定するために、最初に前記ボクセルから前記結腸の中心線を抽出し、次に、ｄｃ（ｘ）を、慣例的な成長戦略を使用し、前記結腸の中心線から計算する。

【００３３】

前記ユーザに指定された開始点とユーザに指定された終了点とによって規定された前記選択された結腸領域の中心線を計算するために、ｄｓ（ｘ）の最大値を捜し出し、ｄｍａｘと示す。次に、興味ある領域内の各々のボクセルに関して、ｄｍａｘ－ｄｓ（ｘ）のコスト値を割り当てる。このようにして、前記結腸表面に近いボクセルは、高いコスト値を有し、前記中心線に近いボクセルは、比較的低いコスト値を有する。次に、前記コスト割り当てに基づいて、当該技術分野において既知である単一始点最短路技術を用い、始点から終点までの最小コスト経路を効率的に計算する。この低コストラインは、調査することを望む前記結腸区分の中心線または輪郭を示す。前記中心線を決定するこの技術は、本発明の好適な技術である。

【００３４】

興味ある領域の内部のボクセルｘに関するポテンシャル値Ｖ（ｘ）を計算するために、以下の式を用いる。

【数１４】

$$V(\mathbf{x}) = C_1 d_t(\mathbf{x})^{\mu} + C_2\left(\frac{d_s(\mathbf{x})}{d_c(\mathbf{x}) + d_s(\mathbf{x})}\right)^{-\nu}, \qquad (8)$$

ここで、C_1、C_2、μおよびυは、タスクに関して選択された定数である。前記仮想カメラと前記仮想結腸表面との間のどのような衝突も回避するために、十分大きいポテンシャル値を、前記結腸の外部のすべての点に割り当てる。前記ポテンシャル場の勾配は、したがって、前記サブマリンモデルカメラが、移動しているとき、前記結腸壁に決して衝突しないようにするため、重要になる。

【００３５】

前記結腸における経路の中心線を決定する他の技術は、“ピールレイヤ”技術と呼ばれ、この技術を図４ないし８において示す。

【００３６】

図４は、前記体積測定結腸の２Ｄ断面を、示している前記結腸の２つの側壁４０１および４０３と共に示す。２つのブロッキング壁を、オペレータによって、調査する興味のある前記結腸の選択を規定するために、選択する。前記ブロッキング壁を超えて見ることはできない。これは、前記仮想表現を表示する場合の計算数を減少するのを助ける。前記ブロッキング壁は、側壁と共に、調査すべき前記結腸の含まれる体積測定形状を明らかにする。

【００３７】

図５は、前記仮想調査の飛行経路の２つの終点、開始体積要素５０１および終了体積要素５０３を示す。前記開始点および終了点を、図１のステップ１０５においてオペレータによって選択する。前記開始点及び終了点と結腸側面との間のボクセルを、図６において“ｘ”で示す領域によって示されるように識別し、マークする。前記ボクセルは、画素の３次元表現である。

【００３８】

次に、前記ピールレイヤ技術を、図６における識別されマークされたボクセルに用いる。すべてのボクセルの最外層（結腸壁に最も近い）を、残りのボクセルのただ１つの内部層が存在するようになるまで、１つずつ剥ぎ取る。すなわち、中心点から最も遠く離れた各ボクセルを、前記開始ボクセルと終了ボクセルとの間の経路の分離を生じなくなるまで除去する。図７は、前記仮想結腸におけるボクセルの除去の多数の反復が完了した後の中間結果を示す。前記結腸壁に最も近いボクセルを除去した。図８は、すべての剥ぎ取り反復

が完了した後の、前記結腸の中心を下った前記カメラモデルの最終飛行経路を示す。これは、本質的に、前記結腸の中心におけるスケルトンを発生し、前記カメラモデルに関する所望の飛行経路になる。

【００３９】

Ｚバッファ可視性支援

図９は、器官の仮想３次元体積表現においてカメラモデルによって見られる仮想画像を表示する実時間可視性技術を説明する。図９は、図１におけるステップ１０９に対応する変更されたＺバッファを使用する表示技術を示す。前記カメラモデルからあるいは見ることができるボクセルの数は、非常に多い。計算し、視覚化しなければならない要素（またはポリゴン）の合計数を、前記走査された環境におけるボクセルの全体の組から減らさなければ、計算の全体数は、大きな内部領域に関して、前記視覚化表示プロセスを非常に遅くする。しかしながら、本発明において、前記結腸表面において可視であるこれらの画像のみを、表示に関して計算する必要がある。前記走査された環境を、より小さい区分またはセルに再分することができる。次に、前記Ｚバッファ技術は、前記カメラから可視であるセルの部分のみをレンダする。前記Ｚバッファ技術を、３次元ボクセル表示にも使用する。変更されたＺバッファの使用は、計算すべき可視ボクセルの数を減らし、医師または医療技術者による前記仮想結腸の実時間調査を可能にする。

【００４０】

前記中心線をステップ１０７において計算した興味ある領域を、前記表示技術を用いる前に再分する。セルは、可視性単位になるボクセルの集合的グループである。各セルは、他のセルを見ることができる多数の門を含む。前記結腸を、前記選択された開始点において開始し、中心線１００１に沿って前記終了点に向かって移動することによって再分する。次に、前記結腸を、前記中心経路に沿った予め規定されたしきい値距離に達した場合、セル（例えば、図１０におけるセル１００３、１００５および１００７）に分割する。前記しきい値距離は、前記視覚化技術を行うプラットフォームの特性と、その格納及び処理容量とに基づく。前記セルサイズは、前記プラットフォームによって格納し、処理することができるボクセル数に直接関係する。大きく変化させることができるが、しきい値距離の一例は５ｃｍである。各々のセルは、図１０に示すようなセルの外側を見る門として２つの断面を有する。

【００４１】

図９におけるステップ９０１は、前記カメラを現在含む選択された器官内のセルを識別する。この現在セルを、前記カメラの方向を与える可視であるすべての他のセルと同様に表示する。ステップ９０３は、以下にさらに詳細に説明するように、（規定された門を経て）前記カメラから可能的に可視であるセルの階層データのスタブツリー（ツリー図）を構成する。前記スタブツリーは、前記カメラに可視であるかもしれないすべてのセルに関するノードを含む。１つ以上のセルは単一方向において可視であるため、前記セルのいくつかは、妨害する物体がなにもなければ、透明であるかも知れない。ステップ９０５は、隣接するセルエッジの交点を含むセルからのボクセルのサブセットを格納し、どのセルが可視であるかをより効率的に決定するために、これらを前記スタブツリーの外部エッジにおいて格納する。

【００４２】

ステップ９０７は、ループノードが前記スタブツリーにおいて存在するかどうかをチェックする。ループノードは、単一セルの２つ以上のエッジが同じ近くのセルに接する場合、生じる。これは、単一セルが他のセルによって囲まれている場合、生じるかもしれない。ループノードが前記スタブツリーにおいて識別された場合、前記方法はステップ９０９に続く。ループノードがない場合、前記プロセスはステップ９１１に進む。

【００４３】

ステップ９０９は、前記ループノードを形成する２つのセルを１つの大きいノードに合体させる。次に、前記スタブツリーを適宜修正する。これは、ループノードのため、同じセルを２回見るという問題を除去する。このステップを、すべての識別されたループノード

において行う。次に、前記プロセスはステップ９１１に続く。

【００４４】

次に、ステップ９１１は、前記Ｚバッファを最も大きいＺ値で開始する。このＺ値は、前記スケルトン経路に沿って前記カメラからの距離を規定する。次に、前記ツリーを横切り、各ノードにおける交点値を最初にチェックする。ノード交点が覆われている場合、現在の門シーケンスが閉じることを意味し（前記Ｚバッファテストによって決定される）、前記ツリーの現在のブランチの横断を停止する。ステップ９１３は、前記ブランチの各々を横断し、前記ノードが覆われていないかどうかをチェックし、覆われていない場合、これらを表示する。

【００４５】

ステップ９１５は、オペレータのスクリーンにおいて表示すべき画像を、ステップ９１３において識別された可視セル内の体積要素から、合成による体積レンダリングのような当該技術分野において既知の種々の技術の１つを使用して構成する。示されるセルは、可能的に可視であると識別されたものだけである。この技術は、実時間表示を達成するために計算を必要とするセルの数を制限し、相応して、よりよい性能のための表示の速度を増す。この技術は、実際に表示されようとされなかろうとすべての可能な可視データ点を計算する従来技術に対する改良である。

【００４６】

図１１Ａは、ガイド付きナビゲーションによって調査されており、オペレータに表示する必要がある器官の２次元画像表現である。器官１１０１は、２つの側壁１１０２と、経路の中心における物体１１０５とを示す。この器官を、４つのセルＡ１１５１、Ｂ１１５３、Ｃ１１５５およびＤ１１５７とに分割した。カメラ１１０３は、セルＤ１１５７の方に面しており、コーン状視野を認めることができる視野ベクトル１１０７、１１０８によって規定される視野を有する。可能的に見ることができるセルは、セルＢ１１５３、Ｃ１１５５およびＤ１１５７である。セルＣ１１５５は、セルＢによって完全に取り囲まれ、したがって、ノードループを構成する。

【００４７】

図１１Ｂは、図１１Ａにおけるセルから構成されたスタブツリーの表現である。前記カメラを含むノードＡ１１０９は、前記ツリーのルートにある。妨害されない可視の経路である視線または視野コーンは、ノードＢ１１１０へ引かれる。ノードＢは、ノードＣ１１１２およびノードＤ１１１４の双方への直接可視視線を有し、これらを接続する矢印によって示す。前記見るカメラの方向におけるノードＣ１１１２の視線は、ノードＢ１１１０と結合する。ノードＣ１１１２およびノードＢ１１１０は、したがって、図１１Ｃに示すような１つの大きいノードＢ´１１２２に合体する。

【００４８】

図１１Ｃは、ノードＢ´１１２２（ノードＢおよびノードＣの双方を含む）およびノードＤ１１１４に隣接する前記カメラを含むノードＡ１１０９を示す。ノードＡ、Ｂ´およびＤを、少なくとも部分的にオペレータに対して表示する。

【００４９】

図１２Ａ－１２Ｅは、視線を妨害する物体を含むセルと共に、前記変更されたＺバッファの使用を説明する。物体を、前記仮想結腸の一部におけるある老廃物とすることができる。図１２Ａは、１０のポテンシャルセル、Ａ１２５１、Ｂ１２５３、Ｃ１２５５、Ｄ１２５７、Ｅ１２５９、Ｆ１２６１、Ｇ１２６３、Ｈ１２６５、Ｉ１２６７およびＪ１２６９を有する仮想空間を示す。前記セルのいくつかは、物体を含む。カメラ１２０１がセルＩ１２６７に位置し、視野ベクトル１２０３によって示されるようにセルＦ１２６１の方を向いている場合、スタブツリーを、図９における流れ図によって示す技術によって発生する。図１２Ｂは、図１２Ａにおいて示すような仮想表現に関して示す交点ノードによって発生されたスタブツリーを示す。図１２Ｂは、カメラ１２１０を含むため、前記ツリーのルートノードとしてセルＩ１２６７を示す。セルＦが前記カメラの視線に直接接続するため、（矢印で示すように）ノードＩ１２１１はノードＦ１２１３をさす。ノードＦ１２１

３は、ノードＢ１２１５およびノードＥ１２１９の双方をさす。ノードＢ１２１５は、ノードＡ１２１７をさす。ノードＣ１２０２は、カメラ１２０１による視線から完全に妨げられ、したがって、前記スタブツリーに含まれない。

【００５０】

図１２Ｃは、ノードＩ１２１１をオペレータ用のディスプレイにおいてレンダした後のスタブツリーを示す。ノードＩ１２１１を、すでに表示されたため、前記スタブツリーから除去し、ノードＦ１２１３はルートになる。図１２Ｄは、ノードＦ１２１３をここでレンダし、ノードＩ１２１１を連結することを示す。次に、矢印によって接続された前記ツリーにおける次のノードをチェックし、これらがすでにカバーされたか（すでに処理されたか）を確かめる。この例において、ノードＢ５１５（と、したがって従属するノードＡと）を前記ディスプレイにおいてレンダする必要がないため、セルＩ１２６７において位置するカメラからの交差したノードのすべてがカバーされている。

【００５１】

図１２Ｅは、ノードＥ５１５をチェックし、その交点がカバーされたかどうかを決定することを示す。カバーされているため、図１２Ａ－１２Ｅのこの例においてレンダされたノードは、ノードＩおよびＦだけであり、ノードＡ、ＢおよびＥは不可視であり、これらのセルが表示される準備ができている必要はない。

【００５２】

図９に示す変更されたＺバッファ技術は、より少ない計算を可能にし、ボクセル、またはポリゴンのような他のデータ要素によって表された物体に用いることができる。

【００５３】

図１３は、その壁の一方に沿って大きいポリープが存在する結腸の２次元仮想ビューを示す。図１３は、さらに調査すべき患者の結腸の選択された区分を示す。このビューは、２つの結腸壁１３０１および１３０３を、１３０５として示す腫瘍と共に示す。層１３０７、１３０９および１３１１は、前記腫瘍の内部層を示す。医師が前記ポリープまたは腫瘍の層を剥がし、任意の癌または他の有害な要素に関して固まりの内部を見ることができることが望ましい。このプロセスは、実際には、前記固まりへ実際に切断することなしに、前記固まりの仮想生体組織検査を行う。前記結腸をボクセルによって仮想的に表現したら、物体の層を剥ぎ取るプロセスは、図４ないし８と共に説明したように、容易に行われる。特定の断面を調査できるように、前記固まりをスライスすることもできる。加えて、ユーザが規定したスライス１３１９を、前記腫瘍において任意の方法で形成することができる。ボクセル１３１９を、以下に説明するように、剥ぎ取ることができ、変更することもできる。

【００５４】

伝達関数を興味ある領域における各ボクセルに行うことができ、各ボクセルの半透明性を表す係数を変化させることによって、前記物体を透明、半透明または不透明にすることができる。不透明度係数を、各ボクセルにその密度に基づいて割り当てる。次に、マッピング関数は、前記密度値を、その半透明性を表す係数に変換する。高密度走査ボクセルは、壁か、単にオープンスペースの以外の他の密な物質のいずれかを示す。次に、オペレータまたはプログラムルーチンは、ボクセルまたはボクセルのグループの不透明度係数を変化させ、これらが前記サブマリンカメラモデルに対して透明または半透明にすることができる。例えば、オペレータは、腫瘍全体の内部または外部の腫瘍を見ることができる。また、透明ボクセルを形成し、図９の表示ステップに関して存在しないかのようにみせる。前記オブジェクトの区分の合成を、当該区分におけるボクセルの不透明度係数の重み付き平均を使用して形成することができる。

【００５５】

医師が、ポリープの種々の層を見て癌の領域を探すことを望む場合、これを、ポリープの外部の層１３０５を除去し、第１層１３０７を生じることによって行うことができる。加えて、第１内部層１３０７を取り除き、第２内部層１３０９を見ることができる。前記第２内部層を取り除き、第３内部層１３１１等を見ることができる。医師は、ポリープ１３

０５をスライスし、所望の区分内のこれらのボクセルのみを見ることもできる。前記スライスする領域を、完全にユーザが規定することができる。

【００５６】

不透明係数を加えることは、仮想システムの調査を援助する他の方法でも使用されるかもしれない。老廃物が存在し、ある既知の範囲内の他の特性として密度を有する場合、前記老廃物を、調査中その不透明度係数を変更することによって前記仮想カメラに対して透明にすることができる。これは、患者が前記手順の前に腸洗浄剤を摂取することを回避することを可能にし、前記調査をより速くより容易にする。他の物体を、実際の適用に応じて同様に消すことができる。加えて、ポリープのようないくつかの物体を、コントラスト剤とそれに続く適切な伝達関数の使用によって電子的に強調することができる。

【００５７】

図１４は、本明細書において記載の技術を使用して人間の器官のような物体の仮想調査を行うシステムを示す。患者１４０１は、プラットフォーム上で横になり、走査装置１４０５は、調査すべき１つ以上の器官を含む領域を調査する。走査装置１４０５は、前記患者の画像を実際に取得する走査部分１４０３と、エレクトロニクス部分１４０６とを含む。エレクトロニクス部分１４０６は、インタフェース１４０７と、中央処理ユニット１４０９と、走査データを一時的に格納するメモリ１４１１と、データを仮想ナビゲーションプラットフォームに送る第２インタフェース１４１３とを具える。インタフェース１４０７および１４１３を、単一のインタフェース構成要素に含めることができ、または、同じ構成要素とすることができる。部分１４０６における構成要素を、慣例的なコネクタによって共に接続することができる。

【００５８】

システム１４００において、装置１４０３の走査部分から与えられたデータを、処理するために部分１４０５に伝送し、メモリ１４１１に格納する。中央処理ユニット１４０９は、走査された２Ｄデータを３Ｄボクセルデータに変換し、その結果をメモリ１４１１の他の部分に格納する。代わりに、前記変換されたデータを、仮想ナビゲーション端末１４１６に伝送するために直接インタフェースユニット１４１３に送ることもできる。前記２Ｄデータの変換を、インタフェース１４１３から伝送した後に、仮想ナビゲーション端末１４１６において行ってもよい。好適実施形態において、オペレータが前記仮想調査を行うために、前記変換されたデータを、キャリア１４１４によって仮想ナビゲーション端末１４１６に伝送する。前記データを、記憶媒体において格納し、端末１４１６に物理的に伝送するか、衛星伝送を使用することによるような他の慣例的な方法において伝送することもできる。

【００５９】

前記走査されたデータをその３Ｄ表現に、前記視覚化レンダリングエンジンが前記データを３Ｄ形式にすることを要求するまで、変換しなくてもいい。これは、計算ステップとメモリ記憶空間とを節約する。

【００６０】

仮想ナビゲーション端末１４１６は、前記仮想器官または他の走査された画像を見るスクリーンと、エレクトロニクス部分１４１５と、キーボード、マウスまたはスペースボールのようなインタフェース制御１４１９とを含む。エレクトロニクス部分１４１５は、インタフェースポート１４２１と、中央処理ユニット１４２３と、前記端末を動作するのに必要な他の構成要素１４２７と、メモリ１４２５とを具える。端末１４１６における構成要素を、慣例的なコネクタによって一緒に接続する。前記変換されたボクセルデータを、インタフェースポート１４２１によって受け、メモリ１４２５に格納する。次に、中央処理ユニット１４２３は、前記３Ｄボクセルを仮想表現に組み立て、図２および３において説明したようなサブマリンカメラモデルを動作し、前記仮想調査を行う。前記サブマリンカメラが前記仮想器官を通って移動しているとき、図９において説明したような可視化技術を使用し、前記仮想カメラから可視のこれらの領域のみを計算し、これらをスクリーン１４１７において表示する。グラフィックスアクセラレータを、前記表示の発生において使

用することもできる。オペレータは、インタフェース装置１４１９を使用し、前記走査された肉体のどの部分を調査したいかを示すことができる。さらに、インタフェース装置１４１９を使用し、図２およびその伴う記述において考察したように望まれるサブマリンカメラを制御し、動かすことができる。端末部分１４１５を、ニューヨーク州立大学ストーニーブロック校におけるコンピュータ科学部から一般的に利用可能なＣｕｂｅ－４専用システムボックスとすることができる。

【００６１】

走査装置１４０５および端末１４１６、またはこれらの部品を、同じユニットの一部とすることができる。単一のプラットフォームを使用し、前記走査画像データを受け、必要ならこれを３Ｄボクセルに接続し、前記ガイド付きナビゲーションを行う。

【００６２】

システム１４００における重要な特徴は、前記仮想器官を、患者の存在なしに、より後の時間において調査することができることである。加えて、前記仮想調査を、患者を走査している間に行うことができる。前記走査データを、２人以上の医師が前記器官の内部を同時に見ることを可能にする多数の端末に送ることもできる。したがって、ニューヨークにおける医師が、カリフォルニアにおける医師と同時に患者の器官の同じ部分を、このケースを討論しながら見ることができる。代わりに、前記データを、異なった時間において見ることができる。２人以上の医師が、異なったケースにおける同じデータの彼ら自身の調査を行うことができる。多数の仮想ナビゲーション端末を使用し、同じ走査データを見ることができる。前記器官をデータの個別の組を有する仮想器官として再生することによって、精度、コストおよび可能なデータ操作のような領域において多数の利点がある。

【００６３】

さらに、上述した技術を、画像分割動作が続く変更された腸準備動作を用いる改善された電子結腸洗浄技術の使用によって、仮想大腸鏡検査用途において拡張することができ、コンピュータ断層撮影（ＣＴ）または磁気共鳴画像（ＭＲＩ）走査中に前記結腸において残る流体および大便を検出し、前記仮想大腸鏡画像から除去することができる。これらのような技術の使用により、前記結腸の慣例的な物理的洗浄と、これに関係する不便さおよび不快さとは、最小になる、または完全に回避される。

【００６４】

図１５を参照し、電子結腸洗浄の第１ステップは、腸準備（ステップ１５１０）であり、このステップは、ＣＴまたは磁気共鳴画像（ＭＲＩ）走査の前に行い、前記結腸において残る残りの大便および流体が、ガスで満たされた結腸内部および結腸壁の画像特性と重大に異なる画像特性を与える条件を形成することを目的とする。好例の腸準備動作は、前記ＣＴまたはＭＲＩ走査の前日中、ニューヨーク、ウェストバリーのＥ－Ｚ－Ｍ，Ｉｎｃ．によって製造されるような２．１％Ｗ／Ｖの硫酸バリウム懸濁液の２５０ｃｃ３回の服用することを含む。前記３回の服用は、１日の間で分散させるべきであり、各々、３回の食事と共に摂ることができる。前記硫酸バリウムは、前記結腸内に残るどのような大便の画像も強調するように働く。前記硫酸バリウムの摂取に加えて、前記ＣＴまたはＭＲＩ走査前日中、液体の摂取を好適には増加させる。水を摂取させることもできるが、クランベリージュースは、腸の流体を増加させることが知られており、好適である。前記ＣＴ走査の前夜と、前記ＣＴ走査の朝との双方において、セントルイス、ミッソーリのマリンクロットによって製造されるＭＤ－ガストロビューとして商業的に利用可能な６０ｍｌのアミドトリゾ酸メグルミンおよびアミドトリゾ酸ナトリウム溶液を摂り、前記結腸流体の画像特性を強調することができる。リン酸ナトリウムを前記溶液に加え、前記結腸内の大便を液化することができ、これは、前記結腸流体および残りの大便のより均一な強調を与える。

【００６５】

上述した好例の予備腸準備動作は、ＣＴスキャン前の１ガロンのゴリテリーの摂取を必要とするかもしれない慣例的な結腸洗浄プロトコルの必要を除去することができる。

【００６６】

前記ＣＴスキャンを行う直前、インディアナポリス、インディアナのエリーリリーアンド

カンパニーによって製造される１ｍｌのグルカゴンの静脈注射を施し、結腸の衰弱を最小にすることができる。次に、前記結腸を、CO_2または空気のような約１０００ｃｃの圧縮ガスを使用して膨張させ、前記ガスを、直腸チューブを経て入れることができる。この時点において、慣例的なＣＴスキャンを行い、前記結腸の領域からデータを取得する（ステップ１５２０）。例えば、データを、５ｍｍ、１．５－２．０：１ピッチのヘリカルモードにおいて動作するＧＥ／ＣＴＩスパイラルモードスキャナを使用して取得することができ、１ｍｍスライスにおいて再生することができ、前記ピッチを、患者の高さに基づいて既知の方法において調節する。１２０ｋＶｐおよび２００－２８０ｍａのルーチンの画像プロトコルを、この動作に使用することができる。前記データを、患者のサイズに応じて３４から４０ｃｍまで変化する視野において５１２×５１２画素のアレイサイズを有する１ｍｍ厚スライス画像として取得し、再生することができる。これらのようなスライスの数は、一般に、前記患者の高さに応じて、３００から４５０までこれらの条件の下で変化する。前記画像データ組を、体積要素またはボクセルに変換する（ステップ１５３０）。

【００６７】

画像分割を、多数の方法において行うことができる。画像分割のある現在の方法において、局所近接技術を使用し、前記画像データのボクセルを、同様の強度値にしたがって分類する。この方法において、取得した画像の各ボクセルを、隣接するボクセルのグループに関して評価する。興味あるボクセルは、中央ボクセルと呼ばれ、関係する強度値を有する。各ボクセルに関する分類指標を、前記中央ボクセルの値をその隣接ボクセルの各々と比較することによって確立する。前記隣接ボクセルが前記中央ボクセルと同じ値を有する場合、前記分類指標の値を増加する。しかしながら、前記隣接ボクセルが前記中央ボクセルと異なった値を有する場合、前記中央ボクセルに関する分類指標を減少する。次に、前記中央ボクセルを、最大の指標値を有するカテゴリに分類し、これは、局所隣接ボクセルの中で最も一様な隣接ボクセルを有する。各々の分類は、特定の強度範囲を示し、この強度範囲は、画像化されている１つ以上の材料形式の表現である。さらに、この方法を、混合確率関数を得られた前記類似性分類に用いることによって拡張することができる。

【００６８】

画像分割の代わりのプロセスを、２つの主な動作、すなわち、低レベル処理と高レベル特徴抽出として行う。低レベル処理中、身体の輪郭の外部の領域を更なる処理から除外し、前記身体輪郭の内部のボクセルを、良好に規定されたク強度特徴のラスに従って大まかに分類する。例えば、腹部領域のＣＴスキャンは、良好に規定された強度分布を示す傾向にあるデータ組を発生する。図１６のグラフは、このような強度分布を、強度しきい値にしたがって分類することができる４つの良好に規定されたピーク、１６０２、１６０４、１６０６、１６０８を有する好例のヒストグラムとして示す。

【００６９】

腹部ＣＴデータ組のボクセルを、強度しきい値にしたがって４つのクラスタに大まかに分類する（ステップ１５４０）。例えば、クラスタ１は、これらの強度が１４０未満のボクセルを含むことができる。このクラスタは、一般に、前記ガスを満たされた結腸内部の最も密度が低い領域に対応する。クラスタ２は、２２００を超える強度値を有するボクセルを含むことができる。これらの強度値は、前記結腸内部の強調された大便および流体と、骨とに対応する。クラスタ３は、約９００から約１０８０の範囲における強度を有するボクセルを含むことができる。この強度範囲は、一般に、おそらく結腸には関係しない、脂肪や筋肉のような柔らかい組織をあらわす。次に、残りのボクセルを共にクラスタ４として分類することができ、これは、前記結腸壁（前記結腸壁の周囲の粘膜および一部の体積混合物を含む）と、肺組織および軟骨に関係すると考えられる。

【００７０】

クラスタ１および３は、前記結腸壁の識別において特に価値がなく、したがって、仮想大腸鏡検査に関する画像分割手順中、実際的な処理を受けない。クラスタ２に関係するボクセルは、前記結腸壁から大便および流体を分離するのに重要であり、前記高レベル特徴抽

出動作中、さらに処理される。低レベル処理を、結腸組織に対応する最も高い可能性を有する第４のクラスタにおいて集中する（ステップ１５５０）。

【００７１】

前記第４クラスタにおける各ボクセルに関して、強度ベクトルを、それ自身およびその周囲のボクセルを使用して発生する。前記強度ベクトルは、所定のボクセルに最も近い隣接ボクセルにおける強度における変化の表示を与える。前記強度ベクトルを確立するのに使用する隣接ボクセルの数は重要ではなく、処理オーバヘッドと精度との間のトレードオフを含む。例えば、簡単なボクセル強度ベクトルを、興味あるボクセルと、３つの相互に直交する軸においてこのボクセルを取り囲む、その前後の隣接ボクセルと、その左右の隣接ボクセルと、その上下の隣接ボクセルとを含む、７ベクトルで確立することができる。図１７は、２５ボクセル強度ベクトルモデルの形態における好例の強度ベクトルを説明する斜視図であり、この強度ベクトルは、選択されたボクセル１７０２と、その第１順、第２順および第３順の隣接ボクセルとを含む。選択されたボクセル１７０２をこのモデルの中心点とし、固定ボクセルと呼ぶ。前記固定ボクセルと同じ平面における１２個の隣接ボクセルを含むボクセルの平面スライスを、固定スライス１７０４と呼ぶ。前記固定スライスに対する隣接平面において、各々５ボクセルを有する２つの最も近いスライス１７０６がある。第１の最も近いスライス１７０６の隣は、各々１つのボクセルを有する２つの第２の最も近いスライス１７０８である。前記第４クラスタにおける各ボクセルに関する強度ベクトルの集合を、局所ベクトル列と呼ぶ。

【００７２】

腹部画像に関するデータ組は、一般に、３００を超えるスライス画像を含み、スライス画像の各々が５１２×５１２ボクセルアレイを有し、各ボクセルが関係する２５のボクセル局所ベクトルを有するため、前記局所ベクトル列において特徴解析を行い（ステップ１５７０）、計算上の負担を減らすことが望ましい。あるこのような特徴解析は、主成分解析（ＰＣＡ）であり、これを前記局所ベクトル列に適用し、特徴ベクトル列の大きさと、クラスタ４のボクセルに関する直交変換行列とを決定することができる。

【００７３】

前記ＣＴ画像強度のヒストグラム（図１６）は、同等の準備および走査パラメータを与えれば、特定のスキャナに関して、患者間でかなり一定になる傾向にある。この観察を信頼し、直交変換行列を確立することができ、この行列は、同じスキャナを同様の条件の下で使用して獲得された訓練データのいくつかの組を使用することによって決定された、予め決定された行列である。このデータから、カールフネン－ロエベ（Ｋ－Ｌ）変換のような変換行列を、既知の方法において発生することができる。前記変換行列を前記局所ベクトル列に用い、特徴ベクトル列を発生することができる。特徴ベクトル空間領域において、ベクトル量子化技術を使用し、前記特徴ベクトル列を分類することができる。

【００７４】

解析的自己適合的アルゴリズムを、前記特徴ベクトルの分類に使用することができる。このアルゴリズムの規定において、$\{X_i \in R^4 : i = 1, 2, 3, \ldots, N\}$を前記特徴ベクトルの列とし、Ｎを特徴ベクトルの数とし、Ｋはクラスの最大数を示し、Ｔを前記データ組に適合するしきい値とする。各クラスに関して、代表的な要素を前記アルゴリズムによって発生する。a_kをクラスｋの代表的な要素とし、n_kをクラスｋにおける特徴ベクトルの数とする。

【００７５】

次に、前記アルゴリズムを以下のように概説することができる。

１．$n_1 = 1$；$a_1 = X_1$；

【外１０】

$\overline{K}$

＝１とおく

２．クラス数［外１０］およびクラスパラメータ（ａｋ，ｎｋ）を得る

（ｉ＝１；ｉ＜Ｎ；ｉ＋＋）と（ｊ＝１；ｊ＜［外１０］；ｊ＋＋）とに関して、
$d_j = dist(X_i, a_j)$を計算し、
$index = ark\ min\ d_j$として、
$(d_{index} < T)^j$または（［外１０］＜Ｋ）ならば、
クラスパラメータを更新する
$a_{index} = (1/(n_{index}+1)) \times (n_{index} \cdot a_{index} + X_i)$
$n_{index} = n_{index} + 1$
$(d_{index} < T)^j$または（［外１０］＜Ｋ）でなければ、
新たなクラスを発生する
【数１５】

$$a_{k+1} = X_i;$$

【数１６】

$$n_{k+1} = 1;$$

［外１０］＝［外１０］＋１
３．各々の特徴ベクトルを、最も近い隣接ルールにしたがって、クラスにラベル付けする
（ｉ＝１；ｉ＜Ｎ；ｉ＋＋）と（ｊ＝１；ｊ＜［外１０］；ｊ＋＋）とに関して、
$d_j = dist(X_i, a_j)$を計算し、
$index = ark\ min\ d_j$
ボクセルｉをクラスインデックスにラベル付けする
【００７６】
このアルゴリズムにおいて、$dist(x, y)$は、ベクトルｘとｙとの間のユークリッド距離であり、$arc\ min\ d_j$は、d_jの最小値を実現する整数である。
【００７７】
上述したアルゴリズムは、パラメータＴおよびＫにのみ依存する。しかしながら、各ボクセルクラスタ内のクラス数に関するＫの値は重要ではなく、Ｋ＝１８のような一定値に設定することができる。しかしながら、ベクトル類似性しきい値であるＴは、分類結果に大きく影響する。Ｔの選択された値が大きすぎる場合、１つのクラスのみが発生する。他方において、Ｔの値が小さすぎる場合、結果として生じるクラスは、望ましくない冗長性を示す。Ｔの値を、前記特徴ベクトル列の最大の構成要素の変化に等しく設定することによって、最大数の別個のクラスが結果として生じる。
【００７８】
前記初期分類処理の結果として、前記選択されたクラスタ内の各ボクセルを１つのクラスに割り当てる（ステップ１５７０）。仮想大腸鏡検査の好例の場合において、クラスタ４内にいくつかのクラスが存在する。したがって、次のタスクは、クラスタ４におけるいくつかのクラスのうちのどれが前記結腸壁に対応するかを決定することである。前記特徴ベクトルの残りの座標は、前記局所隣接ボクセル内の方向強度変化の情報を含む。前記結腸の内部に関する結腸壁ボクセルは、一般に、クラスタ１のガスボクセルの近くにあるため、しきい値間隔を、代表的なＣＴデータ組の代表的な結腸壁強度から選択されたデータ標本によって決定し、結腸壁ボクセル候補を識別することができる。特定のしきい値を、各々の特定の画像プロトコルおよび装置に関して選択する。次に、このしきい値間隔を、（同じ機械から、同じ画像プロトコルを使用して取得された）すべてのＣＴデータ組に用いることができる。前記代表的な要素の第１座標が前記しきい値間隔において位置する場合、対応するクラスを前記結腸壁クラスとみなし、このクラスにおけるすべてのボクセルに結腸壁様ボクセルとラベル付けする。
【００７９】
各々の結腸壁様ボクセルは、コロン壁ボクセルである候補である。結腸壁に属さない３つの可能な結果が存在する。第１の場合は、前記結腸内部の大便／流体に近いボクセルに関係する。第２の場合は、ボクセルが肺組織領域にある場合に生じる。第３の場合は、粘膜

ボクセルを表す。明らかにこのとき、低レベル分類は、ある程度の分類不確実性を伴う。前記低レベル分類不確実性の原因はさまざまである。例えば、２つ以上の材料形式（すなわち、流体および結腸壁）を含むボクセルによる結果として生じる部分的体積効果が、不確実性の第１の場合を導く。不確実性の第２および第３の場合は、前記部分的体積効果と、前記ＣＴ画像が低コントラストなこととの双方による。前記不確実性を除去するために、追加の情報が必要である。したがって、高レベル特徴抽出プロセスを本方法において使用し、前記結腸壁に関するボクセルを他の結腸壁様ボクセルから、前記ＣＴ画像の先験的な解剖知識に基づいてさらに識別する（ステップ１５８０）。

【００８０】

前記高レベル特徴抽出手順の最初のステップを、前記低レベル分類結果から肺組織の領域を除去することとしてもよい。図１８Ａは、肺領域１８０２を明確に説明する好例のスライス画像である。肺領域１８０２は、一般的に、図１８Ｂにおいて説明するような結腸壁様ボクセルによって囲まれた接触する３次元体積として識別可能である。この特性が与えられれば、この技術における第１ステップは、前記腫瘍の領域内で種ボクセルを見つけることである。好適には、前記ＣＴ画像操作を行うオペレータは、画像範囲を設定し、前記ＣＴ走査の最も上部のスライスが結腸ボクセルを含まないようにする。肺の内部が空気で満たされるべきとき、前記種を、前記低レベル分類によって、単に空気ボクセルを選択することによって与える。図１８Ｂの肺領域輪郭が決定されたら、前記肺体積を前記画像スライスから除去することができる（図１８Ｃ）。

【００８１】

高レベル特徴抽出を行うことにおける次のステップを、クラスタ２における強調された大便／流体ボクセルから骨ボクセルを分離することとすることができる。骨組織ボクセル１９０２は、一般に、前記結腸壁から比較的離れており、前記結腸体積の外部に存在する。それと反対に、残りの大便１９０６および流体１９０４は、前記結腸体積内に囲まれる。先験的な解剖知識と、前記低レベル分類プロセスから得られた結腸壁情報とを組み合わせ、大まかな結腸壁体積を発生する。予め決められた数（例えば、３）より多いボクセルユニットによって前記結腸壁から分離され、前記結腸体積の外部のどのベクトルにも、骨とラベル付けし、次に、前記画像から除去する。クラスタ２における残りのボクセルは、前記結腸体積内の大便および液体を表すと仮定することができる（図１９Ａ－Ｃ参照）。

【００８２】

大便１９０６および流体１９０４として識別される前記結腸体積内のボクセルを、前記画像から除去し、きれいな結腸管腔および結腸壁画像を発生することができる。一般に、２種類の大便／流体領域が存在する。一方の領域形式は、前記結腸壁に付着した大便１９０６の残りの領域である。他方の領域形式は、流体１９０４の大きい体積であり、洗面器状の結腸の折りたたみにおいて集まる（図１９Ａ－Ｃ参照）。

【００８３】

付着した残りの大便領域１９０６を、これらは前記低レベル分類プロセス中に発生された大まかな結腸体積の内部にあるため、識別し、除去することができる。前記洗面器状の結腸の折りたたみにおける流体１９０６は、通常、重力の影響により水平面１９０８を有する。前記水平面の上は通常ガス領域であり、このガス領域は前記流体強度に対してきわめて高いコントラストを示す。したがって、前記流体領域の界面を容易に明示することができる。

【００８４】

領域成長戦略を使用し、付着した大便領域１９０６の輪郭を示すことができ、前記結腸壁体積から離れた部分を除去することができる。同様に、流体領域１９０４の輪郭も示すことができる。水平面１９０８を除去した後、前記結腸壁輪郭も除去し、きれいな結腸壁を得る。

【００８５】

前記結腸壁ボクセルから粘膜ボクセルを識別することは困難である。上記３次元処理がいくつかの粘膜ボクセルを除去できたとしても、すべての粘膜ボクセルを除去するのは困難

である。光学大腸鏡検査において、医師は、結腸粘膜を直接検査し、前記粘膜の色および感触に基づいて病変を探す。仮想大腸鏡検査において、前記結腸壁における大部分の粘膜ボクセルを、より多くの情報を保存するために、残すことができる。これは、３次元体積レンダリングに関してきわめて有用であるかもしれない。

【００８６】

前記分割された結腸壁体積から、前記結腸の内部表面、外部表面および壁自体を抽出し、仮想物体として見ることができる。これは、前記結腸の外部壁を内部壁と同様に調査することができるという、慣例的な光学大腸鏡検査に対する独自の利点を提供する。さらに、前記結腸壁および結腸管腔を、前記分割から別々に得ることができる。

【００８７】

前記結腸を、実質上画像化の前に空にするため、一般に遭遇する問題は、前記結腸管腔がある程度までしぼむことである。空気またはCO_2のような圧縮ガスによる前記結腸の膨張は、しぼんだ領域の頻度を減らす。仮想大腸鏡検査を行うことにおいて、前記しぼんだ領域を通じて飛行経路を自動的に保持することが望ましく、前記走査された画像データを使用し、前記しぼんだ領域において前記結腸管腔を少なくとも部分的に再形成することも望ましい。上述した画像分割方法は、前記結腸壁の内部および外部の双方を有効に得るため、この情報を使用し、前記しぼんだ領域を通じて飛行経路の発生を拡張することができる。前記結腸のしぼんだ領域を通じた前記飛行経路の拡張、または、前記結腸のしぼんだ領域の膨張において、第１ステップは、しぼんだ領域を検出することである。前記結腸壁の外側の周囲からの画像データのグレイスケール値は、前記結腸壁それ自体の中や、脂肪、筋肉または他の種類の組織のような他の領域におけるグレイスケール値より劇的により大幅に変化するという前提を使用し、エントロピ解析を使用して、結腸しぼみの領域を検出することができる。

【００８８】

例えば中心線に沿ったグレイスケール値の変化の程度を、エントロピ値によって表し、測定することができる。エントロピ値を計算するために、前記結腸の外側表面におけるボクセルを選択する。これらのような点を、上述した画像分割技術から識別する。５×５×５の立方体ウィンドウを、興味ある画素を中心として前記画素に用いる。前記エントロピ値を計算する前に、前記画像データからノイズをろ過するために、より小さい（３×３×３）ウィンドウを興味ある画素に用いることができる。次に、前記画素について選択されたウィンドウのエントロピ値を、以下の式によって決定することができる。

【数１７】

$$E=\sum_i C(i)\ln(C(i))$$

ここで、Ｅはエントロピ値であり、Ｃ（ｉ）は前記ウィンドウ内のｉ（ｉ＝０，１，２，．．．，２５５）のグレイスケール値を有する点の数である。次に、各々のウィンドウに関して計算されたエントロピ値を、予め決められたしきい値と比較する。空気の領域に関して、前記エントロピ値は、組織の領域と比べると、かなり低くなる。したがって、前記結腸管腔の中心線に沿って、前記エントロピ値が増加し、予め決められたしきい値を超える場合、しぼんだ領域を示す。前記しきい値の正確な値は重要ではなく、画像プロトコルと、画像装置の詳細とに部分的に依存する。

【００８９】

しぼんだ領域が検出されたら、前もって決定された中心線飛行経路を、１ボクセル幅ナビゲーションラインでしぼみの中心を貫通させることによって前記領域を通じて拡張することができる。

【００９０】

前記仮想カメラの飛行経路を前記結腸管腔を通じて自動的に延長することに加えて、前記結腸しぼみの領域を、物理的モデル化技術を使用して仮想的に広げ、前記しぼんだ領域の特性のうちいくつかを回復させることができる。この技術において、前記結腸壁の物理的

特性のモデルを開発する。このモデルに関して、運動パラメータ、質量密度、ダンピング密度、引張係数、および曲げ係数を、ラグランジュ方程式に関して推定する。次に、拡張力モデル（すなわち、前記結腸中に注入された空気のようなガスまたは流体）を、前記ラグランジュ方程式によって規定されるような前記結腸の弾性特性に従って式化し、適用し、前記結腸画像のしぼんだ領域をその自然な形状に復元するようにする。

【００９１】

前記結腸をモデル化するために、有限要素モデルを、前記結腸管腔のしぼんでふさがれた領域に用いる。これを、８ボクセルレンガのような一定のグリッドにおいて前記要素を標本化し、次に、慣例的な体積レンダリング技術を用いることによって行うことができる。代わりに、四面体のような不規則体積表現アプローチを前記しぼんだ領域に用いることができる。

【００９２】

外力（空気注入）モデルを前記結腸モデルに用いることにおいて、前記外力の大きさを最初に決定し、前記しぼんだ結腸壁領域を適切に分離する。三次元成長モデルを使用し、結腸内壁表面および結腸外壁表面を並列にトレースすることができる。個々の表面を、前記しぼんだ領域における開始点から成長源点までマークし、前記外力モデルを用い、前記表面を同様かつ自然なように膨張させる。前記内部表面および外部表面の間の領域、すなわち、結腸壁を、共有領域として分類する。外部斥力モデルをこれらの共有領域に用い、前記しぼんだ結腸壁部分を自然なように分離し、膨張させる。

【００９３】

仮想調査を受ける結腸のような仮想物体の特徴をより明瞭に視覚化するために、前記物体の種々のテクスチャのレンダリングを与えることが有利である。光学大腸鏡検査中に与えられるカラー画像において観察することができるこれらのようなテクスチャは、ＣＴ画像データによって与えられる白黒、グレイスケール画像においてしばしば失われる。したがって、仮想調査中にテクスチャ画像化するシステムおよび方法が要求される。

【００９４】

図２０は、テクスチャ成分を有する仮想画像を発生する本方法を示すフローチャートである。本方法の目的は、例えばビジブルヒューマンからの赤－緑－青（ＲＧＢ）における光学大腸鏡検査画像によって得られたテクスチャを、仮想物体を発生するのに使用されるグレイスケールモノクロームＣＴ画像データ上にマッピングすることである。前記光学大腸鏡検査画像を、ビデオカメラのようなカメラからアナログ光学画像を受け、前記画像を、インタフェースポート１４３１（図１４）を経てＣＰＵ１４２３に供給することができるディジタルデータに変換するディジタル「フレームグラバー」１４２９によるような、慣例的なディジタル画像取得技術によって取得する。このプロセスにおける第１ステップは、前記ＣＴ画像データを分割することである（ステップ２０１０）。上述した画像分割技術を用い、前記グレイスケール画像における強度しきい値を選択し、前記ＣＴ画像データを、骨、結腸壁組織、空気等のような種々の組織形式に分類することができる。

【００９５】

前記ＣＴ画像データにおける画像分割を行うことに加えて、前記光学画像のテクスチャ特徴を、前記光学画像データから抽出することが必要である（ステップ２０２０）。これを行うために、ガウシアンフィルタを前記光学画像データに用いることができ、続いて、前記データをサブ標本化し、多解像度ピラミッドに分解する。ラプラシアンフィルタおよび可変フィルタを前記多解像度ピラミッドに用い、前記データの指向特徴および非指向特徴を得ることもできる。この方法は、前記テクスチャ特徴を抽出し、獲得することにおいて効率的であるが、このアプローチの実施は、大量のメモリおよび処理パワーを必要とする。

【００９６】

前記テクスチャ特徴を前記光学画像から抽出する代わりのアプローチは、ウェーブレット変換を使用することである。しかしながら、ウェーブレット変換は、一般に計算上効率的であるが、慣例的なウェーブレット変換は、軸に平行な方向を持つ特徴のみを獲得するこ

とに制限され、興味ある領域に直接用いることができない。これらの制限を克服するために、分離不可フィルタを用いることができる。例えば、リフティングスキームを用い、２つのステップ、予測および更新アプローチを使用して、任意の次元におけるウェーブレット変換に関するフィルタバンクを構成することができる。これらのようなフィルタバンクを、多次元多項式補間に関するブーアロム（Ｂｏｏｒ－Ｒｏｍ）アルゴリズムによって合成することができる。

【００９７】

前記テクスチャ特徴を前記光学画像データから抽出した後、モデルを発生し、これらの特徴を描かなくてはならない（ステップ２０３０）。これを、例えば、自然のテクスチャに起因する非ガウス分布のエントロピを推定し、操作することを基礎とする非パラメトリック多スケール統計モデルを使用することによって行うことができる。

【００９８】

テクスチャモデルを前記光学画像データから発生したら、テクスチャマッチングを行い、これらのモデルを前記分割されたＣＴ画像データに関連させなければならない（ステップ２０４０）。前記テクスチャが連続的な前記ＣＴ画像データの領域において、対応するテクスチャのクラスは容易に調和する。しかしながら、２つ以上のテクスチャ領域の間の境界領域において、前記プロセスはより複雑になる。境界領域の周囲の前記ＣＴ画像の分割は、しばしば、ぼけたデータを生じ、すなわち、各々の材料または組織からのテクスチャの割合を反映すると共に各々の種々の重み付けに応じて変化する結果を生じる。前記重みの割合を使用し、マッチング基準の重要性を設定することができる。

【００９９】

前記非パラメトリック多スケール統計モデルの場合において、クロスエントロピまたはカルバックライブラー発散アルゴリズムを使用し、境界領域における異なったテクスチャの分布を測定することができる。

【０１００】

テクスチャマッチング後、テクスチャ合成を前記ＣＴ画像データにおいて行う（ステップ２０５０）。これを、前記光学画像データからのテクスチャを前記ＣＴ画像データに融合させることによって行う。骨によって与えられるような等方性「テクスチャパターンに関して、前記テクスチャを前記光学データから前記ＣＴ画像データへ直接標本化することができる。結腸粘膜のような異方性テクスチャ領域に関して、多解像度標本化手順が好ましい。このプロセスにおいて、均質領域および不均質領域に関する選択性再標本化を用いる。

【０１０１】

代わりに、擬似カラーテクスチャを、前記ＣＴデータから直接形成することができる。各ボクセルに関し、局所領域隣接部を具える多数のＣＴ値を評価し、所定のボクセルに関する擬似カラーを決定することができる。例えば、５×５×５ボクセル立方体状領域、または、マンハッタン距離によって測定された３ユニット内のすべてのボクセルを表す二重ピラミッド。次に、このスカラ値のベクトルを評価し、その後の体積レンダリング中にこのボクセルに関して表示すべきカラーにマッピングする。前記値の局所隣接部ベクトルの評価は、これらのようなことを、局所曲率、均質性／不均質性、または他の幾何学的または空間的関数として計算することができる。

【０１０２】

体積レンダリング

上述した画像分割およびテクスチャマッピングに加えて、体積レンダリング技術を仮想大腸鏡検査手順と組み合わせて使用し、結果として生じる画像の忠実度をさらに増す。図２１は、本発明による体積レンダリングに使用することができるパースペクティブ体積光線投射法を説明する。前記結腸管腔内の選択された仮想始点、例えばカメラ位置から、光線を、近似画像画素の各々を経て投影する（ステップ２１００）。各々の光線に関して、第１標本化点を、前記光線に沿った現在画像画素として設定する（ステップ２１１０）。次に、前記現在標本化点と最も近い結腸壁との間の距離（ｄ）を決定する（ステップ２１２

０）。源ｚ内距離（ｄ）を、予め決められた標本化間隔（ｉ）と比較する（ステップ２１３０）。距離（ｄ）が標本化間隔（ｉ）より大きい場合、標本化を行わず、前記光線に沿った次の標本化点を、前記光線に沿って距離ｄジャンプすることによって決定する（ステップ２１４０）。前記距離が標本化間隔（ｉ）以下である場合、慣例的な標本化をこの点において行い（ステップ２１５０）、次の標本化点を標本化間隔（ｉ）にしたがって選択する（ステップ２１６０）。例えば、８個の隣接するボクセルの密度値の間のトリリニア補間を行い、前記標本化点における新たな密度値を決定することができる。

【０１０３】

図２１の方法は、空間跳躍技術を使用し、前記画像面の光線に沿って空の空間を越えて前記結腸壁まで迅速にスキップするため、効率的に光線投影を加速させる。この方法において、標本点から最も近い結腸壁までの距離を、各々の光線に沿って決定する。前記距離が予め決められた間隔（ｉ）より大きい場合、前記光線に沿って次の標本化点までのジャンプを行う。前記最も近い距離情報は、仮想カメラ制御に使用される前記ポテンシャル場からすでに利用可能であるため、追加の距離符号化計算は必要ない。この場合において、表面レンダリングもＺバッファ計算も必要なく、結果として、予備的処理時間およびメモリ空間が節約される。

【０１０４】

代わりに、空間跳躍法は、各々の光線に関する距離情報を、対応する表面レンダリング画像のＺバッファから得ることができる。前記表面レンダリング画像および体積レンダリング画像の双方を発生する場合、このアプローチは、前記Ｚバッファ情報を前記表面レンダリングの結果として与えるため、最小の処理オーバヘッド負担を与える。したがって、この形式の空間跳躍方法は、前記画像空間領域から世界空間領域への深さ変換を行う追加の処理のみを必要とする。

【０１０５】

距離（ｄ）をステップ２１４０において横切った前記光線に沿ったこれらの領域に関して、前記光線に沿った領域は、オープンスペースであり、オープンスペース伝達関数に従って値に割り当てることができる。代表的に、オープンスペースは、最終画素値において寄与しない。標本化を行う各々の点に関して、１つ以上の規定された伝達関数を割り当て、元の体積データの異なった範囲の標本値を、異なった色および不透明度と、あるいは他の表示化のパラメータとにマッピングする。例えば、４つの独立した伝達関数を使用し、ＣＴ密度値の範囲を、赤、緑、青の指定された色と、不透明度とに、各々０から２５５の範囲においてマッピングすることによって、異なった材料を決定した。

【０１０６】

仮想生体組織検査

上述した技術は、柔軟かつ非侵入的生体組織検査を実行するために調査されている領域の仮想電子生体組織検査を行うシステムの基礎を形成することもできる。上記で注意したように、体積レンダリング技術は、１つ以上の規定された伝達関数を使用し、元の体積データの異なった範囲の標本値を、異なった色、不透明度、および、ナビゲーションおよび見ることに関する他の表示可能パラメータにマッピングする。ナビゲーション中、選択された伝達関数は、一般に、最大不透明度を前記結腸壁に割り当て、外側表面が容易に見られるようにする。疑わしい領域を仮想調査中に検出したら、医師は、体積レンダリング手順中に割り当てられた伝達関数をインタラクティブに変更し、結果として、見られている外側表面が実質上透明になり、前記領域の情報が合成され、したがって、前記領域の内部構造が見られるようにする。多数の予め決定された伝達関数を使用し、前記疑わしい領域を、前記プロセスを通じて割り当てられた不透明度を変化させることによって、多数の異なった深さにおいて見ることができる。

【０１０７】

ポリープ検出

本システムおよび方法を使用し、自動化されたポリープ検出を行うことができる。図１３の参照と共に、例えば前記結腸内に生じるポリープ１３０５は、一般に、結腸壁１３０１

から延在する小さな凸面の丘のような構造の形態をとる。このジオメトリは、前記結腸壁の折りたたみと異なる。したがって、異なったジオメトリモデルを使用し、前記結腸壁におけるこれらのようなポリープを検出することができる。

【０１０８】

前記結腸管腔の表面を、Ｃ－２平滑表面モデルを使用するように、３次元ユークリッド空間における連続的な第２の区別可能な表面として表すことができる。このようなモデルは、その全体の参照によってここに含まれる、１９９４年、スプリンガー－バーラグ（Ｓｐｒｉｎｇｅｒ－Ｖｅｒｌａｇ）によって出版された、Ｂ．Ａ．デュブロビン（Ｄｕｂｒｏｖｉｎ）による「現代のジオメトリ方法および用途」に記載されている。このモデルにおいて、前記結腸の表面における各ボクセルは、ガウス曲率フィールドと呼ばれるガウス曲率を有する関連する幾何学的特長を有する。ポリープを示すかもしれない前記表面における凸面の丘は、前記ガウス曲率フィールドにおいてユニークな局部特徴を備える。したがって、前記ガウス曲率フィールドを特定の局部特徴に関して探索することによって、ポリープを検出することができる。検出されたら、疑わしいポリープを強調し、したがって、医師の注意を引かせることができ、医師は前記疑わしいポリープを測定し、上述した仮想生体組織検査方法を使用し、前記疑わしい領域をさらに調査することができる。

【０１０９】

中心飛行経路発生

仮想大腸鏡検査の場合において、前記結腸管腔を通る適切なナビゲーションライン、または、飛行経路は、上述したシステムおよび方法の重要な特徴である。前記仮想カメラモデルの飛行経路を決定するいくつかの技術を、図４－８に関して考察したが、図２２は、前記結腸管腔を通る中心飛行経路を発生する代わりの方法を示す。前記結腸壁を識別した後、上述した画像分割方法等によって、体積減少アルゴリズムを用い、前記結腸管腔の方向を強調し、前記結腸体積内のその後の探索時間を減少することができる（ステップ２３１０）。

【０１１０】

図２３は、多解像度解析モデルに基づく好例の体積減少アルゴリズムのステップをさらに示す。この手順において、前記３次元体積を、同じ行列サイズを有するバイナリ画像のスタックによってあらわす（ステップ２３１０）。集合的に、これらの画像はバイナリデータ組を形成する。離散的ウェーブレット変換を前記バイナリデータ組に用いることができ、これは、前記バイナリデータ組の異なった時間－周波数成分を表す多数のサブデータ組を生じる。例えば、離散的ウェーブレット変換は、８つのサブデータ組を生じるかもしれない。前記サブデータ組を、予め決められたしきい値と比較し、最も低い周波数成分を識別する（ステップ２３３０）。この成分は、多解像度構造において再帰的に用いるその後の離散的ウェーブレット変換およびしきい値処理ステップに関するバイナリデータ組を形成する（ステップ２３４０）。仮想大腸鏡検査の場合において、離散的ウェーブレット変換および関連するしきい値処理を、前記最も低い周波数成分を表すその後のサブデータ組において３回再帰的に用いる（３レベル多解像度分解）。

【０１１１】

図２２に戻って、前記減少した結腸体積モデルから、距離マップ技術を用い、前記結腸の２つの端の間、例えば、直腸から盲腸までの最短距離経路を発生することができる（ステップ２２１５）。この結果として生じる経路は、前記結腸管腔の全体的な方向情報を維持するが、局所的折りたたみによって示される方向を無視する。次に、全体的な結腸内における制御点を、前記最短距離経路を元のデータ空間にマッピングし戻すことによって得ることができる（ステップ２２２０）。例えば、３レベル多解像度分解の場合において、減少した体積は、元の体積の３分の１であり、既知のアフィン変換を使用し、前記減少した体積モデルを正確に原スケールモデルにマッピングし戻すことができる。前記減少した体積の最短距離経路を、前記原スケール体積中に点の列としてマッピングし戻すこともでき、これらの点を前記結腸内の制御点として使用することができる。

【０１１２】

好適な飛行経路は、前記結腸管腔の中心線上におけるものである。しかしながら、初期制御点は、前記結腸管腔の中心において正確に位置しないかもしれない。したがって、前記初期制御点を、２等分面アルゴリズムの使用等によって、中心におく（ステップ２２３０）。例えば、各々の選択された制御点において、２等分面を、前記方向に対して垂直で前記結腸管腔を横切って切断する面として規定することができる。次に、最大ディスクアルゴリズムのような中心化アルゴリズムを各々の２等分面において行うことができる。このようなアルゴリズムは、参照によってここに含まれる、１９９６年、ＰＡＭＩのＩＥＥＥ会報、Ｖｏｌ．１８、１０５５－１０６６ページ、ゲ（Ｇｅ）他による論説「別々のユークリッド距離マップからのスケルトンの発生における」において考察されている。

【０１１３】

前記制御点を中心化したら、前記飛行経路を、これらの点を接続する線を補間することによって決定することができる（ステップ２２４０）。仮想大腸鏡検査の場合において、前記補間された飛行経路は、前記結腸管腔内においてほぼ中心にある滑らかな曲線の形状をとることが望ましい。１９９２年、ケンブリッジ大学出版、プレス他による「Ｃにおける数値レシピ：科学計算の技術」において記載のように、微分幾何学理論におけるセレーフルネ定理に基づく限定されたキュービックＢスプライン補間アルゴリズムを使用し、好適な滑らかにカーブする飛行経路を確立することができる。

【０１１４】

図２４における分割された結腸管腔の絵的表現と、図２５のフローチャートとは、本発明による依然として他の代わりの飛行経路発生方法を説明する。この代わりの方法において、結腸管腔２４００の表現を、最初に、管腔２４００の長さに沿って多数のセグメント２４０２に分割する（ステップ２５００）。各々のセグメント２４０２内から、代表的な点２４０４ａ－ｇを選択する（ステップ２５２０）。次に、各々の代表的な点２４０４ａ－ｇを、個々のセグメントの中心にこれらの点を押すのに使用される物理ベース変形モデルの使用等によって、前記結腸壁に関して中心にする（ステップ２５３０）。前記代表的な点を中心にした後、前記点を順次結合し、前記仮想カメラモデルに関する中心線飛行経路を確立する（ステップ２５４０）。前記セグメントが長さにおいて十分に小さい場合、前記中心化した点を、直線セグメント２４０６ａ－ｆで接続することができる。しかしながら、リニアカーブフィッティング技術を用い、前記中心化した点を結合する場合、より滑らかで連続的な飛行経路が確立される。

【０１１５】

上述した方法の各々を、図１４に示すようなシステムを使用し、適切なソフトウェアを与え、ＣＰＵ１４０９およびＣＰＵ１４２３の動作を制御することによって実現することができる。

【０１１６】

パーソナルコンピュータにおける配備に好適な代わりのハードウェア実施形態を図２６に示す。本システムは、４００ＭＨｚを超えるクロック速度において動作するペンティアム（登録商標）ＩＩＩプロセッサのような高速マルチタスクプロセッサの形態をとるべきプロセッサ２６００を含む。プロセッサ２６００を、高速並列データ伝送を与える慣例的なバス構造２６２０に結合する。バス構造２６２０には、メインメモリ２６３０と、グラフィックスボード２６４０と、体積レンダリングボード２６５０も接続する。グラフィックスボード２６４０を、好適には、ダイアモンドマルチメディアシステムズによって製造されるダイアモンドバイパーｖ７７０ウルトラのような、テクスチャマッピングを行うことができるものとする。堆積レンダリングボード２６５０は、参照によってここに含まれる米国特許第５７６０７８１号および第５８４７７１１号に基づく、ミツビシエレクトリックによるボリュームプロボードの形態をとることができる。慣例的なＳＶＧＡまたはＲＧＢモニタのような表示装置２６４５を、前記画像データを表示するグラフィックスボード２６４０に効率的に結合する。ＭＲＩまたはＣＴスキャナのようなイメージングスキャナからデータを受け、このようなデータをバス構造２６２０に伝送するスキャナインタフェースボード２６６０も設ける。スキャナインタフェースボード２６６０は、選択されたイ

メージングスキャナに関する用途特定インタフェース製品であってもよく、または、一般的な目的の入力／出力カードの形態をとることもできる。ＰＣベースシステム２６００は、一般に、キーボード、ディジタルポインタ（例えば、マウス）等のようなＩ／Ｏ装置２６８０をプロセッサ２６２０に結合するＩ／Ｏインタフェース２６７０を含む。代わりに、前記Ｉ／Ｏインタフェースを、プロセッサ２６２０にバス２６２０を介して結合することができる。

【０１１７】

３次元画像化の場合において、テクスチャ合成、体積レンダリング、多数のデータ処理および処理動作を含むことが必要である。前記結腸管腔およびその周囲の領域によって表されるもののような大きいデータセットに関して、このような処理は、きわめて時間を消費し、メモリが増大するかもしれない。しかしながら、図２７のフローチャートにおいて説明した処理方法にしたがって図２６のトポロジーを使用することによって、これらのような動作を、比較的低コストのパーソナルコンピュータ（ＰＣ）において行うことができる。画像化データを、スキャナインタフェースボード２６６０およびバス構造２６２０を介してプロセッサ２６２０から受け、メインメモリ２６３０に格納する。この画像データ（画素）を体積要素（ボクセル）表現に変換する（ステップ２７１０）。メインメモリ２６３０に格納された前記体積表現を、例えば、主要な体積軸に沿うようなスライス、または、画像化されている領域の他の部分に分割する（ステップ２７２０）。前記体積分割を、次に、前記体積レンダリングボードに伝送し、体積レンダリング動作に関する体積レンダリングメモリ２６５５に一時的に格納する（ステップ２７３０）。局所的に存在する体積レンダリングメモリ２６５５の使用は、全体の体積の各々のスライスのレンダリング中、バス２６２０を越えてデータを交換する必要がないため、体積レンダリングにおける速度を上昇させる。体積レンダリングが前記スライスに関して完了したら、前記レンダリングされたデータを、シーケンシャルバッファにおいてメインメモリ２６３０またはグラフィックスボード２６４０に伝送し戻す（ステップ２７４０）。興味あるすべてのスライスをレンダリングした後、前記シーケンシャルバッファにおける内容を、表示ユニット２６４５における表示に関してグラフィックスボード２６４０によって処理する（ステップ２７５０）。

【０１１８】

多走査ベース仮想調査

上記で考察した技術は、一般に、単一の磁気共鳴画像（ＭＲＩ）またはコンピュータ断層撮影（ＣＴ）走査から取得したデータセットに基づいて仮想画像化を行う。しかしながら、上記で考察した技術は、ある領域の多数の走査を使用してある領域の仮想調査を行うのにも有用である。ある領域の多数の走査を使用することによって、異常な領域の改善された画像化を達成することができ、モーションアーティファクトを減少することができる。ある興味深いこのような用途は、仮想大腸鏡検査を行い、あり得る膀胱のポリープまたは癌に関して患者を選別することにある。

【０１１９】

図２８は、多数のＭＲＩ走査を行い、仮想大腸鏡検査のようなある物体の仮想調査を行う方法を説明するフローチャートである。ＣＴ画像と異なり、膀胱壁を尿と識別することが困難であるかもしれない場合、ＭＲＩ画像において、尿を自然なコントラスト剤として使用し、前記膀胱内壁の輪郭を描くことができる。この目的のため、前画像走査プロトコルを用いる（ステップ２８０５）。４回のＭＲＩ走査の第１のものの約１／２時間前、患者に膀胱を空にし、次に１カップの水を飲むように要求する。約１／２時間後、患者に前記膀胱領域の４回の走査のうちの第１回目を行う（ステップ２８１０）。前記膀胱がいっぱいで膨らんだ第１走査は、Ｔ１重み付き横画像化に関するプロトコルに従う。例えば、上記で参照したピッカー（Ｐｉｃｋｅｒ）スキャナを使用する場合、２５６×２５６行列サイズ、３８ｃｍ視野（ＦＯＶ）、１．５ｍｍスライス厚（隙間なし）、３ミリ秒ＴＥ、９ミリ秒ＴＲ、３０度フリップ角、および、１走査平均を使用するクジェルファスター（ＫＪＥＬＬ　ＦＡＳＴＥＲ）プロトコルを使用することができる。もちろん、これらのパラ

メータはスキャナ特定になる傾向にあり、前記パラメータにおける種々の変更を、許容しうる結果に関して使用することができる。

【０１２０】

前記膀胱がいっぱいのままで、前記患者に第２ＭＲＩ走査、走査２を行う（ステップ２８１５）。前記第２走査は、２５６×２５６行列サイズ、３８ｃｍ視野（ＦＯＶ）、１．５ｍｍスライス厚（隙間なし）、３ミリ秒ＴＥ、９ミリ秒ＴＲ、３０度フリップ角、および、２走査平均を使用するピッカークジェルファスター（Ｐｉｃｋｅｒ　ＫＪＥＬＬ　ＦＡＳＴＥＲ）プロトコルのような、Ｔ１重み付き冠状画像化に関するプロトコルに従う。

【０１２１】

上述した２回の画像走査を、互いに直交する軸に沿って行う。この利点は、一方の走査における重大なモーションアーティファクトの領域が、一般に、直交する走査における最小のモーションアーティファクトの領域に対応することである。したがって、第１走査を横方向に、第２走査を冠状方向にとることによって、前記画像走査を登録することができ、前記データセットにおけるモーションアーティファクトを識別し、補償することができる。

【０１２２】

走査２の後、前記患者に、前記膀胱を開放するように頼み、次に、２回の追加のＭＲＩ走査を行う。第３走査（ステップ２８２０）は、前記第１走査（横画像化）と同じ画像化プロトコルに従う。第４走査（ステップ２８２５）は、前記第２走査（冠状画像化）と同じ画像化プロトコルに従う。

【０１２３】

前記画像走査を、ピッカー１．５Ｔエッジ全身スキャナを使用して取得することができる。Ｔ２画像化プロトコルを使用することもできるが、Ｔ１画像化プロトコルは、脂肪と尿との間の改善された輪郭描写を与え、より短い取得期間しか必要としないため、Ｔ１画像化プロトコルが仮想大腸鏡検査に好適である。代わりに、前記画像操作は、それらの画像化技術に好適なコントラスト剤およびプロトコルを使用するコンピュータ断層撮影または超音波画像走査の形式をとってもよい。

【０１２４】

前記最初の２回の走査（走査１および２）の間、前記膀胱は膨張し、前記膨張壁は比較的薄い。この場合において、腫瘍のような生理学上変化した場所は、変化しない膀胱壁と比べて異なった率において薄くなるかもしれず、これらの状況の下でより明らかになるかもしれない。前記第３および第４走査中、前記膀胱は実質的に空であり、前記膀胱壁はより厚い。より厚い壁により、前記膀胱壁の通常の組織と生理学上変化した組織との間に、より明白な画像コントラストが結果として生じるかもしれない。

【０１２５】

前記４回の走査を取得した後、４つの対応するデータセットを別々に処理する。最初に、図１５と組み合わせるように上述したように（ステップ２８３０）、各々のデータセットを、好適には、画像分割する。画像分割中、前記４つのデータセットのボクセルを、膀胱壁、尿、脂肪、境界等の多数のカテゴリに分類する。前記分類は、前記ボクセルの局所強度ベクトルに基づく。前記ボクセルを分類したら、前記膀胱管腔の内部を、空気ボクセルまたは尿ボクセルを選択することによるような、前記膀胱体積内から選択された種ボクセルで開始する領域成長アルゴリズムを使用して識別することができる。

【０１２６】

前記分割された体積データセットの臨床解析の前に、前記４つのデータセットの共通座標系への登録を行う（ステップ２８３５）。前記膀胱の形状は、走査ごとに変化し、正確なボクセル－ボクセル登録は、実際上の値のものではない。代わりに、柔軟な登録プロセスが好適である。この柔軟な登録プロセスにおいて、興味ある各々の体積（各々の対応する走査に関してレンダリングされた体積）に関して、前記体積の中心を、前記体積におけるすべてのボクセルの３つの座標を平均すること等によって決定する。

【０１２７】

次に、デカルト座標系を構成し、この座標系の原点を前記体積の中心点において位置させる。次に、前記座標系の軸を、多数の方法において方向付けることができる。方向付けの好適な選択は、自然な人間の身体の方向に対応し、例えば、Ｚ軸が前記身体の高さに沿って（例えば、つま先から頭まで）通り、Ｙ軸が後ろから前まで通り、Ｘ軸が横に（例えば、左から右に）通る。この座標系における長さの単位を、１ボクセル長の任意の単位に対して便利に設定することができ、その絶対値は、ＭＲＩ走査に関する取得特性に基づいて変化する。同じ画素間隔をすべての走査において使用し、４つのデータセットのすべてを獲得する限りは、前記４つのデータセットの各々に関して一様な値が結果として生じる。

【０１２８】

登録後、前記４つのデータセットからの画像を、別々にまたは同時に見ることができる（ステップ２８４５）。好例の表示ウィンドウを図２９および３０に示す。図２９を参照し、前記表示を、各々走査１、走査２、走査３および走査４に対応する４つのサブウィンドウ２９０５、２９１０、２９１５、２９２０に分割する。制御パネル選択２９２５を、前記表示のある部分において与え、グラフィカルユーザインタフェース（ＧＵＩ）を確立し、表示およびナビゲーション機能をユーザに与えることもできる。オペレータが前記画像サブウィンドウの１つにおいてビューを拡大するようなナビゲーションをすると、好適には、対応する動作が他のサブウィンドウビューにおいても同様に起こる。ユーザは、単一ウィンドウ表示への拡張に関して前記ビューのうち１つを選択することもできる。

【０１２９】

同時に処理されるデータの量を減らすために、前記データセットを、８つの部分またはオクタント等に分割することができる（ステップ２８４０）。これを、多数の方法において行うことができる。例えば、図２９に示すデカルト座標系への参照と共に、前記データを前記座標系の８つの領域、（１）Ｘ，Ｙ，Ｚ；（２）Ｘ，－Ｙ，Ｚ；（３）Ｘ，Ｙ，－Ｚ；（４）Ｘ，－Ｙ，－Ｚ；（５）－Ｘ，Ｙ，Ｚ；（６）－Ｘ，－Ｙ，Ｚ；（７）－Ｘ，Ｙ，－Ｚ；および（８）－Ｘ，－Ｙ，－Ｚに分割することができる。

【０１３０】

図２９は、前記４回の走査の各々から得られた前記膀胱管腔の外側の４つのビューを示す。図３０は、前記４回の走査の各々から得られた前記膀胱管腔の内側の一部の４つのビューを示す。

【０１３１】

多解像度画像化および仮想喉頭鏡検査

ここで説明したシステムおよび方法を適合させ、用いて、仮想喉頭鏡検査に好適な多解像度画像化を行うことができる。図３１は、仮想喉頭鏡検査を行う方法を説明するフローチャートである。第１に、患者の喉頭の領域の画像走査を取得する（ステップ３１０５）。これを、コンピュータ断層撮影（ＣＴ）または磁気共鳴画像（ＭＲＩ）技術を使用して行うことができる。しかしながら、この領域におけるＣＴ走査は、重大により速い取得時間（ＭＲＩに関する７分に対して３０秒）とより高い解像度（ＭＲＩに関する１ｍｍ立方体ボクセルに対して０．３ｍｍ立方体ボクセル）を与えるため、ＣＴ走査が好適である。ＣＴ走査データを取得するために、ＧＥ／ＣＴＩスパイラル走査ＣＴスキャナを使用することができる。好適な走査プロトコルは、１２０ｋｅＶ、２００ｍａ、５１２×５１２行列サイズ、１５ｃｍ視野および３ｍｍ／２．０：１ピッチである。この走査は、約３０秒において計算され、結果として、０．３ｍｍ厚の３５１の画像スライスを生じ、結果として、０．３ｍｍ立方体ボクセルを生じる。

【０１３２】

画像分割を使用し、ボクセルを多数のカテゴリに分類することができる（ステップ３１１０）。この動作において、変形した自己適合オンラインベクトル量子化（ＳＯＶＱ）アルゴリズムを使用することができる。このような場合において、前記アルゴリズムは、各々のボクセルを３次までの隣接ボクセルに関して解析し、局所密度特徴を決定する。前記取得されたデータセットにおける各ボクセルは、関連する局所密度ボクセルを有する。前記局所密度ベクトルをカールフネン－ロエベ（Ｋ－Ｌ）変換を使用して変換することによっ

て、前記体積画像におけるボクセルに関する特徴ベクトルを得ることができる。前記特徴ベクトルに基づいて、前記ボクセルを分類し、ラベル付けする。ボクセル分類は、局所ボクセル密度ベクトルと、最大クラスタ数（ＭＣＮ）と呼ばれる１つのプリセットパラメータとに部分的に依存する。ＭＣＮは、前記データセットに用いられるボクセル分類の数を設定する。ＣＴ画像の場合において、人間の目は、４つの識別可能な組織／材料形式を識別することができる。５のＭＣＮ値がこの場合において好適である。ＭＲＩ画像に関し、人間の目は、６つの異なった組織形式の間に差異を認めることができ、７のＭＣＮ値を使用することができる。

【０１３３】

前記画像分割プロセスの一部として、拡張されたデータセットを、前記測定されたデータ点の間の補間によって発生する。例えば、ＳＯＶＱアルゴリズムの前に、１次ラグランジュ補間を、前記データセットにおける各々のスライスに用いることができる。これは、前記データセットの原スライスの２５６×２５６行列サイズを５１２×５１２行列サイズに拡張する。加えて、スライス内補間を行い、実際のスライス間の前記データセットをさらに拡張することができる。前記補間されたデータセットを、拡大データセットと呼ぶ。拡大データセットの発生に加え、前記補間プロセスは、前記データにおいてローパスフィルタ効果を有するため、ノイズを抑制し、部分的体積効果を減少させる。

【０１３４】

２次元ビューイングツールを使用し、種ボクセルを前記喉頭管腔内で選択し、成長アルゴリズムを用いて、前記データセットから喉頭体積を抽出する（ステップ３１１５）。いくつかの接続されない体積領域が存在するかもしれない前記喉頭のこれらの領域において、多数の種点を選択することができる。

【０１３５】

前記識別された喉頭体積と、画像分割によって分類された前記領域のボクセルとに関して、次のタスクは、前記仮想喉頭管腔の効率的なナビゲーションおよびビューイングを可能にするように前記データを管理することである。この場合において、詳細レベル（ＬＯＤ）アプローチを、本方法における使用に適合させ、変更する。このＬＯＤ方法において、減少したデータセットを前記拡大データセットから発生する。例えば、５１２×５１２×２５６拡大データセットを、３レベルのしきい値処理を伴う多解像度分解を使用することによって、６４×６４×３２減少体積データセットに減少することができる。次に、前記拡大および減少体積データセットの双方において体積画像をレンダリングするのに使用されるポリゴンを抽出することができる。慣例的なマーチングキューブ法を使用し、前記喉頭の表面に適合するポリゴンを抽出することができる。

【０１３６】

先行技術において遭遇する１つの問題は、必要なポリゴンの最大数を管理し、前記拡大データセットに関する３次元画像を発生することである。この問題を、本方法において、前記拡大データセットをバイナリ空間分割（ＢＳＰ）ツリーデータ構造において組織化することによって解決する（ステップ３１３０）。前記原画像体積を、前記ツリーのルートとして選択する。次に、前記空間を、ほぼ等しい数のポリゴンを含む２つのサブ空間に分割する。この再分プロセスを、各々の結果として生じるサブ空間におけるポリゴン数がしきい値未満になるまで繰り返す。前記しきい値は、システム性能および適用必要条件に基づいて変化することができる。最後の結果として生じるサブ空間を、前記ツリーのリーフノードと呼ぶ。前記再分プロセスが完了したら、前記拡大データセットのボクセルのすべてを、前記ＢＳＰツリーのリーフノードに格納する。

【０１３７】

ナビゲーションまたはビューイング中、ポリゴン選別を、完全に視界の外側のこれらのリーフノードを現在の処理動作から最初に除去することによって適用することができる。残りのポリゴンを前記ＢＳＰツリーから呼び戻し、選別されていないこれらの空間において配列し、レンダリングする。したがって、前記ＢＳＰツリーは、特定のナビゲーションまたは表示動作に関して前記データセットの関連する部分を選択する有効なツールを提供す

る。
【０１３８】
前記拡大および減少データセットを、２レベルＬＯＤレンダリングモードにおいて協働して使用する。ユーザが前記物体と、前記視界において回転、シフトまたは他の変更を行うような相互作用をする場合（ステップ３１３５）、前記減少データセット（６４サイズ）からのポリゴンをレンダリングする（ステップ３１４０）。含まれるポリゴン数が重大により少ないため、前記減少データセット体積との相互作用を、より速く、少ない処理オーバヘッドで行うことができる。増加する速度とのトレードオフは、減少した画像解像度である。予め決められた期間後、ユーザからの相互作用がない場合、拡大データセット（５１２サイズ）のポリゴンを前記ＢＳＰツリーから選択し、レンダリングし、現在の視野の高解像度画像を与える（ステップ３１４５）。
【０１３９】
仮想血管造影法
仮想画像化およびナビゲーションに関する前記技術を、仮想血管造影法に適合させ、用いることもできる。この技術を、循環系の種々の異常および疾病の検出および測定に使用することができる。
【０１４０】
仮想血管造影法のこれらのような用途の１つは、一般に大動脈管の小さい拡大として始まり、大動脈瘤のサイズの増加と共に破裂するより大きな危険性を示す腹部の大動脈瘤の検出である。以前は、唯一の有効な治療方法は切開手術であり、大動脈瘤のレベルにおいて大動脈内に移植用片を配置していた。しかしながらこの手順は、高い程度の関連する不健全性および死亡率を有する。最近開発された、皮膚ごとに配置される大動脈ステントグラフト技術は、著しくより低い複雑割合を持っている。仮想血管造影法は、これらのあまり侵害しない手順を計画するのを助ける有効な方法であり、大動脈瘤を検出し、大動脈瘤の成長を追跡し、手術が必要な場合を決定する有効なツールでもあり得る。
【０１４１】
図３２のフローチャートは、本仮想血管造影法の概要を与える、仮想血管造影法を行うことにおいて、大動脈のような血管の画像走査を取得しなければならない（ステップ３２０５）。コンピュータ断層撮影（ＣＴ）、磁気共鳴画像（ＭＲＩ）および超音波のような種々の画像化技術を使用することができる。しかしながら、大動脈ＣＴ走査が、ＣＴ画像において結果として生じる、血と、柔らかい組織と、カルシウム堆積物との間のコントラストのため、一般に好適である。
【０１４２】
画像走査データセットを取得したら、画像分割技術を前記データセットに用い、前記データセットのボクセルを多数のカテゴリに分類する（ステップ３２１０）。図１５と組み合わせたような上述した画像分割技術は、一般的に利用可能である。この場合において、前記ボクセルの種々の特徴ベクトル値を、血、柔らかい組織およびカルシウム堆積物のようなカテゴリにしたがってグループ化する。血液ボクセルを種として使用し、領域成長アルゴリズムを使用して、前記大動脈管腔の体積および大きさを決定することができる。
【０１４３】
前記ＣＴ画像において、大動脈瘤は、隣接する柔らかい組織によく似た画像特徴を有する。結果として、前記大動脈瘤の完全な輪郭を確立することは困難であるかもしれない。しかしながら、カルシウム堆積物を有する領域は、前記ＣＴ走査において重大なコントラストを提供し、これらを使用し、前記血管壁における大動脈瘤の終了点のような、前記大動脈瘤の部分を識別することができる（ステップ３２１５）。
【０１４４】
大動脈瘤の一部を検出した後、１つ以上の閉表面を発生し、前記大動脈瘤の輪郭の推定を規定することができる（ステップ３２２０）。凸面閉表面を、非一様、非論理的なＢスプラインを使用し、識別された前記大動脈瘤の点を通るか、これらの近くを通る表面を発生することによって確立することができる。

【０１４５】
前記閉表面を発生した後、前記大動脈瘤の体積を推定することができる（ステップ３２２５）。前記体積を推定する１つの方法は、前記推定された閉表面によって囲まれたボクセルの数を計数することである。加えて、前記大動脈瘤のボクセル内で、血流の方向に沿った中心線を、距離変換技術を使用することによって決定することができる。次に、連続的な局所座標系をこの中心線に沿って確立し、前記大動脈瘤の直径を決定することができる。仮想ナビゲーションをこの中心線に沿って、前記結腸のような管腔を通るナビゲーションに関して上述したものと一致するように行う。

【０１４６】
図３３Ａ－Ｃを参照し、上述した仮想血管造影法を使用し、ステントグラフトの発生および配置において補助し、腹部の大動脈瘤をバイパスするのに使用することができる。図３３Ａは、腎臓部の動脈の下で前記大動脈の二股の上に位置する腹部の大動脈瘤の単純化した図を示す。前記大動脈の特定の解剖と、前記腹部の大動脈瘤のサイズおよび位置における患者間の変化のため、ステントグラフトを使用して大動脈瘤をバイパスするため、前記グラフトを、個々の大動脈セグメントに特に適合するように設計し、構成しなければならない。図３３Ｂに示すように、これは、とりわけ、必要なグラフトの長さと、前記バイパスされる領域の各々の端におけるインタフェースの点における直径と、インタフェースの角度とを知ることを必要とする。図３３Ｂおよび３３Ｃに示すように、前記大動脈瘤が動脈の枝の近くに位置する場合、二股に分かれたステントグラフトの二股に分かれた端のサイズおよび角度も決定しなければならない。

【０１４７】
現在まで、これらのような測定は、鼠蹊領域のレベルにおいて行われる挿入により前記大動脈中に挿入されるカテーテルを使用する侵入的な較正血管造影像この技術を、本仮想血管造影法を使用して補足し、ひょっとすると取って代わることができ、この仮想血管造影法は、前記大動脈管腔のブランチを通って構成された中心線を使用する仮想ナビゲーションを使用してこれらのような距離および角度を決定することができる。加えて、前記仮想血管造影法を使用し、ステントグラフトを挿入することができる領域の仮想試験切除を行うことができる。これは、手術者が、動脈表面の下を見ることを可能にし、血栓、堆積物、石灰化像、または、ステントグラフト手順の使用に禁忌を示す他の要因に関する領域を検査することを可能にする。

【０１４８】
仮想血管造影法の他の用途は、脳に血流を供給する頚動脈を通る画像化、調査およびナビゲーションである。仮想内視鏡検査に関して上述した技術は、血管の場合において完全に適用可能である。例えば、興味ある血管を、取得した画像データから画像分割技術を使用して抽出する。次に、ナビゲーション飛行経路を、前記血管を通って確立することができる。好適には、ポテンシャル場を、ナビゲーションにおける使用に関して前記血管内に構成する。結腸のような他の器官に関するように、前記血管の体積レンダリングされたモデルを発生することができる。前記飛行経路およびポテンシャル場を使用して、前記体積レンダリングされた血管管腔の内部を通ってナビゲーションすることによって、血管狭窄およびプラーク形成のような異常を観察することができる。加えて、仮想試験切除に関して考察した技術を、この文脈において用い、血管壁を評価し、プラークのような血管壁表面における構造を特徴付けることができる。

【０１４９】
仮想内視鏡検査に関するツリーブランチ探索

中空の器官または物体を通る仮想ナビゲーションに関する経路探索は、重要な仕事である。この目的を達成するために、飛行経路発生のような種々の技術が考察されてきた。多ブランチ構造を与えるような、調査されている物体のジオメトリがより複雑になるにつれて、前記経路探索の仕事はさらにより複雑になる。主要な管腔の中心線を決定するだけでなく、前記主要な管腔から延びる任意のブランチを識別し、位置付けることが望ましい。複雑なブランチ構造を有する器官の一般の例は、主な気道および肺と、心臓血管系と、結腸

膨起の折りたたみの存在のため結腸とを含む。各々の器官または物体は、一般に、該物体に関する経路またはスケルトンを規定する特定の挑戦を示す。しかしながら、このようなスケルトンを発生する一般化された技術を、図３４のフローチャートにおいて説明した。

【０１５０】

図３４を参照し、コンピュータ断層撮影（ＣＴ）または磁気共鳴画像（ＭＲＩ）走査のような、興味ある領域の画像走査を取得する（ステップ３４０５）。上記で考察したように、前記画像走査を、前記画像走査のバイナリ画像を重ね、これらの重ねられた画像から３次元体積ユニットまたはボクセルを規定することによって、３次元体積に変換する（ステップ３４１０）。前記興味ある領域の体積および複雑さに応じて、前記スケルトンを発生する前に、前記３次元体積のデータセットのサイズに減少することが望ましい。この目的のため、以下により詳細に考察する多解像度データ減少プロセスを使用することができる（ステップ３４１５）。

【０１５１】

前記スケルトンは、前記３次元体積のサブセットである。好適には、以下の属性、すなわち、１）前記ツリーのホモトピーを保存する、２）２６接続されている、３）１ボクセル厚である、４）前記ブランチの中央軸を推定する、５）比較的滑らかである、を有する。ホモトピーの程度は、ある程度用途特定である。例えば、結腸管腔のスケルトンの発生において、前記スケルトンは、一般に、数ボクセル深さであるかもしれない多数の結腸膨起の折りたたみの存在にもかかわらず、端から端まで単一経路である。しかしながら、心臓血管系および肺系において、数ボクセル深さであるルートからの小さい分枝が、前記系における正当なブランチを表すことができる。

【０１５２】

図３４に戻って、興味ある体積において、ルートボクセルを前記体積において識別する（ステップ３４２０）。仮想内視鏡検査を行うことにおいて、これを、評価している構造のジオメトリの理解に基づいて手動で行うことができる。

【０１５３】

次に、距離マップを発生し、前記ツリーにおけるブランチと、前記ブランチおよびルートボクセルの終了点間の距離とを識別する（ステップ３４２５）。この方法において用いられる仮定は、前記ツリーのルートまで最も長い距離を示す各ブランチにおいて１つのユニークな終了点が存在することである。図３５は、２６接続ボクセルと呼ばれる３×３×３立方体ボクセル配置を説明する図式的な図である。この配置の中心において、ゼロの距離重みが割り当てられた種ボクセル３５０５がある。種ボクセル３５０５の周囲に、２６個の接続された隣接ボクセルがあり、これらの隣接ボクセルには、各々の隣接ボクセルと種ボクセルとの間の各々のユークリッド距離に基づいた距離重みが割り当てられる。立方体配置において、ユークリッド距離は、１、１．４および１．７にほぼ等しい

【外１１】

$$1, \sqrt{2}, \sqrt{3}$$

の正規化値をとることができる。簡単に処理するために、前記ボクセルに１０、１４および１７の整数値重みを割り当て、関連するユークリッド距離を近似することができる。

【０１５４】

図３６は、図３５の２６接続立方体距離プレートのユークリッド重み付き距離を使用して前記体積におけるボクセルからルートまでの距離マップを決定するアルゴリズムの擬似コード表現である。発生された距離マップから、ブランチを識別し、前記ブランチの終了点を決定する（ステップ３４３０）。

【０１５５】

図３６を参照し、前記体積のルートに整数値０をラベル付けする。次に、前記体積におけるボクセルに関して処理待ち行列を形成する。次に、前記ボクセルに、先入れ先出し方法において、前記待ち行列の先頭におけるボクセルとルートボクセルとの間のユークリッド距離を加算することによってラベル付けする。このプロセスを、前記体積におけるボクセ

ルのすべてが前記距離マップにおける値を割り当てられるまで繰り返す。

【０１５６】

前記距離マップにおけるボクセルのラベル付けは、前記待ち行列の順序に部分的に依存するため、結果として生じる距離マップは、ユニークな解を与えない。しかしながら、前記待ち行列順序にかかわらず、各部ランチに関して少なくとも１つの最も遠い点が常に存在する。加えて、各々のボクセルに関して、ルートボクセルのほかに、前記体積において前記ルートに対してより短い距離を有する少なくとも２６の接続された隣接ボクセルが存在する。したがって、前記ブランチの終了点は、前記距離マップを局所最大距離（局所最大値）に関して探索することによって、容易に検出可能である（ステップ３４３０）。この局所最大値という用語は、相対的な用語である。前記体積を局所最大値に関して評価することにおいて、前記体積を、評価されている物体に適切な種々のサブ空間に分割すべきである。期待される特徴サイズ、ブランチ長、ブランチ直径等を、前記サブ空間分割を決定することにおいて一般に考慮する。

【０１５７】

前記ブランチの終了点を決定したら、前記終了点からルートボクセルまでの最短経路を決定する（ステップ３４３５）。前記終了点からルートボクセルまでの最短経路は、前記ツリーのブランチの基本的構造を規定し、前記ブランチの中心線を近似する。これを、前記体積のラフスケルトンと呼ぶ。前記最短経路を、好適には、前記ツリーの最も遠い端におけるブランチから、これらのブランチの端から始めて発生する。最も遠いブランチ終了点から、第１ボクセルを選択し、その２６の接続された隣接ボクセルを解析し、どのボクセルが前記終了点からルートまでの最短距離経路においてあるかを決定する。このプロセスを、選択されたボクセルがルートに達するまで繰り返す。これは、結果として、前記最も遠い端からルートまでの１ボクセル幅経路を生じる。他のブランチに関する最短経路の探索も同様である。しかしながら、その後のブランチに関して、前記選択プロセスは、現在経路が以前に割り当てられた経路に達する場合、終了することができる（例えば、前記経路は、前記ルートへのすべての道を導く必要はない）。前記相互接続された最短経路のすべての集合は、前記物体の結果として生じるラフスケルトンである。

【０１５８】

前記結果として生じるラフスケルトンの用途に応じて、前記ラフスケルトンを改良することが望ましいかもしれない。前記スケルトンを改良するあるステップは、前記スケルトンを前記ブランチ内で中心に集めることである。最も長いブランチから開始して、一様な間隔を、一般に４－８ボクセルの範囲において、前記ブランチに沿って選択する。各々の間隔に関して、前記ラフスケルトンにおけるボクセルの接線方向を計算し、前記接線方向に対して垂直なボクセルと交差する面を決定する。前記面およびボクセルの交線によって規定される２次元領域を形成し、この交線の中心を既知の最大ディスク技術を使用して計算することができる。次に、前記交線の中心をバイキュービックスプラインＢ補間または他の曲線フィッティング方法を使用して接続することができる。残りのブランチに関して、他のブランチまたはルートに達する終了点を最初に調節し、以前に中心化されたスケルトンブランチの位置を調和させる。次に、中心化を、前記最も長いブランチに関して説明したのと同じように続ける。

【０１５９】

ステップ３４１５に戻って参照し、大きいデータセットが含まれる場合、前記データセットのサイズを減少して、処理をスピードアップすると共に処理コストを減少することが必要であるか、少なくとも望ましいかもしれない。前記ツリー構造がある範囲のスケール内で保存され得ることに注意することによって、大きい体積を、構造解析のためのより小さいスケール空間に縮小することができる。

【０１６０】

多解像度解析に基づく縮小方法を使用することができる。入力データは、ＣＴまたはＭＲＩ走査の分割結果から得ることができる同じサイズのバイナリ画像のスタックである。ｘ方向をスライス画像幅に沿ってとり、ｙ方向はスライス画像高さに沿い、ｚ方向はステッ

プずつの方向に沿う。前記ツリー体積における前景ボクセルを１２８（最大）の値に設定し、背景ボクセルを０（最小）の値に設定する。すべての有理係数にダウベッチーズ（Ｄａｕｂｅｃｈｉｅｓ）の両直交ウェーブレット変換を用いる。この１次元（１Ｄ）離散ウェーブレット変換（ＤＷＴ）を、最初にｘ方向に沿って１行ずつ用いる。前記ＤＷＴの適用から、より低い周波数成分のみが保持され、もたらされる。前記ＤＴＭをバイナリ信号に用いることに注意し、前記より低い周波数成分を結果として生じる２種類の非ゼロ係数が存在する。第１は値１２８であり、この種類の係数は前記体積内部において位置する。第２は１２８に等しくない値であり、これらの係数は前記体積の境界に位置する。

【０１６１】

前記第２の種類の係数を、予め決められたしきい値と比較する。その絶対値が、予め設定されたしきい値Ｔ１より大きい場合、前記係数の値を１２８に設定し、そうでなければ０に設定する。これは、結果として、原データセットの半分の行サイズを有するバイナリ画像のスタックを生じる。次に、同様のしきい値処理を、より低い周波数成分に用いる場合、同じＤＷＴを、前記結果として生じたデータセットに、ｙ方向に沿って、１列ずつ用いる。この結果は、再びバイナリ画像のスタックだが、ここでは、原データセットと比較して半分の行および列サイズを有する。最後に、前記ＤＷＴを、前記最後の結果に、ｚ方向に沿って用い、より低い周波数成分を保持する。このステップは、第１レベル分解を完了する。

【０１６２】

前記第１レベル分解の結果として生じるデータセットは、原データセットと比較して３方向すべてにおいて半分のサイズのものである。前記縮小手順がこのレベルにおいて停止する場合、最後のしきい値処理を用いる。非ゼロおよび非１２８値のこれらの係数を再評価する。この種類の係数の絶対値が予め設定されたしきい値Ｔ２より大きい場合、１２８として再評価し、そうでなければ０として再評価する。更なる縮小が必要な場合、同じしきい値アルゴリズムをしきい値Ｔ１によって用いる。上述したような更なる縮小プロセスを、結果として生じる体積が所望の減少したデータ体積に達するまで再帰的に用いることができる。仮想内視鏡検査において、前記スライス画像を５１２×５１２画素サイズとする。最大分解レベルは、通常３であり、結果として６４×６４減少画素サイズを生じる。

【０１６３】

前記体積を、前記与えた方法によってすべての方向において等方的に縮小する。２つのプリセットしきい値Ｔ１およびＴ２を使用し、縮小の程度を制御する。前記体積が著しく過縮小である場合、前記減少した体積において連結度が失われてしまうかもしれない。より小さい程度に過縮小である場合、前記減少した体積データセットにおいて２つの別個のブランチが１つのブランチに合体するかもしれない。前記２つのしきい値がより大きくなると、より薄く減少した体積になる。これらの２つのしきい値の範囲は、［０，ｒ×１２８］であり、０＜ｒ＜１である。好適には、仮想内視鏡検査に関する範囲は、Ｔ１に関してｒ∈（０．０８，０．２８）、Ｔ２に関してｒ∈（０．７，０．９８）である。正確な決定は、特定の用途の特徴サイズに依存し、縮小体積における構造特徴の忠実度を保持しながら、減少を達成するように選択される。

【０１６４】

原体積の縮小後、前記ツリーブランチ探索手順を、前記より小さい体積に用いることができる（ステップ３４２０－３４４０）。結果として生じるスケルトンを、原スケール空間にマッピングし戻すことができる。原空間に対して測った場合、より小さいスケールのスケルトンの画像は、もはや、前記原スケール空間にける接続された経路のままではない。前記画像におけるこれらのボクセルは、最終スケルトンに関する制御点として働く。前記制御点を、前に説明したようなアルゴリズムを使用して中心に集め、次に、これらを補間し、前記オブジェクトに関する最終スケルトンを形成する。

【０１６５】

コンピュータ支援診断

ここに説明した仮想調査技術は、種々の条件のコンピュータ支援診断（ＣＡＤ）に関する

用途に適する。例えば、上述したように、器官組織のジオメトリをガウス曲線に関して調査することによって、結腸管腔内部のポリープのような異常ジオメトリを有する領域を自動的に識別することができる。この技術を一般化し、テクスチャ特徴と共に使用して、多数の用途に関するＣＡＤ機能性を与えることができる。

【０１６６】

例えば、上述した膀胱の多走査画像化を使用し、膀胱壁における腫瘍の自動検出を行うことができる。この場合において、一般に膀胱壁内における腫瘍侵入の程度を使用し、膀胱癌の段階を規定する。上述した多走査画像化および画像分割技術を使用し、前記膀胱壁の領域の輪郭を容易に描くことができる。通常の膀胱組織の領域は、一般に、実質的に一様なテクスチャ特徴を示す。しかしながら、腫瘍が前記領域において存在する場合、前記一様なテクスチャ特徴は中断される。したがって、テクスチャ解析を使用し、前記膀胱壁を評価することによって、腫瘍を示すかもしれない領域は、前記一様なテクスチャ内の乱れまたは“ノイジー領域”としてそれ自身を示す。

【０１６７】

領域のテクスチャを、規定された範囲内のボクセル間の強度相関を特徴付ける確率分布関数（ＰＤＦ）によって表すことができる。２次元ＰＤＦを使用し、テクスチャ特徴を表すことができる。このようなＰＤＦは、すべての方向に沿った２つの最も近いボクセル間の相関を特徴付ける。前記ＰＤＦを評価するために、興味ある領域における任意の２つの最も近い隣接ボクセルの強度を、前記興味ある領域に関する標本ベクトルとして記録することができる（例えば文脈）。多数のこのような標本ベクトルを使用し、この文脈に関して前記ＰＤＦを評価する累積分布関数（ＣＤＦ）を発生することができる。各ボクセルに関して、その隣接ボクセルのある範囲内の標本ベクトルを使用し、局所ＣＤＦを発生することもできる。

【０１６８】

コルモロゴフ－スミルノフテストのような統計テストを前記ＣＤＦに用い、前記文脈のＣＤＦおよび局所ＣＤＦが統計的に等価であるか、例えば、予め規定された信頼レベル内であるかどうかを決定することができる。そうであるならば、現在ボクセルの周囲の局所テクスチャ特徴を前記文脈と同一であるとみなす。そうでなければ、現在ボクセルは、前記文脈のテクスチャ特徴と異なったテクスチャ特徴を示し、腫瘍のような潜在的な異常とみなしてもよい。あるボクセルが前記文脈と統計的に等価であるかどうかを決定するのに使用される信頼レベルを変化させ、検出の感度を増減させることができる。

【０１６９】

テクスチャ解析にＰＤＦまたはＣＤＦを用いる代わりの方法において、各々のＣＤＦまたはＰＤＦを、機能的線形空間における点とみなすことができる。この空間における２つのＤＣＦまたはＰＤＦの間の距離を、スコロホールド（Ｓｋｏｒｏｈｏｌｄ）距離等によって測定することができる。この距離は、ＰＤＦの類似性の程度の測定を与える。例えば、局所ＣＤＦと文脈ＣＤＦとの間の距離を計算することができ、結果として生じる距離を１つ以上の距離しきい値と比較することができる。前記距離が大きい場合、前記局所テクスチャを、前記文脈と異なると考え、このことは、このようなボクセルが、潜在的な異常または腫瘍を有する領域に属することを示すことができる。好適には、前記距離しきい値を、統計的に十分に既知のデータセットの評価に基づいて決定する。

【０１７０】

上記で計算した距離を、ここで説明したような視覚化技術および体積レンダリング技術と共に使用することができる。例えば、原データセットと比較し得るサイズを有する特徴体積データセットを形成することができる。この新たなデータセットにおける各ボクセルに関する強度を、前記局所ＣＤＦと文脈のＣＤＦとの間の距離に基づいて割り当てることができる。この３次元体積データセットを体積レンダリング技術によって見る場合、疑わしい腫瘍を含む領域は、周囲の領域よりも高い画像強度を示す。

【０１７１】

ポリープの自動検出に関して上記で考察したように、管腔の表面を、Ｃ－２滑らか表面モ

デル等を使用することによって、３次元ユークリッド空間における連続的に二次微分可能表面として表すことができる。このようなモデルにおいて、前記結腸の表面における各ボクセルは、ガウス曲率場と呼ばれる、ガウス曲率を有する関連する幾何学的特長を有する。種々の器官に関して、ある予想される局所特徴を、別個の曲率テンプレートによって特徴付けることができる。例えば、前記結腸の文脈において、予想される局所特徴は、滑らかな湾曲表面と、リング折りたたみと、滑らかな面からの凸面の丘と、滑らかな表面からの台地とを含む。これらの少なくとも２つの特徴は、ポリープまたは腫瘍を表すかもしれない。したがって、前記ガウス曲率場を特定の予め決められた局所特徴テンプレートに関して探索することによって、ポリープ、腫瘍、および、興味ある他の異常を自動的に検出することができる。コンピュータ支援診断を行うことへの表面ジオメトリのこの使用を、単独で使用することもでき、または、上述したテクスチャベースＣＡＤ技術と共に使用することもできる。

【０１７２】

器官全体または興味ある領域をレンダリングして見る代わりとして、観察されている表面を小さい領域またはパッチに分割することができ、これらのパッチを、前記局所曲率テンプレートによって規定する。各々のパッチは、共通の幾何学的特長または曲率テンプレートを有するボクセルを含むべきである。次に、前記パッチのすべてのボクセルを観察することを可能にする単一の視点を、前記パッチに関して決定する。次に、前記パッチに、該パッチがポリープまたは他の異常を表す可能性を示す優先度スコアを割り当てる。次に、オペレータが前記内蔵体積全体をナビゲートして疑わしい領域を探し出すのではなく、前記パッチを、優先度順に別々に観察することができる。もちろん、好適な診断システムは、オペレータが、あるパッチを見ることから、前記器官の文脈におけるパッチを見ることへ容易に変更することができるように、ビューの間で切り替える能力を含む。代わりに、これら２つのビューを同時に与えることができる。再び、前記テクスチャベースアプローチを使用し、このアプローチを補うことができる。前記テクスチャ解析の結果を調査している前記パッチにマッピングすることによって、前記テクスチャ情報を観察し、診断に使用することもできる。

【０１７３】

上記は、本画像化および調査システムおよび方法の原理を単に説明する。したがって、当業者が、ここに明白に図示または説明していないが、本発明の原理を具体化し、したがって、請求項によって規定される本発明の精神および範囲内である多数のシステム、装置および方法を考案することができることは明らかであろう。

【０１７４】

例えば、ここで説明した方法およびシステムを用い、動物、魚、または無生物を仮想調査することができる。医療分野における指定された使用に加え、前記技術の用途を使用し、開くことができない密封された物体の内容を検出することができる。前記技術を、ビルディングまたは洞窟のような建築上の構造内で使用することもでき、オペレータが前記構造中をナビゲートすることを可能にすることができる。

【図面の簡単な説明】

【図１】本発明による、物体、特に結腸の仮想調査を行うステップのフローチャートである。

【図２】仮想器官におけるガイド付きナビゲーションを行う「サブマリン」カメラモデルの説明である。

【図３】「サブマリン」カメラのピッチおよびロールをモデル化するのに使用される振り子の説明である。

【図４】２つのブロッキング壁を識別する体積測定結腸の二次元断面を説明する図である。

【図５】開始および終了体積要素を選択する体積測定結腸の二次元断面を説明する図である。

【図６】前記ブロッキング壁および結腸表面によって閉じた離散的サブ体積を示す体積測

定結腸の二次元断面を説明する図である。
【図７】多数の層を剥ぎ取られた体積測定結腸の二次元断面を説明する図である。
【図８】残りの飛行経路を含む堆積測定結腸の二次元断面を説明する図である。
【図９】走査された結腸の体積視覚化を発生するステップのフローチャートである。
【図１０】セルに再分された仮想結腸の説明である。
【図１１】Ａは仮想調査されている器官のグラフィカル描写であり、ＢはＡにおける器官を描写すると同時に、発生されたスタブツリーのグラフィカル描写であり、ＣはＡにおける器官を描写すると同時に、発生されたスタブツリーの他のグラフィカル描写である。
【図１２】Ａはレンダリングすべきシーンおよび前記シーンの特定のセル内の物体のグラフィカル描写であり、ＢはＡにおける画像を描写すると同時に、発生されたスタブツリーのグラフィカル描写であり、Ｃ－ＥはＡにおける画像を描写すると同時に、発生されたスタブツリーの他のグラフィカル描写である。
【図１３】層を除去したポリープを含む仮想結腸の２次元表現である。
【図１４】本発明による人間の器官の仮想調査を行うのに使用されるシステムの図である。
【図１５】改善された画像分割方法を示すフローチャートである。
【図１６】代表的な腹部ＣＴデータセットのボクセル強度対周波数のグラフである。
【図１７】興味あるボクセルと、その選択された隣接ボクセルとを含む強度ベクトル構造の斜視図である。
【図１８】Ａは肺を含む領域を第１に説明する人間の腹部領域のＣＴ走査からの好例の画像スライスであり、ＢはＡの画像スライスにおける肺領域の識別を説明する絵的図であり、ＣはＢにおいて識別された肺体積の除去を説明する絵的図である。
【図１９】Ａは結腸および骨の一部を含む領域を第１に説明する人間の腹部領域のＣＴ走査からの好例の画像スライスであり、ＢはＡの画像スライスからの結腸および骨領域の識別を説明する絵的図であり、Ｃは骨の領域を除去したＡの画像走査を説明する絵的図である。
【図２０】テクスチャをモノクローム画像データに用いる方法を説明するフローチャートである。
【図２１】高速パースペクティブ光線投影技術を用いて体積レンダリングする方法を説明するフローチャートである。
【図２２】体積縮小技術を用いて結腸管腔を通る中心飛行経路を決定する方法を説明するフローチャートである。
【図２３】図２２に示す方法において使用する体積縮小技術をさらに説明するフローチャートである。
【図２４】発生された中心飛行経路による分割された結腸管腔の３次元絵的表現である。
【図２５】分割技術を用いて結腸管腔を通る中心飛行経路を発生する方法を説明するフローチャートである。
【図２６】パーソナルコンピュータバスアーキテクチャに基づくシステム実施形態のブロック図である。
【図２７】図２６のシステムを使用して体積画像化を行う方法を説明するフローチャートである。
【図２８】膀胱のような物体の仮想調査（仮想膀胱鏡検査）を行う多走査方法を説明するフローチャートである。
【図２９】図２８の仮想膀胱鏡検査による画像化結果を与え、膀胱構造の説明的外側ビューを与えるのに好適な表示ウィンドウの絵的表現である。
【図３０】図２８の仮想膀胱鏡検査による画像化結果を与え、膀胱構造の説明的内側ビューを与えるのに好適な表示ウィンドウの絵的表現である。
【図３１】多解像度ビューイングを使用して喉頭のような物体の仮想調査を行う方法のフローチャートである。
【図３２】仮想血管造影検査を行う方法のフローチャートである。

【図３３】Ａ－Ｃは腹部大動脈瘤の存在を説明する大動脈の一部の絵的ビューである。
【図３４】物体のスケルトン構造を発生する方法を説明するフローチャートである。
【図３５】２６接続ユークリッド重み付き立方体距離プレートの図式的な図である。
【図３６】図３４の方法において使用する距離マップを発生するプロセスの擬似コードを説明する図である。

【国際公開パンフレット】

(12) INTERNATIONAL APPLICATION PUBLISHED UNDER THE PATENT COOPERATION TREATY (PCT)

(19) World Intellectual Property Organization
International Bureau

(43) International Publication Date
11 April 2002 (11.04.2002)

PCT

(10) International Publication Number
WO 02/29764 A1

(51) International Patent Classification⁷: G09B 23/28, G06F 17/00, G06T 1/00, 13/00, 15/00, 15/50, 17/00

(21) International Application Number: PCT/US01/30704

(22) International Filing Date: 1 October 2001 (01.10.2001)

(25) Filing Language: English

(26) Publication Language: English

(30) Priority Data:
60/237,665 3 October 2000 (03.10.2000) US
09/777,120 5 February 2001 (05.02.2001) US

(71) Applicant: THE RESEARCH FOUNDATION OF STATE UNIVERSITY OF NEW YORK [US/US]; Office of Technology Licensing, State University of New York at Stony Brook, Stony Brook, NY 11794 (US).

(72) Inventors: KAUFMAN, Arie, E.; 94 Cedar Drive W., Plainview, NY 11803 (US). LIANG, Zhengrong; 28 Houghton Boulevard, Stony Brook, NY 11790 (US). WAX, Mark, R.; 6 E. Sanders Street, Greenlawn, NY 11740 (US). WAN, Ming; 459 Chapin Complex, Stony Brook, NY 11790 (US). CHEN, Dongqing; 100 Ronkonkoma Avenue E1, Lake Ronkonkoma, NY 11779 (US). LI, Bin; Apt. 3F, 1 Williams Boulevard, Lake Grove, NY 11755 (US).

(74) Agents: TANG, Henry et al.; Baker Botts, LLP, 30 Rockefeller Plaza, New York, NY 10112-0228 (US).

(81) Designated States (national): AE, AG, AL, AM, AT, AU, AZ, BA, BB, BG, BR, BY, BZ, CA, CH, CN, CO, CR, CU, CZ, DE, DK, DM, DZ, EC, EE, ES, FI, GB, GD, GE, GH, GM, HR, HU, ID, IL, IN, IS, JP, KE, KG, KP, KR, KZ, LC, LK, LR, LS, LT, LU, LV, MA, MD, MG, MK, MN, MW, MX, MZ, NO, NZ, PH, PL, PT, RO, RU, SD, SE, SG, SI, SK, SL, TJ, TM, TR, TT, TZ, UA, UG, UZ, VN, YU, ZA, ZW.

(84) Designated States (regional): ARIPO patent (GH, GM, KE, LS, MW, MZ, SD, SL, SZ, TZ, UG, ZW), Eurasian patent (AM, AZ, BY, KG, KZ, MD, RU, TJ, TM), European patent (AT, BE, CH, CY, DE, DK, ES, FI, FR, GB, GR, IE, IT, LU, MC, NL, PT, SE, TR), OAPI patent (BF, BJ, CF, CG, CI, CM, GA, GN, GQ, GW, ML, MR, NE, SN, TD, TG).

Published:
— with international search report

For two-letter codes and other abbreviations, refer to the "Guidance Notes on Codes and Abbreviations" appearing at the beginning of each regular issue of the PCT Gazette

WO 02/29764 A1

(54) Title: SYSTEM AND METHOD FOR PERFORMING A THREE-DIMENSIONAL VIRTUAL EXAMINATION OF OBJECTS, SUCH AS INTERNAL ORGANS

(57) Abstract: Methods for generating a three-dimensional visualization image of an object, such as an internal organ, using volume visualization techniques are provided. The techniques includes a multi-scan imaging method, a multi-resolution imaging method, and a method for generating a skeleton of a complex three dimension object. The applications include virtual cystoscopy, virtual laryngoscopy, virtual angiography, among others.

SYSTEM AND METHOD FOR PERFORMING A THREE-DIMENSIONAL VIRTUAL EXAMINATION OF OBJECTS, SUCH AS INTERNAL ORGANS

SPECIFICATION

TECHNICAL FIELD

The present invention relates to a system and method for performing a volume based three-dimensional virtual examination, and more particularly relates to a system which offers enhanced visualization and navigation properties.

BACKGROUND OF THE INVENTION

Colon cancer continues to be a major cause of death throughout the world. Early detection of cancerous growths, which in the human colon initially manifest themselves as polyps, can greatly improve a patient's chance of recovery. Presently, there are two conventional ways of detecting polyps or other masses in the colon of a patient. The first method is a colonoscopy procedure, which uses a flexible fiber-optic tube called a colonoscope to visually examine the colon by way of physical rectal entry with the scope. The doctor can manipulate the tube to search for any abnormal growths in the colon. The colonoscopy, although reliable, is both relatively costly in money and time, and is an invasive, uncomfortable painful procedure for the patient.

The second detection technique is the use of a barium enema and two-dimensional X-ray imaging of the colon. The barium enema is used to coat the colon with barium, and a two-dimensional X-ray image is taken to capture an image of the colon. However, barium enemas may not always provide a view of the entire colon, require extensive pretreatment and patient manipulation, is often operator-dependent when performing the operation, exposes the patient to excessive radiation and can be less sensitive than a colonoscopy. Due to deficiencies in the conventional practices described above, a more reliable, less intrusive and less expensive way to examine the

colon for polyps is desirable. A method to examine other human organs, such as the lungs, for masses in a reliable, cost effective way and with less patient discomfort is also desirable.

Another leading cause of cancer deaths in the United States is bladder cancer. In 1995, there were 50,000 new cases of bladder cancer reported and 11,000 deaths were reported as a result of this disease. The most common test for bladder cancer is the use of a urine "dipstick" or conventional urinalysis. However, such tests are generally only effective at detecting bladder cancer in its later developed stages and does not provide any information regarding the size or location of a cancerous growth. Cystoscopy, the main method of investigating bladder abnormalities at present, provides accurate results and can provide information regarding the relative size and location of any abnormalities. However, cystoscopy is an invasive procedure which offers a physician a limited field of view and lacks an objective indication of size. In addition, cystoscopy is contra-indicated for those patients who have severe urethral strictures or active vesical bleeding. Thus, it is desirable to develop alternative procedures for screening patients for bladder cancer, especially at early stages of cancer development.

Two-dimensional ("2D") visualization of human organs employing currently available medical imaging devices, such as computed tomography and MRI (magnetic resonance imaging), has been widely used for patient diagnosis. Three-dimensional images can be formed by stacking and interpolating between two-dimensional pictures produced from the scanning machines. Imaging an organ and visualizing its volume in three-dimensional space would be beneficial due to its lack of physical intrusion and the ease of data manipulation. However, the exploration of the three-dimensional volume image must be properly performed in order to fully exploit the advantages of virtually viewing an organ from the inside.

When viewing the three dimensional ("3D") volume virtual image of an environment, a functional model must be used to explore the virtual space. One possible model is a virtual camera which can be used as a point of reference for the viewer to explore the virtual space. Camera control in the context of navigation within a general 3D virtual environment has been previously studied. There are two

conventional types of camera control offered for navigation of virtual space. The first gives the operator full control of the camera which allows the operator to manipulate the camera in different positions and orientations to achieve the view desired. The operator will in effect pilot the camera. This allows the operator to explore a particular section of interest while ignoring other sections. However, complete control of a camera in a large domain would be tedious and tiring, and an operator might not view all the important features between the start and finishing point of the exploration.

The second technique of camera control is a planned navigation method, which assigns the camera a predetermined path to take and which cannot be changed by the operator. This is akin to having an engaged "autopilot". This allows the operator to concentrate on the virtual space being viewed, and not have to worry about steering into walls of the environment being examined. However, this second technique does not give the viewer the flexibility to alter the course or investigate an interesting area viewed along the flight path.

It would be desirable to use a combination of the two navigation techniques described above to realize the advantages of both techniques while minimizing their respective drawbacks. It would be desirable to apply a flexible navigation technique to the examination of human or animal organs which are represented in virtual 3D space in order to perform a non-intrusive painless thorough examination. The desired navigation technique would further allow for a complete examination of a virtual organ in 3D space by an operator allowing flexibility while ensuring a smooth path and complete examination through and around the organ. It would be additionally desirable to be able to display the exploration of the organ in a real time setting by using a technique which minimizes the computations necessary for viewing the organ. The desired technique should also be equally applicable to exploring any virtual object.

It is another object of the invention to assign opacity coefficients to each volume element in the representation in order to make particular volume elements transparent or translucent to varying degrees in order to customize the

visualization of the portion of the object being viewed. A section of the object can also be composited using the opacity coefficients.

SUMMARY OF THE INVENTION

The invention generates a three-dimensional visualization image of an object such as a human organ using volume visualization techniques and explores the virtual image using a guided navigation system which allows the operator to travel along a predefined flight path and to adjust both the position and viewing angle to a particular portion of interest in the image away from the predefined path in order to identify polyps, cysts or other abnormal features in the organ.

A method for performing virtual examination of an object includes performing at least one imaging scan of an object with the object distended by the presence of a contrast agent. In addition, at least one imaging scan of the object is acquired with the object relieved of the contrast agent. The scans are converted to corresponding volume datasets formed with a plurality of voxels. Image segmentation is then performed to classify the voxels of each scan into a plurality of categories. The volume datasets of each scan are registered to a common coordinate system. A displaying operation can then be performed where corresponding images at least two of the volume datasets are substantially simultaneously displayed. Virtual navigation operations performed in one of the volume datasets results in having the corresponding navigation operations take place in at least one other volume dataset.

Preferably, the at least one scan of the distended object includes a transverse scan and a coronal scan of the object. Similarly, it is preferable that the at least one scan of the relieved object includes a transverse scan and a coronal scan of the object. This procedure is particularly well suited for performing virtual cystoscopy, where the object is the bladder. In this case, the scan generally takes the form of a magnetic resonance imaging scan and the contrast agent can be urine.

Another method in accordance with the present invention is for performing virtual examination of an object. In this method, an imaging scan of the object is performed to acquire image scan data. The acquired image scan data is converted to a plurality of volume units, or voxels. By interpolating between the

voxels, an expanded dataset is generated. Image segmentation can then be performed to classify the voxels into a plurality of categories. A volume of the object interior is extracted from the expanded dataset, such as by using a region growing algorithm from a seed voxel within the object lumen. A reduced resolution dataset is then generated from the expanded dataset. To efficiently store and recall the data from the expanded data set, this data is stored in a tree data structure. Images can then be rendered for both the expanded dataset and reduced resolution dataset. One of these images is then selected for viewing. Generally, the reduced resolution dataset is selected during navigation or image interaction whereas the expanded dataset is selected for high resolution, static display.

A method of performing virtual angiography is also provided. In this method, imaging scan data is acquired of at least a portion of the aorta. The imaging scan data is converted to a volume representation including a plurality of voxels. The volume representation is segmented to classify the voxels into one of a plurality of categories. The segmented volume representation is then analyzed to identify voxels indicative of at least a portion of an aneurysm in the aortic wall. From the portions of the aneurysm which are identified, at least one closing surface is generated around the voxels indicative of at least a portion of an aneurysm. The closing surface provides an estimate of the contour of the aneurysm. A navigation path can be established through the aortic lumen and characteristics of the aneurysm, such as length, diameter, volume and composition, can be determined.

The method of performing virtual angiography can be used to detect and monitor the progression of aneurysms and can also be used in determining the characteristics needed to place a stent graft.

Also provided is a method of defining a skeleton for a three dimensional image representation of a hollow object formed with a plurality of voxels. A root voxel is first identified within the hollow object. A distance map is then generated for all voxels within the hollow object. The distance map is formed using a 26-connected cubic plate having Euclidian weighted distances. Those voxels having a local maxima in the distance map are identified as endpoints of branches in the hollow object. For each local maxima voxel, a shortest connected path to either

the root voxel or a previously defined shortest path, is determined. The collection of shortest paths is the rough skeleton of the object. This technique is particularly well suited for multibranch structures such as the respiratory system and cardio vascular system.

BRIEF DESCRIPTION OF THE DRAWINGS

Further objects, features and advantages of the invention will become apparent from the following detailed description taken in conjunction with the accompanying figures showing a preferred embodiment of the invention, on which:

Figure 1 is a flow chart of the steps for performing a virtual examination of an object, specifically a colon, in accordance with the invention;

Figure 2 is an illustration of a "submarine" camera model which performs guided navigation in the virtual organ;

Figure 3 is an illustration of a pendulum used to model pitch and roll of the "submarine" camera;

Figure 4 is a diagram illustrating a two dimensional cross-section of a volumetric colon which identifies two blocking walls;

Figure 5 is a diagram illustrating a two dimensional cross-section of a volumetric colon upon which start and finish volume elements are selected;

Figure 6 is a diagram illustrating a two dimensional cross-section of a volumetric colon which shows a discrete sub-volume enclosed by the blocking walls and the colon surface;

Figure 7 is a diagram illustrating a two dimensional cross-section of a volumetric colon which has multiple layers peeled away;

Figure 8 is a diagram illustrating a two dimensional cross-section of a volumetric colon which contains the remaining flight path;

Figure 9 is a flow chart of the steps of generating a volume visualization of the scanned organ;

Figure 10 is an illustration of a virtual colon which has been sub-divided into cells;

Figure 11A is a graphical depiction of an organ which is being virtually examined;

Figure 11B is a graphical depiction of a stab tree generated when depicting the organ in Fig. 11A;

Figure 11C is a further graphical depiction of a stab tree generated while depicting the organ in Fig. 11A;

Figure 12A is a graphical depiction of a scene to be rendered with objects within certain cells of the scene;

Figure 12B is a graphical depiction of a stab tree generated while depicting the scene in Fig. 12A;

Figures 12C-12E are further graphical depictions of stab trees generated while depicting the image in Fig. 12A;

Figure 13 is a two dimensional representation of a virtual colon containing a polyp whose layers can be removed;

Figure 14 is a diagram of a system used to perform a virtual examination of a human organ in accordance with the invention;

Figure 15 is a flow chart depicting an improved image segmentation method;

Figure 16 is a graph of voxel intensity versus frequency of a typical abdominal CT data set;

Figure 17 is a perspective view diagram of an intensity vector structure including a voxel of interest and its selected neighbors;

Figure 18A is an exemplary image slice from a CT scan of a human abdominal region, primarily illustrating a region including the lungs;

Figure 18B is a pictorial diagram illustrating the identification of the lung region in the image slice of Figure 18A;

Figure 18C is a pictorial diagram illustrating the removal of the lung volume identified in Figure 18B;

Figure 19A is a exemplary image slice form a CT scan of a human abdominal region, primarily illustrating a region including a portion of the colon and bone;

Figure 19B is a pictorial diagram illustrating the identification of the colon and bone region from the image slice of Figure 19A;

Figure 19C is a pictorial diagram illustrating the image scan of figure 19a with the regions of bone removed; and

Figure 20 is a flowchart illustrating a method for applying texture to monochrome image data.

Figure 21 is a flowchart illustrating a method for volume rendering employing a fast perspective ray casting technique;

Figure 22 is a flowchart illustrating a method for determining the central flight path through a colon lumen employing a volume shrinking technique.

Figure 23 is a flowchart further illustrating a volume shrinking technique for use in the method illustrated in Figure 22.

Figure 24 is a three dimensional pictorial representation of a segmented colon lumen with a central fly-path generated therein.

Figure 25 is a flow chart illustrating a method of generating a central flight path through a colon lumen employing a segmentation technique.

Figure 26 is a block diagram of a system embodiment based on a personal computer bus architecture.

Figure 27 is a flow chart illustrating a method of performing volume imaging using the system of Figure 26.

Figure 28 is a flow chart illustrating a multi-scan method for performing virtual examination of an object, such as a bladder (virtual cystoscopy).

Figure 29 is a pictorial representation of a display window suitable for presenting imaging results from the virtual cystoscopy method of Figure 28 and providing illustrative outside views of a bladder structure.

Figure 30 is a pictorial representation of a display window suitable for presenting imaging results from the virtual cystoscopy method of Figure 28 and providing illustrative interior views of a bladder structure.

Figure 31 is a flow chart of a method of performing virtual examination of an object, such as the larynx, using multiresolution viewing.

Figure 32 is a flow chart of a method for performing virtual angiography.

Figures 33A-C are pictorial views of a portion of the aorta illustrating the presence of an abdominal aortic aneurysm.

Figure 34 is a flow chart illustrating a method for generating a skeleton structure of an object.

Figure 35 is a schematic diagram of a 26-connected, Euclidean weighted, cubic distance plate.

Figure 36 is a diagram illustrating pseudo-code of a process for generating a distance map for use in the method of Figure 34.

DETAILED DESCRIPTION OF PREFERRED EMBODIMENTS

While the methods and systems described in this application can be applied to any object to be examined, the preferred embodiment which will be described is the examination of an organ in the human body, specifically the colon. The colon is long and twisted which makes it especially suited for a virtual examination saving the patient both money and the discomfort and danger of a physical probe. Other examples of organs which can be examined, without limitation, include the lungs, stomach and portions of the gastro-intestinal system, the heart and blood vessels.

Fig. 1 illustrates the steps necessary to perform a virtual colonoscopy using volume visualization techniques. Step 101 prepares the colon to be scanned in order to be viewed for examination if required by either the doctor or the particular scanning instrument. This preparation could include cleansing the colon with a "cocktail" or liquid which enters the colon after being orally ingested and passed through the stomach. The cocktail forces the patient to expel waste material that is present in the colon. One example of a substance used is Golytely. Additionally, in the case of the colon, air or CO_2 can be forced into the colon in order to expand it to make the colon easier to scan and examine. This is accomplished with a small tube placed in the rectum with approximately 1,000 cc of air pumped into the colon to distend the colon. Depending upon the type of scanner used, it may be necessary for

the patient to drink a contrast substance such as barium to coat any unexpunged stool in order to distinguish the waste in the colon from the colon walls themselves. Alternatively, the method for virtually examining the colon can remove the virtual waste prior to or during the virtual examination as explained later in this specification. Step 101 does not need to be performed in all examinations as indicated by the dashed line in Fig. 1.

Step 103 scans the organ which is to be examined. The scanner can be an apparatus well known in the art, such as a spiral CT-scanner for scanning a colon or a Zenita MRI machine for scanning a lung labeled for example with xenon gas. The scanner must be able to take multiple images from different positions around the body during suspended respiration, in order to produce the data necessary for the volume visualization. An example of a single CT-image would use an X-ray beam of 5mm width, 1:1 to 2:1 pitch, with a 40cm field-of-view being performed from the top of the splenic flexure of the colon to the rectum.

Discrete data representations of said object can be produced by other methods besides scanning. Voxel data representing an object can be derived from a geometric model by techniques described in U.S. Pat. No. 5,038,302 entitled "Method of Converting Continuous Three-Dimensional Geometrical Representations into Discrete Three-Dimensional Voxel-Based Representations Within a Three-Dimensional Voxel-Based System" by Kaufman, issued Aug. 8, 1991, filed July 26, 1988, which is hereby incorporated by reference. Additionally, data can be produced by a computer model of an image which can be converted to three-dimension voxels and explored in accordance with this invention. One example of this type of data is a computer simulation of the turbulence surrounding a space shuttle craft.

Step 104 converts the scanned images into three-dimensional volume elements (Voxels). In the preferred embodiment for examining a colon, the scan data is reformatted into 5mm thick slices at increments of 1mm or 2.5mm and reconstructed in 1mm slices, with each slice represented as a matrix of 512 by 512 pixels. By doing this, voxels of approximately 1 cubic mm are created. Thus a large number of 2D slices are generated depending upon the length of the scan. The set of 2D slices is then reconstructed to 3D voxels. The conversion process of 2D

images from the scanner into 3D voxels can either be performed by the scanning machine itself or by a separate machine such as a computer with techniques which are well known in the art (for example, see U.S. Pat. No. 4,985,856 entitled "Method and Apparatus for Storing, Accessing, and Processing Voxel-based Data" by Kaufman et al.; issued Jan. 15, 1991, filed Nov. 11, 1988; which is hereby incorporated by reference).

Step 105 allows the operator to define the portion of the selected organ to be examined. A physician may be interested in a particular section of the colon likely to develop polyps. The physician can view a two dimensional slice overview map to indicate the section to be examined. A starting point and finishing point of a path to be viewed can be indicated by the physician/operator. A conventional computer and computer interface (e.g., keyboard, mouse or spaceball) can be used to designate the portion of the colon which is to be inspected. A grid system with coordinates can be used for keyboard entry or the physician/operator can "click" on the desired points. The entire image of the colon can also be viewed if desired.

Step 107 performs the planned or guided navigation operation of the virtual organ being examined. Performing a guided navigation operation is defined as navigating through an environment along a predefined or automatically predetermined flight path which can be manually adjusted by an operator at any time. After the scan data has been converted to 3D voxels, the inside of the organ must be traversed from the selected start to the selected finishing point. The virtual examinations is modeled on having a tiny camera traveling through the virtual space with a lens pointing towards the finishing point. The guided navigation technique provides a level of interaction with the camera, so that the camera can navigate through a virtual environment automatically in the case of no operator interaction, and at the same time, allow the operator to manipulate the camera when necessary. The preferred embodiment of achieving guided navigation is to use a physically based camera model which employs potential fields to control the movement of the camera and which are described in detail in Figs. 2 and 3.

Step 109, which can be performed concurrently with step 107, displays the inside of the organ from the viewpoint of the camera model along the selected

pathway of the guided navigation operation. Three-dimensional displays can be generated using techniques well known in the art such as the marching cubes technique. However, in order to produce a real time display of the colon, a technique is required which reduces the vast number of computations of data necessary for the display of the virtual organ. Fig. 9 describe this display step in more detail.

The method described in Figure 1 can also be applied to scanning multiple organs in a body at the same time. For example, a patient may be examined for cancerous growths in both the colon and lungs. The method of Figure 1 would be modified to scan all the areas of interest in step 103 and to select the current organ to be examined in step 105. For example, the physician/operator may initially select the colon to virtually explore and later explore the lung. Alternatively, two different doctors with different specialties may virtually explore different scanned organs relating to their respective specialties. Following step 109, the next organ to be examined is selected and its portion will be defined and explored. This continues until all organs which need examination have been processed.

The steps described in conjunction with Figure 1 can also be applied to the exploration of any object which can be represented by volume elements. For example, an architectural structure or inanimate object can be represented and explored in the same manner.

Figure 2 depicts a "submarine" camera control model which performs the guided navigation technique in step 107. When there is no operator control during guided navigation, the default navigation is similar to that of planned navigation which automatically directs the camera along a flight path from one selected end of the colon to another. During the planned navigation phase, the camera stays at the center of the colon for obtaining better views of the colonic surface. When an interesting region is encountered, the operator of the virtual camera using guided navigation can interactively bring the camera close to a specific region and direct the motion and angle of the camera to study the interesting area in detail, without unwillingly colliding with the walls of the colon. The operator can control the camera with a standard interface device such as a keyboard, mouse or non-standard device such as a spaceball. In order to fully operate a camera in a virtual environment, six

degrees of freedom for the camera is required. The camera must be able to move in the horizontal, vertical, and Z direction (axes 217), as well as being able to rotate in another three degrees of freedom (axes 219) to allow the camera to move and scan all sides and angles of a virtual environment. The camera model for guided navigation includes an inextensible, weightless rod 201 connecting two particles x_1 203 and x_2 205, both particles being subjected to a potential field 215. The potential field is defined to be highest at the walls of the organ in order to push the camera away from the walls.

The positions of the particles are given by x_1 and x_2, and they are assumed to have the same mass m. A camera is attached at the head of the submarine x_1 203, whose viewing direction coincides with x_2x_1. The submarine can perform translation and rotation around the center of mass x of the model as the two particles are affected by the forces from the potential field $V(x)$ which is defined below, any friction forces, and any simulated external force. The relations between x_1, x_2, and x are as follows:

$$\begin{aligned} x &= (x,y,z), \\ r &= (r\sin\theta\cos\varphi, r\sin\theta\sin\varphi, r\cos\theta), \\ x_1 &= x + r, \\ x_2 &= x - r, \end{aligned} \qquad (1)$$

where r, θ and φ are the polar coordinates of the vector xx_1.

The kinetic energy of the model, T, is defined as the summation of the kinetic energies of the movements of x_1 and x_2:

$$\begin{aligned} T &= \frac{m}{2}(\dot{x}_1^2 + \dot{x}_2^2) \\ &= m\dot{x}^2 + m\dot{r}^2 \\ &= m(\dot{x}^2 + \dot{y}^2 + \dot{z}^2) + mr^2(\dot{\theta}^2 + \dot{\phi}^2\sin^2\theta). \end{aligned} \qquad (2)$$

Then, the equations for the motion of the submarine model are obtained by using LaGrange's equation:

$$\frac{d}{dt}\left(\frac{\partial T}{\partial \dot{q}_j}\right) - \frac{\partial T}{\partial q_j} = \sum_{i=1}^{2}\left(\mathbf{F}_i \cdot \frac{\partial \mathbf{x}_i}{\partial q_j}\right), \tag{3}$$

where the q_js are the *generalized coordinates* of the model and can be considered as the variables of time t as:

$$(q_1, q_2, q_3, q_4, q_5, q_6) = (x, y, z, \theta, \phi, \psi) = \mathbf{q}(t), \tag{4}$$

with ψ denoting the *roll angle* of our camera system, which will be explained later. The $\mathbf{F}_i$s are called the *generalized forces*. The control of the submarine is performed by applying a simulated external force to x_1,

$$\mathbf{F}_{ext} = (F_x, F_y, F_z),$$

and it is assumed that both x_1 and x_2 are affected by the forces from the potential field and the frictions which act in the opposite direction of each particle's velocity. Consequently, the generalized forces are formulated as follows:

$$\begin{aligned} \mathbf{F}_1 &= -m\nabla V(\mathbf{x}_1) - k\dot{\mathbf{x}}_1 + \mathbf{F}_{ext}, \\ \mathbf{F}_2 &= -m\nabla V(\mathbf{x}_2) - k\dot{\mathbf{x}}_2, \end{aligned} \tag{5}$$

where k denotes the friction coefficient of the system. The external force $\mathbf{F}_{ext}$ is applied by the operator by simply clicking the mouse button in the desired direction 207 in the generated image, as shown in Figure 2. This camera model would then be moved in that direction. This allows the operator to control at least five degrees of freedom of the camera with only a single click of the mouse button. From Equations (2), (3) and (5), it can be derived that the accelerations of the five parameters of our submarine model as:

$$
\begin{aligned}
\ddot{x} &= -\frac{1}{2}\left(\frac{\partial V(\mathbf{x}_1)}{\partial x}+\frac{\partial V(\mathbf{x}_2)}{\partial x}\right)-\frac{k\dot{x}}{m}+\frac{F_x}{2m},\\
\ddot{y} &= -\frac{1}{2}\left(\frac{\partial V(\mathbf{x}_1)}{\partial y}+\frac{\partial V(\mathbf{x}_2)}{\partial y}\right)-\frac{k\dot{y}}{m}+\frac{F_y}{2m},\\
\ddot{z} &= -\frac{1}{2}\left(\frac{\partial V(\mathbf{x}_1)}{\partial z}+\frac{\partial V(\mathbf{x}_2)}{\partial z}\right)-\frac{k\dot{z}}{m}+\frac{F_z}{2m},\\
\ddot{\theta} &= \dot{\phi}^2\sin\theta\cos\theta\\
&\quad -\frac{1}{2r}\{\cos\theta\{\cos\phi\left(\frac{\partial V(\mathbf{x}_1)}{\partial x}-\frac{\partial V(\mathbf{x}_2)}{\partial x}\right)+\sin\phi\left(\frac{\partial V(\mathbf{x}_1)}{\partial y}-\frac{\partial V(\mathbf{x}_2)}{\partial y}\right)\}\\
&\quad -\sin\theta\left(\frac{\partial V(\mathbf{x}_1)}{\partial z}-\frac{\partial V(\mathbf{x}_2)}{\partial z}\right)]\\
&\quad -\frac{k}{m}\dot{\theta}+\frac{1}{2mr}(F_x\cos\theta\cos\phi+F_y\cos\theta\sin\phi-F_z\sin\theta),\\
\ddot{\phi} &= \frac{1}{\sin\theta}[-2\dot{\theta}\dot{\phi}\cos\theta\\
&\quad -\frac{1}{2r}\{-\sin\phi\left(\frac{\partial V(\mathbf{x}_1)}{\partial x}-\frac{\partial V(\mathbf{x}_2)}{\partial x}\right)+\cos\phi\left(\frac{\partial V(\mathbf{x}_1)}{\partial y}-\frac{\partial V(\mathbf{x}_2)}{\partial y}\right)\}\\
&\quad -\frac{k}{m}\dot{\phi}\sin\theta+\frac{1}{2mr}(-F_x\sin\phi+F_y\cos\phi)],
\end{aligned}
\tag{6}
$$

where $\dot{x}$ and $\ddot{x}$ denote the first and the second derivative of x, respectively, and

$\left(\frac{\partial V(x)}{\partial x},\frac{\partial V(x)}{\partial y},\frac{\partial V(x)}{\partial z}\right)$ denotes the gradient of the potential at a point x.

The terms $\dot{\phi}^2\sin\theta\cos\theta$ of $\ddot{\theta}$ and $-\frac{2\dot{\theta}\dot{\phi}\cos\theta}{\sin\theta}$ of $\ddot{\phi}$ are called the

centrifugal force and the *Coriolis force*, respectively, and they are concerned with the exchange of angular velocities of the submarine. Since the model does not have the moment of inertia defined for the rod of the submarine, these terms tend to cause an overflow of the numeric calculation of φ. Fortunately, these terms become significant

only when the angular velocities of the submarine model are significant, which essentially means that the camera moves too fast. Since it is meaningless to allow the camera to move so fast because the organ could not be properly viewed, these terms are minimized in our implementation to avoid the overflow problem.

From the first three formulas of Equation (6), it is known that the submarine cannot be propelled by the external force against the potential field if the following condition is satisfied:

$$|\nabla V(\mathbf{x}_1) + \nabla V(\mathbf{x}_2)| > \frac{|\mathbf{F}_{ext}|}{m}.$$

Since the velocity of the submarine and the external force $\mathbf{F}_{ext}$ have upper limits in our implementation, by assigning sufficiently high potential values at the boundary of the objects, it can be guaranteed that the submarine never bumps against the objects or walls in the environment.

As mentioned previously, the roll angle ψ of the camera system needs to be considered. One possible option allows the operator full control of the angle ψ. However, although the operator can rotate the camera freely around the rod of the model, he or she can easily become disoriented. The preferred technique assumes that the upper direction of the camera is connected to a pendulum with mass m_2 301, which rotates freely around the rod of the submarine, as shown in Figure 3. The direction of the pendulum, $\mathbf{r}_2$, is expressed as:

$$\mathbf{r}_2 = r_2(\cos\theta\cos\phi\sin\psi + \sin\phi\cos\psi, \cos\theta\sin\phi\sin\psi - \cos\phi\cos\psi, -\sin\theta\sin\psi).$$

although it is possible to calculate the accurate movement of this pendulum along with the movement of the submarine, it makes the system equations too complicated. Therefore, it is assumed that all the generalized coordinates except the roll angle ψ are constants, and thus define the independent kinetic energy for the pendulum system as:

$$T_p = \frac{m_2}{2}\dot{r}_2^2 = \frac{m_2 r_2^2}{2}\dot{\psi}^2.$$

This simplifies the model for the roll angle. Since it is assumed in this model that the gravitational force

$$\mathbf{F}_g = m_2\mathbf{g} = (m_2 g_x, m_2 g_y, m_2 g_z)$$

acts at the mass point m_2, the acceleration of ψ can be derived using LaGrange's equation as:

$$\begin{aligned}\ddot{\psi} &= \frac{1}{r_2}\{g_x(\cos\theta\cos\phi\cos\psi - \sin\phi\sin\psi) \\ &\quad + g_y(\cos\theta\sin\phi\cos\psi + \cos\phi\sin\psi) \\ &\quad + g_z(-\sin\theta\cos\psi)\} - \frac{k_2}{m_2}\dot{\psi}. \qquad (7)\end{aligned}$$

From Equations (6) and (7), the generalized

coordinates q(t) and their derivatives $\dot{\mathbf{q}}(t)$ are calculated asymptotically by using *Taylor series* as:

$$\begin{aligned}\mathbf{q}(t+h) &= \mathbf{q}(t) + h\dot{\mathbf{q}}(t) + \frac{h^2}{2}\ddot{\mathbf{q}}(t) + O(h^3), \\ \dot{\mathbf{q}}(t+h) &= \dot{\mathbf{q}}(t) + h\ddot{\mathbf{q}}(t) + O(h^2),\end{aligned}$$

to freely move the submarine. To smooth the submarine's motion, the time step h is selected as an equilibrium value between being as small as possible to smooth the motion but as large as necessary to reduce computation cost.

Definition of the Potential Field

The potential field in the submarine model in Figure 2 defines the boundaries (walls or other matter) in the virtual organ by assigning a high potential to the boundary in order to ensure that the submarine camera does not collide with the walls or other boundary. If the camera model is attempted to be moved into a high potential area by the operator, the camera model will be restrained from doing so unless the operator wishes to examine the organ behind the boundary or inside a polyp, for example. In the case of performing a virtual colonoscopy, a potential field value is assigned to each piece of volumetric colon data (volume element). When a particular region of interest is designated in step 105 of Fig. 1 with a start and finish point, the voxels within the selected area of the scanned colon are identified using conventional blocking operations. Subsequently, a potential value is assigned to every voxel x of the selected volume based on the following three distance values: the distance from the finishing point dt(x), the distance from the colon surface ds(x) and the distance from the center-line of the colon space dc(x). dt(x) is calculated by using a conventional growing strategy. The distance from the colon surface, ds(x), is computed using a conventional technique of growing from the surface voxels inwards. To determine dc(x), the center-line of the colon from the voxel is first extracted, and then dc(x) is computed using the conventional growing strategy from the center-line of the colon.

To calculate the center-line of the selected colon area defined by the user-specified start point and the user-specified finish point, the maximum value of ds(x) is located and denoted dmax. Then for each voxel inside the area of interest, a cost value of dmax - ds(x) is assigned. Thus the voxels which are close to the colon surface have high cost values and the voxels close to the center line have relatively low cost values. Then, based on the cost assignment, the single-source shortest path technique which is well known in the art is applied to efficiently compute a minimum cost path from the source point to the finish point. This low cost line indicates the center-line or skeleton of the colon section which is desired to be explored. This technique for determining the center-line is the preferred technique of the invention.

To compute the potential value V(x) for a voxel x inside the area of interest, the following formula is employed:

$$V(\mathbf{x}) = C_1 d_t(\mathbf{x})^{\mu} + C_2\left(\frac{d_s(\mathbf{x})}{d_c(\mathbf{x}) + d_s(\mathbf{x})}\right)^{-\nu}, \qquad (8)$$

where C_1, C_2, μ and ν are constants chosen for the task. In order to avoid any collision between the virtual camera and the virtual colonic surface, a sufficiently large potential value is assigned for all points outside the colon. The gradient of the potential field will therefore become so significant that the submarine model camera will never collide with the colonic wall when being run.

Another technique to determine the center-line of the path in the colon is called the "peel-layer" technique and is shown in Figure 4 through Figure 8.

Figure 4 shows a 2D cross-section of the volumetric colon, with the two side walls 401 and 403 of the colon being shown. Two blocking walls are selected by the operator in order to define the section of the colon which is of interest to examine. Nothing can be viewed beyond the blocking walls. This helps reduce the number of computations when displaying the virtual representation. The blocking walls together with side walls identify a contained volumetric shape of the colon which is to be explored.

Figure 5 shows two end points of the flight path of the virtual examination, the start volume element 501 and the finish volume element 503. The start and finish points are selected by the operator in step 105 of Fig. 1. The voxels between the start and finish points and the colon sides are identified and marked, as indicated by the area designated with "x"s in Fig. 6. The voxels are three-dimensional representations of the picture element.

The peel-layer technique is then applied to the identified and marked voxels in Fig. 6. The outermost layer of all the voxels (closest to the colon walls) is peeled off step-by-step, until there is only one inner layer of voxels remaining. Stated differently, each voxel furthest away from a center point is removed if the removal does not lead to a disconnection of the path between the start voxel and the finish

voxel. Figure 7 shows the intermediate result after a number of iterations of peeling the voxels in the virtual colon are complete. The voxels closest to the walls of the colon have been removed. Fig. 8 shows the final flight path for the camera model down the center of the colon after all the peeling iterations are complete. This produces essentially a skeleton at the center of the colon and becomes the desired flight path for the camera model.

Z- Buffer assisted visibility

Figure 9 describes a real time visibility technique to display of virtual images seen by the camera model in the virtual three-dimensional volume representation of an organ. Figure 9 shows a display technique using a modified Z buffer which corresponds to step 109 in Fig. 1. The number of voxels which could be possibly viewed from the camera model is extremely large. Unless the total number of elements (or polygons) which must be computed and visualized is reduced from an entire set of voxels in the scanned environment, the overall number of computations will make the visualization display process exceedingly slow for a large internal area. However, in the present invention only those images which are visible on the colon surface need to be computed for display. The scanned environment can be subdivided into smaller sections, or cells. The Z buffer technique then renders only a portion of the cells which are visible from the camera. The Z buffer technique is also used for three-dimensional voxel representations. The use of a modified Z buffer reduces the number of visible voxels to be computed and allows for the real time examination of the virtual colon by a physician or medical technician.

The area of interest from which the center-line has been calculated in step 107 is subdivided into cells before the display technique is applied. Cells are collective groups of voxels which become a visibility unit. The voxels in each cell will be displayed as a group. Each cell contains a number of portals through which the other cells can be viewed. The colon is subdivided by beginning at the selected start point and moving along the center-line 1001 towards the finish point. The colon is then partitioned into cells (for example, cells 1003, 1005 and 1007 in Fig. 10) when a predefined threshold distance along the center-path is reached. The threshold

distance is based upon the specifications of the platform upon which the visualization technique is performed and its capabilities of storage and processing. The cell size is directly related to the number of voxels which can be stored and processed by the platform. One example of a threshold distance is 5cm, although the distance can greatly vary. Each cell has two cross-sections as portals for viewing outside of the cell as shown in Fig. 10.

Step 901 in Fig. 9 identifies the cell within the selected organ which currently contains the camera. The current cell will be displayed as well as all other cells which are visible given the orientation of the camera. Step 903 builds a stab tree (tree diagram) of hierarchical data of potentially visible cells from the camera (through defined portals), as will be described in further detail hereinbelow. The stab tree contains a node for every cell which may be visible to the camera. Some of the cells may be transparent without any blocking bodies present so that more than one cell will be visible in a single direction. Step 905 stores a subset of the voxels from a cell which include the intersection of adjoining cell edges and stores them at the outside edge of the stab tree in order to more efficiently determine which cells are visible.

Step 907 checks if any loop nodes are present in the stab tree. A loop node occurs when two or more edges of a single cell both border on the same nearby cell. This may occur when a single cell is surrounded by another cell. If a loop node is identified in the stab tree, the method continues with step 909. If there is no loop node, the process goes to step 911.

Step 909 collapses the two cells making up the loop node into one large node. The stab tree is then corrected accordingly. This eliminates the problem of viewing the same cell twice because of a loop node. The step is performed on all identified loop nodes. The process then continues with step 911.

Step 911 then initiates the Z-buffer with the largest Z value. The Z value defines the distance away from the camera along the skeleton path. The tree is then traversed to first check the intersection values at each node. If a node intersection is covered, meaning that the current portal sequence is occluded (which is determined by the Z buffer test), then the traversal of the current branch in the tree is

stopped. Step 913 traverses each of the branches to check if the nodes are covered and displays them if they are not.

Step 915 then constructs the image to be displayed on the operator's screen from the volume elements within the visible cells identified in step 913 using one of a variety of techniques known in the art, such as volume rendering by compositing. The only cells shown are those which are identified as potentially visible. This technique limits the number of cells which requires calculations in order to achieve a real time display and correspondingly increases the speed of the display for better performance. This technique is an improvement over prior techniques which calculate all the possible visible data points whether or not they are actually viewed.

Figure 11A is a two dimensional pictorial representation of an organ which is being explored by guided navigation and needs to be displayed to an operator. Organ 1101 shows two side walls 1102 and an object 1105 in the center of the pathway. The organ has been divided into four cells A 1151, B 1153, C 1155 and D 1157. The camera 1103 is facing towards cell D 1157 and has a field of vision defined by vision vectors 1107, 1108 which can identify a cone-shaped field. The cells which can be potentially viewed are cells B 1153, C 1155 and D 1157. Cell C 1155 is completely surrounded by Cell B and thus constitutes a node loop.

Fig. 11B is a representation of a stab tree built from the cells in Fig. 11A. Node A 1109 which contains the camera is at the root of the tree. A sight line or sight cone, which is a visible path without being blocked, is drawn to node B 1110. Node B has direct visible sight lines to both node C 1112 and node D 1114 and which is shown by the connecting arrows. The sight line of node C 1112 in the direction of the viewing camera combines with node B 1110. Node C 1112 and node B 1110 will thus be collapsed into one large node B' 1122 as shown in Fig. 11C.

Fig. 11C shows node A 1109 containing the camera adjacent to node B' 1122 (containing both nodes B and node C) and node D 1114. The nodes A, B' and D will be displayed at least partially to the operator.

Figs 12A - 12E illustrate the use of the modified Z buffer with cells that contain objects which obstruct the views. An object could be some waste

material in a portion of the virtual colon. Fig. 12A shows a virtual space with 10 potential cells: A 1251, B 1253, C 1255, D 1257, E 1259, F 1261, G 1263, H 1265, I 1267 and J 1269. Some of the cells contain objects. If the camera 1201 is positioned in cell I 1267 and is facing toward cell F 1261 as indicated by the vision vectors 1203, then a stab tree is generated in accordance with the technique illustrated by the flow diagram in Fig. 9. Fig. 12B shows the stab tree generated with the intersection nodes showing for the virtual representation as shown in Fig. 12A. Fig. 12B shows cell I 1267 as the root node of the tree because it contains the camera 1201. Node I 1211 is pointing to node F 1213 (as indicated with an arrow), because cell F is directly connected to the sight line of the camera. Node F 1213 is pointing to both node B 1215 and node E 1219. Node B 1215 is pointing to node A 1217. Node C 1202 is completely blocked from the line of sight by camera 1201 so is not included in the stab tree.

Fig. 12C shows the stab tree after node I 1211 is rendered on the display for the operator. Node I 1211 is then removed from the stab tree because it has already been displayed and node F 1213 becomes the root. Fig. 12D shows that node F 1213 is now rendered to join node I 1211. The next nodes in the tree connected by arrows are then checked to see if they are already covered (already processed). In this example, all of the intersected nodes from the camera positioned in cell I 1267 has been covered so that node B 515 (and therefore dependent node A) do not need to be rendered on the display.

Fig. 12E shows node E 515 being checked to determine if its intersection has been covered. Since it has, the only rendered nodes in this example of Figure 12A-12E are nodes I and F while nodes A, B and E are not visible and do not need to have their cells prepared to be displayed.

The modified Z buffer technique described in Figure 9 allows for fewer computations and can be applied to an object which has been represented by voxels or other data elements, such as polygons.

Figure 13 shows a two dimensional virtual view of a colon with a large polyp present along one of its walls. Figure 13 shows a selected section of a patient's colon which is to be examined further. The view shows two colon walls 1301 and

1303 with the growth indicated as 1305. Layers 1307, 1309, and 1311 show inner layers of the growth. It is desirable for a physician to be able to peel the layers of the polyp or tumor away to look inside of the mass for any cancerous or other harmful material. This process would in effect perform a virtual biopsy of the mass without actually cutting into the mass. Once the colon is represented virtually by voxels, the process of peeling away layers of an object is easily performed in a similar manner as described in conjunction with Figs. 4 through 8. The mass can also be sliced so that a particular cross-section can be examined. In Fig. 13, a planar cut 1313 can be made so that a particular portion of the growth can be examined. Additionally, a user-defined slice 1319 can be made in any manner in the growth. The voxels 1319 can either be peeled away or modified as explained below.

A transfer function can be performed to each voxel in the area of interest which can make the object transparent, semi-transparent or opaque by altering coefficients representing the translucently for each voxel. An opacity coefficient is assigned to each voxel based on its density. A mapping function then transforms the density value to a coefficient representing its translucency. A high density scanned voxel will indicate either a wall or other dense matter besides simply open space. An operator or program routine could then change the opacity coefficient of a voxel or group of voxels to make them appear transparent or semi-transparent to the submarine camera model. For example, an operator may view a tumor within or outside of an entire growth. Or a transparent voxel will be made to appear as if it is not present for the display step of Figure 9. A composite of a section of the object can be created using a weighted average of the opacity coefficients of the voxels in that section.

If a physician desires to view the various layers of a polyp to look for a cancerous areas, this can be performed by removing the outer layer of polyp 1305 yielding a first layer 1307. Additionally, the first inner layer 1307 can be stripped back to view second inner layer 1309. The second inner layer can be stripped back to view third inner layer 1311, etc. The physician could also slice the polyp 1305 and view only those voxels within a desired section. The slicing area can be completely user-defined.

Adding an opacity coefficient can also be used in other ways to aid in the exploration of a virtual system. If waste material is present and has a density as other properties within a certain known range, the waste can be made transparent to the virtual camera by changing its opacity coefficient during the examination. This will allow the patient to avoid ingesting a bowel cleansing agent before the procedure and make the examination faster and easier. Other objects can be similarly made to disappear depending upon the actual application. Additionally, some objects like polyps could be enhanced electronically by a contrast agent followed by a use of an appropriate transfer function.

Figure 14 shows a system for performing the virtual examination of an object such as a human organ using the techniques described in this specification. Patient 1401 lies down on a platform 1402 while scanning device 1405 scans the area that contains the organ or organs which are to be examined. The scanning device 1405 contains a scanning portion 1403 which actually takes images of the patient and an electronics portion 1406. Electronics portion 1406 comprises an interface 1407, a central processing unit 1409, a memory 1411 for temporarily storing the scanning data, and a second interface 1413 for sending data to the virtual navigation platform. Interface 1407 and 1413 could be included in a single interface component or could be the same component. The components in portion 1406 are connected together with conventional connectors.

In system 1400, the data provided from the scanning portion of device 1403 is transferred to portion 1405 for processing and is stored in memory 1411. Central processing unit 1409 converts the scanned 2D data to 3D voxel data and stores the results in another portion of memory 1411. Alternatively, the converted data could be directly sent to interface unit 1413 to be transferred to the virtual navigation terminal 1416. The conversion of the 2D data could also take place at the virtual navigation terminal 1416 after being transmitted from interface 1413. In the preferred embodiment, the converted data is transmitted over carrier 1414 to the virtual navigation terminal 1416 in order for an operator to perform the virtual examination. The data could also be transported in other conventional ways such as

storing the data on a storage medium and physically transporting it to terminal 1416 or by using satellite transmissions.

The scanned data may not be converted to its 3D representation until the visualization rendering engine requires it to be in 3D form. This saves computational steps and memory storage space.

Virtual navigation terminal 1416 includes a screen for viewing the virtual organ or other scanned image, an electronics portion 1415 and interface control 1419 such as a keyboard, mouse or spaceball. Electronics portion 1415 comprises a interface port 1421, a central processing unit 1423, other components 1427 necessary to run the terminal and a memory 1425. The components in terminal 1416 are connected together with conventional connectors. The converted voxel data is received in interface port 1421 and stored in memory 1425. The central processor unit 1423 then assembles the 3D voxels into a virtual representation and runs the submarine camera model as described in Figures 2 and 3 to perform the virtual examination. As the submarine camera travels through the virtual organ, the visibility technique as described in Figure 9 is used to compute only those areas which are visible from the virtual camera and displays them on screen 1417. A graphics accelerator can also be used in generating the representations. The operator can use interface device 1419 to indicate which portion of the scanned body is desired to be explored. The interface device 1419 can further be used to control and move the submarine camera as desired as discussed in Figure 2 and its accompanying description. Terminal portion 1415 can be the Cube-4 dedicated system box, generally available from the Department of Computer Science at the State University of New York at Stony Brook.

Scanning device 1405 and terminal 1416, or parts thereof, can be part of the same unit. A single platform would be used to receive the scan image data, connect it to 3D voxels if necessary and perform the guided navigation.

An important feature in system 1400 is that the virtual organ can be examined at a later time without the presence of the patient. Additionally, the virtual examination could take place while the patient is being scanned. The scan data can also be sent to multiple terminals which would allow more than one doctor to view

the inside of the organ simultaneously. Thus a doctor in New York could be looking at the same portion of a patient's organ at the same time with a doctor in California while discussing the case. Alternatively, the data can be viewed at different times. Two or more doctors could perform their own examination of the same data in a difficult case. Multiple virtual navigation terminals could be used to view the same scan data. By reproducing the organ as a virtual organ with a discrete set of data, there are a multitude of benefits in areas such as accuracy, cost and possible data manipulations.

The above described techniques can be further enhanced in virtual colonoscopy applications through the use of an improved electronic colon cleansing technique which employs modified bowel preparation operations followed by image segmentation operations, such that fluid and stool remaining in the colon during a computed tomographic (CT) or magnetic resonance imaging (MRI) scan can be detected and removed from the virtual colonoscopy images. Through the use of such techniques, conventional physical washing of the colon, and its associated inconvenience and discomfort, is minimized or completely avoided.

Referring to Figure 15, the first step in electronic colon cleansing is bowel preparation (step 1510), which takes place prior to conducting the CT or magnetic resonance imaging (MRI) scan and is intended to create a condition where residual stool and fluid remaining in the colon present significantly different image properties from that of the gas-filled colon interior and colon wall. An exemplary bowel preparation operation includes ingesting three 250 cc doses of Barium Sulfate suspension of 2.1 % W/V, such as manufactured by E-Z-EM, Inc.,of Westbury, New York, during the day prior the CT or MRI scan. The three doses should be spread out over the course of the day and can be ingested along with three meals, respectively. The Barium Sulfate serves to enhance the images of any stool which remains in the colon. In addition to the intake of Barium Sulfate, fluid intake is preferably increased during the day prior to the CT or MRI scan. Cranberry juice is known to provide increased bowel fluids and is preferred, although water can also be ingested. In both the evening prior to the CT scan and the morning of the CT scan, 60 ml of a Diatrizoate Meglumine and Diaztrizoate Sodium Solution, which is commercially

available as MD-Gastroview, manufactured by Mallinckrodt, Inc. of St. Louis, Missouri, can be consumed to enhance image properties of the colonic fluid. Sodium phosphate can also be added to the solution to liquidize the stool in the colon, which provides for more uniform enhancement of the colonic fluid and residual stool.

The above described exemplary preliminary bowel preparation operation can obviate the need for conventional colonic washing protocols, which can call for the ingestion of a gallon of Golytely solution prior to a CT scan.

Just prior to conducting the CT scan, an intravenous injection of 1 ml of Glucagon, manufactured by Ely Lily and Company, of Indianapolis, Indiana can be administered to minimize colon collapse. Then, the colon can be inflated using approximately 1000cc of compressed gas, such as CO_2, or room air, which can be introduced through a rectum tube. At this point, a conventional CT scan is performed to acquire data from the region of the colon (step 1520). For example, data can be acquired using a GE/CTI spiral mode scanner operating in a helical mode of 5mm, 1.5-2.0:1 pitch, reconstructed in 1mm slices, where the pitch is adjusted based upon the patient's height in a known manner. A routine imaging protocol of 120 kVp and 200-280 ma can be utilized for this operation. The data can be acquired and reconstructed as 1mm thick slice images having an array size of 512x512 pixels in the field of view, which varies from 34 to 40 cm depending on the patient's size. the number of such slices generally varies under these conditions from 300 to 450, depending on the patient's height. The image data set is converted to volume elements or voxels (step 1530).

Image segmentation can be performed in a number of ways. In one present method of image segmentation, a local neighbor technique is used to classify voxels of the image data in accordance with similar intensity values. In this method, each voxel of an acquired image is evaluated with respect to a group of neighbor voxels. The voxel of interest is referred to as the central voxel and has an associated intensity value. A classification indicator for each voxel is established by comparing the value of the central voxel to each of its neighbors. If the neighbor has the same value as the central voxel, the value of the classification indicator is incremented. However, if the neighbor has a different value from the central voxel, the

classification indicator for the central voxel is decremented. The central voxel is then classified to that category which has the maximum indicator value, which indicates the most uniform neighborhood among the local neighbors. Each classification is indicative of a particular intensity range, which in turn is representative of one or more material types being imaged. The method can be further enhanced by employing a mixture probability function to the similarity classifications derived.

An alternate process of image segmentation is performed as two major operations: low level processing and high level feature extraction. During low level processing, regions outside the body contour are eliminated from further processing and voxels within the body contour are roughly categorized in accordance with well defined classes of intensity characteristics. For example, a CT scan of the abdominal region generates a data set which tends to exhibit a well defined intensity distribution. The graph of Figure 16 illustrates such an intensity distribution as an exemplary histogram having four, well defined peaks, 1602, 1604, 1606, 1608, which can be classified according to intensity thresholds.

The voxels of the abdominal CT data set are roughly classified as four clusters by intensity thresholds (step 1540). For example, Cluster 1 can include voxels whose intensities are below 140. This cluster generally corresponds to the lowest density regions within the interior of the gas filled colon. Cluster 2 can include voxels which have intensity values in excess of 2200. These intensity values correspond to the enhanced stool and fluid within the colon as well as bone. Cluster 3 can include voxels with intensities in the range of about 900 to about 1080. This intensity range generally represents soft tissues, such as fat and muscle, which are unlikely to be associated with the colon. The remaining voxels can then be grouped together as cluster 4, which are likely to be associated with the colon wall (including mucosa and partial volume mixtures around the colon wall) as well as lung tissue and soft bones.

Clusters 1 and 3 are not particularly valuable in identifying the colon wall and, therefore are not subject to substantial processing during image segmentation procedures for virtual colonoscopy. The voxels associated with cluster 2 are important for segregating stool and fluid from the colon wall and are processed

further during the high-level feature extraction operations. Low level processing is concentrated on the fourth cluster, which has the highest likelihood of corresponding to colon tissue (step 1550).

For each voxel in the fourth cluster, an intensity vector is generated using itself and its neighbors. The intensity vector provides an indication of the change in intensity in the neighborhood proximate a given voxel. The number of neighbor voxels which are used to establish the intensity vector is not critical, but involves a tradeoff between processing overhead and accuracy. For example, a simple voxel intensity vector can be established with seven (7) voxels, which includes the voxel of interest, its front and back neighbors, its left and right neighbors and its top and bottom neighbors, all surrounding the voxel of interest on three mutually perpendicular axes. Figure 17 is a perspective view illustrating an exemplary intensity vector in the form of a 25 voxel intensity vector model, which includes the selected voxel 1702 as well as its first, second and third order neighbors. The selected voxel 1702 is the central point of this model and is referred to as the fixed voxel. A planar slice of voxels, which includes 12 neighbors on the same plane as the fixed voxel, is referred to as the fixed slice 1704. On adjacent planes to the fixed slice are two nearest slices 1706, having five voxels each. Adjacent to the first nearest slices 1706 are two second nearest slices 1708, each having a single voxel. The collection of intensity vectors for each voxel in the fourth cluster is referred to as a local vector series.

Because the data set for an abdominal image generally includes more than 300 slice images, each with a 512 x 512 voxel array, and each voxel having an associated 25 voxel local vector, it is desirable to perform feature analysis (step 1570) on the local vector series to reduce the computational burden. One such feature analysis is a principal component analysis (PCA), which can be applied to the local vector series to determine the dimension of a feature vector series and an orthogonal transformation matrix for the voxels of cluster 4.

It has been found that the histogram (Figure 16) of the CT image intensities tends to be fairly constant from patient to patient for a particular scanner, given equivalent preparation and scanning parameters. Relying on this observation,

an orthogonal transformation matrix can be established which is a predetermined matrix determined by using several sets of training data acquired using the same scanner under similar conditions. From this data, a transformation matrix, such as a Karhunen-Loéve (K-L) transformation, can be generated in a known manner. The transformation matrix is applied to the local vector series to generate feature vector series. Once in the feature-vector space domain, vector quantization techniques can be used to classify the feature vector series.

An analytical, self-adaptive algorithm can be used for the classification of the feature vectors. In defining this algorithm, let $\{X_i \in R^1; i = 1,2,3,...,N\}$ be the series of the feature vectors, where N is the number of feature vectors; K denotes the maximum number of classes; and T is a threshold which is adaptive to the data set. For each class, a representative element is generated by the algorithm. Let a_k be a representative element of class k and n_k be the number of feature vectors in that class.

The algorithm can then be outlined as:

1. $Set\ n_1=1;\ a_1=X_1;\ \overline{K}=1;$

2. obtain the class number $\overline{K}$ and class parameters (a_k, n_k)
   for (i=1; i<N; i++)
      for ($j=1; j<\overline{K}; j++$)
         calculate $d_j = dist(X_i, a_j)$;
      end for
      index=arc min d_j;
      if $\{(d_{index} < T)\ or\ (\overline{K}=K)\}$

         update class parameters:

$$a_{index} = \frac{1}{n_{index}+1} \times (n_{index} * a_{index} + X_i);$$
$$n_{index} = n_{index} + 1;$$

end if

else

generate new class

$$a_{\overline{K}+1} = X_i;$$
$$n_{\overline{K}+1} = 1;$$
$$\overline{K} = \overline{K}+1;$$

end else

end for

3. label each feature vector to a class according to the nearest neighbor rule

for {i=1; i<N; i++}

for {j=1; j<$\overline{K}$; j++}

calculate $d_j = dist(X_i, a_j)$;

end for

index = *arc* min d_j

label voxel *i* to class *index*.

end for

In this algorithm, *dist(x,y)* is the Euclidean distance between vector *x* and *y* and *arc* min d_j gives the integer *j* which realizes the minimum value of d_j.

The above described algorithm is dependent only on the parameters *T* and *K*. However, the value of K, which relates to the number of classes within each voxel cluster, is not critical and can be set to a constant value, such as K=18. However, T, which is the vector similarity threshold, greatly influences the classification results. If the selected value of T is too large, only a single class will be generated. On the other hand, if the value of T is too small, the resulting classes will exhibit undesirable redundancy. By setting the value of T to be equal to the maximum component variance of the feature vector series, the maximum number of distinct classes results.

As a result of the initial classification process, each voxel within the selected cluster is assigned to a class (step 1570). In the exemplary case of virtual colonoscopy, there are several classes within cluster 4. Thus, the next task is to determine which of the several classes in cluster 4 corresponds to the colon wall. The first coordinate of the feature vector, which is that coordinate of the feature vector exhibiting the highest variance, reflects the information of the average of the 3D local voxel intensities. The remaining coordinates of the feature vector contain the information of directional intensity change within the local neighbors. Because the colon wall voxels for the interior of the colon are generally in close proximity to the gas voxels of cluster 1, a threshold interval can be determined by data samples selected from typical colon wall intensities of a typical CT data set to roughly distinguish colon wall voxel candidates. The particular threshold value is selected for each particular imaging protocol and device. This threshold interval can then applied to all CT data sets (acquired from the same machine, using the same imaging protocol). If the first coordinate of the representative element is located in the threshold interval, the corresponding class is regarded as the colon wall class and all voxels in that class are labeled as colon wall-like voxels.

Each colon wall-like voxel is a candidate to be a colon wall voxel. There are three possible outcomes of not belonging to the colon wall. The first case relates to voxels which are close to the stool/liquid inside the colon. The second case occurs when voxels are in the lung tissue regions. The third case represents mucosa voxels. Clearly then, low level classification carries a degree of classification uncertainty. The causes of the low-level classification uncertainty vary. For example, a partial-volume effect resulting from voxels containing more than one material type (i.e., fluid and colon wall) leads to the first case of uncertainty. The second and the third cases of uncertainty are due to both the partial volume effect as well as the low contrast of CT images. To resolve the uncertainty, additional information is needed. Thus, a high-level feature extraction procedure is used in the present method to further distinguish candidates for the colon wall from other colon wall-like voxels, based on a *priori* anatomical knowledge of the CT images (step 1580).

An initial step of the high-level feature extraction procedure can be to eliminate the region of lung tissue from the low-level classification results. Figure 18A is an exemplary slice image clearly illustrating the lung region 1802. The lung region 1802 is identifiable as a generally contiguous three dimensional volume enclosed by colon wall-like voxels, as illustrated in Figure 18B. Given this characteristic, the lung region can be identified using a region growing strategy. The first step in this technique is to find a seed voxel within the region of growing. Preferably, the operator performing the CT imaging scan sets the imaging range such that the top most slice of the CT scan does not contain any colon voxels. As the interior of lung should be filled with air, the seed is provided by the low-level classification simply by selecting an air voxel. Once the lung region outline of Figure 18B is determined, the lung volume can be removed from the image slice (Figure 18C).

A next step in performing high-level feature extraction can be to separate the bone voxels from enhanced stool/fluid voxels in cluster 2. The bone tissue voxels 1902 are generally relatively far away from the colon wall and resides outside the colon volume. To the contrary, the residual stool 1906 and fluid 1904 are enclosed inside the colon volume. Combining the *a priori* proximity information and the colon wall information obtained from the low-level classification process, a rough colon wall volume is generated. Any voxel separated by more than a predetermined number (e.g., 3) of voxel units from the colon wall, and outside the colon volume, will be labeled as bone and then removed from the image. The remaining voxels in cluster 2 can be assumed to represent stool and fluid within the colon volume (see Figures 19A-C).

The voxels within the colon volume identified as stool 1906 and fluid 1904 can be removed from the image to generate a clean colon lumen and colon wall image. In general, there are two kinds of stool/fluid regions. One region type is small residual areas of stool 1906 attached to the colon wall. The other region type is large volumes of fluid 1904, which collect in basin-like colonic folds (see Figures 19A-C).

The attached residual stool regions 1906 can be identified and removed because they are inside the rough colon volume generated during the low-level

classification process. The fluid 1906 in the basin-like colon fold usually has a horizontal surface 1908 due to the effect of gravity. Above the surface is always a gas region, which exhibits a very high contrast to the fluid intensity. Thus, the surface interface of the fluid regions can be easily marked.

Using a region growing strategy, the contour of the attached stool regions 1906 can be outlined, and the part which is away from the colon wall volume can be removed. Similarly, the contour of the fluid regions 1904 can also be outlined. After eliminating the horizontal surfaces 1908, the colon wall contour is revealed and the clean colon wall is obtained.

It is difficult to distinguish the mucosa voxels from the colon wall voxels. Even though the above three dimensional processing can remove some mucosa voxels, it is difficult to remove all mucosa voxels. In optical colonoscopy, physicians directly inspect the colonic mucosa and search for lesions based on the color and texture of the mucosa. In virtual colonoscopy, most mucosa voxels on the colon wall can be left intact in order to preserve more information. This can be very useful for three dimensional volume rendering.

From the segmented colon wall volume, the inner surface, the outer surface and the wall itself of the colon can be extracted and viewed as a virtual object. This provides a distinct advantage over conventional optical colonoscopy in that the exterior wall of the colon can be examined as well as the interior wall. Furthermore, the colon wall and the colon lumen can be obtained separately from the segmentation.

Because the colon is substantially evacuated prior to imaging, a commonly encountered problem is that the colon lumen collapses in spots. While the inflation of the colon with compressed gas, such as air or CO_2, reduces the frequency of collapsed regions, such areas still occur. In performing a virtual colonoscopy, it is desirable to automatically maintain a flight path through the collapsed regions and it is also desirable to use the scanned image data to at least partially recreate the colon lumen in the collapsed regions. Since the above described image segmentation methods effectively derive both the interior and exterior of the colon wall, this information can be used to enhance the generation of the fly path through the collapsed regions.

In extending the flight path through collapsed regions of the colon or expanding a collapsed region of the colon, the first step is to detect a collapsed region. Using the premise that the grayscale values of the image data from around the outside of the colon wall change much more dramatically than the greyscale values within the colon wall itself, as well as in other regions such as fat, muscle and other kinds of tissue, an entropy analysis can be used to detect areas of colon collapse.

The degree of change in greyscale value, for example along the centerline, can be expressed and measured by an entropy value. To calculate an entropy value, voxels on the outer surface of the colon wall are selected. Such points are identified from the above described image segmentation techniques. A 5x5x5 cubic window can be applied to the pixels, centered on the pixel of interest. Prior to calculating the entropy value, a smaller (3x3x3) window can be applied to the pixels of interest in order to filter out noise from the image data. The entropy value of a selected window about the pixel can then be determined by the equation:

$$E=\sum_{i} C(i)\ln(C(i))$$

where E is the entropy and C(i) is the number of points in the window with the grayscale of i (i=0,1,2,. . ., 255). The calculated entropy values for each window are then compared against a predetermined threshold value. For regions of air, the entropy values will be fairly low, when compared to regions of tissue. Therefore, along the centerline of the colon lumen, when the entropy values increase and exceed the predetermined threshold value, a collapsed region is indicated. The exact value of the threshold is not critical and will depend in part on the imaging protocol and particulars of the imaging device.

Once a collapsed region is detected, the previously determined centerline flight path can be extended through the region by piercing through the center of the collapse with a one voxel wide navigation line.

In addition to automatically continuing the flight path of the virtual camera through the colon lumen, the region of colon collapse can be virtually opened using a physical modeling technique to recover some of the properties of the collapsed

region. In this technique, a model of the physical properties of the colon wall is developed. From this model, parameters of motion, mass density, damping density, stretching and bending coefficients are estimated for a Lagrange equation. Then, an expanding force model (i.e., gas or fluid, such as air, pumped into the colon) is formulated and applied in accordance with the elastic properties of the colon, as defined by the Lagrange equation, such that the collapsed region of the colon image is restored to its natural shape.

To model the colon, a finite-element model can be applied to the collapsed or obstructed regions of the colon lumen. This can be performed by sampling the elements in a regular grid, such as an 8 voxel brick, and then applying traditional volume rendering techniques. Alternatively, an irregular volume representation approach, such as tetrahedrons can be applied to the collapsed regions.

In applying the external force (air pumping) model to the colon model, the magnitude of the external force is first determined to properly separate the collapsed colon wall regions. A three dimensional growing model can be used to trace the internal and external colon wall surfaces in a parallel manner. The respective surfaces are marked from a starting point at the collapsed region to a growing source point, and the force model is applied to expand the surfaces in a like and natural manner. The region between the internal and external surfaces, i.e., the colon wall, are classified as sharing regions. The external repulsive force model is applied to these sharing regions to separate and expand the collapsed colon wall segments in a natural manner.

To more clearly visualize the features of a virtual object, such as the colon, which is subjected to virtual examination, it is advantageous to provide a rendering of the various textures of the object. Such textures, which can be observed in the color images presented during optical colonoscopy, are often lost in the black and white, grey scale images provided by the CT image data. Thus a system and method for texture imaging during virtual examination is required.

Figure 20 is a flow chart depicting a present method for generating virtual objects having a texture component. The purpose of this method is to map textures obtained by optical colonoscopy images in the red-green-blue (RGB) color

space, as for example from the Visible Human, onto the gray scale monochrome CT image data used to generate virtual objects. The optical colonoscopy images are acquired by conventional digital image acquisition techniques, such as by a digital "frame grabber" 1429 which receives analog optical images from a camera, such as a video camera, and converts the image to digital data which can be provided to CPU 1423 via interface port 1431 (Figure 14). The first step in this process is to segment the CT image data (step 2010). The above described image segmentation techniques can be applied to choose intensity thresholds in the grey scale image to classify the CT image data into various tissue types, such as bone, colon wall tissue, air, and the like.

In addition to performing image segmentation on the CT image data, the texture features of the optical image need to be extracted from the optical image data (step 2020). To do this, a gausian filter can be applied to the optical image data followed by sub-sampling to decompose the data into a multiresolutional pyramid. A laplacian filter and steerable filter can also be applied to the multiresolutional pyramid to obtain oriented and non-oriented features of the data. While this method is effective at extracting and capturing the texture features, the implementation of this approach requires a large amount of memory and processing power.

An alternative approach to extracting the texture features from the optical image is to utilize a wavelet transform. However, while wavelet transformations are generally computationally efficient, conventional wavelet transforms are limited in that they only capture features with orientations parallel to the axes and cannot be applied directly to a region of interest. To overcome these limitations, a non-separable filter can be employed. For example, a lifting scheme can be employed to build filter banks for wavelets transform in any dimension using a two step, prediction and updating approach. Such filter banks can be synthesized by the Boor-Rom algorithm for multidimensional polynomial interpolation.

After the textural features are extracted from the optical image data, models must be generated to describe these features (step 2030). This can be performed, for example, by using a non-parametric multi-scale statistical model which is based on estimating and manipulating the entropy of non-Gausian distributions attributable to the natural textures.

Once texture models are generated from the optical image data, texture matching must be performed to correlate these models to the segmented CT image data (step 2050). In regions of the CT image data where the texture is continuous, corresponding classes of texture are easily matched. However, in boundary regions between two or more texture regions, the process is more complex. Segmentation of the CT data around a boundary region often leads to data which is fuzzy, i.e., the results reflect a percentage of texture from each material or tissue and vary depending on the various weighting of each. The weighting percentage can be used to set the importance of matching criteria.

In the case of the non-parametric multi-scale statistical model, the cross entropy or a Kullback-Leiber divergence algorithm can be used to measure the distribution of different textures in a boundary region.

After texture matching, texture synthesis is performed on the CT image data (step 2050). This is done by fusing the textures from the optical image data in to the CT image data. For isotropic texture patterns, such as presented by bone, the texture can be sampled directly from the optical data to the segmented CT image data. For anisotropic texture regions, such as colon mucosa, a multiresolution sampling procedure is preferred. In this process, selective re-sampling for homogenous and heterogenous regions is employed.

Alternatively, pseudocolor texture can be created directly from the CT data. For each voxel, multiple CT values, comprising a local area neighborhood, can be evaluated to determine a pseudocolor for the given voxel. For each voxel the local neighborhood consists of the voxels that are within some given distance of the center voxel. For example a 5x5x5 voxel cubic shaped region, or the double pyramid which represents all voxels within 3 units measured by Manhattan distance. This vector of scalar values is then evaluated to map to a color to be displayed for this voxel during subsequent volume rendering. The evaluation of the local neighborhood vector of values can compute such things as local curvature, homo/heterogeneity, or other geometric or spatial functions.

Volume Rendering

In addition to image segmentation and texture mapping described above, volume rendering techniques can be used in connection with virtual colonoscopy procedures to further enhance the fidelity of the resulting image. Figure 21 illustrates a perspective volume ray-casting method which can be used for volume rendering in accordance with the present invention. From a selected virtual viewpoint, e.g., camera position, such as within the colon lumen, rays are cast through each of the proximate image pixels (step 2100). For each ray, the first sampling point is set as the current image pixel along the ray (step 2110). The distance (d) between the current sampling point and the nearest colon wall is then determined (step 2120). The current distance (d) is compared to a predetermined sampling interval (i) (step 2130). If the distance (d) is greater than the sampling interval (i) then no sampling occurs and the next sampling point along the ray is determined by jumping the distance d along the ray (step 2140). If the distance is less than or equal to the sampling interval (i) then conventional sampling is performed on this point (step 2150) and the next sampling point is selected in accordance with the sampling interval (i) (step 2160). For example, trilinear interpolation between the density values of 8 neighboring voxels can be performed to determine the new density value at the sampling point.

The method of Figure 21 effectively accelerates ray-casting because a space leaping technique is used to quickly skip over empty space along the ray of the image plane to the colon wall. In this method, a distance from a sample point to the nearest colon wall is determined along each ray. If the distance is larger than a predetermined sampling interval (i), a jump to the next sampling point along the ray is performed. Since the closest distance information is already available from the potential field which is used for virtual camera control, no additional distance coding calculations are required. In this case, neither surface rendering nor Z-buffer transform is required, which results in savings in preprocessing time and memory space.

Alternatively, a space leaping method can derive distance information for each ray from the Z-buffer of the corresponding surface rendering image. If the surface rendering image and volume rendering image will both be generated, this

approach provides minimal processing overhead burden as the Z-buffer information is provided as a result of the surface rendering methods. Thus, this form of space leaping method only requires additional processing to perform a depth transformation from the image space domain to the world space domain.

For those regions along the ray where the distance (d) was traversed in step 2140, the region along the ray corresponds to open space and can be assigned a value according to an open space transfer function. Typically, open space will have no contribution on the final pixel value. For each point where sampling takes place, one or more defined transfer functions can be assigned to map different ranges of sample values of the original volume data to different colors and opacities and possibly other displayable parameters. For example, four independent transfer functions have been used to determine different material by mapping ranges of CT density values into specified colors of red, green, blue and opacity, each in the range of 0 to 255.

Virtual Biopsy

The above described techniques can also form the basis of a system for performing virtual electronic biopsy of a region being examined to effect a flexible and non-invasive biopsy. As noted above, volume rendering techniques use one or more defined transfer functions to map different ranges of sample values of the original volume data to different colors, opacities and other displayable parameters for navigation and viewing. During navigation, the selected transfer function generally assigns maximum opacity to the colon wall such that the outer surface is easily viewed. Once a suspicious area is detected during virtual examination, the physician can interactively change the transfer function assigned during the volume rendering procedure such that the outer surface being viewed becomes substantially transparent, allowing the region information to be composited and thus the interior structure of the region to be viewed. Using a number of predetermined transfer functions, the suspicious area can be viewed at a number of different depths, with varying degrees of opacity assigned throughout the process.

Polyp Detection

The present system and methods can be used to perform automated polyp detection. With reference to Figure 13, polyps 1305, which occur, for example, within the colon, generally take the form of small convex hill-like structures extending from the colon wall 1301. This geometry is distinct from the fold of the colon wall. Thus, a differential geometry model can be used to detect such polyps on the colon wall.

The surface of the colon lumen can be represented as a continuously second differentiable surface in three dimensional Euclidean space, such as by using a C-2 smoothness surface model. Such a model is described in "Modern Geometry Methods and Applications" by B.A. Dubrovin et al, published by Springer-Verlag 1994, which is hereby incorporated by reference in its entirety. In this model, each voxel on the surface of the colon has an associated geometrical feature which has a Gauss curvature, referred to as Gauss curvature fields. A convex hill on the surface, which may be indicative of a polyp, possesses a unique local feature in the Gauss curvature fields. Accordingly, by searching the Gauss curvature fields for specific local features, polyps can be detected. Once detected, the suspected polyps can be highlighted and thus brought to the attention of the physician where the physician can measure the suspected polyp and use the above described virtual biopsy methods to further investigate the suspicious region.

Central Fly-Path Generation

In the case of virtual colonoscopy, determining a proper navigation line, or fly-path, through the colon lumen is an important aspect of the described systems and methods. While certain techniques for determining the fly-path of the virtual camera model were discussed with respect to Figures 4-8, Figure 22 illustrates an alternate method of generating the central fly-path through the colon lumen. After the colon wall is identified, such as by the image segmentation methods described herein, a volume shrinking algorithm can be employed to emphasize the trend of the colon lumen and reduce subsequent searching time within the lumen volume (step 2310).

Figure 23 further illustrates the steps of an exemplary volume shrinking algorithm, which is based on a multiresolution analysis model. In this procedure, the three dimensional volume is represented by a stack of binary images which have the same matrix size (step 2310). Collectively, these images form a binary data set. A discrete wavelet transformation can be applied to the binary data set which results in a number of sub-data sets representing different time-frequency components of the binary data set (step 2320). For example, the discrete wavelet transformation may yield eight (8) sub-data sets. The sub-data sets are compared against predetermined threshold values such that the lowest frequency component is identified (step 2330). This component forms the binary data set for subsequent discrete wavelet transformation and thresholding steps, which are recursively applied in a multi-resolution structure (step 2340). In the case of virtual colonoscopy, the discrete wavelet transformation and associated thresholding can be applied three times recursively on the subsequent sub-dataset that represents the lowest frequency component (a 3-level multi-resolution decomposition).

Returning to Figure 22, from the reduced colon volume model, a distance map technique can be employed to generate a minimum distance path between the two ends of the colon, e.g., from the rectum to the cecum (step 2215). The resulting path preserves the global trend information of the colon lumen, but ignores the trends exhibited by local folds. Control points within the global colon can then be determined by mapping the minimum distance path back to the original data space (Step 2220). For example, in the case of a 3-level multi-resolution decomposition, the reduced volume is three times smaller than the original volume and an affine transformation, which is well known, can be used to map the reduced volume model exactly back to the original scale volume. The minimum distance path of the reduced value can also be mapped back into the original scale volume as a series of points, which can be used as the control points within the colon.

The preferred fly path is one which is on the centerline of the colon lumen. However, the initial control points may not be exactly located in the center of the colon lumen. Thus, the initial control points can be centered, such as by the use of a bi-section plane algorithm (step 2230). For example, at each selected control point,

a bi-section plane can be defined as a plane normal to the trend direction and cutting across the colon lumen. A centralization algorithm, such as a maximum disk algorithm, can then be performed on each bi-section plane. Such an algorithm is discussed in the article "On the Generation of Skeletons from Discrete Euclidean Distance Maps" by Ge et al., IEEE Transactions on PAMI, Vol. 18, pp. 1055-1066, 1996 which is hereby incorporated by reference.

Once the control points are centralized, the flight path can be determined by interpolating a line connecting these points (step 2240). In the case of virtual colonoscopy, it is desirable that the interpolated flight path take the form of a smooth curve which is substantially centered within the colon lumen. A constrained cubic B-spline interpolation algorithm based on Serret-Frenet Theorem in differential geometry theory can be used to establish a suitable smooth curved flight path, such as is described in "Numerical Recipes in C: The Art of Scientific Computing," by Press et al., Second Edition, Cambridge University Press, 1992.

The pictorial representation of a segmented colon lumen in Figures 24 and the flow chart of Figure 25 set forth yet another alternate fly-path generation method in accordance with the present invention. In this alternate method, the representation of the colon lumen 2400 is first partitioned into a number of segments 2402 a-g along the length of the lumen 2400 (step 2500). From within each segment 2402 a representative point is selected 2404 a-g (step 2520). Each representative point 2404 a-g is then centered with respect to the colon wall (step 2530), such as by the use of a physically-based deformable model which is used to push the points to the center of the respective segment. After the representative points are centered, the points are sequentially joined to establish the center-line fly-path for the virtual camera model (step 2540). If the segments are sufficiently small in length, the centered points can be connected with straight line segments 2406 a-f. However, when linear curve fitting techniques are applied to join the centered points, a smoother, continuous flight path is established.

Each of the foregoing methods can be implemented using a system as illustrated in Figure 14, with appropriate software being provided to control the operation of CPU 1409 and CPU 1423.

An alternate hardware embodiment, suitable for deployment on a personal computer, is illustrated in Figure 26. The system includes a processor 2600 which should take the form of a high speed, multitasking processor such as a Pentium III processor operating at a clock speed in excess of 400 MHZ. The processor 2600 is coupled to a conventional bus structure 2620 which provides for high speed parallel data transfer. Also coupled to the bus structure 2620 are main memory 2630, a graphics board 2640, and a volume rendering board 2650. The graphics board 2640 is preferably one which can perform texture mapping, such as the Diamond Viper v770 Ultra manufactured by Diamond Multimedia Systems. The volume rendering board 2650 can take the form of the VolumePro board from Mitsubishi Electric, which is based on U.S. Patent Nos. 5,760,781 and 5,847,711, which are hereby incorporated by reference. A display device 2645, such as a conventional SVGA or RGB monitor, is operatively coupled to the graphics board 2640 for displaying the image data. A scanner interface board 2660 is also provided for receiving data from an imaging scanner, such as an MRI or CT scanner, and transmitting such data to the bus structure 2620. The scanner interface board 2660 may be an application specific interface product for a selected imaging scanner or can take the form of a general purpose input/output card. The PC based system 2600 will generally include an I/O interface 2670 for coupling I/O devices 2680, such as a keyboard, digital pointer (e.g., mouse) and the like to the processor 2620. Alternatively, the I/O interface can be coupled to the processor 2620 via the bus 2620.

In the case of three dimensional imaging, including texture synthesis and volume rendering, numerous data handling and processing operations are required. For large datasets, such as those represented by the colon lumen and its surrounding area, such processing can be very time consuming and memory intense. However, using the topology of Figure 26 in accordance with the processing method illustrated in the flow chart of Figure 27, such operations can be performed on a relatively low cost personal computer (PC). Imaging data is received by the processor 2620 and stored in main memory 2630 via the scanner interface board 2660 and bus structure 2620. This image data (pixels) is converted into a volume element (voxel) representation (step 2710). The volume representation, which is stored in main

memory 2630, is partitioned, for example into slices, such as along a major volume axis or other portions of the region being imaged (step 2720). The volume partitions are then transferred to the volume rendering board and temporarily stored in volume rendering memory 2655 for volume rendering operations (step 2730). The use of locally resident volume rendering memory 2655 provides for enhanced speed in volume rendering as data need not be exchanged over the bus 2620 during rendering of each slice of the total volume. Once volume rendering is complete for the slice, the rendered data is transferred back to main memory 2630 or the graphics board 2640 in a sequential buffer (step 2740). After all slices of interest have been subjected to rendering, the contents of the sequential buffer are processed by the graphics board 2640 for display on the display unit 2645 (step 2750).

Multi-scan Based Virtual Examination

The techniques discussed above generally perform virtual imaging based on a dataset acquired from a single magnetic resonance imaging (MRI) or computed tomography (CT) scan. However, the techniques discussed above are also useful for performing virtual examination of a region using multiple scans of a region. By using multiple scans of a region, improved imaging of regions of pathology can be achieved and motion artifacts can be reduced. One such application of interest is in performing virtual cystoscopy to screen a patient for possible polyps or cancer of the bladder.

Figure 28 is a flow chart which illustrates a method of employing multiple MRI scans to perform virtual examination of an object, such as virtual cystoscopy. Unlike CT images, where the bladder wall can be difficult to distinguish from urine, in MRI images, urine can be used as a natural contrast agent to delineate the inner bladder wall. To this end, a pre-image scan protocol is employed (step 2805). Approximately ½ hour prior to the first of four MRI scans, the patient is requested to empty the bladder and then consume one cup of water. After approximately ½ hour, the patient is subjected to the first of four MRI scans of the bladder region (step 2810). The first scan, with the bladder full and distended, follows protocol for T1-weighted transverse imaging. For example, when using the Picker scanner referenced above, a

KJELL FASTER protocol using a 256x256 matrix size, a 38 cm field of view (FOV), a 1.5 mm slice thickness (no gap), a 3 ms TE, a 9 ms TR, a 30 degree flip angle and one scan average can be used. Of course, these parameters tend to be scanner specific and various changes in the parameters can be used with acceptable results.

With the bladder still full, the patient is subjected to a second MRI scan, scan 2 (step 2815). The second scan follows a protocol for T1-weighted coronal imaging, such as the Picker KJELL FASTER protocol with a 256x256 matrix size, a 38 cm field of view (FOV), a 1.5 mm slice thickness (no gap), a 3 ms TE, a 9 ms TR, a 30 degree flip angle and a two-scan average.

The two image scans described above are taken along orthongal axes with respect to one another. The advantage of this is that regions of significant motion artifacts in one scan, generally correspond to regions of minimal motion artifacts in the orthogonal scan. Accordingly, by taking a first scan in the transverse direction and a second scan in the coronal direction, the image scans can be registered and motion artifacts in the data set can be identified and compensated for.

After the scan 2, the patient is asked to relieve the bladder and is then subjected to two additional MRI scans. The third scan (step 2820) follows the same imaging protocol as the first scan (transverse imaging). The fourth scan (step 2825) follows the same imaging protocol as the second scan (coronal imaging).

The image scans can be acquired using a Picker 1.5 T Edge whole-body scanner. Although a T2 imaging protocol can be used, a T1 imaging protocol is preferred for virtual cystoscopy because this protocol provides improved delineation between fat and urine and offers a shorter acquisition period. Alternatively, the image scans can take the form of computed tomography or ultrasound imaging scans using suitable contrast agents and protocols for these imaging techniques.

During the first two scans (scan 1 and scan 2), the bladder is distended and the bladder wall is relatively thin. In this case, physiologically altered locations, such as tumors, may thin at a different rate as compared to the unaltered bladder wall and may become more apparent under these conditions. During the third and fourth scans, the bladder is substantially empty and the bladder wall is thicker. With a thicker

wall, a more pronounced image contrast may result between normal tissue of the bladder wall and that of physiologically altered tissue.

After the four scans are acquired, the four corresponding datasets can then be individually processed. Initially, each scan data set is preferably subjected to image segmentation, as discussed above (step 2830), such as in connection with Figure 15. During image segmentation, the voxels of the four datasets are classified into a number of categories, such as bladder wall, urine, fat, boundary, etc. The classification is based on the local intensity vectors of the voxels. Once the voxels are classified, the interior of the bladder lumen can be identified using a region growing algorithm beginning with a seed voxel selected from within the bladder volume, such as by selecting an air voxel or urine voxel.

Prior to clinical analysis of the segmented volume data sets, registration of the four data sets to a common coordinate system is performed (step 2835). Because the shape of the bladder varies from scan to scan, an exact voxel-voxel registration is not of practical value. Instead a flexible registration process is preferred. In the present flexible registration process, for each volume of interest (volume rendered for each corresponding scan) the center of the volume is determined, such as by averaging the three coordinates of all the voxels in the volume.

A Cartesian coordinate system can then be constructed with the origin of the system located at the center point of the volume. The axes of the system can then be oriented in a number of ways. A suitable selection of orientation corresponds to the orientation of the natural human body, e.g., with the Z-Axis running along the height of the body (e.g., from toe to head) the Y-axis oriented from back to front and the X-axis running laterally (e.g., from left to right). The units of length in this coordinate system can be conveniently set to an arbitrary unit of one voxel length, the absolute magnitude of which will vary based on acquisition properties for the MRI scans. So long as the same pixel spacing is used in all scans to acquire all four data sets, this will result in a uniform value for each of the four data sets.

After registration, the images from the four data sets can be viewed individually or simultaneously (step 2845). An exemplary display window is illustrated in Figures 29 and 30. Referring to Figure 29, the display is partitioned into

four sub windows 2905, 2910, 2915, 2920 which correspond to scan 1, scan 2, scan 3 and scan 4, respectively. A control panel section 2925 can also be provided on a portion of the display to establish a graphical user interface (GUI) to offer display and navigation functions to the user. As an operator navigates in one of the image sub windows, such as magnifying the view, the corresponding operation preferably takes place in the other sub window views as well. A user can also select one of the views for expansion to a single window display.

To reduce the amount of data which is simultaneously processed, the data sets can be partitioned, such as into 8 parts or octants (step 2840). This can be performed in a number of ways. For example, with reference to the Cartesian coordinate system illustrated in Figure 29, the data can be portioned into the eight regions of the coordinate system: (1) X, Y, Z; (2) X, -Y, Z; (3) X, Y, -Z; (4) X, -Y, -Z; (5) -X, Y, Z; (6) -X, -Y, Z; (7) -X, Y, -Z; and (8) -X, -Y, -Z.

Figure 29 illustrates four views of the outside of the bladder lumen taken from each of the four scans. Figure 30 illustrates fours views of a portion of the interior of the bladder lumen also taken from each of the four scans.

Multi-Resolution Imaging and Virtual Laryngoscopy

The systems and methods described herein can be adapted and applied to perform multiresolution imaging which is well suited for virtual laryngoscopy. Figure 31 is a flow chart illustrating a method for performing virtual laryngoscopy. First, an imaging scan of the region of a patient's larynx is acquired (step 3105). This can be performed using computed tomography (CT) or magnetic resonance imaging (MRI) techniques. However, because the CT scan in this region offers significantly faster acquisition time (30 seconds versus over 7 minutes for MRI) and higher resolution (0.3mm cubic voxel compared to 1mm cubic voxel for MRI), the CT scan is preferred. To acquire the CT scan data a GE/CTI spiral scan CT scanner can be used. A suitable scan protocol is 120 keV, 200 ma, 512x512 matrix size, 15 cm field-of-view and 3mm/2.0:1 pitch. The scan is completed in approximately 30 seconds and results in 351 image slices of 0.3mm thickness and results in 0.3mm cubic voxels.

Image segmentation can be used to classify voxels into a number of categories (step 3110). In this operation, a modified self-adaptive on-line vector quantization (SOVQ) algorithm can be used. In such a case, the algorithm analyzes each voxel with respect to neighbors of up to the third order to determine local density features. Each voxel in the acquired dataset has an associated local density vector. By transforming the local density vectors using the Karhunen-Loéve (K-L) transform, feature vectors for the voxels in the volume image can be obtained. Based upon the feature vectors, the voxels can be classified and labeled. Voxel classification is dependent in part on the choice of a local voxel density vector and one preset parameter, referred to as the maximum cluster number (MCN). The MCN sets the number of voxel classifications that will be applied to the dataset. In the case of the CT images, the human eye can discern four (4) distinguishable tissue/material types. An MCN value of 5 is suitable in this case. For an MRI image, the human eye can differentiate among 6 different tissue types, and an MCN value of 7 can be used.

As part of the image segmentation process, an expanded data set is generated by interpolation between the measured data points. For example, prior to employing the SOVQ algorithm, a first order Lagrange interpolation can be applied to each slice in the dataset. This expands the 256x256 matrix size of the original slices of the data set to a 512 x 512 matrix size. In addition, inter-slice interpolation can be performed to further expand the dataset between actual slices. The interpolated dataset is referred to as the enlarged dataset. In addition to generating an enlarged dataset, the interpolation process also suppresses noise and reduces the partial-volume effect, as the interpolation process has a low-pass filtering effect on the data.

Using a two dimensional viewing tool, a seed voxel can be selected within the larynx lumen and a growing algorithm applied to extract the larynx volume from the dataset (step 3115). In those regions of the larynx where there may be several unconnected volume regions, multiple seed points can be selected.

With the larynx volume identified and the voxels of the regions classified through image segmentation, the next task is to manage the data in a manner which allows efficient navigation and viewing of the virtual larynx. In this case, a level-of-detail (LOD) approach is adopted and modified for use in the present method.

In this LOD method, a reduced dataset is generated from the enlarged data set. For example, the 512x512x256 enlarged dataset can be reduced to a 64 x 64 x 32 reduced volume dataset using a multi-resolution decomposition with three levels of thresholding (step 3120). Next, polygons used to render the volume images in both the enlarged and reduced volume datasets can be extracted. A traditional Marching Cubes method can be used to extract polygons to fit the surface of the larynx.

One problem encountered in the prior art is managing the large number of polygons required to generate the three dimensional image for the enlarged dataset. This problem is solved in the present method by organizing the enlarged dataset in a Binary Space Partitioning (BSP) tree data structure (step 3130). The original image volume is selected as the root of the tree. The space is then partitioned into two subspaces containing an approximately equal number of polygons. This subdivision process is iteratively repeated until the number of polygons in each resulting subspace is below a threshold value. The threshold value can vary based on system performance and application requirements. The last resulting subspaces are referred to as leaf nodes of the tree. Once the subdivision process is complete, all of the voxels of the expanded dataset are stored in the leaf nodes of the BSP tree.

During navigation or viewing, polygon culling can be applied by first removing those leaf nodes that are completely outside the field-of-view from current processing operations. The remaining polygons are recalled from the BSP tree, ordered and rendered in those spaces which were not culled. Thus, the BSP tree provides an effective tool for selecting a relevant portion of the dataset for a particular navigation or display operation.

The enlarged and reduced datasets are cooperatively used in a two level LOD rendering mode. If a user is interacting with the object (step 3135), such as rotating, shifting or effecting other changes in the field of view, the polygons from the reduced dataset (64-sized) are rendered (step 3140). Because of the significantly lower number of polygons involved, interaction with the reduced dataset volume can be performed faster and with less processing overhead. The tradeoff for the increased speed is reduced image resolution. If there is no interaction from the user after a predetermined time period, the polygons of the enlarged dataset (512-sized) are

selected from the BSP tree and are rendered to provide a high resolution image of the current field of view (step 3145).

Virtual Angiography

The techniques for virtual imaging and navigation can also be adapted and applied to virtual angiography. This technique can be used for detection and measurement of various abnormalities and disease of the circulatory system.

One such application of virtual angiography is the detection of abdominal aortic aneurysms, which generally start as small enlargements of the aortic vessel and exhibit a greater risk to rupture with increasing size of the aneurysm. Previously, the only effective method of treatment was open surgery, placing a graft within the aorta at the level of the aneurysm. However, this procedure has a high degree of associated morbidity and mortality. Recently developed per cutaneous placed aortic stent graft techniques have a significantly lower complication rate. Virtual angiography is an effective method to help plan these less invasive procedures and can also be an effective tool for detecting the presence of an aneurysm and tracking the growth of an aneurysm to determine if and when surgery is indicated.

Figure 32 in a flow chart which provides an overview of the present virtual angiography method. In performing a virtual angiography, an image scan of the vessel, such as the aorta must be acquired (step 3205). Various imaging techniques can be used, such as Computed Tomography (CT), Magnetic Resonance Imaging (MRI) and ultrasound. However, an aortic CT scan is generally preferred because of the contrast between blood, soft tissue and calcium deposits which results in the CT image.

Once an image scan data set is acquired, image segmentation techniques are then applied to the data set to classify the voxels of the dataset into a number of categories (step 3210). The image segmentation techniques described above, such as in connection with Figure 15, are generally applicable. In this case, the various feature vector values of the voxels will be grouped according to categories such as blood, soft tissue and calcium deposits. Using a blood voxel as a seed, a region growing algorithm can be used to determine the volume and extent of the aortic lumen.

In the CT image, an aneurysm has image features which closely resemble the neighboring soft tissue. As a result, the full contour of the aneurysm can be difficult to establish. However, regions with calcium deposits offer significant contrast on the CT scan and can be used to identify portions of the aneurysm, such as the endpoints of the aneurysm on the vessel wall (step 3215).

After a portion of an aneurysm is detected, one or more closing surfaces can be generated to define an estimation of the aneurysm's contour (step 3220). A convex closing surface can be established using a non-uniform, non-rational B-spline to generate a surface which runs through or near the points of the aneurysm which were identified.

After the closing surface is generated, the volume of the aneurysm can be estimated (step 3225). One method for estimating the volume is to count the number of voxels which are enclosed by the estimated closing surface. In addition, within the volume of the aneurysm, the centerline along the direction of blood flow can be determined by using a distance transform technique. Continuous local coordinate systems can then be established along this centerline and the diameter of the aneurysm determined. Virtual navigation can take place along this centerline, in a manner consistent with that described above for navigating through a lumen, such as the colon.

Referring to Figures 33A-C, the described method of virtual angiography can be used to assist in the generation and placement of a stent graft to bypass an abdominal aortic aneurysm. Figure 33A illustrates a simplified diagram of an abdominal aortic aneurysm located below the renal arteries and above the bifurcation of the aorta. Because of variations from patient to patient in the specific anatomy of the aorta and the size and location of an abdominal aortic aneurysm therein, when a stent graft is to be used to bypass an aneurysm, the graft must be designed and built to specifically fit the particular aortic segment. As illustrated in Figure 33B, this can require identifying the length of the required graft, the diameter at the points of interface on each end of the bypassed region, the angles of interface, among other variables. If the aneurysm is located near an arterial branch, the size and angles of the bifurcated ends of a bifurcated stent graft must also be determined, as illustrated in Figures 33B and 33C.

To date, such measurements have been performed through invasive calibrated angiograms using a catheter inserted into the aorta from an insertion made at the level of the groin region, rapid injection of a large amount of iodinated contrast and rapid radiographic imaging. This technique can be supplemented and perhaps supplanted using the present virtual angiography techniques, which can resolve such distances and angles using virtual navigation using centerlines constructed through the branches of the aortic lumen. In addition, the virtual angioscopy can be used to perform a virtual biopsy of the region where a stent graft may be inserted. This allows the operator to view beneath the arterial surface and examine the region for thrombus deposits, calcification or other factors which would contra-indicate the use of a stent graft procedure.

Another application of virtual angiography is the imaging, examination and navigation through the carotid arteries which supply blood flow to the brain. The techniques described herein with respect to virtual endoscopy are fully applicable in the case of blood vessels. For example, the vessels of interest are extracted from the acquired image data using image-segmentation techniques. Next, a navigation flight path can be established through the vessel(s). Preferably, potential fields are built up within the vessel for use in navigation. As with other organs, such as the colon, a volume-rendered model of the vessels of interest can be generated. Using the flight path and potential fields to navigate through the interior of the volume rendered blood vessel lumen, abnormalities such as vessel narrowing and plaque build up can be observed. In addition, the techniques discussed regarding virtual biopsy can be applied in this context to evaluate vessel wall and characterize build up on the wall surface, such as plaque.

Tree Branch Searching for Virtual Endoscopy

Path planning for virtual navigation through a hollow organ or object is an important task. Various techniques have been discussed, such as fly-path generation, to achieve this goal. As the geometry of the object being studied becomes

more complex, such as presenting a multi-branch structure, the task of path planning becomes even more complex. It is desirable to determine not only the center line of a primary lumen, but also to identify and locate any branches extending from the primary lumen. Common examples of organs having a complex branch structure include the main airway and lungs, the cardiovascular system and, because of the presence of haustral folds, the colon. Each organ or object generally presents specific challenges for defining a path, or skeleton, for the object. However, a generalized technique for generating such a skeleton is illustrated in the flow chart of Figure 34.

Referring to Figure 34, an imaging scan of the region of interest, such as a computed tomography (CT) or Magnetic Resonance Imaging (MRI) scan, is acquired (step 3405). As discussed above, the imaging scan is transformed into a three dimensional volume of the region by stacking the binary images of the imaging scan and defining three dimensional volume units, or voxels, from these stacked images (step 3410). Depending on the volume and complexity of the region of interest, it may be desirable to reduce to size of the dataset of the three dimensional volume prior to generating the skeleton. To this end, a multiresolution data reduction process, which is discussed in more detail below, can be used (step 3415).

The skeleton is a subset of the three dimensional volume. Preferably, the skeleton has the following attributes: 1) it preserves the homotopy of the tree; 2) it is 26-connected; 3) it is one voxel thick; 4) it approximates the central axes of the branches; and 5) it is relatively smooth. The degree of homotopy is somewhat application specific. For example, in generating a skeleton of the colon lumen, the skeleton will generally be a single path from end to end, despite the presence of numerous haustral folds which can be several voxels deep. However, in the cardiovascular system and pulmonary system, a small offshoot from the root which is several voxels deep can represent a legitimate branch in the system.

Returning to Figure 34, in the volume of interest, a root voxel is identified in the volume (step 3420). In performing virtual endoscopy, this can be performed manually based on an understanding of the geometry of the structure being evaluated.

A distance map can then be generated to identify the branches in the tree and the distances between the endpoints of the branches and the root voxel (step 3425). A presumption applied in this method is that there exists one unique endpoint on each branch which exhibits the longest distance to the root of the tree. Figure 35 is a schematic diagram illustrating a 3x3x3 cubic voxel arrangement which is referred to as a 26-connected voxel cubic distance plate. In the center of this arrangement is a seed voxel 3505, which is assigned a distance weight of zero. Around the seed voxel 3505 are 26 connected neighbor voxels which are assigned distance weights based on the respective Euclidean distance between the respective neighbor voxel and the seed. In a cubic arrangement the Euclidian distance can assume a normalized value of $1\sqrt{2},\sqrt{3}$ which is approximately equal to 1, 1.4 and 1.7. To simplify processing, the voxels can be assigned integer value weights of 10, 14, and 17 to approximate the relative Euclidian distances.

Figure 36 is a pseudo-code representation of an algorithm for determining the distance map from a voxel in the volume to the root using the Euclidian weighted distances of the 26-connected cubic distance plate of Figure 35. From the generated distance map, branches are identified and the endpoints of the branches are determined (step 3430).

Referring to Figure 36, the root of the volume is labeled with the integer value 0. A processing queue is then formed with the voxels in the volume. The voxels are then labeled in a first-in, first out manner by adding the Euclidian distances between the voxel at the top of the queue and the root voxel. This process is repeated until all of the voxels in the volume are assigned a value in the distance map.

Because the labeling of voxels in the distance map will depend, in part, on the queuing order, the resulting distance map does not provide a unique solution. However, regardless of the queuing order, there is always at least one farthest point for each branch. In addition, for each voxel, other than the root voxel, there is always at least one 26-connected neighbor in the volume which has a shorter distance to the root. Thus, the endpoints of the branches are readily detectable by searching the distance map for local maximum distances (local maxima) (step 3430). The term local maxima is a relative term. In evaluating the volume for local maxima, the volume should be

partitioned into various subspaces which are appropriate to the object being evaluated. The expected feature size, branch length, branch diameter, etc. are generally considered in determining the subspace partitions.

Once the endpoints of the branches are determined, the shortest path from the endpoint to the root voxel is determined (step 3435). The shortest paths from the endpoints to the root define the basic structure of the branches of the tree and approximate the centerline of the branches. This is referred to as the rough skeleton of the volume. The shortest paths are preferably generated from the branches at farthest end of the tree and begin from the end of those branches. From the most remote branch endpoint, the first voxel is selected and its 26-connected neighbors are analyzed to determine which voxel is in the minimal distance path from endpoint to root. This process is repeated until a selected voxel meets the root. This results in a one-voxel wide path from the farthest end to the root. Searching for the shortest path for other branches is similar. However, for subsequent branches, the selection process can terminate when the current path reaches a previously assigned path (e.g., the path need not lead all the way to the root). The collection of all of the interconnected shortest paths is the resulting rough skeleton of the object.

Depending on the application of the resulting rough skeleton, it may be desirable to refine the rough skeleton (step 3440). One step of refining the skeleton is to centralize the skeleton within the branches. Centralization preferably takes place branch by branch from the longest branch to the shortest. Starting with the longest branch, a uniform interval is selected, generally in the range of 4-8 voxels, along the branch. For each interval, the tangent direction of the voxel on the rough skeleton is calculated and a plane crossing the voxel perpendicular to the tangent direction is determined. A two dimensional area defined by the intersection of the plane and the volume is created and the center of this intersection can be computed using the known maximum disk technique. The centers of intersection can then be connected using a bi-cubic, B-spline interpolation or other curve fitting method. For the remaining branches, the endpoint which meets another branch or the root must first be adjusted to match the position of the previously centered skeleton branch. Then, centralization can proceed in the same manner as described for the longest branch.

Referring back to step 3415, when a large dataset is involved, it may be required, or at least desirable, to reduce the size of the dataset to speed up processing and reduce processing cost. Noting that the tree structure can be preserved within a range of scales, the large volume can be shrunk to a smaller scale space for structure analysis.

A shrinking method based on multiresolution analysis theory can be used. The input data is the stack of binary images of the same size which can be obtained from the segmentation results of the CT or MRI scan. The x-direction is taken along the slice image width, the y-direction is along the slice image height, and the z-direction is along the direction of slice by slice. The foreground voxels in the tree volume are set to value of 128 (maximum) and the background voxels are set to value 0 (minimum). A Daubechies' bi-orthogonal wavelet transform with all rational coefficients is employed. This one-dimensional (1D) discrete wavelet transformation (DWT) is first applied along to the x-direction row by row. From application of the DWT only the lower frequency components are retained and packed. The computation is preferably implemented in floating points. Noting that the DWT is applied to the binary signal, there are two kinds of nonzero coefficients which result in the lower frequency component. The first is of value 128 and this kind of coefficients are located in the interior of the volume. The second is of a value not equal to 128 and these coefficients locate the boundary of the volume.

The coefficients of the second kind are compared against a predetermined threshold value. If its absolute value is larger than a pre-set threshold T1, the value of the coefficient is set to 128; otherwise, it is set to 0. This results in a stack of binary images with a row size of half of the original dataset. The same DWT is then applied to the resulting dataset along the y-direction column by column, where the similar thresholding is employed to the lower frequency components. The result is again a stack of binary images, but now with both half row and column size as compared to the original dataset. Finally, the DWT is applied to the last result along the z-direction and the lower frequency components are retained. This step completes the first level decomposition.

The resulting dataset of the first level decomposition is of half size in all three directions as compared to the original dataset. If the shrinking procedure stops at this level, the finial thresholding is applied. It revalues those coefficients of nonzero and non-128 value. If the absolute value of this kind of coefficient is larger than a pre-set threshold **T2**, it will be revalued as 128; otherwise, it is revalued as 0. If further shrinking is needed, the same thresholding algorithm is applied with the threshold **T1**. Further shrinking proceeds as previously described, but is applied to the dataset shrunk at the last previous level. The decomposition procedure can be recursively applied until the resulting volume meets the desired reduced data volume. In virtual endoscopy, the slice images are of 512X512 pixel size. The maximum decomposition level is usually three, resulting in a 64x64 reduced pixel size.

The volume is isotropically shrank in all directions with the presented method. The two pre-set thresholds, **T1** and **T2**, are used to control the degree of shrinking. If the volume is significantly over shrunk, connectivity may be lost in the reduced volume. If it is over shrunk to a leaser degree, two separate branches may merge into one branch in the reduced volume dataset. The larger the two threshold values, the thinner the reduced volume is. The range of those two thresholds is [0, r x 128], where $0<r<1$. Preferably, the range for virtual endoscopy is $r \in (0.08, 0.28)$ for **T1** and $r \in (0.7, 0.98)$ for **T2**. The exact determination is dependant on the feature size of the particular application and is selected to achieve reduction while retaining the fidelity of the structure information in the shrunk volume.

After shrinking the original volume, the tree branch searching procedure can be applied to the smaller volume (steps 3420-3440). The resultant skeleton can be mapped back into the original scale space. When scaled to the original space, the image of the smaller scale skeleton no longer remain a connected path in the original scale space. These voxels in the image act as control points for the final skeleton. The control points are centralized using the algorithm as described previously, and then, they are interpolated to form the final skeleton of the object.

Computer Assisted Diagnosis

The virtual examination techniques described herein lend themselves to applications for the computer assisted diagnosis (CAD) of various conditions. For example, as described above, by examining the geometry of an organs tissue for local Gausian curvatures, regions with abnormal geometry, such as polyps inside a colon lumen, can automatically be identified. This technique can be generalized and used in conjunction with texture features to provide CAD functionality for a number of applications.

For example, using the multi-scan imaging of the bladder described above, automated detection or tumors in the bladder wall can be performed. In this case, the degree of tumor invasion within the bladder wall is generally used to define the stage of bladder cancer. Using the multi-scan imaging and image segmentation techniques described above, the region of the bladder wall can be readily delineated. Regions of normal bladder tissue generally exhibit a substantially uniform texture feature. However, if a tumor is present in the region, the uniform texture feature will be interrupted. Thus, using texture analysis to evaluate the wall of the bladder, a region which may exhibit a tumor will present itself as a disturbance, or "noisy region" within the uniform texture.

The texture of a region can be represented by a probability distribution function (PDF) which characterizes the intensity correlation between voxels within a defined range. A two-dimensional PDF can be used to represent a texture feature. Such a PDF characterizes the correlation between two closest voxels along all directions. To estimate the PDF, the intensities of any two closest neighbor voxels in a region of interest can be recorded as a sample vector for the region of interest (e.g., context). Using a number of such sample vectors, a cumulating distribution function (CDF) can be generated which estimates the PDF for that context. For each voxel, sample vectors within a range of its neighbor can also be used to generate a local CDF.

A statistical test, such as a Kolmogorov-Smirnov test, can be applied to the CDF to determine whether the CDF of the context and the local CDF are statistically equivalent, e.g., within a predefined confidence level. If so, the local texture feature around the current voxel is regarded as identical to the context. Otherwise, the current voxel exhibits a different texture feature from that of the

context and may be regarded as a potential abnormality, such as a tumor. The level of confidence used to determine whether a voxel is statistically equivalent to the context can be varied to increase or decrease the sensitivity of detection.

In an alternative method of applying the PDF or CDF for texture analyis, each CDF or PDF can be regarded as a point in a functional linear space. The distance between two CDF's or PDF's in that space can be measured, such as in terms of the Skorohold metric. This distance provides a measure of the degree of similarity of PDF's. For example, the distance between a local CDF and the context CDF can be calculated and the resulting distance can be compared to one or more distancing thresholds. If the distance is large, the local texture may be considered different from the context, which can indicate that such a voxel belongs to a region with a potential abnormality or tumor. Preferably, the distancing thresholds are determined based on evaluation of a statistically sufficient known data sets.

The distance calculated above can be used with visualization techniques and volume rendering techniques, such as those described herein. For example, a feature volume dataset having a size comparable to the original dataset can be created. The intensity for each voxel in the new dataset can then be assigned based upon the distance between the local CDF and the CDF of the context. When this three dimensional volume dataset is viewed through volume rendering techniques, the regions which contain suspected tumors will exhibit a higher image intensity than the surrounding area.

As was discussed above in connection with automatic detection of polyps, the surface of a lumen can be represented as a continuously second differentiable surface in three dimensional Euclidean space, such as by using a C-2 smoothness surface model. In such a model, each voxel on the surface of the colon has an associated geometrical feature which has a Gauss curvature, referred to as Gauss curvature fields. For various organs, certain expected local features can be characterized by distinct curvature templates. For example, in the context of the colon, the expected local features include smooth curve surfaces, ring folds, convex hills from a smooth surface and plateaus from a smooth surface. These last two local features may be indicative of a polyp or tumor. Accordingly, by searching the Gauss curvature

fields for specific predetermined local feature templates, polyps, tumors and other abnormalities of interest can be automatically detected. This use of surface geometry to perform computer assisted diagnosis can be used alone, or in conjunction with the texture-based CAD techniques described above.

As an alternative to rendering and viewing the entire organ or region of interest, the surface under observation can be partitioned into small areas, or patches, which are defined by the local curvature templates. Each patch should contain voxels which have a common geometry feature, or curvature template. A single viewing point is then determined for the patch which allows all voxels of the patch to be observed. The patches are then assigned a priority score indicating the probability that the patch represents a polyp or other abnormality. The patches can then be observed individually, in priority order, rather than requiring the operator to navigate the entire organ volume to search out suspect areas. Of course, a preferred diagnostic system includes the ability to toggle between views such that an operator can readily change from viewing a patch to viewing the patch in the context of the organ. Alternatively, these two views can be presented simultaneously. Again, the texture based approaches can be used to supplement this approach. By mapping the results of texture analysis onto the patches being observed, the texture information can also be observed and used in diagnoses.

The foregoing merely illustrates the principles of the present imaging and examination systems and methods. It will thus be appreciated that those skilled in the art will be able to devise numerous systems, apparatus and methods which, although not explicitly shown or described herein, embody the principles of the invention and are thus within the spirit and scope of the invention as defined by its claims.

For example, the methods and systems described herein could be applied to virtually examine an animal, fish or inanimate object. Besides the stated uses in the medical field, applications of the technique could be used to detect the contents of sealed objects which cannot be opened. The techniques can also be used inside an architectural structure such as a building or cavern and enable the operator to navigate through the structure.

CLAIMS

1. A method for performing virtual examination of an object comprising:

performing at least one scan of an object with the object distended by the presence of a contrast agent;

performing at least one scan of the object with the object relieved of the contrast agent;

converting the scans to corresponding volume datasets comprising a plurality of voxels;

performing image segmentation to classify the voxels of each scan into a plurality of categories;

registering the volume datasets of each scan to a common coordinate system;

displaying at least two of the volume datasets in a substantially simultaneous manner; and

performing virtual navigation operations in one of the volume datasets and having the corresponding navigation operations take place in at least one other volume dataset.

2. The method for performing virtual examination according to claim 1, wherein the at least one scan of the distended object includes a transverse scan and a coronal scan of the object.

3. The method for performing virtual examination according to claim 2, wherein the at least one scan of the relieved object includes a transverse scan and a coronal scan of the object.

4. The method for performing virtual examination according to claim 3, wherein the object is a bladder.

5. The method of performing virtual examination according to claim 4, wherein the scans are computed tomography scans.

6. The method of performing virtual examination according to claim 4, wherein the scans are ultrasound imaging scans.

7. The method of performing virtual examination according to claim 4, wherein the scans are magnetic resonance imaging scans.

8 The method of performing virtual examination according to claim 7, wherein the contrast agent is urine.

9. The method for performing virtual examination according to claim 1, wherein the at least one scan of the relieved object includes a transverse scan and a coronal scan of the object.

10. The method for performing virtual examination according to claim 1, wherein the object is a bladder.

11. The method of performing virtual examination according to claim 10, wherein the scans are computed tomography scans.

12. The method of performing virtual examination according to claim 10, wherein the scans are ultrasound imaging scans.

13. The method of performing virtual examination according to claim 10, wherein the scans are magnetic resonance imaging scans

14. The method of performing virtual examination according to claim 13, wherein the contrast agent is urine.

15. The method of performing virtual examination according to claim 1, further comprising evaluating the at least one scan with the object distended and the at least one scan with the object relieved to identify regions where contrast is more visible in one of said scans and evaluating the scan with more contrast in a region of interest to determine physiological characteristics of the object.

16. The method of performing virtual examination according to claim 15, wherein said step of image segmentation includes classifying voxels based on local intensity vectors of the voxels.

17. The method of performing virtual examination according to claim 16, wherein the step of image segmentation further includes using a region growing algorithm to identify regions of the object based on the classified voxels.

18. The method of performing virtual examination according to claim 1, further comprising partitioning the volume image datasets into a plurality of regions related to the coordinate system.

19. The method of performing virtual examination according to claim 18, wherein the plurality of regions include eight regions defined in a three dimensional coordinate system.

20. A method for performing virtual examination of an object comprising:

performing an imaging scan of the object to acquire image scan data;

converting the acquired image scan data to a plurality of voxels;

interpolating between the voxels to generate an expanded dataset;

performing image segmentation to classify the voxels into a plurality of categories;

extracting a volume of the object interior from the expanded dataset;

generating a reduced resolution dataset from the expanded dataset;

storing the expanded dataset in a tree data structure;

rendering images for the expanded dataset and reduced resolution dataset; and

selecting at least one of the reduced resolution dataset or expanded dataset renderings for display.

21. The method for performing virtual examination of an object of claim 20, wherein the selecting step comprises:

selecting the reduced resolution dataset during image interaction; and

selecting the expanded dataset rendering if no image interaction has occurred in a predetermined time period.

22. The method for performing virtual examination of an object of claim 20, wherein the imaging scan is a computed tomography scan.

23. The method for performing virtual examination of an object of claim 20, wherein the imaging scan is a magnetic resonance imaging scan.

24. The method for performing virtual examination of an object of claim 20, wherein the imaging scan is an ultrasound imaging scan.

25. The method for performing virtual examination of an object of claim 20, wherein the object is the larynx.

26. The method for performing virtual examination of an object of claim 20, wherein the tree structure is a binary space partition tree structure.

27. A method of performing virtual angiography comprising:

acquiring imaging scan data including at least a portion of the aorta;

converting the imaging scan data to a volume representation including a plurality of voxels;

segmenting the volume representation to classify the voxels into one of a plurality of categories;

analyzing the segmented volume representation to identify voxels indicative of at least a portion of an aneurysm in the aortic wall; and

generating at least one closing surface around the voxels indicative of at least a portion of an aneurysm to estimate the contour of the aneurysm.

28. The method of performing virtual angiography of claim 27, wherein the imaging scan is a computed tomography scan.

29. The method of performing virtual angiography of claim 27, wherein the imaging scan is a magnetic resonance imaging scan.

30. The method of performing virtual angiography of claim 27, wherein the segmenting operation classifies voxels in at least the categories of blood, tissue, and calcium deposits.

31. The method of performing virtual angiography of claim 27, further comprising estimating the volume of the aneurysm using the generated closing surfaces.

32. The method of performing virtual angiography of claim 27, further comprising generating a navigation path through the aortic lumen.

33. The method of performing virtual angiography of claim 32, further comprising estimating the length of the aneurysm based on the navigation path.

34. A method of performing virtual endoscopy of a blood vessel comprising:

acquiring imaging scan data including at least a portion of the vessel;

converting the imaging scan data to a volume representation including a plurality of voxels;

segmenting the volume representation to classify the voxels into one of a plurality of categories including the categories of blood, tissue, and calcium deposits; and

generating a navigation path through the vessel.

35. The method of performing virtual endoscopy of claim 34, wherein the vessel is a carotid artery.

36. The method of performing virtual endoscopy of claim 34, further comprising the step of determining the diameter of the carotid artery along the navigation path to identify regions of narrowing.

37. The method of performing virtual angiography of claim 34, wherein the imaging scan is a computed tomography scan.

38. The method of performing virtual angiography of claim 34, wherein the imaging scan is a magnetic resonance imaging scan.

39. A method of determining the characteristics of a stent graft using virtual angioscopy, comprising:

acquiring imaging scan data including at least a portion of the aorta;

converting the imaging scan data to a volume representation including a plurality of voxels;

segmenting the volume representation to classify the voxels into one of a plurality of categories;

analyzing the segmented volume representation to identify voxels indicative of at least a portion of an aneurysm in the aortic wall;

generating at least one closing surface around the voxels indicative of at least a portion of an aneurysm to estimate the contour of the aneurysm;

identifying the location of the endpoints of the aneurysm contour;

calculating the length between the endpoints of the aneurysm contour to determine the length of the stent graft; and

calculating the diameter of the aortic lumen at the endpoints of the aneurysm contour to determine the required outside diameters of the stent graft.

40. The method of determining the characteristics of a stent graft of claim 39, further comprising determining the angle of interface of the aneurysm and normal aortic lumen to determine an angular direction of a corresponding end of the stent graft.

41. The method of determining the characteristics of a stent graft of claim 39, further comprising locating arterial branches proximate the aneurysm to determine a maximum length of the stent graft.

42. The method of determining the characteristics of a stent graft of claim 41, wherein the arterial branches proximate the aneurysm include at least one of the renal and femoral arterial branches.

43. The method of determining the characteristics of a stent graft of claim 39, further comprising conducting a virtual biopsy of the aortic region proximate the ends of the aneurysm to determine the nature of the tissue at the anticipated graft interface locations.

44. A method of defining a skeleton for a three dimensional image representation of a hollow object formed with a plurality of voxels comprising:

identifying a root voxel within the hollow object;

generating a distance map for all voxels within the hollow object, the distance map being formed using a 26-connected cubic plate of neighboring voxels having Euclidian weighted distances;

identifying voxels having a local maxima in the distance map as endpoints of branches in the hollow object; and

for each local maxima voxel, determining a shortest connected path to one of the root voxel or a previously defined shortest path.

45. The method of defining a skeleton for a three dimensional image representation of claim 44 further comprising performing multi-resolution data reduction to the three dimensional image representation to generate a reduced data set for the generating and identifying operations.

46. The method of defining a skeleton for a three dimensional image representation of claim 44 further comprising centralizing the shortest paths within the respective branches of the object.

47. The method of defining a skeleton for a three dimensional image representation of claim 44, wherein the object includes at least one blood vessel.

48. The method of defining a skeleton for a three dimensional image representation of claim 44, wherein the object includes the airways of a lung.

49. The method of defining a skeleton for a three dimensional image representation of claim 44, wherein the object includes the bladder.

50. The method of defining a skeleton for a three dimensional image representation of claim 44, wherein the object includes the spinal cord of a vertebrate animal.

51. A method of performing computed assisted diagnosis of a region of interest, comprising:

acquiring imaging scan data including at least a portion of the region of interest;

converting the imaging scan data to a volume representation including a plurality of voxels, at least a portion of the voxels representing a surface of the region of interest; and

analyzing said portion of voxels representing a surface for at least one of a geometric feature and a textural feature indicative of an abnormality.

52. The method of performing computed assisted diagnosis according to claim 51, wherein the textural feature is included in a probability density function characterizing a correlation between two voxels of the portion of voxels.

53 The method of performing computed assisted diagnosis according to claim 52, wherein the two voxels are adjacent voxels.

54. The method of performing computer assisted diagnosis according to claim 52, wherein intensities of said portion of voxels are used to generate an estimate of the probability density function.

55. The method of performing computer assisted diagnosis according to claim 54, wherein a plurality of voxel intensities are used to generate a cumulating distribution function of the region of interest and a local cumulating distribution function, and wherein the local cumulating distribution function is compared against the context cumulating distribution function to identify regions of abnormality.

56. The method of performing computer assisted diagnosis according to claim 55, wherein a distance is determined between said local cumulating distribution function and said context cumulating distribution function, the distance providing a measure of abnormality.

57. The method of performing computer assisted diagnosis according to claim 56, wherein the distance is used to assign intensity values to the voxels representing a

surface of the region of interest and wherein said method further comprises displaying said voxels such that variations in intensity represent regions of abnormality.

58. The method of performing computer assisted diagnosis according to claim 57, wherein the region of interest includes the colon and wherein the abnormality includes polyps.

59. The method of performing computer assisted diagnosis according to claim 51, wherein the region of interest includes the aorta and wherein the abnormality includes abdominal aortic aneurysms.

60. The method of performing computer assisted diagnosis according to claim 51 wherein the surface is represented as a second differentiable surface where each surface volume unit has an associate Gauss curvature and wherein said Gauss curvatures combine to form said geometric features.

61. The method of performing computer assisted diagnosis according to claim 59 wherein a plurality of predetermined geometrical feature templates are defined and wherein the geometric features of said surface are compared to said templates to determine a geometric feature classification.

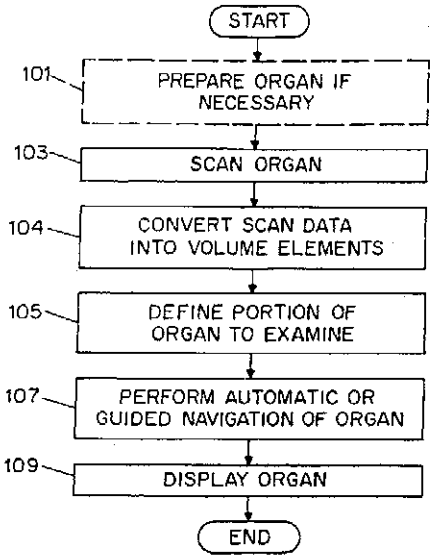
START
101
PREPARE ORGAN IF NECESSARY
103
SCAN ORGAN
104
CONVERT SCAN DATA INTO VOLUME ELEMENTS
105
DEFINE PORTION OF ORGAN TO EXAMINE
107
PERFORM AUTOMATIC OR GUIDED NAVIGATION OF ORGAN
109
DISPLAY ORGAN
END

FIG. 1

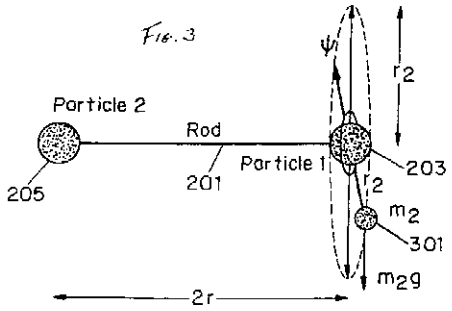
Fig. 3
Particle 2
Rod
Particle 1
205
201
203
r2
r2
m2
301
m29
2r

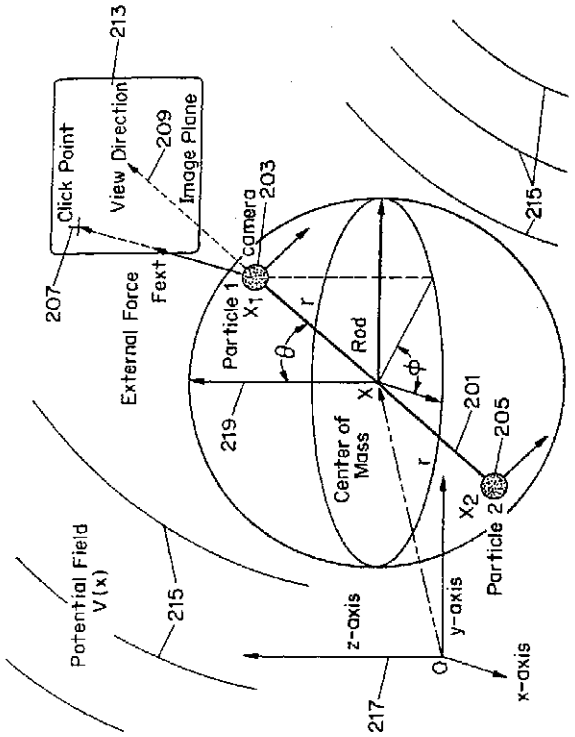
213
View Direction
209
Image Plane
Click Point
207
External Force
Fext
Camera
203
Particle 1
X1
r
θ
Rod
φ
X
Center of Mass
219
201
205
r
X2
Particle 2
215
215
Potential Field
V(x)
z-axis
y-axis
0
x-axis
217

FIG. 2

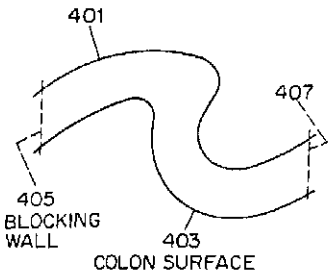

FIG. 4

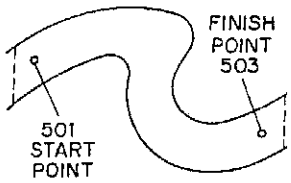

FIG. 5

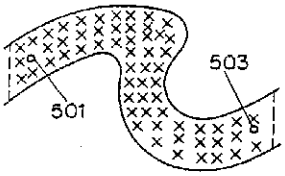

FIG. 6

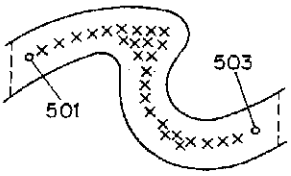

FIG. 7

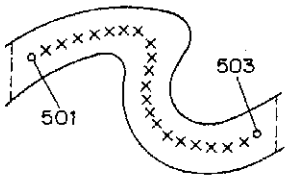

FIG. 8

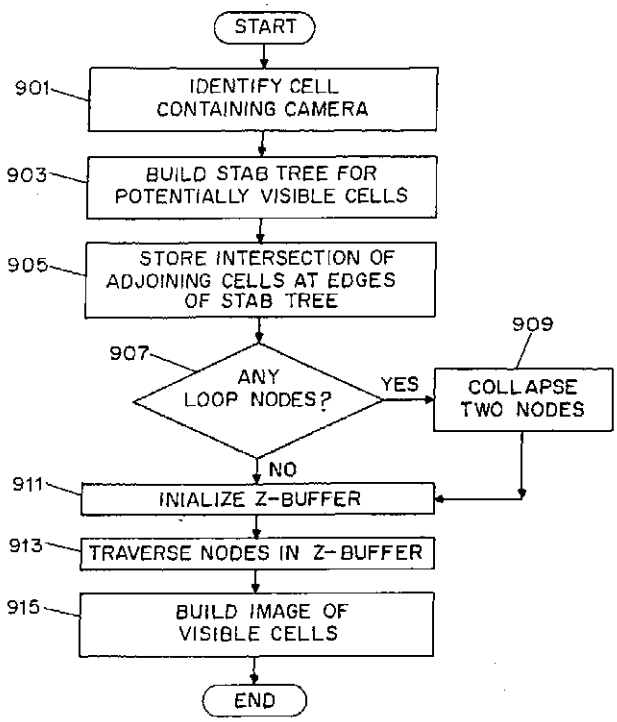
START
901
IDENTIFY CELL CONTAINING CAMERA
903
BUILD STAB TREE FOR POTENTIALLY VISIBLE CELLS
905
STORE INTERSECTION OF ADJOINING CELLS AT EDGES OF STAB TREE
907
ANY LOOP NODES?
YES
909
COLLAPSE TWO NODES
NO
911
INIALIZE Z-BUFFER
913
TRAVERSE NODES IN Z-BUFFER
915
BUILD IMAGE OF VISIBLE CELLS
END

FIG. 9

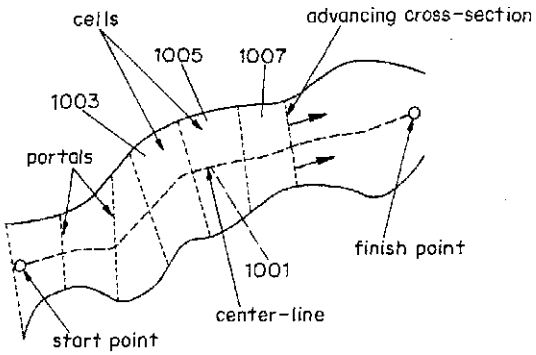

FIG. 10

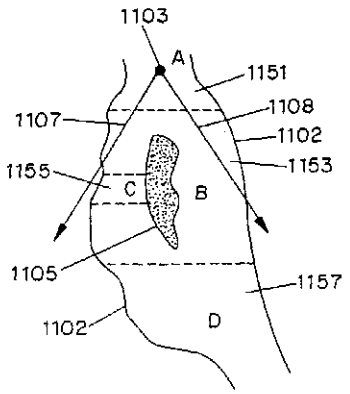

FIG. 11(a)

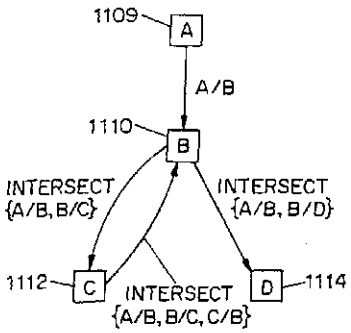

FIG. 11(b)

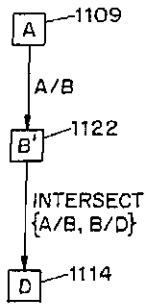

FIG. 11(c)

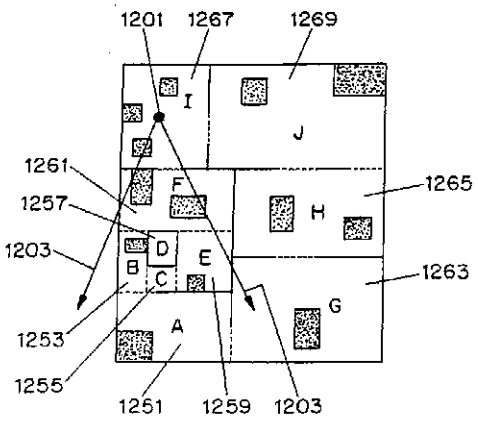

FIG. 12(a)

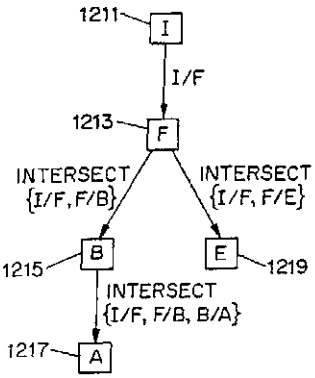

FIG. 12(b)

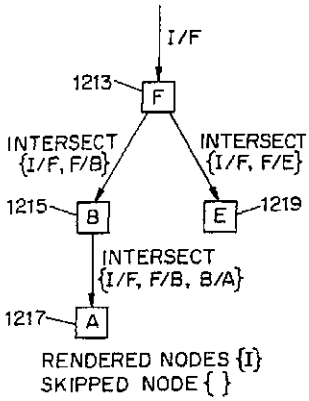

FIG. 12(c)

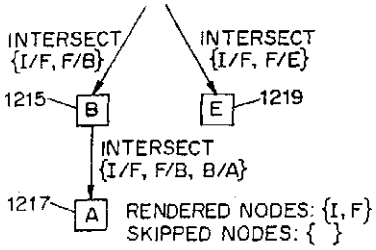

FIG. 12(d)

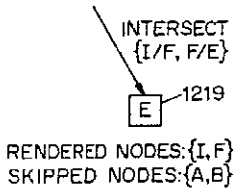

FIG. 12(e)

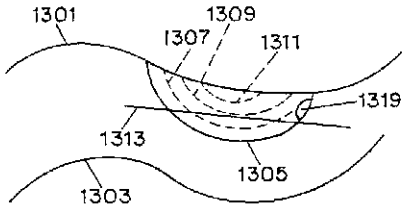

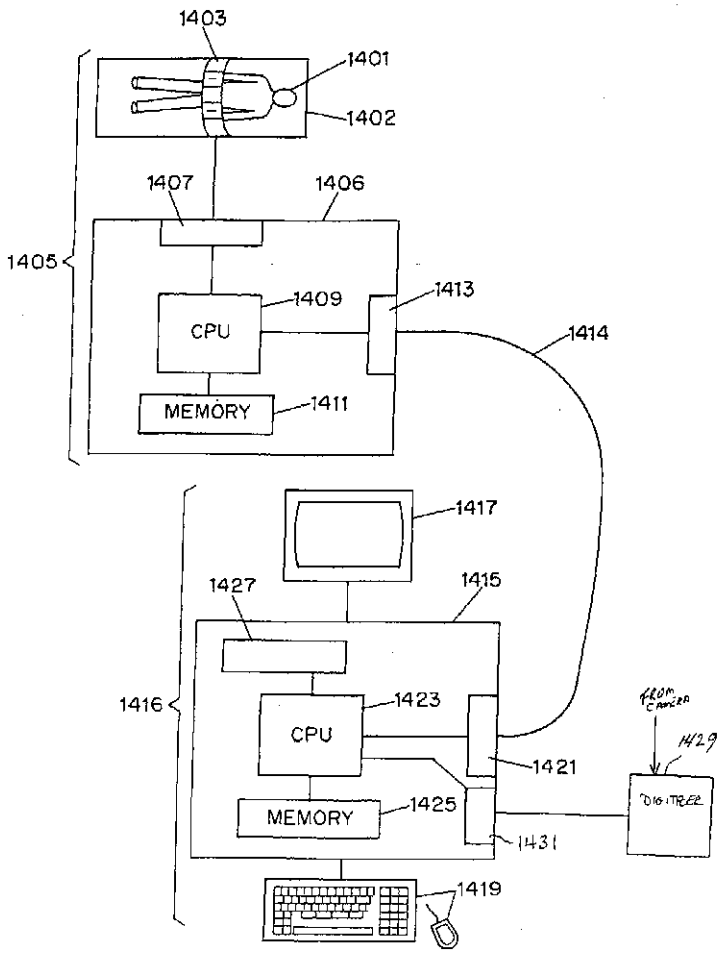
1403
1401
1402
1407
1406
1405
CPU
1409
1413
1414
MEMORY
1411
1417
1427
1415
1416
1423
CPU
1421
MEMORY
1425
1431
1419

FIG. 14

Fig. 15

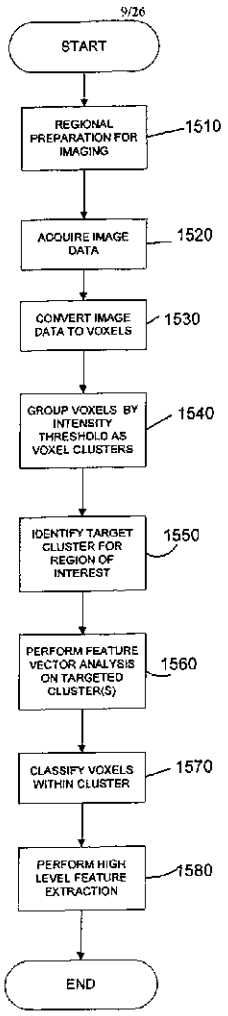
START
REGIONAL PREPARATION FOR IMAGING
1510
ACQUIRE IMAGE DATA
1520
CONVERT IMAGE DATA TO VOXELS
1530
GROUP VOXELS BY INTENSITY THRESHOLD AS VOXEL CLUSTERS
1540
IDENTIFY TARGET CLUSTER FOR REGION OF INTEREST
1550
PERFORM FEATURE VECTOR ANALYSIS ON TARGETED CLUSTER(S)
1560
CLASSIFY VOXELS WITHIN CLUSTER
1570
PERFORM HIGH LEVEL FEATURE EXTRACTION
1580
END

Fig. 16

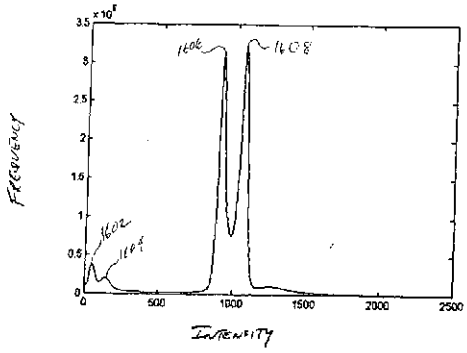
3.5 x 10^5
3
2.5
2
1.5
1
0.5
0
0
500
1000
1500
2000
2500
1606
1608
1602
1604
FREQUENCY
INTENSITY

Fig. 17

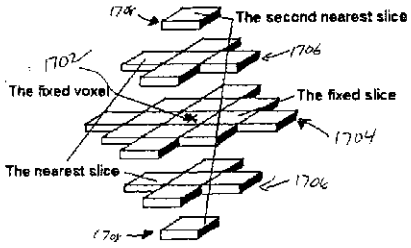
1704
The second nearest slice
1706
1702
The fixed voxel
The fixed slice
1704
The nearest slice
1706
1706

Fig. 18A

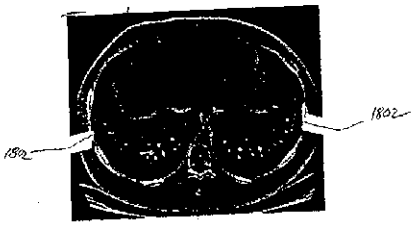

Fig 18B

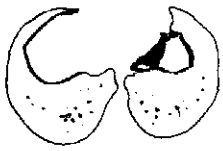

Fig. 18C

Fig. 20

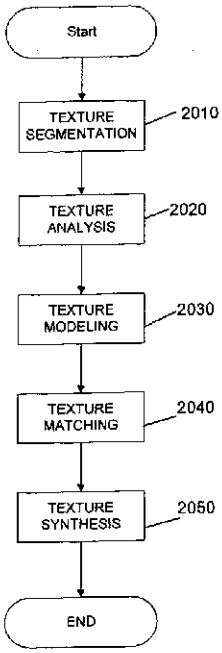
Start
TEXTURE SEGMENTATION
2010
TEXTURE ANALYSIS
2020
TEXTURE MODELING
2030
TEXTURE MATCHING
2040
TEXTURE SYNTHESIS
2050
END

FIG. 21

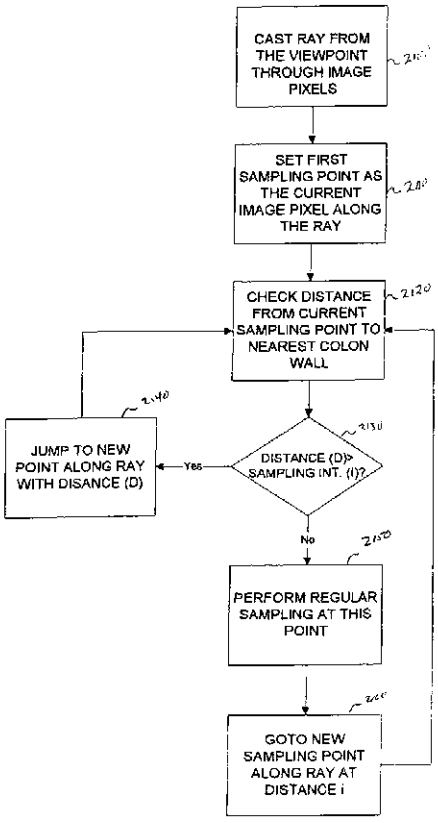
CAST RAY FROM THE VIEWPOINT THROUGH IMAGE PIXELS
SET FIRST SAMPLING POINT AS THE CURRENT IMAGE PIXEL ALONG THE RAY
CHECK DISTANCE FROM CURRENT SAMPLING POINT TO NEAREST COLON WALL
DISTANCE (D)> SAMPLING INT. (I)?
Yes
JUMP TO NEW POINT ALONG RAY WITH DISANCE (D)
No
PERFORM REGULAR SAMPLING AT THIS POINT
GOTO NEW SAMPLING POINT ALONG RAY AT DISTANCE i

FIG. 22

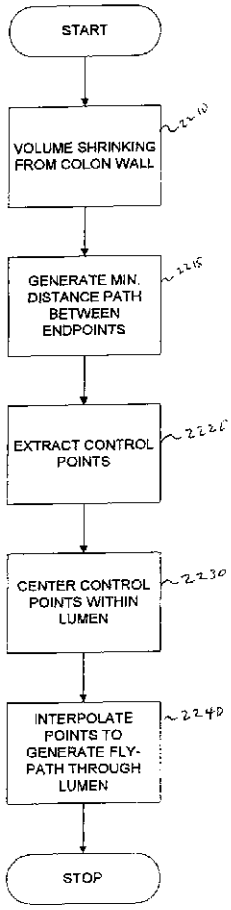
START
VOLUME SHRINKING FROM COLON WALL
2210
GENERATE MIN. DISTANCE PATH BETWEEN ENDPOINTS
2215
EXTRACT CONTROL POINTS
2220
CENTER CONTROL POINTS WITHIN LUMEN
2230
INTERPOLATE POINTS TO GENERATE FLY-PATH THROUGH LUMEN
2240
STOP

FIG. 23

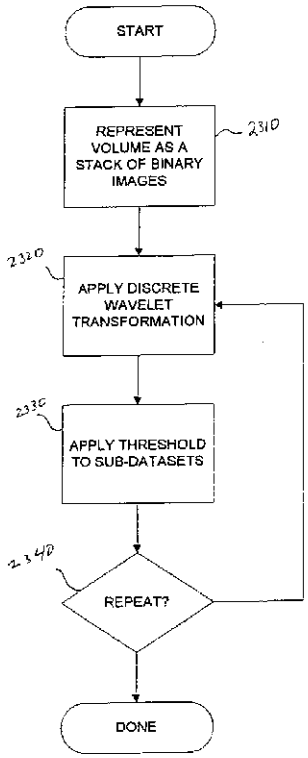
START
REPRESENT VOLUME AS A STACK OF BINARY IMAGES
2310
2320
APPLY DISCRETE WAVELET TRANSFORMATION
2330
APPLY THRESHOLD TO SUB-DATASETS
2340
REPEAT?
DONE

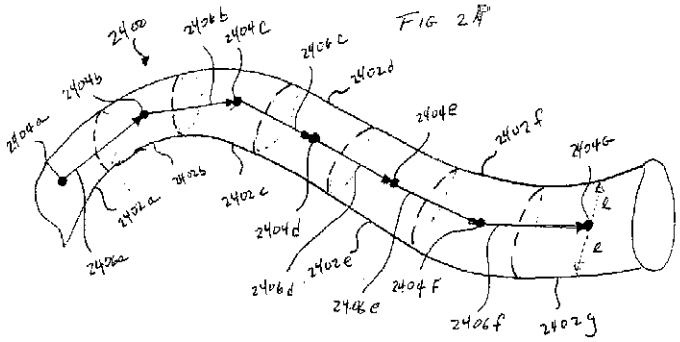
FIG 24
2400
2406b
2404c
2406c
2402d
2404b
2404a
2404e
2402f
2406g
2402a
2406a
2402c
2404d
2406d
2402e
2406e
2404F
2406f
2402g
ℓ
ℓ

FIG. 25

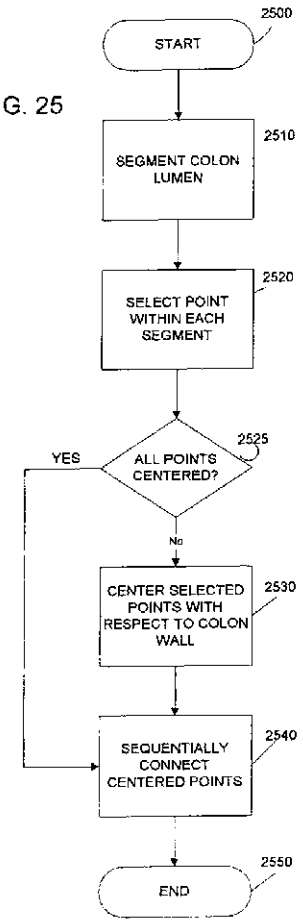
2500
START
2510
SEGMENT COLON LUMEN
2520
SELECT POINT WITHIN EACH SEGMENT
2525
ALL POINTS CENTERED?
YES
No
2530
CENTER SELECTED POINTS WITH RESPECT TO COLON WALL
2540
SEQUENTIALLY CONNECT CENTERED POINTS
2550
END

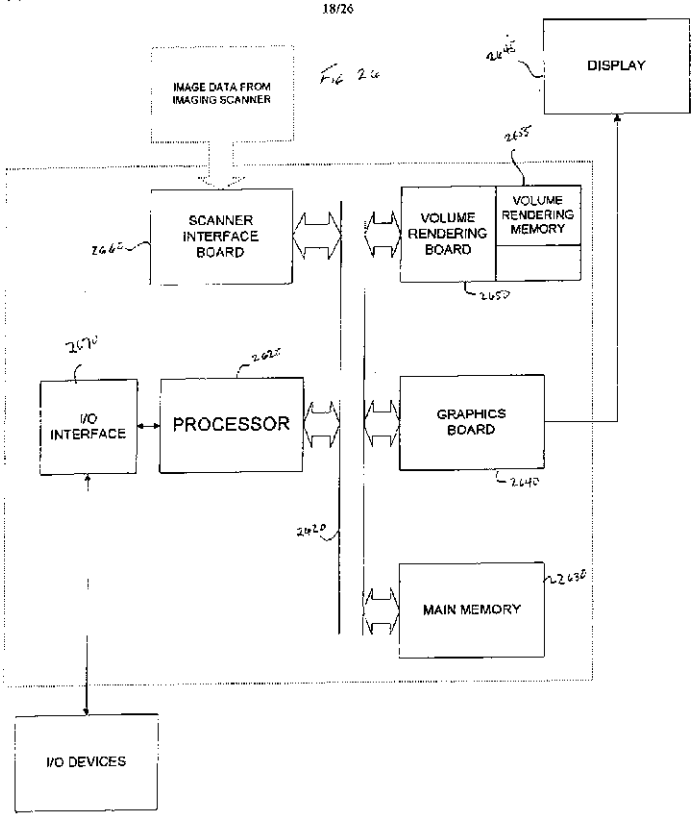
IMAGE DATA FROM IMAGING SCANNER
DISPLAY
SCANNER INTERFACE BOARD
VOLUME RENDERING BOARD
VOLUME RENDERING MEMORY
I/O INTERFACE
PROCESSOR
GRAPHICS BOARD
MAIN MEMORY
I/O DEVICES

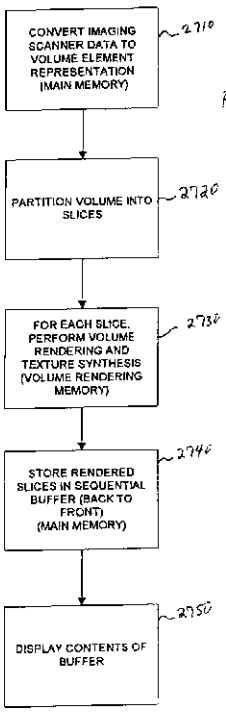
CONVERT IMAGING SCANNER DATA TO VOLUME ELEMENT REPRESENTATION (MAIN MEMORY)
2710
PARTITION VOLUME INTO SLICES
2720
FOR EACH SLICE, PERFORM VOLUME RENDERING AND TEXTURE SYNTHESIS (VOLUME RENDERING MEMORY)
2730
STORE RENDERED SLICES IN SEQUENTIAL BUFFER (BACK TO FRONT) (MAIN MEMORY)
2740
DISPLAY CONTENTS OF BUFFER
2750

Fig. 27

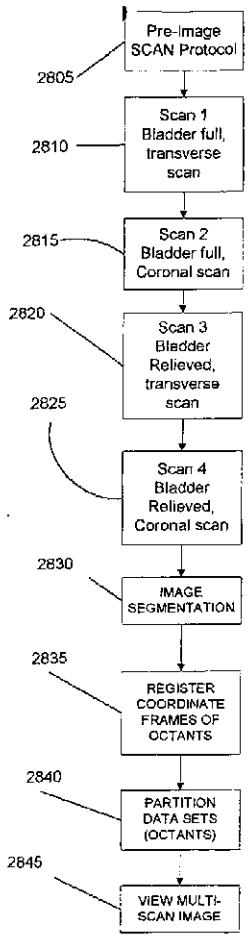
Pre-Image SCAN Protocol
2805
Scan 1 Bladder full, transverse scan
2810
Scan 2 Bladder full, Coronal scan
2815
Scan 3 Bladder Relieved, transverse scan
2820
Scan 4 Bladder Relieved, Coronal scan
2825
IMAGE SEGMENTATION
2830
REGISTER COORDINATE FRAMES OF OCTANTS
2835
PARTITION DATA SETS (OCTANTS)
2840
VIEW MULTI-SCAN IMAGE
2845

Fig. 28

FIG. 29

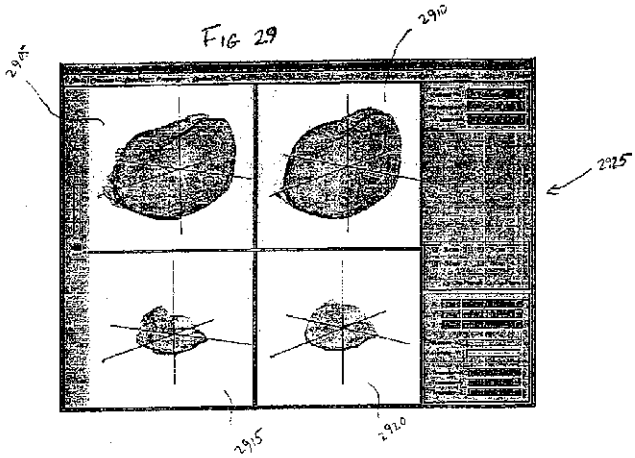

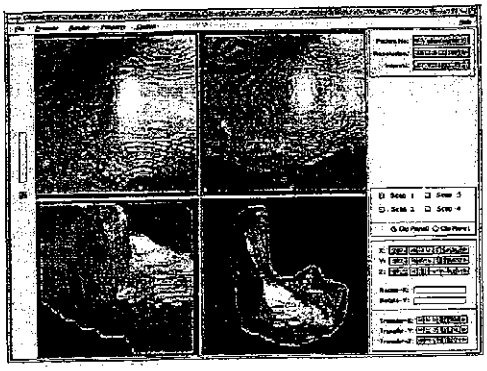

FIG. 30

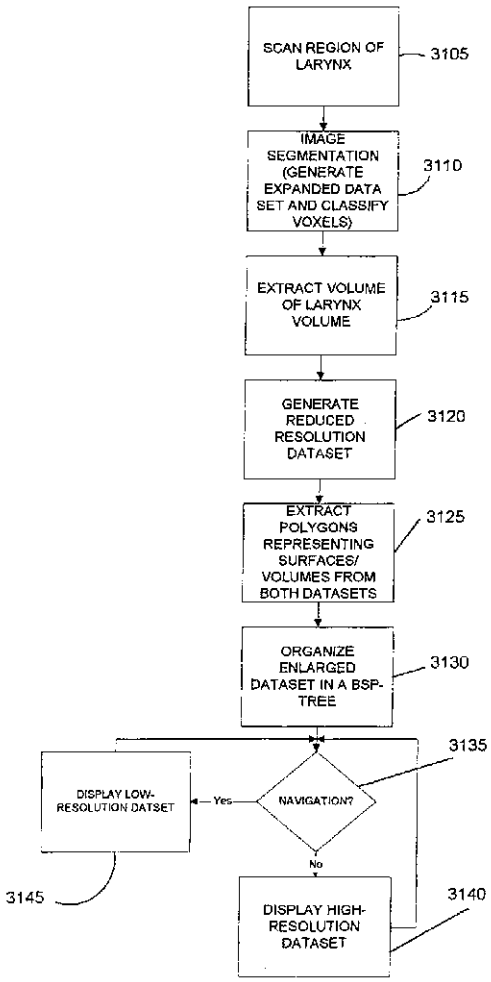
SCAN REGION OF LARYNX
3105
IMAGE SEGMENTATION (GENERATE EXPANDED DATA SET AND CLASSIFY VOXELS)
3110
EXTRACT VOLUME OF LARYNX VOLUME
3115
GENERATE REDUCED RESOLUTION DATASET
3120
EXTRACT POLYGONS REPRESENTING SURFACES/ VOLUMES FROM BOTH DATASETS
3125
ORGANIZE ENLARGED DATASET IN A BSP-TREE
3130
3135
NAVIGATION?
Yes
No
DISPLAY LOW-RESOLUTION DATSET
3145
DISPLAY HIGH-RESOLUTION DATASET
3140

F 3 β1

FIG. 32

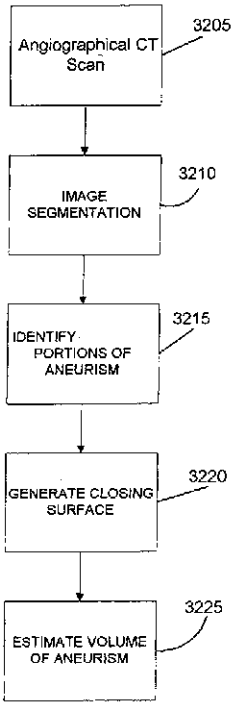
Angiographical CT Scan
3205
IMAGE SEGMENTATION
3210
IDENTIFY PORTIONS OF ANEURISM
3215
GENERATE CLOSING SURFACE
3220
ESTIMATE VOLUME OF ANEURISM
3225

FIG. 33A FIG. 33B FIG 33C

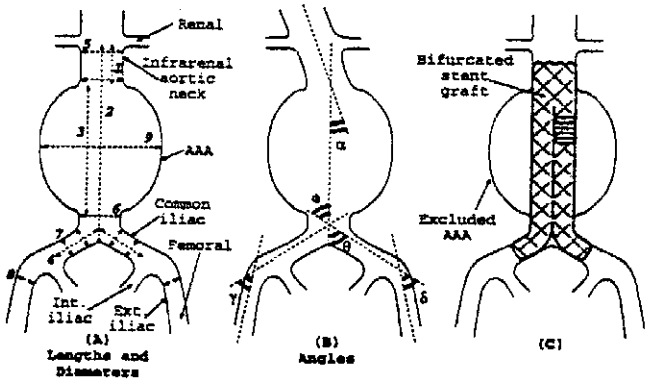

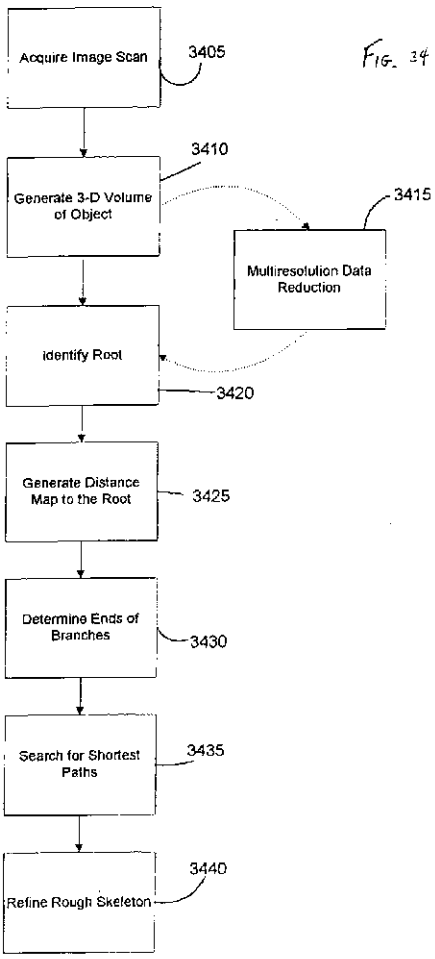
Acquire Image Scan
3405
Generate 3-D Volume of Object
3410
Multiresolution Data Reduction
3415
Identify Root
3420
Generate Distance Map to the Root
3425
Determine Ends of Branches
3430
Search for Shortest Paths
3435
Refine Rough Skeleton
3440

Fig. 34

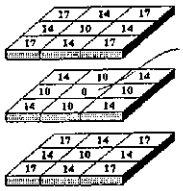

3505

FIG. 35

FIG. 36

```
1) Label root voxel with integer 0;
2) Construct a queue and line up the root in the queue;
3) If( There is at least one voxel in the queue )
     Serve the voxel x on the top of the queue;
     For( each of x's 26-connected neighbor voxel y) {
       If( y in the volume and has not been labeled yet ) {
         Line up the y in the queue;

         /* label the voxel y */
         Set dist = 999999 ;
         For( each of y's 26-connected neighbor voxel z ) {
           If( z in the volume and has been already labeled with an integer of n_z ) {
             d_z = n_z + d(y,z);
             where d(y,z) is 10, 14 or 17 if the Euclidean distance between y and z is
             1, √2, or √3, respectively;
           }
           If( dist > d_z ) {
             label y with integer dist ;
             dist = d_z ;
           }
         }
       }
     }
     x leaves the queue;
   }
   Else {
     end of calculating the distance map.
   }
```

【国際公開パンフレット（コレクトバージョン）】

(12) INTERNATIONAL APPLICATION PUBLISHED UNDER THE PATENT COOPERATION TREATY (PCT)

CORRECTED VERSION

(19) World Intellectual Property Organization
International Bureau

(43) International Publication Date
11 April 2002 (11.04.2002)

PCT

(10) International Publication Number
WO 02/029764 A1

(51) International Patent Classification[7]: G09B 23/28, G06F 17/00, G06T 1/00, 13/00, 15/50, 17/00

(21) International Application Number: PCT/US01/30703

(22) International Filing Date: 1 October 2001 (01.10.2001)

(25) Filing Language: English

(26) Publication Language: English

(30) Priority Data:
60/237,665 3 October 2000 (03.10.2000) US
09/777,120 5 February 2001 (05.02.2001) US

(71) Applicant: THE RESEARCH FOUNDATION OF STATE UNIVERSITY OF NEW YORK [US/US]; Office of Technology Licensing, State University of New York at Stony Brook, Stony Brook, NY 11794 (US).

(72) Inventors: KAUFMAN, Arie, E.; 94 Cedar Drive W., Plainview, NY 11803 (US). LIANG, Zhengrong; 28 Houghton Boulevard, Stony Brook, NY 11790 (US). WAX, Mark, R.; 5 E. Sanders Street, Greenlawn, NY 11740 (US). WAN, Ming; 439 Chapin Complex, Stony Brook, NY 11790 (US). CHEN, Dongqing; 100 Ronkonkoma Avenue #1, Lake Ronkonkoma, NY 11779 (US). LI, Bin; Apt. 2F, 1 Williams Boulevard, Lake Grove, NY 11755 (US).

(74) Agent: TANG, Henry et al.; Baker Botts, LLP, 30 Rockefeller Plaza, New York, NY 10112-0228 (US).

(81) Designated States (national): AE, AG, AL, AM, AT, AU, AZ, BA, BB, BG, BR, BY, BZ, CA, CH, CN, CO, CR, CU, CZ, DE, DK, DM, DZ, EC, EE, ES, FI, GB, GD, GE, GH, GM, HR, HU, ID, IL, IN, IS, JP, KE, KG, KP, KR, KZ, LC, LK, LR, LS, LT, LU, LV, MA, MD, MG, MK, MN, MW, MX, MZ, NO, NZ, PH, PL, PT, RO, RU, SD, SE, SG, SI, SK, SL, TJ, TM, TR, TT, TZ, UA, UG, UZ, VN, YU, ZA, ZW.

(84) Designated States (regional): ARIPO patent (GH, GM, KE, LS, MW, MZ, SD, SL, SZ, TZ, UG, ZW), Eurasian patent (AM, AZ, BY, KG, KZ, MD, RU, TJ, TM), European patent (AT, BE, CH, CY, DE, DK, ES, FI, FR, GB, GR, IE, IT, LU, MC, NL, PT, SE, TR), OAPI patent (BF, BJ, CF, CG, CI, CM, GA, GN, GQ, GW, ML, MR, NE, SN, TD, TG).

Published:
— with international search report

(48) Date of publication of this corrected version:
23 January 2003

(15) Information about Correction:
see PCT Gazette No. 04/2003 of 23 January 2003, Section II

For two-letter codes and other abbreviations, refer to the "Guidance Notes on Codes and Abbreviations" appearing at the beginning of each regular issue of the PCT Gazette.

WO 02/029764 A1

(54) Title: SYSTEM AND METHOD FOR PERFORMING A THREE-DIMENSIONAL VIRTUAL EXAMINATION OF OBJECTS, SUCH AS INTERNAL ORGANS

(57) Abstract: Methods for generating a three-dimensional visualization image of an object, such as an internal organ, using volume visualization techniques are provided. The techniques includes a multi-scan imaging method, a preparation imaging method and a method for generating a skeleton of a complex three dimension object. The applications include virtual cystoscopy, virtual laryngoscopy, virtual angiography, among others.

SYSTEM AND METHOD FOR PERFORMING A THREE-DIMENSIONAL VIRTUAL EXAMINATION OF OBJECTS, SUCH AS INTERNAL ORGANS

SPECIFICATION

TECHNICAL FIELD

The present invention relates to a system and method for performing a volume based three-dimensional virtual examination, and more particularly relates to a system which offers enhanced visualization and navigation properties.

BACKGROUND OF THE INVENTION

Colon cancer continues to be a major cause of death throughout the world. Early detection of cancerous growths, which in the human colon initially manifest themselves as polyps, can greatly improve a patient's chance of recovery. Presently, there are two conventional ways of detecting polyps or other masses in the colon of a patient. The first method is a colonoscopy procedure, which uses a flexible fiber-optic tube called a colonoscope to visually examine the colon by way of physical rectal entry with the scope. The doctor can manipulate the tube to search for any abnormal growths in the colon. The colonoscopy, although reliable, is both relatively costly in money and time, and is an invasive, uncomfortable painful procedure for the patient.

The second detection technique is the use of a barium enema and two-dimensional X-ray imaging of the colon. The barium enema is used to coat the colon with barium, and a two-dimensional X-ray image is taken to capture an image of the colon. However, barium enemas may not always provide a view of the entire colon, require extensive pretreatment and patient manipulation, is often operator-dependent when performing the operation, exposes the patient to excessive radiation and can be less sensitive than a colonoscopy. Due to deficiencies in the conventional practices described above, a more reliable, less intrusive and less expensive way to examine the

colon for polyps is desirable. A method to examine other human organs, such as the lungs, for masses in a reliable, cost effective way and with less patient discomfort is also desirable.

Another leading cause of cancer deaths in the United States is bladder cancer. In 1995, there were 50,000 new cases of bladder cancer reported and 11,000 deaths were reported as a result of this disease. The most common test for bladder cancer is the use of a urine "dipstick" or conventional urinalysis. However, such tests are generally only effective at detecting bladder cancer in its later developed stages and does not provide any information regarding the size or location of a cancerous growth. Cystoscopy, the main method of investigating bladder abnormalities at present, provides accurate results and can provide information regarding the relative size and location of any abnormalities. However, cystoscopy is an invasive procedure which offers a physician a limited field of view and lacks an objective indication of size. In addition, cystoscopy is contra-indicated for those patients who have severe urethral strictures or active vesical bleeding. Thus, it is desirable to develop alternative procedures for screening patients for bladder cancer, especially at early stages of cancer development.

Two-dimensional ("2D") visualization of human organs employing currently available medical imaging devices, such as computed tomography and MRI (magnetic resonance imaging), has been widely used for patient diagnosis. Three-dimensional images can be formed by stacking and interpolating between two-dimensional pictures produced from the scanning machines. Imaging an organ and visualizing its volume in three-dimensional space would be beneficial due to its lack of physical intrusion and the ease of data manipulation. However, the exploration of the three-dimensional volume image must be properly performed in order to fully exploit the advantages of virtually viewing an organ from the inside.

When viewing the three dimensional ("3D") volume virtual image of an environment, a functional model must be used to explore the virtual space. One possible model is a virtual camera which can be used as a point of reference for the viewer to explore the virtual space. Camera control in the context of navigation within a general 3D virtual environment has been previously studied. There are two

conventional types of camera control offered for navigation of virtual space. The first gives the operator full control of the camera which allows the operator to manipulate the camera in different positions and orientations to achieve the view desired. The operator will in effect pilot the camera. This allows the operator to explore a particular section of interest while ignoring other sections. However, complete control of a camera in a large domain would be tedious and tiring, and an operator might not view all the important features between the start and finishing point of the exploration.

The second technique of camera control is a planned navigation method, which assigns the camera a predetermined path to take and which cannot be changed by the operator. This is akin to having an engaged "autopilot". This allows the operator to concentrate on the virtual space being viewed, and not have to worry about steering into walls of the environment being examined. However, this second technique does not give the viewer the flexibility to alter the course or investigate an interesting area viewed along the flight path.

It would be desirable to use a combination of the two navigation techniques described above to realize the advantages of both techniques while minimizing their respective drawbacks. It would be desirable to apply a flexible navigation technique to the examination of human or animal organs which are represented in virtual 3D space in order to perform a non-intrusive painless thorough examination. The desired navigation technique would further allow for a complete examination of a virtual organ in 3D space by an operator allowing flexibility while ensuring a smooth path and complete examination through and around the organ. It would be additionally desirable to be able to display the exploration of the organ in a real time setting by using a technique which minimizes the computations necessary for viewing the organ. The desired technique should also be equally applicable to exploring any virtual object.

It is another object of the invention to assign opacity coefficients to each volume element in the representation in order to make particular volume elements transparent or translucent to varying degrees in order to customize the

visualization of the portion of the object being viewed. A section of the object can also be composited using the opacity coefficients.

SUMMARY OF THE INVENTION

The invention generates a three-dimensional visualization image of an object such as a human organ using volume visualization techniques and explores the virtual image using a guided navigation system which allows the operator to travel along a predefined flight path and to adjust both the position and viewing angle to a particular portion of interest in the image away from the predefined path in order to identify polyps, cysts or other abnormal features in the organ.

A method for performing virtual examination of an object includes performing at least one imaging scan of an object with the object distended by the presence of a contrast agent. In addition, at least one imaging scan of the object is acquired with the object relieved of the contrast agent. The scans are converted to corresponding volume datasets formed with a plurality of voxels. Image segmentation is then performed to classify the voxels of each scan into a plurality of categories. The volume datasets of each scan are registered to a common coordinate system. A displaying operation can then be performed where corresponding images at least two of the volume datasets are substantially simultaneously displayed. Virtual navigation operations performed in one of the volume datasets results in having the corresponding navigation operations take place in at least one other volume dataset.

Preferably, the at least one scan of the distended object includes a transverse scan and a coronal scan of the object. Similarly, it is preferable that the at least one scan of the relieved object includes a transverse scan and a coronal scan of the object. This procedure is particularly well suited for performing virtual cystoscopy, where the object is the bladder. In this case, the scan generally takes the form of a magnetic resonance imaging scan and the contrast agent can be urine.

Another method in accordance with the present invention is for performing virtual examination of an object. In this method, an imaging scan of the object is performed to acquire image scan data. The acquired image scan data is converted to a plurality of volume units, or voxels. By interpolating between the

voxels, an expanded dataset is generated. Image segmentation can then be performed to classify the voxels into a plurality of categories. A volume of the object interior is extracted from the expanded dataset, such as by using a region growing algorithm from a seed voxel within the object lumen. A reduced resolution dataset is then generated from the expanded dataset. To efficiently store and recall the data from the expanded data set, this data is stored in a tree data structure. Images can then be rendered for both the expanded dataset and reduced resolution dataset. One of these images is then selected for viewing. Generally, the reduced resolution dataset is selected during navigation or image interaction whereas the expanded dataset is selected for high resolution, static display.

A method of performing virtual angiography is also provided. In this method, imaging scan data is acquired of at least a portion of the aorta. The imaging scan data is converted to a volume representation including a plurality of voxels. The volume representation is segmented to classify the voxels into one of a plurality of categories. The segmented volume representation is then analyzed to identify voxels indicative of at least a portion of an aneurysm in the aortic wall. From the portions of the aneurysm which are identified, at least one closing surface is generated around the voxels indicative of at least a portion of an aneurysm. The closing surface provides an estimate of the contour of the aneurysm. A navigation path can be established through the aortic lumen and characteristics of the aneurysm, such as length, diameter, volume and composition, can be determined.

The method of performing virtual angiography can be used to detect and monitor the progression of aneurysms and can also be used in determining the characteristics needed to place a stent graft.

Also provided is a method of defining a skeleton for a three dimensional image representation of a hollow object formed with a plurality of voxels. A root voxel is first identified within the hollow object. A distance map is then generated for all voxels within the hollow object. The distance map is formed using a 26-connected cubic plate having Euclidian weighted distances. Those voxels having a local maxima in the distance map are identified as endpoints of branches in the hollow object. For each local maxima voxel, a shortest connected path to either

the root voxel or a previously defined shortest path, is determined. The collection of shortest paths is the rough skeleton of the object. This technique is particularly well suited for multibranch structures such as the respiratory system and cardio vascular system.

BRIEF DESCRIPTION OF THE DRAWINGS

Further objects, features and advantages of the invention will become apparent from the following detailed description taken in conjunction with the accompanying figures showing a preferred embodiment of the invention, on which:

Figure 1 is a flow chart of the steps for performing a virtual examination of an object, specifically a colon, in accordance with the invention;

Figure 2 is an illustration of a "submarine" camera model which performs guided navigation in the virtual organ;

Figure 3 is an illustration of a pendulum used to model pitch and roll of the "submarine" camera;

Figure 4 is a diagram illustrating a two dimensional cross-section of a volumetric colon which identifies two blocking walls;

Figure 5 is a diagram illustrating a two dimensional cross-section of a volumetric colon upon which start and finish volume elements are selected;

Figure 6 is a diagram illustrating a two dimensional cross-section of a volumetric colon which shows a discrete sub-volume enclosed by the blocking walls and the colon surface;

Figure 7 is a diagram illustrating a two dimensional cross-section of a volumetric colon which has multiple layers peeled away;

Figure 8 is a diagram illustrating a two dimensional cross-section of a volumetric colon which contains the remaining flight path;

Figure 9 is a flow chart of the steps of generating a volume visualization of the scanned organ;

Figure 10 is an illustration of a virtual colon which has been sub-divided into cells;

Figure 11A is a graphical depiction of an organ which is being virtually examined;

Figure 11B is a graphical depiction of a stab tree generated when depicting the organ in Fig. 11A;

Figure 11C is a further graphical depiction of a stab tree generated while depicting the organ in Fig. 11A;

Figure 12A is a graphical depiction of a scene to be rendered with objects within certain cells of the scene;

Figure 12B is a graphical depiction of a stab tree generated while depicting the scene in Fig. 12A;

Figures 12C-12E are further graphical depictions of stab trees generated while depicting the image in Fig. 12A;

Figure 13 is a two dimensional representation of a virtual colon containing a polyp whose layers can be removed;

Figure 14 is a diagram of a system used to perform a virtual examination of a human organ in accordance with the invention;

Figure 15 is a flow chart depicting an improved image segmentation method;

Figure 16 is a graph of voxel intensity versus frequency of a typical abdominal CT data set;

Figure 17 is a perspective view diagram of an intensity vector structure including a voxel of interest and its selected neighbors;

Figure 18A is an exemplary image slice from a CT scan of a human abdominal region, primarily illustrating a region including the lungs;

Figure 18B is a pictorial diagram illustrating the identification of the lung region in the image slice of Figure 18A;

Figure 18C is a pictorial diagram illustrating the removal of the lung volume identified in Figure 18B;

Figure 19A is a exemplary image slice form a CT scan of a human abdominal region, primarily illustrating a region including a portion of the colon and bone;

Figure 19B is a pictorial diagram illustrating the identification of the colon and bone region from the image slice of Figure 19A;

Figure 19C is a pictorial diagram illustrating the image scan of figure 19a with the regions of bone removed; and

Figure 20 is a flowchart illustrating a method for applying texture to monochrome image data.

Figure 21 is a flowchart illustrating a method for volume rendering employing a fast perspective ray casting technique;

Figure 22 is a flowchart illustrating a method for determining the central flight path through a colon lumen employing a volume shrinking technique.

Figure 23 is a flowchart further illustrating a volume shrinking technique for use in the method illustrated in Figure 22.

Figure 24 is a three dimensional pictorial representation of a segmented colon lumen with a central fly-path generated therein.

Figure 25 is a flow chart illustrating a method of generating a central flight path through a colon lumen employing a segmentation technique.

Figure 26 is a block diagram of a system embodiment based on a personal computer bus architecture.

Figure 27 is a flow chart illustrating a method of performing volume imaging using the system of Figure 26.

Figure 28 is a flow chart illustrating a multi-scan method for performing virtual examination of an object, such as a bladder (virtual cystoscopy).

Figure 29 is a pictorial representation of a display window suitable for presenting imaging results from the virtual cystoscopy method of Figure 28 and providing illustrative outside views of a bladder structure.

Figure 30 is a pictorial representation of a display window suitable for presenting imaging results from the virtual cystoscopy method of Figure 28 and providing illustrative interior views of a bladder structure.

Figure 31 is a flow chart of a method of performing virtual examination of an object, such as the larynx, using multiresolution viewing.

Figure 32 is a flow chart of a method for performing virtual angiography.

Figures 33A-C are pictorial views of a portion of the aorta illustrating the presence of an abdominal aortic aneurysm.

Figure 34 is a flow chart illustrating a method for generating a skeleton structure of an object.

Figure 35 is a schematic diagram of a 26-connected, Euclidean weighted, cubic distance plate.

Figure 36 is a diagram illustrating pseudo-code of a process for generating a distance map for use in the method of Figure 34.

DETAILED DESCRIPTION OF PREFERRED EMBODIMENTS

While the methods and systems described in this application can be applied to any object to be examined, the preferred embodiment which will be described is the examination of an organ in the human body, specifically the colon. The colon is long and twisted which makes it especially suited for a virtual examination saving the patient both money and the discomfort and danger of a physical probe. Other examples of organs which can be examined, without limitation, include the lungs, stomach and portions of the gastro-intestinal system, the heart and blood vessels.

Fig. 1 illustrates the steps necessary to perform a virtual colonoscopy using volume visualization techniques. Step 101 prepares the colon to be scanned in order to be viewed for examination if required by either the doctor or the particular scanning instrument. This preparation could include cleansing the colon with a "cocktail" or liquid which enters the colon after being orally ingested and passed through the stomach. The cocktail forces the patient to expel waste material that is present in the colon. One example of a substance used is Golytely. Additionally, in the case of the colon, air or CO_2 can be forced into the colon in order to expand it to make the colon easier to scan and examine. This is accomplished with a small tube placed in the rectum with approximately 1,000 cc of air pumped into the colon to distend the colon. Depending upon the type of scanner used, it may be necessary for

the patient to drink a contrast substance such as barium to coat any unexpunged stool in order to distinguish the waste in the colon from the colon walls themselves. Alternatively, the method for virtually examining the colon can remove the virtual waste prior to or during the virtual examination as explained later in this specification. Step 101 does not need to be performed in all examinations as indicated by the dashed line in Fig. 1.

Step 103 scans the organ which is to be examined. The scanner can be an apparatus well known in the art, such as a spiral CT-scanner for scanning a colon or a Zenita MRI machine for scanning a lung labeled for example with xenon gas. The scanner must be able to take multiple images from different positions around the body during suspended respiration, in order to produce the data necessary for the volume visualization. An example of a single CT-image would use an X-ray beam of 5mm width, 1:1 to 2:1 pitch, with a 40cm field-of-view being performed from the top of the splenic flexure of the colon to the rectum.

Discrete data representations of said object can be produced by other methods besides scanning. Voxel data representing an object can be derived from a geometric model by techniques described in U.S. Pat. No. 5,038,302 entitled "Method of Converting Continuous Three-Dimensional Geometrical Representations into Discrete Three-Dimensional Voxel-Based Representations Within a Three-Dimensional Voxel-Based System" by Kaufman, issued Aug. 8, 1991, filed July 26, 1988, which is hereby incorporated by reference. Additionally, data can be produced by a computer model of an image which can be converted to three-dimension voxels and explored in accordance with this invention. One example of this type of data is a computer simulation of the turbulence surrounding a space shuttle craft.

Step 104 converts the scanned images into three-dimensional volume elements (Voxels). In the preferred embodiment for examining a colon, the scan data is reformatted into 5mm thick slices at increments of 1mm or 2.5mm and reconstructed in 1mm slices, with each slice represented as a matrix of 512 by 512 pixels. By doing this, voxels of approximately 1 cubic mm are created. Thus a large number of 2D slices are generated depending upon the length of the scan. The set of 2D slices is then reconstructed to 3D voxels. The conversion process of 2D

images from the scanner into 3D voxels can either be performed by the scanning machine itself or by a separate machine such as a computer with techniques which are well known in the art (for example, see U.S. Pat. No. 4,985,856 entitled "Method and Apparatus for Storing, Accessing, and Processing Voxel-based Data" by Kaufman et al.; issued Jan. 15, 1991, filed Nov. 11, 1988; which is hereby incorporated by reference).

Step 105 allows the operator to define the portion of the selected organ to be examined. A physician may be interested in a particular section of the colon likely to develop polyps. The physician can view a two dimensional slice overview map to indicate the section to be examined. A starting point and finishing point of a path to be viewed can be indicated by the physician/operator. A conventional computer and computer interface (e.g., keyboard, mouse or spaceball) can be used to designate the portion of the colon which is to be inspected. A grid system with coordinates can be used for keyboard entry or the physician/operator can "click" on the desired points. The entire image of the colon can also be viewed if desired.

Step 107 performs the planned or guided navigation operation of the virtual organ being examined. Performing a guided navigation operation is defined as navigating through an environment along a predefined or automatically predetermined flight path which can be manually adjusted by an operator at any time. After the scan data has been converted to 3D voxels, the inside of the organ must be traversed from the selected start to the selected finishing point. The virtual examinations is modeled on having a tiny camera traveling through the virtual space with a lens pointing towards the finishing point. The guided navigation technique provides a level of interaction with the camera, so that the camera can navigate through a virtual environment automatically in the case of no operator interaction, and at the same time, allow the operator to manipulate the camera when necessary. The preferred embodiment of achieving guided navigation is to use a physically based camera model which employs potential fields to control the movement of the camera and which are described in detail in Figs. 2 and 3.

Step 109, which can be performed concurrently with step 107, displays the inside of the organ from the viewpoint of the camera model along the selected

pathway of the guided navigation operation. Three-dimensional displays can be generated using techniques well known in the art such as the marching cubes technique. However, in order to produce a real time display of the colon, a technique is required which reduces the vast number of computations of data necessary for the display of the virtual organ. Fig. 9 describe this display step in more detail.

The method described in Figure 1 can also be applied to scanning multiple organs in a body at the same time. For example, a patient may be examined for cancerous growths in both the colon and lungs. The method of Figure 1 would be modified to scan all the areas of interest in step 103 and to select the current organ to be examined in step 105. For example, the physician/operator may initially select the colon to virtually explore and later explore the lung. Alternatively, two different doctors with different specialties may virtually explore different scanned organs relating to their respective specialties. Following step 109, the next organ to be examined is selected and its portion will be defined and explored. This continues until all organs which need examination have been processed.

The steps described in conjunction with Figure 1 can also be applied to the exploration of any object which can be represented by volume elements. For example, an architectural structure or inanimate object can be represented and explored in the same manner.

Figure 2 depicts a "submarine" camera control model which performs the guided navigation technique in step 107. When there is no operator control during guided navigation, the default navigation is similar to that of planned navigation which automatically directs the camera along a flight path from one selected end of the colon to another. During the planned navigation phase, the camera stays at the center of the colon for obtaining better views of the colonic surface. When an interesting region is encountered, the operator of the virtual camera using guided navigation can interactively bring the camera close to a specific region and direct the motion and angle of the camera to study the interesting area in detail, without unwillingly colliding with the walls of the colon. The operator can control the camera with a standard interface device such as a keyboard, mouse or non-standard device such as a spaceball. In order to fully operate a camera in a virtual environment, six

degrees of freedom for the camera is required. The camera must be able to move in the horizontal, vertical, and Z direction (axes 217), as well as being able to rotate in another three degrees of freedom (axes 219) to allow the camera to move and scan all sides and angles of a virtual environment. The camera model for guided navigation includes an inextensible, weightless rod 201 connecting two particles x_1 203 and x_2 205, both particles being subjected to a potential field 215. The potential field is defined to be highest at the walls of the organ in order to push the camera away from the walls.

The positions of the particles are given by x_1 and x_2, and they are assumed to have the same mass *m*. A camera is attached at the head of the submarine x_1 203, whose viewing direction coincides with x_2x_1. The submarine can perform translation and rotation around the center of mass x of the model as the two particles are affected by the forces from the potential field *V(x)* which is defined below, any friction forces, and any simulated external force. The relations between x_1, x_2, and x are as follows:

$$x = (x,y,z),$$
$$r = (r\sin\theta\cos\varphi, r\sin\theta\sin\varphi, r\cos\theta),$$
$$\mathbf{x}_1 = \mathbf{x} + \mathbf{r},$$
$$\mathbf{x}_2 = \mathbf{x} - \mathbf{r}, \qquad (1)$$

where r, θ and φ are the polar coordinates of the vector xx_1.

The kinetic energy of the model, T, is defined as the summation of the kinetic energies of the movements of x_1 and x_2:

$$\begin{aligned} T &= \frac{m}{2}(\dot{\mathbf{x}}_1^2 + \dot{\mathbf{x}}_2^2) \\ &= m\dot{\mathbf{x}}^2 + m\dot{\mathbf{r}}^2 \\ &= m(\dot{x}^2 + \dot{y}^2 + \dot{z}^2) + mr^2(\dot{\theta}^2 + \dot{\phi}^2\sin^2\theta). \end{aligned} \qquad (2)$$

Then, the equations for the motion of the submarine model are obtained by using LaGrange's equation:

$$\frac{d}{dt}\left(\frac{\partial T}{\partial \dot{q}_j}\right) - \frac{\partial T}{\partial q_j} = \sum_{i=1}^{2}\left(\mathbf{F}_i \cdot \frac{\partial \mathbf{x}_i}{\partial q_j}\right), \tag{3}$$

where the q_js are the *generalized coordinates* of the model and can be considered as the variables of time t as:

$$(q_1, q_2, q_3, q_4, q_5, q_6) = (x, y, z, \theta, \phi, \psi) = \mathbf{q}(t), \tag{4}$$

with ψ denoting the *roll angle* of our camera system, which will be explained later. The $\mathbf{F}_j$s are called the *generalized forces*. The control of the submarine is performed by applying a simulated external force to x_1,

$$\mathbf{F}_{ext} = \left(F_x, F_y, F_z\right),$$

and it is assumed that both x_1 and x_2 are affected by the forces from the potential field and the frictions which act in the opposite direction of each particle's velocity. Consequently, the generalized forces are formulated as follows:

$$\begin{aligned} \mathbf{F}_1 &= -m\nabla V(\mathbf{x}_1) - k\dot{\mathbf{x}}_1 + \mathbf{F}_{ext}, \\ \mathbf{F}_2 &= -m\nabla V(\mathbf{x}_2) - k\dot{\mathbf{x}}_2, \end{aligned} \tag{5}$$

where k denotes the friction coefficient of the system. The external force $\mathbf{F}_{ext}$ is applied by the operator by simply clicking the mouse button in the desired direction 207 in the generated image, as shown in Figure 2. This camera model would then be moved in that direction. This allows the operator to control at least five degrees of freedom of the camera with only a single click of the mouse button. From Equations (2), (3) and (5), it can be derived that the accelerations of the five parameters of our submarine model as:

$$
\begin{aligned}
\ddot{x} &= -\frac{1}{2}\left(\frac{\partial V(\mathbf{x}_1)}{\partial x}+\frac{\partial V(\mathbf{x}_2)}{\partial x}\right)-\frac{k\dot{x}}{m}+\frac{F_x}{2m},\\
\ddot{y} &= -\frac{1}{2}\left(\frac{\partial V(\mathbf{x}_1)}{\partial y}+\frac{\partial V(\mathbf{x}_2)}{\partial y}\right)-\frac{k\dot{y}}{m}+\frac{F_y}{2m},\\
\ddot{z} &= -\frac{1}{2}\left(\frac{\partial V(\mathbf{x}_1)}{\partial z}+\frac{\partial V(\mathbf{x}_2)}{\partial z}\right)-\frac{k\dot{z}}{m}+\frac{F_z}{2m},\\
\ddot{\theta} &= \dot{\phi}^2\sin\theta\cos\theta\\
&\quad -\frac{1}{2r}\left[\cos\theta\left\{\cos\phi\left(\frac{\partial V(\mathbf{x}_1)}{\partial x}-\frac{\partial V(\mathbf{x}_2)}{\partial x}\right)+\sin\phi\left(\frac{\partial V(\mathbf{x}_1)}{\partial y}-\frac{\partial V(\mathbf{x}_2)}{\partial y}\right)\right\}\right.\\
&\quad \left.-\sin\theta\left(\frac{\partial V(\mathbf{x}_1)}{\partial z}-\frac{\partial V(\mathbf{x}_2)}{\partial z}\right)\right]\\
&\quad -\frac{k}{m}\dot{\theta}+\frac{1}{2mr}\left(F_x\cos\theta\cos\phi+F_y\cos\theta\sin\phi-F_z\sin\theta\right),\\
\ddot{\phi} &= \frac{1}{\sin\theta}\left[-2\dot{\theta}\dot{\phi}\cos\theta\right.\\
&\quad -\frac{1}{2r}\left\{-\sin\phi\left(\frac{\partial V(\mathbf{x}_1)}{\partial x}-\frac{\partial V(\mathbf{x}_2)}{\partial x}\right)+\cos\phi\left(\frac{\partial V(\mathbf{x}_1)}{\partial y}-\frac{\partial V(\mathbf{x}_2)}{\partial y}\right)\right\}\\
&\quad \left.-\frac{k}{m}\dot{\phi}\sin\theta+\frac{1}{2mr}\left(-F_x\sin\phi+F_y\cos\phi\right)\right], \qquad (6)
\end{aligned}
$$

where $\dot{x}$ and $\ddot{x}$ denote the first and the second derivative of x, respectively, and

$\left(\frac{\partial V(x)}{\partial x}, \frac{\partial V(x)}{\partial Y}, \frac{\partial V(x)}{\partial z}\right)$ denotes the gradient of the potential at a point x.

The terms $\dot{\phi}^2\sin\theta\cos\theta$ of $\ddot{\theta}$ and $-\frac{2\dot{\theta}\dot{\phi}\cos\theta}{\sin\theta}$ of $\ddot{\phi}$ are called the

centrifugal force and the *Coriolis force*, respectively, and they are concerned with the exchange of angular velocities of the submarine. Since the model does not have the moment of inertia defined for the rod of the submarine, these terms tend to cause an overflow of the numeric calculation of φ. Fortunately, these terms become significant

only when the angular velocities of the submarine model are significant, which essentially means that the camera moves too fast. Since it is meaningless to allow the camera to move so fast because the organ could not be properly viewed, these terms are minimized in our implementation to avoid the overflow problem.

From the first three formulas of Equation (6), it is known that the submarine cannot be propelled by the external force against the potential field if the following condition is satisfied:

$$|\nabla V(\mathbf{x}_1) + \nabla V(\mathbf{x}_2)| > \frac{|\mathbf{F}_{ext}|}{m}.$$

Since the velocity of the submarine and the external force F_{ext} have upper limits in our implementation, by assigning sufficiently high potential values at the boundary of the objects, it can be guaranteed that the submarine never bumps against the objects or walls in the environment.

As mentioned previously, the roll angle υ of the camera system needs to be considered. One possible option allows the operator full control of the angle ψ. However, although the operator can rotate the camera freely around the rod of the model, he or she can easily become disoriented. The preferred technique assumes that the upper direction of the camera is connected to a pendulum with mass m_2 301, which rotates freely around the rod of the submarine, as shown in Figure 3. The direction of the pendulum, r_2, is expressed as:

$$\mathbf{r}_2 = r_2\{\cos\theta\cos\phi\sin\psi + \sin\phi\cos\psi, \cos\theta\sin\phi\sin\psi - \cos\phi\cos\psi, -\sin\theta\sin\psi\},$$

although it is possible to calculate the accurate movement of this pendulum along with the movement of the submarine, it makes the system equations too complicated. Therefore, it is assumed that all the generalized coordinates except the roll angle ψ are constants, and thus define the independent kinetic energy for the pendulum system as:

$$T_p = \frac{m_2}{2}\dot{r}_2^2 = \frac{m_2 r_2^2}{2}\dot{\psi}^2.$$

This simplifies the model for the roll angle. Since it is assumed in this model that the gravitational force

$$\mathbf{F}_g = m_2\mathbf{g} = (m_2 g_x, m_2 g_y, m_2 g_z)$$

acts at the mass point m_2, the acceleration of ψ can be derived using LaGrange's equation as:

$$\begin{aligned}\ddot{\psi} = \frac{1}{r_2}\{&g_x(\cos\theta\cos\phi\cos\psi - \sin\phi\sin\psi)\\ &+g_y(\cos\theta\sin\phi\cos\psi + \cos\phi\sin\psi)\\ &+g_z(-\sin\theta\cos\psi)\} - \frac{k_2}{m_2}\dot{\psi}.\end{aligned} \tag{7}$$

From Equations (6) and (7), the generalized

coordinates **q**(t) and their derivatives **q**(t) are calculated asymptotically by using *Taylor series* as:

$$\begin{aligned}\mathbf{q}(t+h) &= \mathbf{q}(t) + h\dot{\mathbf{q}}(t) + \frac{h^2}{2}\ddot{\mathbf{q}}(t) + O(h^3),\\ \dot{\mathbf{q}}(t+h) &= \dot{\mathbf{q}}(t) + h\ddot{\mathbf{q}}(t) + O(h^2),\end{aligned}$$

to freely move the submarine. To smooth the submarine's motion, the time step **h** is selected as an equilibrium value between being as small as possible to smooth the motion but as large as necessary to reduce computation cost.

Definition of the Potential Field

The potential field in the submarine model in Figure 2 defines the boundaries (walls or other matter) in the virtual organ by assigning a high potential to the boundary in order to ensure that the submarine camera does not collide with the walls or other boundary. If the camera model is attempted to be moved into a high potential area by the operator, the camera model will be restrained from doing so unless the operator wishes to examine the organ behind the boundary or inside a polyp, for example. In the case of performing a virtual colonoscopy, a potential field value is assigned to each piece of volumetric colon data (volume element). When a particular region of interest is designated in step 105 of Fig. 1 with a start and finish point, the voxels within the selected area of the scanned colon are identified using conventional blocking operations. Subsequently, a potential value is assigned to every voxel x of the selected volume based on the following three distance values: the distance from the finishing point dt(x), the distance from the colon surface ds(x) and the distance from the center-line of the colon space dc(x). dt(x) is calculated by using a conventional growing strategy. The distance from the colon surface, ds(x), is computed using a conventional technique of growing from the surface voxels inwards. To determine dc(x), the center-line of the colon from the voxel is first extracted, and then dc(x) is computed using the conventional growing strategy from the center-line of the colon.

To calculate the center-line of the selected colon area defined by the user-specified start point and the user-specified finish point, the maximum value of ds(x) is located and denoted dmax. Then for each voxel inside the area of interest, a cost value of dmax - ds(x) is assigned. Thus the voxels which are close to the colon surface have high cost values and the voxels close to the center line have relatively low cost values. Then, based on the cost assignment, the single-source shortest path technique which is well known in the art is applied to efficiently compute a minimum cost path from the source point to the finish point. This low cost line indicates the center-line or skeleton of the colon section which is desired to be explored. This technique for determining the center-line is the preferred technique of the invention.

To compute the potential value V(x) for a voxel x inside the area of interest, the following formula is employed:

$$V(\mathbf{x}) = C_1 d_t(\mathbf{x})^{\mu} + C_2\left(\frac{d_s(\mathbf{x})}{d_c(\mathbf{x}) + d_s(\mathbf{x})}\right)^{-\nu}, \qquad (8)$$

where C_1, C_2, μ and ν are constants chosen for the task. In order to avoid any collision between the virtual camera and the virtual colonic surface, a sufficiently large potential value is assigned for all points outside the colon. The gradient of the potential field will therefore become so significant that the submarine model camera will never collide with the colonic wall when being run.

Another technique to determine the center-line of the path in the colon is called the "peel-layer" technique and is shown in Figure 4 through Figure 8.

Figure 4 shows a 2D cross-section of the volumetric colon, with the two side walls 401 and 403 of the colon being shown. Two blocking walls are selected by the operator in order to define the section of the colon which is of interest to examine. Nothing can be viewed beyond the blocking walls. This helps reduce the number of computations when displaying the virtual representation. The blocking walls together with side walls identify a contained volumetric shape of the colon which is to be explored.

Figure 5 shows two end points of the flight path of the virtual examination, the start volume element 501 and the finish volume element 503. The start and finish points are selected by the operator in step 105 of Fig. 1. The voxels between the start and finish points and the colon sides are identified and marked, as indicated by the area designated with "x"s in Fig. 6. The voxels are three-dimensional representations of the picture element.

The peel-layer technique is then applied to the identified and marked voxels in Fig. 6. The outermost layer of all the voxels (closest to the colon walls) is peeled off step-by-step, until there is only one inner layer of voxels remaining. Stated differently, each voxel furthest away from a center point is removed if the removal does not lead to a disconnection of the path between the start voxel and the finish

voxel. Figure 7 shows the intermediate result after a number of iterations of peeling the voxels in the virtual colon are complete. The voxels closest to the walls of the colon have been removed. Fig. 8 shows the final flight path for the camera model down the center of the colon after all the peeling iterations are complete. This produces essentially a skeleton at the center of the colon and becomes the desired flight path for the camera model.

Z- Buffer assisted visibility

Figure 9 describes a real time visibility technique to display of virtual images seen by the camera model in the virtual three-dimensional volume representation of an organ. Figure 9 shows a display technique using a modified Z buffer which corresponds to step 109 in Fig. 1. The number of voxels which could be possibly viewed from the camera model is extremely large. Unless the total number of elements (or polygons) which must be computed and visualized is reduced from an entire set of voxels in the scanned environment, the overall number of computations will make the visualization display process exceedingly slow for a large internal area. However, in the present invention only those images which are visible on the colon surface need to be computed for display. The scanned environment can be subdivided into smaller sections, or cells. The Z buffer technique then renders only a portion of the cells which are visible from the camera. The Z buffer technique is also used for three-dimensional voxel representations. The use of a modified Z buffer reduces the number of visible voxels to be computed and allows for the real time examination of the virtual colon by a physician or medical technician.

The area of interest from which the center-line has been calculated in step 107 is subdivided into cells before the display technique is applied. Cells are collective groups of voxels which become a visibility unit. The voxels in each cell will be displayed as a group. Each cell contains a number of portals through which the other cells can be viewed. The colon is subdivided by beginning at the selected start point and moving along the center-line 1001 towards the finish point. The colon is then partitioned into cells (for example, cells 1003, 1005 and 1007 in Fig. 10) when a predefined threshold distance along the center-path is reached. The threshold

distance is based upon the specifications of the platform upon which the visualization technique is performed and its capabilities of storage and processing. The cell size is directly related to the number of voxels which can be stored and processed by the platform. One example of a threshold distance is 5cm, although the distance can greatly vary. Each cell has two cross-sections as portals for viewing outside of the cell as shown in Fig. 10.

Step 901 in Fig. 9 identifies the cell within the selected organ which currently contains the camera. The current cell will be displayed as well as all other cells which are visible given the orientation of the camera. Step 903 builds a stab tree (tree diagram) of hierarchical data of potentially visible cells from the camera (through defined portals), as will be described in further detail hereinbelow. The stab tree contains a node for every cell which may be visible to the camera. Some of the cells may be transparent without any blocking bodies present so that more than one cell will be visible in a single direction. Step 905 stores a subset of the voxels from a cell which include the intersection of adjoining cell edges and stores them at the outside edge of the stab tree in order to more efficiently determine which cells are visible.

Step 907 checks if any loop nodes are present in the stab tree. A loop node occurs when two or more edges of a single cell both border on the same nearby cell. This may occur when a single cell is surrounded by another cell. If a loop node is identified in the stab tree, the method continues with step 909. If there is no loop node, the process goes to step 911.

Step 909 collapses the two cells making up the loop node into one large node. The stab tree is then corrected accordingly. This eliminates the problem of viewing the same cell twice because of a loop node. The step is performed on all identified loop nodes. The process then continues with step 911.

Step 911 then initiates the Z-buffer with the largest Z value. The Z value defines the distance away from the camera along the skeleton path. The tree is then traversed to first check the intersection values at each node. If a node intersection is covered, meaning that the current portal sequence is occluded (which is determined by the Z buffer test), then the traversal of the current branch in the tree is

stopped. Step 913 traverses each of the branches to check if the nodes are covered and displays them if they are not.

Step 915 then constructs the image to be displayed on the operator's screen from the volume elements within the visible cells identified in step 913 using one of a variety of techniques known in the art, such as volume rendering by compositing. The only cells shown are those which are identified as potentially visible. This technique limits the number of cells which requires calculations in order to achieve a real time display and correspondingly increases the speed of the display for better performance. This technique is an improvement over prior techniques which calculate all the possible visible data points whether or not they are actually viewed.

Figure 11A is a two dimensional pictorial representation of an organ which is being explored by guided navigation and needs to be displayed to an operator. Organ 1101 shows two side walls 1102 and an object 1105 in the center of the pathway. The organ has been divided into four cells A 1151, B 1153, C 1155 and D 1157. The camera 1103 is facing towards cell D 1157 and has a field of vision defined by vision vectors 1107, 1108 which can identify a cone-shaped field. The cells which can be potentially viewed are cells B 1153, C 1155 and D 1157. Cell C 1155 is completely surrounded by Cell B and thus constitutes a node loop.

Fig. 11B is a representation of a stab tree built from the cells in Fig. 11A. Node A 1109 which contains the camera is at the root of the tree. A sight line or sight cone, which is a visible path without being blocked, is drawn to node B 1110. Node B has direct visible sight lines to both node C 1112 and node D 1114 and which is shown by the connecting arrows. The sight line of node C 1112 in the direction of the viewing camera combines with node B 1110. Node C 1112 and node B 1110 will thus be collapsed into one large node B' 1122 as shown in Fig. 11C.

Fig. 11C shows node A 1109 containing the camera adjacent to node B' 1122 (containing both nodes B and node C) and node D 1114. The nodes A, B' and D will be displayed at least partially to the operator.

Figs 12A - 12B illustrate the use of the modified Z buffer with cells that contain objects which obstruct the views. An object could be some waste

material in a portion of the virtual colon. Fig. 12A shows a virtual space with 10 potential cells: A 1251, B 1253, C 1255, D 1257, E 1259, F 1261, G 1263, H 1265, I 1267 and J 1269. Some of the cells contain objects. If the camera 1201 is positioned in cell I 1267 and is facing toward cell F 1261 as indicated by the vision vectors 1203, then a stab tree is generated in accordance with the technique illustrated by the flow diagram in Fig. 9. Fig. 12B shows the stab tree generated with the intersection nodes showing for the virtual representation as shown in Fig. 12A. Fig. 12B shows cell I 1267 as the root node of the tree because it contains the camera 1201. Node I 1211 is pointing to node F 1213 (as indicated with an arrow), because cell F is directly connected to the sight line of the camera. Node F 1213 is pointing to both node B 1215 and node E 1219. Node B 1215 is pointing to node A 1217. Node C 1202 is completely blocked from the line of sight by camera 1201 so is not included in the stab tree.

Fig. 12C shows the stab tree after node I 1211 is rendered on the display for the operator. Node I 1211 is then removed from the stab tree because it has already been displayed and node F 1213 becomes the root. Fig. 12D shows that node F 1213 is now rendered to join node I 1211. The next nodes in the tree connected by arrows are then checked to see if they are already covered (already processed). In this example, all of the intersected nodes from the camera positioned in cell I 1267 has been covered so that node B 515 (and therefore dependent node A) do not need to be rendered on the display.

Fig. 12E shows node E 515 being checked to determine if its intersection has been covered. Since it has, the only rendered nodes in this example of Figure 12A-12E are nodes I and F while nodes A, B and E are not visible and do not need to have their cells prepared to be displayed.

The modified Z buffer technique described in Figure 9 allows for fewer computations and can be applied to an object which has been represented by voxels or other data elements, such as polygons.

Figure 13 shows a two dimensional virtual view of a colon with a large polyp present along one of its walls. Figure 13 shows a selected section of a patient's colon which is to be examined further. The view shows two colon walls 1301 and

1303 with the growth indicated as 1305. Layers 1307, 1309, and 1311 show inner layers of the growth. It is desirable for a physician to be able to peel the layers of the polyp or tumor away to look inside of the mass for any cancerous or other harmful material. This process would in effect perform a virtual biopsy of the mass without actually cutting into the mass. Once the colon is represented virtually by voxels, the process of peeling away layers of an object is easily performed in a similar manner as described in conjunction with Figs. 4 through 8. The mass can also be sliced so that a particular cross-section can be examined. In Fig. 13, a planar cut 1313 can be made so that a particular portion of the growth can be examined. Additionally, a user-defined slice 1319 can be made in any manner in the growth. The voxels 1319 can either be peeled away or modified as explained below.

A transfer function can be performed to each voxel in the area of interest which can make the object transparent, semi-transparent or opaque by altering coefficients representing the translucently for each voxel. An opacity coefficient is assigned to each voxel based on its density. A mapping function then transforms the density value to a coefficient representing its translucency. A high density scanned voxel will indicate either a wall or other dense matter besides simply open space. An operator or program routine could then change the opacity coefficient of a voxel or group of voxels to make them appear transparent or semi-transparent to the submarine camera model. For example, an operator may view a tumor within or outside of an entire growth. Or a transparent voxel will be made to appear as if it is not present for the display step of Figure 9. A composite of a section of the object can be created using a weighted average of the opacity coefficients of the voxels in that section.

If a physician desires to view the various layers of a polyp to look for a cancerous areas, this can be performed by removing the outer layer of polyp 1305 yielding a first layer 1307. Additionally, the first inner layer 1307 can be stripped back to view second inner layer 1309. The second inner layer can be stripped back to view third inner layer 1311, etc. The physician could also slice the polyp 1305 and view only those voxels within a desired section. The slicing area can be completely user-defined.

Adding an opacity coefficient can also be used in other ways to aid in the exploration of a virtual system. If waste material is present and has a density as other properties within a certain known range, the waste can be made transparent to the virtual camera by changing its opacity coefficient during the examination. This will allow the patient to avoid ingesting a bowel cleansing agent before the procedure and make the examination faster and easier. Other objects can be similarly made to disappear depending upon the actual application. Additionally, some objects like polyps could be enhanced electronically by a contrast agent followed by a use of an appropriate transfer function.

Figure 14 shows a system for performing the virtual examination of an object such as a human organ using the techniques described in this specification. Patient 1401 lies down on a platform 1402 while scanning device 1405 scans the area that contains the organ or organs which are to be examined. The scanning device 1405 contains a scanning portion 1403 which actually takes images of the patient and an electronics portion 1406. Electronics portion 1406 comprises an interface 1407, a central processing unit 1409, a memory 1411 for temporarily storing the scanning data, and a second interface 1413 for sending data to the virtual navigation platform. Interface 1407 and 1413 could be included in a single interface component or could be the same component. The components in portion 1406 are connected together with conventional connectors.

In system 1400, the data provided from the scanning portion of device 1403 is transferred to portion 1405 for processing and is stored in memory 1411. Central processing unit 1409 converts the scanned 2D data to 3D voxel data and stores the results in another portion of memory 1411. Alternatively, the converted data could be directly sent to interface unit 1413 to be transferred to the virtual navigation terminal 1416. The conversion of the 2D data could also take place at the virtual navigation terminal 1416 after being transmitted from interface 1413. In the preferred embodiment, the converted data is transmitted over carrier 1414 to the virtual navigation terminal 1416 in order for an operator to perform the virtual examination. The data could also be transported in other conventional ways such as

storing the data on a storage medium and physically transporting it to terminal 1416 or by using satellite transmissions.

The scanned data may not be converted to its 3D representation until the visualization rendering engine requires it to be in 3D form. This saves computational steps and memory storage space.

Virtual navigation terminal 1416 includes a screen for viewing the virtual organ or other scanned image, an electronics portion 1415 and interface control 1419 such as a keyboard, mouse or spaceball. Electronics portion 1415 comprises a interface port 1421, a central processing unit 1423, other components 1427 necessary to run the terminal and a memory 1425. The components in terminal 1416 are connected together with conventional connectors. The converted voxel data is received in interface port 1421 and stored in memory 1425. The central processor unit 1423 then assembles the 3D voxels into a virtual representation and runs the submarine camera model as described in Figures 2 and 3 to perform the virtual examination. As the submarine camera travels through the virtual organ, the visibility technique as described in Figure 9 is used to compute only those areas which are visible from the virtual camera and displays them on screen 1417. A graphics accelerator can also be used in generating the representations. The operator can use interface device 1419 to indicate which portion of the scanned body is desired to be explored. The interface device 1419 can further be used to control and move the submarine camera as desired as discussed in Figure 2 and its accompanying description. Terminal portion 1415 can be the Cube-4 dedicated system box, generally available from the Department of Computer Science at the State University of New York at Stony Brook.

Scanning device 1405 and terminal 1416, or parts thereof, can be part of the same unit. A single platform would be used to receive the scan image data, connect it to 3D voxels if necessary and perform the guided navigation.

An important feature in system 1400 is that the virtual organ can be examined at a later time without the presence of the patient. Additionally, the virtual examination could take place while the patient is being scanned. The scan data can also be sent to multiple terminals which would allow more than one doctor to view

the inside of the organ simultaneously. Thus a doctor in New York could be looking at the same portion of a patient's organ at the same time with a doctor in California while discussing the case. Alternatively, the data can be viewed at different times. Two or more doctors could perform their own examination of the same data in a difficult case. Multiple virtual navigation terminals could be used to view the same scan data. By reproducing the organ as a virtual organ with a discrete set of data, there are a multitude of benefits in areas such as accuracy, cost and possible data manipulations.

The above described techniques can be further enhanced in virtual colonoscopy applications through the use of an improved electronic colon cleansing technique which employs modified bowel preparation operations followed by image segmentation operations, such that fluid and stool remaining in the colon during a computed tomographic (CT) or magnetic resonance imaging (MRI) scan can be detected and removed from the virtual colonoscopy images. Through the use of such techniques, conventional physical washing of the colon, and its associated inconvenience and discomfort, is minimized or completely avoided.

Referring to Figure 15, the first step in electronic colon cleansing is bowel preparation (step 1510), which takes place prior to conducting the CT or magnetic resonance imaging (MRI) scan and is intended to create a condition where residual stool and fluid remaining in the colon present significantly different image properties from that of the gas-filled colon interior and colon wall. An exemplary bowel preparation operation includes ingesting three 250 cc doses of Barium Sulfate suspension of 2.1 % W/V, such as manufactured by E-Z-EM, Inc.,of Westbury, New York, during the day prior the CT or MRI scan. The three doses should be spread out over the course of the day and can be ingested along with three meals, respectively. The Barium Sulfate serves to enhance the images of any stool which remains in the colon. In addition to the intake of Barium Sulfate, fluid intake is preferably increased during the day prior to the CT or MRI scan. Cranberry juice is known to provide increased bowel fluids and is preferred, although water can also be ingested. In both the evening prior to the CT scan and the morning of the CT scan, 60 ml of a Diatrizoate Meglumine and Diatrizoate Sodium Solution, which is commercially

available as MD-Gastroview, manufactured by Mallinckrodt, Inc. of St. Louis, Missouri, can be consumed to enhance image properties of the colonic fluid. Sodium phosphate can also be added to the solution to liquidize the stool in the colon, which provides for more uniform enhancement of the colonic fluid and residual stool.

The above described exemplary preliminary bowel preparation operation can obviate the need for conventional colonic washing protocols, which can call for the ingestion of a gallon of Golytely solution prior to a CT scan.

Just prior to conducting the CT scan, an intravenous injection of 1 ml of Glucagon, manufactured by Ely Lily and Company, of Indianapolis, Indiana can be administered to minimize colon collapse. Then, the colon can be inflated using approximately 1000cc of compressed gas, such as CO_2, or room air, which can be introduced through a rectum tube. At this point, a conventional CT scan is performed to acquire data from the region of the colon (step 1520). For example, data can be acquired using a GE/CTI spiral mode scanner operating in a helical mode of 5mm, 1.5-2.0:1 pitch, reconstructed in 1mm slices, where the pitch is adjusted based upon the patient's height in a known manner. A routine imaging protocol of 120 kVp and 200-280 ma can be utilized for this operation. The data can be acquired and reconstructed as 1mm thick slice images having an array size of 512x512 pixels in the field of view, which varies from 34 to 40 cm depending on the patient's size. the number of such slices generally varies under these conditions from 300 to 450, depending on the patient's height. The image data set is converted to volume elements or voxels (step 1530).

Image segmentation can be performed in a number of ways. In one present method of image segmentation, a local neighbor technique is used to classify voxels of the image data in accordance with similar intensity values. In this method, each voxel of an acquired image is evaluated with respect to a group of neighbor voxels. The voxel of interest is referred to as the central voxel and has an associated intensity value. A classification indicator for each voxel is established by comparing the value of the central voxel to each of its neighbors. If the neighbor has the same value as the central voxel, the value of the classification indicator is incremented. However, if the neighbor has a different value from the central voxel, the

classification indicator for the central voxel is decremented. The central voxel is then classified to that category which has the maximum indicator value, which indicates the most uniform neighborhood among the local neighbors. Each classification is indicative of a particular intensity range, which in turn is representative of one or more material types being imaged. The method can be further enhanced by employing a mixture probability function to the similarity classifications derived.

An alternate process of image segmentation is performed as two major operations: low level processing and high level feature extraction. During low level processing, regions outside the body contour are eliminated from further processing and voxels within the body contour are roughly categorized in accordance with well defined classes of intensity characteristics. For example, a CT scan of the abdominal region generates a data set which tends to exhibit a well defined intensity distribution. The graph of Figure 16 illustrates such an intensity distribution as an exemplary histogram having four, well defined peaks, 1602, 1604, 1606, 1608, which can be classified according to intensity thresholds.

The voxels of the abdominal CT data set are roughly classified as four clusters by intensity thresholds (step 1540). For example, Cluster 1 can include voxels whose intensities are below 140. This cluster generally corresponds to the lowest density regions within the interior of the gas filled colon. Cluster 2 can include voxels which have intensity values in excess of 2200. These intensity values correspond to the enhanced stool and fluid within the colon as well as bone. Cluster 3 can include voxels with intensities in the range of about 900 to about 1080. This intensity range generally represents soft tissues, such as fat and muscle, which are unlikely to be associated with the colon. The remaining voxels can then be grouped together as cluster 4, which are likely to be associated with the colon wall (including mucosa and partial volume mixtures around the colon wall) as well as lung tissue and soft bones.

Clusters 1 and 3 are not particularly valuable in identifying the colon wall and, therefore are not subject to substantial processing during image segmentation procedures for virtual colonoscopy. The voxels associated with cluster 2 are important for segregating stool and fluid from the colon wall and are processed

further during the high-level feature extraction operations. Low level processing is concentrated on the fourth cluster, which has the highest likelihood of corresponding to colon tissue (step 1550).

For each voxel in the fourth cluster, an intensity vector is generated using itself and its neighbors. The intensity vector provides an indication of the change in intensity in the neighborhood proximate a given voxel. The number of neighbor voxels which are used to establish the intensity vector is not critical, but involves a tradeoff between processing overhead and accuracy. For example, a simple voxel intensity vector can be established with seven (7) voxels, which includes the voxel of interest, its front and back neighbors, its left and right neighbors and its top and bottom neighbors, all surrounding the voxel of interest on three mutually perpendicular axes. Figure 17 is a perspective view illustrating an exemplary intensity vector in the form of a 25 voxel intensity vector model, which includes the selected voxel 1702 as well as its first, second and third order neighbors. The selected voxel 1702 is the central point of this model and is referred to as the fixed voxel. A planar slice of voxels, which includes 12 neighbors on the same plane as the fixed voxel, is referred to as the fixed slice 1704. On adjacent planes to the fixed slice are two nearest slices 1706, having five voxels each. Adjacent to the first nearest slices 1706 are two second nearest slices 1708, each having a single voxel. The collection of intensity vectors for each voxel in the fourth cluster is referred to as a local vector series.

Because the data set for an abdominal image generally includes more than 300 slice images, each with a 512 x 512 voxel array, and each voxel having an associated 25 voxel local vector, it is desirable to perform feature analysis (step 1570) on the local vector series to reduce the computational burden. One such feature analysis is a principal component analysis (PCA), which can be applied to the local vector series to determine the dimension of a feature vector series and an orthogonal transformation matrix for the voxels of cluster 4.

It has been found that the histogram (Figure 16) of the CT image intensities tends to be fairly constant from patient to patient for a particular scanner, given equivalent preparation and scanning parameters. Relying on this observation,

an orthogonal transformation matrix can be established which is a predetermined matrix determined by using several sets of training data acquired using the same scanner under similar conditions. From this data, a transformation matrix, such as a Karlhunen-Loéve (K-L) transformation, can be generated in a known manner. The transformation matrix is applied to the local vector series to generate feature vector series. Once in the feature-vector space domain, vector quantization techniques can be used to classify the feature vector series.

An analytical, self-adaptive algorithm can be used for the classification of the feature vectors. In defining this algorithm, let $\{X_i \in R^l; i = 1,2,3,...,N\}$ be the series of the feature vectors, where N is the number of feature vectors; K denotes the maximum number of classes; and T is a threshold which is adaptive to the data set. For each class, a representative element is generated by the algorithm. Let a_k be a representative element of class k and n_k be the number of feature vectors in that class.

The algorithm can then be outlined as:

1. Set $n_1=1$; $a_1=X_1$; $\overline{K}=1$;

2. obtain the class number $\overline{K}$ and class parameters (a_k, n_k)
   for ($i=1$; $i<N$; $i++$)
      for ($j=1$; $j<\overline{K}$; $j++$)
         calculate $d_j = dist(X_i, a_j)$;
      end for
      index=arc min d_j;
      if ($(d_{index} < T)$ OR $(\overline{K}=K)$)

         update class parameters:

$$a_{index} = \frac{1}{n_{index}+1} \times (n_{index} * a_{index} + X_i);$$
$$n_{index} = n_{index} + 1;$$

end if

else

generate new class

$$a_{\bar{K}+1} = X_i;$$
$$n_{\bar{K}+1} = 1;$$
$$\bar{K} = \bar{K}+1;$$

end else

end for

3. label each feature vector to a class according to the nearest neighbor rule

for ($i=1; i<N; i++$)

for ($j=1; j<\bar{K}; j++$)

calculate $d_j = dist(X_i, a_j)$;

end for

index = *arc* min d_j

label voxel *i* to class *index*.

end for

In this algorithm, *dist(x,y)* is the Euclidean distance between vector *x* and *y* and *arc* min d_j gives the integer *j* which realizes the minimum value of d_j.

The above described algorithm is dependent only on the parameters *T* and *K*. However, the value of K, which relates to the number of classes within each voxel cluster, is not critical and can be set to a constant value, such as K=18. However, T, which is the vector similarity threshold, greatly influences the classification results. If the selected value of T is too large, only a single class will be generated. On the other hand, if the value of T is too small, the resulting classes will exhibit undesirable redundancy. By setting the value of T to be equal to the maximum component variance of the feature vector series, the maximum number of distinct classes results.

As a result of the initial classification process, each voxel within the selected cluster is assigned to a class (step 1570). In the exemplary case of virtual colonoscopy, there are several classes within cluster 4. Thus, the next task is to determine which of the several classes in cluster 4 corresponds to the colon wall. The first coordinate of the feature vector, which is that coordinate of the feature vector exhibiting the highest variance, reflects the information of the average of the 3D local voxel intensities. The remaining coordinates of the feature vector contain the information of directional intensity change within the local neighbors. Because the colon wall voxels for the interior of the colon are generally in close proximity to the gas voxels of cluster 1, a threshold interval can be determined by data samples selected from typical colon wall intensities of a typical CT data set to roughly distinguish colon wall voxel candidates. The particular threshold value is selected for each particular imaging protocol and device. This threshold interval can then applied to all CT data sets (acquired from the same machine, using the same imaging protocol). If the first coordinate of the representative element is located in the threshold interval, the corresponding class is regarded as the colon wall class and all voxels in that class are labeled as colon wall-like voxels.

Each colon wall-like voxel is a candidate to be a colon wall voxel. There are three possible outcomes of not belonging to the colon wall. The first case relates to voxels which are close to the stool/liquid inside the colon. The second case occurs when voxels are in the lung tissue regions. The third case represents mucosa voxels. Clearly then, low level classification carries a degree of classification uncertainty. The causes of the low-level classification uncertainty vary. For example, a partial-volume effect resulting from voxels containing more than one material type (i.e., fluid and colon wall) leads to the first case of uncertainty. The second and the third cases of uncertainty are due to both the partial volume effect as well as the low contrast of CT images. To resolve the uncertainty, additional information is needed. Thus, a high-level feature extraction procedure is used in the present method to further distinguish candidates for the colon wall from other colon wall-like voxels, based on a *priori* anatomical knowledge of the CT images (step 1580).

An initial step of the high-level feature extraction procedure can be to eliminate the region of lung tissue from the low-level classification results. Figure 18A is an exemplary slice image clearly illustrating the lung region 1802. The lung region 1802 is identifiable as a generally contiguous three dimensional volume enclosed by colon wall-like voxels, as illustrated in Figure 18B. Given this characteristic, the lung region can be identified using a region growing strategy. The first step in this technique is to find a seed voxel within the region of growing. Preferably, the operator performing the CT imaging scan sets the imaging range such that the top most slice of the CT scan does not contain any colon voxels. As the interior of lung should be filled with air, the seed is provided by the low-level classification simply by selecting an air voxel. Once the lung region outline of Figure 18B is determined, the lung volume can be removed from the image slice (Figure 18C).

A next step in performing high-level feature extraction can be to separate the bone voxels from enhanced stool/fluid voxels in cluster 2. The bone tissue voxels 1902 are generally relatively far away from the colon wall and resides outside the colon volume. To the contrary, the residual stool 1906 and fluid 1904 are enclosed inside the colon volume. Combining the a *priori* proximity information and the colon wall information obtained from the low-level classification process, a rough colon wall volume is generated. Any voxel separated by more than a predetermined number (e.g., 3) of voxel units from the colon wall, and outside the colon volume, will be labeled as bone and then removed from the image. The remaining voxels in cluster 2 can be assumed to represent stool and fluid within the colon volume (see Figures 19A-C).

The voxels within the colon volume identified as stool 1906 and fluid 1904 can be removed from the image to generate a clean colon lumen and colon wall image. In general, there are two kinds of stool/fluid regions. One region type is small residual areas of stool 1906 attached to the colon wall. The other region type is large volumes of fluid 1904, which collect in basin-like colonic folds (see Figures 19A-C).

The attached residual stool regions 1906 can be identified and removed because they are inside the rough colon volume generated during the low-level

classification process. The fluid 1906 in the basin-like colon fold usually has a horizontal surface 1908 due to the effect of gravity. Above the surface is always a gas region, which exhibits a very high contrast to the fluid intensity. Thus, the surface interface of the fluid regions can be easily marked.

Using a region growing strategy, the contour of the attached stool regions 1906 can be outlined, and the part which is away from the colon wall volume can be removed. Similarly, the contour of the fluid regions 1904 can also be outlined. After eliminating the horizontal surfaces 1908, the colon wall contour is revealed and the clean colon wall is obtained.

It is difficult to distinguish the mucosa voxels from the colon wall voxels. Even though the above three dimensional processing can remove some mucosa voxels, it is difficult to remove all mucosa voxels. In optical colonoscopy, physicians directly inspect the colonic mucosa and search for lesions based on the color and texture of the mucosa. In virtual colonoscopy, most mucosa voxels on the colon wall can be left intact in order to preserve more information. This can be very useful for three dimensional volume rendering.

From the segmented colon wall volume, the inner surface, the outer surface and the wall itself of the colon can be extracted and viewed as a virtual object. This provides a distinct advantage over conventional optical colonoscopy in that the exterior wall of the colon can be examined as well as the interior wall. Furthermore, the colon wall and the colon lumen can be obtained separately from the segmentation.

Because the colon is substantially evacuated prior to imaging, a commonly encountered problem is that the colon lumen collapses in spots. While the inflation of the colon with compressed gas, such as air or CO_2, reduces the frequency of collapsed regions, such areas still occur. In performing a virtual colonoscopy, it is desirable to automatically maintain a flight path through the collapsed regions and it is also desirable to use the scanned image data to at least partially recreate the colon lumen in the collapsed regions. Since the above described image segmentation methods effectively derive both the interior and exterior of the colon wall, this information can be used to enhance the generation of the fly path through the collapsed regions.

In extending the flight path through collapsed regions of the colon or expanding a collapsed region of the colon, the first step is to detect a collapsed region. Using the premise that the grayscale values of the image data from around the outside of the colon wall change much more dramatically than the greyscale values within the colon wall itself, as well as in other regions such as fat, muscle and other kinds of tissue, an entropy analysis can be used to detect areas of colon collapse.

The degree of change in greyscale value, for example along the centerline, can be expressed and measured by an entropy value. To calculate an entropy value, voxels on the outer surface of the colon wall are selected. Such points are identified from the above described image segmentation techniques. A 5x5x5 cubic window can be applied to the pixels, centered on the pixel of interest. Prior to calculating the entropy value, a smaller (3x3x3) window can be applied to the pixels of interest in order to filter out noise from the image data. The entropy value of a selected window about the pixel can then be determined by the equation:

$$E=\sum_i C(i)\ln(C(i))$$

where E is the entropy and C(i) is the number of points in the window with the grayscale of i (i=0,1,2,. . ., 255). The calculated entropy values for each window are then compared against a predetermined threshold value. For regions of air, the entropy values will be fairly low, when compared to regions of tissue. Therefore, along the centerline of the colon lumen, when the entropy values increase and exceed the predetermined threshold value, a collapsed region is indicated. The exact value of the threshold is not critical and will depend in part on the imaging protocol and particulars of the imaging device.

Once a collapsed region is detected, the previously determined centerline flight path can be extended through the region by piercing through the center of the collapse with a one voxel wide navigation line.

In addition to automatically continuing the flight path of the virtual camera through the colon lumen, the region of colon collapse can be virtually opened using a physical modeling technique to recover some of the properties of the collapsed

region. In this technique, a model of the physical properties of the colon wall is developed. From this model, parameters of motion, mass density, damping density, stretching and bending coefficients are estimated for a Lagrange equation. Then, an expanding force model (i.e., gas or fluid, such as air, pumped into the colon) is formulated and applied in accordance with the elastic properties of the colon, as defined by the Lagrange equation, such that the collapsed region of the colon image is restored to its natural shape.

To model the colon, a finite-element model can be applied to the collapsed or obstructed regions of the colon lumen. This can be performed by sampling the elements in a regular grid, such as an 8 voxel brick, and then applying traditional volume rendering techniques. Alternatively, an irregular volume representation approach, such as tetrahedrons can be applied to the collapsed regions.

In applying the external force (air pumping) model to the colon model, the magnitude of the external force is first determined to properly separate the collapsed colon wall regions. A three dimensional growing model can be used to trace the internal and external colon wall surfaces in a parallel manner. The respective surfaces are marked from a starting point at the collapsed region to a growing source point, and the force model is applied to expand the surfaces in a like and natural manner. The region between the internal and external surfaces, i.e., the colon wall, are classified as sharing regions. The external repulsive force model is applied to these sharing regions to separate and expand the collapsed colon wall segments in a natural manner.

To more clearly visualize the features of a virtual object, such as the colon, which is subjected to virtual examination, it is advantageous to provide a rendering of the various textures of the object. Such textures, which can be observed in the color images presented during optical colonoscopy, are often lost in the black and white, grey scale images provided by the CT image data. Thus a system and method for texture imaging during virtual examination is required.

Figure 20 is a flow chart depicting a present method for generating virtual objects having a texture component. The purpose of this method is to map textures obtained by optical colonoscopy images in the red-green-blue (RGB) color

space, as for example from the Visible Human, onto the gray scale monochrome CT image data used to generate virtual objects. The optical colonoscopy images are acquired by conventional digital image acquisition techniques, such as by a digital "frame grabber" 1429 which receives analog optical images from a camera, such as a video camera, and converts the image to digital data which can be provided to CPU 1423 via interface port 1431 (Figure 14). The first step in this process is to segment the CT image data (step 2010). The above described image segmentation techniques can be applied to choose intensity thresholds in the grey scale image to classify the CT image data into various tissue types, such as bone, colon wall tissue, air, and the like.

In addition to performing image segmentation on the CT image data, the texture features of the optical image need to be extracted from the optical image data (step 2020). To do this, a gausian filter can be applied to the optical image data followed by sub-sampling to decompose the data into a multiresolutional pyramid. A laplacian filter and steerable filter can also be applied to the multiresolutional pyramid to obtain oriented and non-oriented features of the data. While this method is effective at extracting and capturing the texture features, the implementation of this approach requires a large amount of memory and processing power.

An alternative approach to extracting the texture features from the optical image is to utilize a wavelet transform. However, while wavelet transformations are generally computationally efficient, conventional wavelet transforms are limited in that they only capture features with orientations parallel to the axes and cannot be applied directly to a region of interest. To overcome these limitations, a non-separable filter can be employed. For example, a lifting scheme can be employed to build filter banks for wavelets transform in any dimension using a two step, prediction and updating approach. Such filter banks can be synthesized by the Boor-Rom algorithm for multidimensional polynomial interpolation.

After the textural features are extracted from the optical image data, models must be generated to describe these features (step 2030). This can be performed, for example, by using a non-parametric multi-scale statistical model which is based on estimating and manipulating the entropy of non-Gausian distributions attributable to the natural textures.

Once texture models are generated from the optical image data, texture matching must be performed to correlate these models to the segmented CT image data (step 2050). In regions of the CT image data where the texture is continuous, corresponding classes of texture are easily matched. However, in boundary regions between two or more texture regions, the process is more complex. Segmentation of the CT data around a boundary region often leads to data which is fuzzy, i.e., the results reflect a percentage of texture from each material or tissue and vary depending on the various weighting of each. The weighting percentage can be used to set the importance of matching criteria.

In the case of the non-parametric multi-scale statistical model, the cross entropy or a Kullback-Leiber divergence algorithm can be used to measure the distribution of different textures in a boundary region.

After texture matching, texture synthesis is performed on the CT image data (step 2050). This is done by fusing the textures from the optical image data in to the CT image data. For isotropic texture patterns, such as presented by bone, the texture can be sampled directly from the optical data to the segmented CT image data. For anisotropic texture regions, such as colon mucosa, a multiresolution sampling procedure is preferred. In this process, selective re-sampling for homogenous and heterogenous regions is employed.

Alternatively, pseudocolor texture can be created directly from the CT data. For each voxel, multiple CT values, comprising a local area neighborhood, can be evaluated to determine a pseudocolor for the given voxel. For each voxel the local neighborhood consists of the voxels that are within some given distance of the center voxel. For example a 5x5x5 voxel cubic shaped region, or the double pyramid which represents all voxels within 3 units measured by Manhattan distance. This vector of scalar values is then evaluated to map to a color to be displayed for this voxel during subsequent volume rendering. The evaluation of the local neighborhood vector of values can compute such things as local curvature, homo/heterogeneity, or other geometric or spatial functions.

Volume Rendering

In addition to image segmentation and texture mapping described above, volume rendering techniques can be used in connection with virtual colonoscopy procedures to further enhance the fidelity of the resulting image. Figure 21 illustrates a perspective volume ray-casting method which can be used for volume rendering in accordance with the present invention. From a selected virtual viewpoint, e.g., camera position, such as within the colon lumen, rays are cast through each of the proximate image pixels (step 2100). For each ray, the first sampling point is set as the current image pixel along the ray (step 2110). The distance (d) between the current sampling point and the nearest colon wall is then determined (step 2120). The current distance (d) is compared to a predetermined sampling interval (i) (step 2130). If the distance (d) is greater than the sampling interval (i) then no sampling occurs and the next sampling point along the ray is determined by jumping the distance d along the ray (step 2140). If the distance is less than or equal to the sampling interval (i) then conventional sampling is performed on this point (step 2150) and the next sampling point is selected in accordance with the sampling interval (i) (step 2160). For example, trilinear interpolation between the density values of 8 neighboring voxels can be performed to determine the new density value at the sampling point.

The method of Figure 21 effectively accelerates ray-casting because a space leaping technique is used to quickly skip over empty space along the ray of the image plane to the colon wall. In this method, a distance from a sample point to the nearest colon wall is determined along each ray. If the distance is larger than a predetermined sampling interval (i), a jump to the next sampling point along the ray is performed. Since the closest distance information is already available from the potential field which is used for virtual camera control, no additional distance coding calculations are required. In this case, neither surface rendering nor Z-buffer transform is required, which results in savings in preprocessing time and memory space.

Alternatively, a space leaping method can derive distance information for each ray from the Z-buffer of the corresponding surface rendering image. If the surface rendering image and volume rendering image will both be generated, this

approach provides minimal processing overhead burden as the Z-buffer information is provided as a result of the surface rendering methods. Thus, this form of space leaping method only requires additional processing to perform a depth transformation from the image space domain to the world space domain.

For those regions along the ray where the distance (d) was traversed in step 2140, the region along the ray corresponds to open space and can be assigned a value according to an open space transfer function. Typically, open space will have no contribution on the final pixel value. For each point where sampling takes place, one or more defined transfer functions can be assigned to map different ranges of sample values of the original volume data to different colors and opacities and possibly other displayable parameters. For example, four independent transfer functions have been used to determine different material by mapping ranges of CT density values into specified colors of red, green, blue and opacity, each in the range of 0 to 255.

Virtual Biopsy

The above described techniques can also form the basis of a system for performing virtual electronic biopsy of a region being examined to effect a flexible and non-invasive biopsy. As noted above, volume rendering techniques use one or more defined transfer functions to map different ranges of sample values of the original volume data to different colors, opacities and other displayable parameters for navigation and viewing. During navigation, the selected transfer function generally assigns maximum opacity to the colon wall such that the outer surface is easily viewed. Once a suspicious area is detected during virtual examination, the physician can interactively change the transfer function assigned during the volume rendering procedure such that the outer surface being viewed becomes substantially transparent, allowing the region information to be composited and thus the interior structure of the region to be viewed. Using a number of predetermined transfer functions, the suspicious area can be viewed at a number of different depths, with varying degrees of opacity assigned throughout the process.

Polyp Detection

The present system and methods can be used to perform automated polyp detection. With reference to Figure 13, polyps 1305, which occur, for example, within the colon, generally take the form of small convex hill-like structures extending from the colon wall 1301. This geometry is distinct from the fold of the colon wall. Thus, a differential geometry model can be used to detect such polyps on the colon wall.

The surface of the colon lumen can be represented as a continuously second differentiable surface in three dimensional Euclidean space, such as by using a C-2 smoothness surface model. Such a model is described in "Modern Geometry Methods and Applications" by B.A. Dubrovin et al, published by Springer-Verlag 1994, which is hereby incorporated by reference in its entirety. In this model, each voxel on the surface of the colon has an associated geometrical feature which has a Gauss curvature, referred to as Gauss curvature fields. A convex hill on the surface, which may be indicative of a polyp, possesses a unique local feature in the Gauss curvature fields. Accordingly, by searching the Gauss curvature fields for specific local features, polyps can be detected. Once detected, the suspected polyps can be highlighted and thus brought to the attention of the physician where the physician can measure the suspected polyp and use the above described virtual biopsy methods to further investigate the suspicious region.

Central Fly-Path Generation

In the case of virtual colonoscopy, determining a proper navigation line, or fly-path, through the colon lumen is an important aspect of the described systems and methods. While certain techniques for determining the fly-path of the virtual camera model were discussed with respect to Figures 4-8, Figure 22 illustrates an alternate method of generating the central fly-path through the colon lumen. After the colon wall is identified, such as by the image segmentation methods described herein, a volume shrinking algorithm can be employed to emphasize the trend of the colon lumen and reduce subsequent searching time within the lumen volume (step 2310).

Figure 23 further illustrates the steps of an exemplary volume shrinking algorithm, which is based on a multiresolution analysis model. In this procedure, the three dimensional volume is represented by a stack of binary images which have the same matrix size (step 2310). Collectively, these images form a binary data set. A discrete wavelet transformation can be applied to the binary data set which results in a number of sub-data sets representing different time-frequency components of the binary data set (step 2320). For example, the discrete wavelet transformation may yield eight (8) sub-data sets. The sub-data sets are compared against predetermined threshold values such that the lowest frequency component is identified (step 2330). This component forms the binary data set for subsequent discrete wavelet transformation and thresholding steps, which are recursively applied in a multi-resolution structure (step 2340). In the case of virtual colonoscopy, the discrete wavelet transformation and associated thresholding can be applied three times recursively on the subsequent sub-dataset that represents the lowest frequency component (a 3-level multi-resolution decomposition).

Returning to Figure 22, from the reduced colon volume model, a distance map technique can be employed to generate a minimum distance path between the two ends of the colon, e.g., from the rectum to the cecum (step 2215). The resulting path preserves the global trend information of the colon lumen, but ignores the trends exhibited by local folds. Control points within the global colon can then be determined by mapping the minimum distance path back to the original data space (Step 2220). For example, in the case of a 3-level multi-resolution decomposition, the reduced volume is three times smaller than the original volume and an affine transformation, which is well known, can be used to map the reduced volume model exactly back to the original scale volume. The minimum distance path of the reduced value can also be mapped back into the original scale volume as a series of points, which can be used as the control points within the colon.

The preferred fly path is one which is on the centerline of the colon lumen. However, the initial control points may not be exactly located in the center of the colon lumen. Thus, the initial control points can be centered, such as by the use of a bi-section plane algorithm (step 2230). For example, at each selected control point,

a bi-section plane can be defined as a plane normal to the trend direction and cutting across the colon lumen. A centralization algorithm, such as a maximum disk algorithm, can then be performed on each bi-section plane. Such an algorithm is discussed in the article "On the Generation of Skeletons from Discrete Euclidean Distance Maps" by Ge et al., IEEE Transactions on PAMI, Vol. 18, pp. 1055-1066, 1996 which is hereby incorporated by reference.

Once the control points are centralized, the flight path can be determined by interpolating a line connecting these points (step 2240). In the case of virtual colonoscopy, it is desirable that the interpolated flight path take the form of a smooth curve which is substantially centered within the colon lumen. A constrained cubic B-spline interpolation algorithm based on Serret-Frenet Theorem in differential geometry theory can be used to establish a suitable smooth curved flight path, such as is described in "Numerical Recipes in C: The Art of Scientific Computing," by Press et al., Second Edition, Cambridge University Press, 1992.

The pictorial representation of a segmented colon lumen in Figures 24 and the flow chart of Figure 25 set forth yet another alternate fly-path generation method in accordance with the present invention. In this alternate method, the representation of the colon lumen 2400 is first partitioned into a number of segments 2402 a-g along the length of the lumen 2400 (step 2500). From within each segment 2402 a representative point is selected 2404 a-g (step 2520). Each representative point 2404 a-g is then centered with respect to the colon wall (step 2530), such as by the use of a physically-based deformable model which is used to push the points to the center of the respective segment. After the representative points are centered, the points are sequentially joined to establish the center-line fly-path for the virtual camera model (step 2540). If the segments are sufficiently small in length, the centered points can be connected with straight line segments 2406 a-f. However, when linear curve fitting techniques are applied to join the centered points, a smoother, continuous flight path is established.

Each of the foregoing methods can be implemented using a system as illustrated in Figure 14, with appropriate software being provided to control the operation of CPU 1409 and CPU 1423.

An alternate hardware embodiment, suitable for deployment on a personal computer, is illustrated in Figure 26. The system includes a processor 2600 which should take the form of a high speed, multitasking processor such as a Pentium III processor operating at a clock speed in excess of 400 MHZ. The processor 2600 is coupled to a conventional bus structure 2620 which provides for high speed parallel data transfer. Also coupled to the bus structure 2620 are main memory 2630, a graphics board 2640, and a volume rendering board 2650. The graphics board 2640 is preferably one which can perform texture mapping, such as the Diamond Viper v770 Ultra manufactured by Diamond Multimedia Systems. The volume rendering board 2650 can take the form of the VolumePro board from Mitsubishi Electric, which is based on U.S. Patent Nos. 5,760,781 and 5,847,711, which are hereby incorporated by reference. A display device 2645, such as a conventional SVGA or RGB monitor, is operatively coupled to the graphics board 2640 for displaying the image data. A scanner interface board 2660 is also provided for receiving data from an imaging scanner, such as an MRI or CT scanner, and transmitting such data to the bus structure 2620. The scanner interface board 2660 may be an application specific interface product for a selected imaging scanner or can take the form of a general purpose input/output card. The PC based system 2600 will generally include an I/O interface 2670 for coupling I/O devices 2680, such as a keyboard, digital pointer (e.g., mouse) and the like to the processor 2620. Alternatively, the I/O interface can be coupled to the processor 2620 via the bus 2620.

In the case of three dimensional imaging, including texture synthesis and volume rendering, numerous data handling and processing operations are required. For large datasets, such as those represented by the colon lumen and its surrounding area, such processing can be very time consuming and memory intense. However, using the topology of Figure 26 in accordance with the processing method illustrated in the flow chart of Figure 27, such operations can be performed on a relatively low cost personal computer (PC). Imaging data is received by the processor 2620 and stored in main memory 2630 via the scanner interface board 2660 and bus structure 2620. This image data (pixels) is converted into a volume element (voxel) representation (step 2710). The volume representation, which is stored in main

memory 2630, is partitioned, for example into slices, such as along a major volume axis or other portions of the region being imaged (step 2720). The volume partitions are then transferred to the volume rendering board and temporarily stored in volume rendering memory 2655 for volume rendering operations (step 2730). The use of locally resident volume rendering memory 2655 provides for enhanced speed in volume rendering as data need not be exchanged over the bus 2620 during rendering of each slice of the total volume. Once volume rendering is complete for the slice, the rendered data is transferred back to main memory 2630 or the graphics board 2640 in a sequential buffer (step 2740). After all slices of interest have been subjected to rendering, the contents of the sequential buffer are processed by the graphics board 2640 for display on the display unit 2645 (step 2750).

Multi-scan Based Virtual Examination

The techniques discussed above generally perform virtual imaging based on a dataset acquired from a single magnetic resonance imaging (MRI) or computed tomography (CT) scan. However, the techniques discussed above are also useful for performing virtual examination of a region using multiple scans of a region. By using multiple scans of a region, improved imaging of regions of pathology can be achieved and motion artifacts can be reduced. One such application of interest is in performing virtual cystoscopy to screen a patient for possible polyps or cancer of the bladder.

Figure 28 is a flow chart which illustrates a method of employing multiple MRI scans to perform virtual examination of an object, such as virtual cystoscopy. Unlike CT images, where the bladder wall can be difficult to distinguish from urine, in MRI images, urine can be used as a natural contrast agent to delineate the inner bladder wall. To this end, a pre-image scan protocol is employed (step 2805). Approximately ½ hour prior to the first of four MRI scans, the patient is requested to empty the bladder and then consume one cup of water. After approximately ½ hour, the patient is subjected to the first of four MRI scans of the bladder region (step 2810). The first scan, with the bladder full and distended, follows protocol for T1-weighted transverse imaging. For example, when using the Picker scanner referenced above, a

KJELL FASTER protocol using a 256x256 matrix size, a 38 cm field of view (FOV), a 1.5 mm slice thickness (no gap), a 3 ms TE, a 9 ms TR, a 30 degree flip angle and one scan average can be used. Of course, these parameters tend to be scanner specific and various changes in the parameters can be used with acceptable results.

With the bladder still full, the patient is subjected to a second MRI scan, scan 2 (step 2815). The second scan follows a protocol for T1-weighted coronal imaging, such as the Picker KJELL FASTER protocol with a 256x256 matrix size, a 38 cm field of view (FOV), a 1.5 mm slice thickness (no gap), a 3 ms TE, a 9 ms TR, a 30 degree flip angle and a two-scan average.

The two image scans described above are taken along orthongal axes with respect to one another. The advantage of this is that regions of significant motion artifacts in one scan, generally correspond to regions of minimal motion artifacts in the orthogonal scan. Accordingly, by taking a first scan in the transverse direction and a second scan in the coronal direction, the image scans can be registered and motion artifacts in the data set can be identified and compensated for.

After the scan 2, the patient is asked to relieve the bladder and is then subjected to two additional MRI scans. The third scan (step 2820) follows the same imaging protocol as the first scan (transverse imaging). The fourth scan (step 2825) follows the same imaging protocol as the second scan (coronal imaging).

The image scans can be acquired using a Picker 1.5 T Edge whole-body scanner. Although a T2 imaging protocol can be used, a T1 imaging protocol is preferred for virtual cystoscopy because this protocol provides improved delineation between fat and urine and offers a shorter acquisition period. Alternatively, the image scans can take the form of computed tomography or ultrasound imaging scans using suitable contrast agents and protocols for these imaging techniques.

During the first two scans (scan 1 and scan 2), the bladder is distended and the bladder wall is relatively thin. In this case, physiologically altered locations, such as tumors, may thin at a different rate as compared to the unaltered bladder wall and may become more apparent under these conditions. During the third and fourth scans, the bladder is substantially empty and the bladder wall is thicker. With a thicker

wall, a more pronounced image contrast may result between normal tissue of the bladder wall and that of physiologically altered tissue.

After the four scans are acquired, the four corresponding datasets can then be individually processed. Initially, each scan data set is preferably subjected to image segmentation, as discussed above (step 2830), such as in connection with Figure 15. During image segmentation, the voxels of the four datasets are classified into a number of categories, such as bladder wall, urine, fat, boundary, etc. The classification is based on the local intensity vectors of the voxels. Once the voxels are classified, the interior of the bladder lumen can be identified using a region growing algorithm beginning with a seed voxel selected from within the bladder volume, such as by selecting an air voxel or urine voxel.

Prior to clinical analysis of the segmented volume data sets, registration of the four data sets to a common coordinate system is performed (step 2835). Because the shape of the bladder varies from scan to scan, an exact voxel-voxel registration is not of practical value. Instead a flexible registration process is preferred. In the present flexible registration process, for each volume of interest (volume rendered for each corresponding scan) the center of the volume is determined, such as by averaging the three coordinates of all the voxels in the volume.

A Cartesian coordinate system can then be constructed with the origin of the system located at the center point of the volume. The axes of the system can then be oriented in a number of ways. A suitable selection of orientation corresponds to the orientation of the natural human body, e.g., with the Z-Axis running along the height of the body (e.g., from toe to head) the Y-axis oriented from back to front and the X-axis running laterally (e.g., from left to right). The units of length in this coordinate system can be conveniently set to an arbitrary unit of one voxel length, the absolute magnitude of which will vary based on acquisition properties for the MRI scans. So long as the same pixel spacing is used in all scans to acquire all four data sets, this will result in a uniform value for each of the four data sets.

After registration, the images from the four data sets can be viewed individually or simultaneously (step 2845). An exemplary display window is illustrated in Figures 29 and 30. Referring to Figure 29, the display is partitioned into

four sub windows 2905, 2910, 2915, 2920 which correspond to scan 1, scan 2, scan 3 and scan 4, respectively. A control panel section 2925 can also be provided on a portion of the display to establish a graphical user interface (GUI) to offer display and navigation functions to the user. As an operator navigates in one of the image sub windows, such as magnifying the view, the corresponding operation preferably takes place in the other sub window views as well. A user can also select one of the views for expansion to a single window display.

To reduce the amount of data which is simultaneously processed, the data sets can be partitioned, such as into 8 parts or octants (step 2840). This can be performed in a number of ways. For example, with reference to the Cartesian coordinate system illustrated in Figure 29, the data can be portioned into the eight regions of the coordinate system: (1) X, Y, Z; (2) X, -Y, Z; (3) X, Y, -Z; (4) X, -Y, -Z; (5) -X, Y, Z; (6) -X, -Y, Z; (7) -X, Y, -Z; and (8) -X, -Y, -Z.

Figure 29 illustrates four views of the outside of the bladder lumen taken from each of the four scans. Figure 30 illustrates fours views of a portion of the interior of the bladder lumen also taken from each of the four scans.

Multi-Resolution Imaging and Virtual Laryngoscopy

The systems and methods described herein can be adapted and applied to perform multiresolution imaging which is well suited for virtual laryngoscopy. Figure 31 is a flow chart illustrating a method for performing virtual laryngoscopy. First, an imaging scan of the region of a patient's larynx is acquired (step 3105). This can be performed using computed tomography (CT) or magnetic resonance imaging (MRI) techniques. However, because the CT scan in this region offers significantly faster acquisition time (30 seconds versus over 7 minutes for MRI) and higher resolution (0.3mm cubic voxel compared to 1mm cubic voxel for MRI), the CT scan is preferred. To acquire the CT scan data a GE/CTI spiral scan CT scanner can be used. A suitable scan protocol is 120 keV, 200 ma, 512x512 matrix size, 15 cm field-of-view and 3mm/2.0:1 pitch. The scan is completed in approximately 30 seconds and results in 351 image slices of 0.3mm thickness and results in 0.3mm cubic voxels.

Image segmentation can be used to classify voxels into a number of categories (step 3110). In this operation, a modified self-adaptive on-line vector quantization (SOVQ) algorithm can be used. In such a case, the algorithm analyzes each voxel with respect to neighbors of up to the third order to determine local density features. Each voxel in the acquired dataset has an associated local density vector. By transforming the local density vectors using the Karhunen-Loéve (K-L) transform, feature vectors for the voxels in the volume image can be obtained. Based upon the feature vectors, the voxels can be classified and labeled. Voxel classification is dependent in part on the choice of a local voxel density vector and one preset parameter, referred to as the maximum cluster number (MCN). The MCN sets the number of voxel classifications that will be applied to the dataset. In the case of the CT images, the human eye can discern four (4) distinguishable tissue/material types. An MCN value of 5 is suitable in this case. For an MRI image, the human eye can differentiate among 6 different tissue types, and an MCN value of 7 can be used.

As part of the image segmentation process, an expanded data set is generated by interpolation between the measured data points. For example, prior to employing the SOVQ algorithm, a first order Lagrange interpolation can be applied to each slice in the dataset. This expands the 256x256 matrix size of the original slices of the data set to a 512 x 512 matrix size. In addition, inter-slice interpolation can be performed to further expand the dataset between actual slices. The interpolated dataset is referred to as the enlarged dataset. In addition to generating an enlarged dataset, the interpolation process also suppresses noise and reduces the partial-volume effect, as the interpolation process has a low-pass filtering effect on the data.

Using a two dimensional viewing tool, a seed voxel can be selected within the larynx lumen and a growing algorithm applied to extract the larynx volume from the dataset (step 3115). In those regions of the larynx where there may be several unconnected volume regions, multiple seed points can be selected.

With the larynx volume identified and the voxels of the regions classified through image segmentation, the next task is to manage the data in a manner which allows efficient navigation and viewing of the virtual larynx. In this case, a level-of-detail (LOD) approach is adopted and modified for use in the present method.

In this LOD method, a reduced dataset is generated from the enlarged data set. For example, the 512x512x256 enlarged dataset can be reduced to a 64 x 64 x 32 reduced volume dataset using a multi-resolution decomposition with three levels of thresholding (step 3120). Next, polygons used to render the volume images in both the enlarged and reduced volume datasets can be extracted. A traditional Marching Cubes method can be used to extract polygons to fit the surface of the larynx.

One problem encountered in the prior art is managing the large number of polygons required to generate the three dimensional image for the enlarged dataset. This problem is solved in the present method by organizing the enlarged dataset in a Binary Space Partitioning (BSP) tree data structure (step 3130). The original image volume is selected as the root of the tree. The space is then partitioned into two subspaces containing an approximately equal number of polygons. This subdivision process is iteratively repeated until the number of polygons in each resulting subspace is below a threshold value. The threshold value can vary based on system performance and application requirements. The last resulting subspaces are referred to as leaf nodes of the tree. Once the subdivision process is complete, all of the voxels of the expanded dataset are stored in the leaf nodes of the BSP tree.

During navigation or viewing, polygon culling can be applied by first removing those leaf nodes that are completely outside the field-of-view from current processing operations. The remaining polygons are recalled from the BSP tree, ordered and rendered in those spaces which were not culled. Thus, the BSP tree provides an effective tool for selecting a relevant portion of the dataset for a particular navigation or display operation.

The enlarged and reduced datasets are cooperatively used in a two level LOD rendering mode. If a user is interacting with the object (step 3135), such as rotating, shifting or effecting other changes in the field of view, the polygons from the reduced dataset (64-sized) are rendered (step 3140). Because of the significantly lower number of polygons involved, interaction with the reduced dataset volume can be performed faster and with less processing overhead. The tradeoff for the increased speed is reduced image resolution. If there is no interaction from the user after a predetermined time period, the polygons of the enlarged dataset (512-sized) are

selected from the BSP tree and are rendered to provide a high resolution image of the current field of view (step 3145).

Virtual Angiography

The techniques for virtual imaging and navigation can also be adapted and applied to virtual angiography. This technique can be used for detection and measurement of various abnormalities and disease of the circulatory system.

One such application of virtual angiography is the detection of abdominal aortic aneurysms, which generally start as small enlargements of the aortic vessel and exhibit a greater risk to rupture with increasing size of the aneurysm. Previously, the only effective method of treatment was open surgery, placing a graft within the aorta at the level of the aneurysm. However, this procedure has a high degree of associated morbidity and mortality. Recently developed per cutaneous placed aortic stent graft techniques have a significantly lower complication rate. Virtual angiography is an effective method to help plan these less invasive procedures and can also be an effective tool for detecting the presence of an aneurysm and tracking the growth of an aneurysm to determine if and when surgery is indicated.

Figure 32 in a flow chart which provides an overview of the present virtual angiography method. In performing a virtual angiography, an image scan of the vessel, such as the aorta must be acquired (step 3205). Various imaging techniques can be used, such as Computed Tomography (CT), Magnetic Resonance Imaging (MRI) and ultrasound. However, an aortic CT scan is generally preferred because of the contrast between blood, soft tissue and calcium deposits which results in the CT image.

Once an image scan data set is acquired, image segmentation techniques are then applied to the data set to classify the voxels of the dataset into a number of categories (step 3210). The image segmentation techniques described above, such as in connection with Figure 15, are generally applicable. In this case, the various feature vector values of the voxels will be grouped according to categories such as blood, soft tissue and calcium deposits. Using a blood voxel as a seed, a region growing algorithm can be used to determine the volume and extent of the aortic lumen.

In the CT image, an aneurysm has image features which closely resemble the neighboring soft tissue. As a result, the full contour of the aneurysm can be difficult to establish. However, regions with calcium deposits offer significant contrast on the CT scan and can be used to identify portions of the aneurysm, such as the endpoints of the aneurysm on the vessel wall (step 3215).

After a portion of an aneurysm is detected, one or more closing surfaces can be generated to define an estimation of the aneurysm's contour (step 3220). A convex closing surface can be established using a non-uniform, non-rational B-spline to generate a surface which runs through or near the points of the aneurysm which were identified.

After the closing surface is generated, the volume of the aneurysm can be estimated (step 3225). One method for estimating the volume is to count the number of voxels which are enclosed by the estimated closing surface. In addition, within the volume of the aneurysm, the centerline along the direction of blood flow can be determined by using a distance transform technique. Continuous local coordinate systems can then be established along this centerline and the diameter of the aneurysm determined. Virtual navigation can take place along this centerline, in a manner consistent with that described above for navigating through a lumen, such as the colon.

Referring to Figures 33A-C, the described method of virtual angiography can be used to assist in the generation and placement of a stent graft to bypass an abdominal aortic aneurysm. Figure 33A illustrates a simplified diagram of an abdominal aortic aneurysm located below the renal arteries and above the bifurcation of the aorta. Because of variations from patient to patient in the specific anatomy of the aorta and the size and location of an abdominal aortic aneurysm therein, when a stent graft is to be used to bypass an aneurysm, the graft must be designed and built to specifically fit the particular aortic segment. As illustrated in Figure 33B, this can require identifying the length of the required graft, the diameter at the points of interface on each end of the bypassed region, the angles of interface, among other variables. If the aneurysm is located near an arterial branch, the size and angles of the bifurcated ends of a bifurcated stent graft must also be determined, as illustrated in Figures 33B and 33C.

To date, such measurements have been performed through invasive calibrated angiograms using a catheter inserted into the aorta from an insertion made at the level of the groin region, rapid injection of a large amount of iodinated contrast and rapid radiographic imaging. This technique can be supplemented and perhaps supplanted using the present virtual angiography techniques, which can resolve such distances and angles using virtual navigation using centerlines constructed through the branches of the aortic lumen. In addition, the virtual angioscopy can be used to perform a virtual biopsy of the region where a stent graft may be inserted. This allows the operator to view beneath the arterial surface and examine the region for thrombus deposits, calcification or other factors which would contra-indicate the use of a stent graft procedure.

Another application of virtual angiography is the imaging, examination and navigation through the carotid arteries which supply blood flow to the brain. The techniques described herein with respect to virtual endoscopy are fully applicable in the case of blood vessels. For example, the vessels of interest are extracted from the acquired image data using image-segmentation techniques. Next, a navigation flight path can be established through the vessel(s). Preferably, potential fields are built up within the vessel for use in navigation. As with other organs, such as the colon, a volume-rendered model of the vessels of interest can be generated. Using the flight path and potential fields to navigate through the interior of the volume rendered blood vessel lumen, abnormalities such as vessel narrowing and plaque build up can be observed. In addition, the techniques discussed regarding virtual biopsy can be applied in this context to evaluate vessel wall and characterize build up on the wall surface, such as plaque.

Tree Branch Searching for Virtual Endoscopy

Path planning for virtual navigation through a hollow organ or object is an important task. Various techniques have been discussed, such as fly-path generation, to achieve this goal. As the geometry of the object being studied becomes

more complex, such as presenting a multi-branch structure, the task of path planning becomes even more complex. It is desirable to determine not only the center line of a primary lumen, but also to identify and locate any branches extending from the primary lumen. Common examples of organs having a complex branch structure include the main airway and lungs, the cardiovascular system and, because of the presence of haustral folds, the colon. Each organ or object generally presents specific challenges for defining a path, or skeleton, for the object. However, a generalized technique for generating such a skeleton is illustrated in the flow chart of Figure 34.

Referring to Figure 34, an imaging scan of the region of interest, such as a computed tomography (CT) or Magnetic Resonance Imaging (MRI) scan, is acquired (step 3405). As discussed above, the imaging scan is transformed into a three dimensional volume of the region by stacking the binary images of the imaging scan and defining three dimensional volume units, or voxels, from these stacked images (step 3410). Depending on the volume and complexity of the region of interest, it may be desirable to reduce to size of the dataset of the three dimensional volume prior to generating the skeleton. To this end, a multiresolution data reduction process, which is discussed in more detail below, can be used (step 3415).

The skeleton is a subset of the three dimensional volume. Preferably, the skeleton has the following attributes: 1) It preserves the homotopy of the tree; 2) it is 26-connected; 3) it is one voxel thick; 4) it approximates the central axes of the branches; and 5) it is relatively smooth. The degree of homotopy is somewhat application specific. For example, in generating a skeleton of the colon lumen, the skeleton will generally be a single path from end to end, despite the presence of numerous haustral folds which can be several voxels deep. However, in the cardiovascular system and pulmonary system, a small offshoot from the root which is several voxels deep can represent a legitimate branch in the system.

Returning to Figure 34, in the volume of interest, a root voxel is identified in the volume (step 3420). In performing virtual endoscopy, this can be performed manually based on an understanding of the geometry of the structure being evaluated.

A distance map can then be generated to identify the branches in the tree and the distances between the endpoints of the branches and the root voxel (step 3425). A presumption applied in this method is that there exists one unique endpoint on each branch which exhibits the longest distance to the root of the tree. Figure 35 is a schematic diagram illustrating a 3x3x3 cubic voxel arrangement which is referred to as a 26-connected voxel cubic distance plate. In the center of this arrangement is a seed voxel 3505, which is assigned a distance weight of zero. Around the seed voxel 3505 are 26 connected neighbor voxels which are assigned distance weights based on the respective Euclidean distance between the respective neighbor voxel and the seed. In a cubic arrangement the Euclidian distance can assume a normalized value of $1, \sqrt{2}, \sqrt{3}$ which is approximately equal to 1, 1.4 and 1.7. To simplify processing, the voxels can be assigned integer value weights of 10, 14, and 17 to approximate the relative Euclidian distances.

Figure 36 is a pseudo-code representation of an algorithm for determining the distance map from a voxel in the volume to the root using the Euclidian weighted distances of the 26-connected cubic distance plate of Figure 35. From the generated distance map, branches are identified and the endpoints of the branches are determined (step 3430).

Referring to Figure 36, the root of the volume is labeled with the integer value 0. A processing queue is then formed with the voxels in the volume. The voxels are then labeled in a first-in, first out manner by adding the Euclidian distances between the voxel at the top of the queue and the root voxel. This process is repeated until all of the voxels in the volume are assigned a value in the distance map.

Because the labeling of voxels in the distance map will depend, in part, on the queuing order, the resulting distance map does not provide a unique solution. However, regardless of the queuing order, there is always at least one farthest point for each branch. In addition, for each voxel, other than the root voxel, there is always at least one 26-connected neighbor in the volume which has a shorter distance to the root. Thus, the endpoints of the branches are readily detectable by searching the distance map for local maximum distances (local maxima) (step 3430). The term local maxima is a relative term. In evaluating the volume for local maxima, the volume should be

partitioned into various subspaces which are appropriate to the object being evaluated. The expected feature size, branch length, branch diameter, etc. are generally considered in determining the subspace partitions.

Once the endpoints of the branches are determined, the shortest path from the endpoint to the root voxel is determined (step 3435). The shortest paths from the endpoints to the root define the basic structure of the branches of the tree and approximate the centerline of the branches. This is referred to as the rough skeleton of the volume. The shortest paths are preferably generated from the branches at farthest end of the tree and begin from the end of those branches. From the most remote branch endpoint, the first voxel is selected and its 26-connected neighbors are analyzed to determine which voxel is in the minimal distance path from endpoint to root. This process is repeated until a selected voxel meets the root. This results in a one-voxel wide path from the farthest end to the root. Searching for the shortest path for other branches is similar. However, for subsequent branches, the selection process can terminate when the current path reaches a previously assigned path (e.g., the path need not lead all the way to the root). The collection of all of the interconnected shortest paths is the resulting rough skeleton of the object.

Depending on the application of the resulting rough skeleton, it may be desirable to refine the rough skeleton (step 3440). One step of refining the skeleton is to centralize the skeleton within the branches. Centralization preferably takes place branch by branch from the longest branch to the shortest. Starting with the longest branch, a uniform interval is selected, generally in the range of 4-8 voxels, along the branch. For each interval, the tangent direction of the voxel on the rough skeleton is calculated and a plane crossing the voxel perpendicular to the tangent direction is determined. A two dimensional area defined by the intersection of the plane and the volume is created and the center of this intersection can be computed using the known maximum disk technique. The centers of intersection can then be connected using a bi-cubic, B-spline interpolation or other curve fitting method. For the remaining branches, the endpoint which meets another branch or the root must first be adjusted to match the position of the previously centered skeleton branch. Then, centralization can proceed in the same manner as described for the longest branch.

Referring back to step 3415, when a large dataset is involved, it may be required, or at least desirable, to reduce the size of the dataset to speed up processing and reduce processing cost. Noting that the tree structure can be preserved within a range of scales, the large volume can be shrunk to a smaller scale space for structure analysis.

A shrinking method based on multiresolution analysis theory can be used. The input data is the stack of binary images of the same size which can be obtained from the segmentation results of the CT or MRI scan. The x-direction is taken along the slice image width, the y-direction is along the slice image height, and the z-direction is along the direction of slice by slice. The foreground voxels in the tree volume are set to value of 128 (maximum) and the background voxels are set to value 0 (minimum). A Daubechies' bi-orthogonal wavelet transform with all rational coefficients is employed. This one-dimensional (1D) discrete wavelet transformation (DWT) is first applied along to the x-direction row by row. From application of the DWT only the lower frequency components are retained and packed. The computation is preferably implemented in floating points. Noting that the DWT is applied to the binary signal, there are two kinds of nonzero coefficients which result in the lower frequency component. The first is of value 128 and this kind of coefficients are located in the interior of the volume. The second is of a value not equal to 128 and these coefficients locate the boundary of the volume.

The coefficients of the second kind are compared against a predetermined threshold value. If its absolute value is larger than a pre-set threshold T1, the value of the coefficient is set to 128; otherwise, it is set to 0. This results in a stack of binary images with a row size of half of the original dataset. The same DWT is then applied to the resulting dataset along the y-direction column by column, where the similar thresholding is employed to the lower frequency components. The result is again a stack of binary images, but now with both half row and column size as compared to the original dataset. Finally, the DWT is applied to the last result along the z-direction and the lower frequency components are retained. This step completes the first level decomposition.

The resulting dataset of the first level decomposition is of half size in all three directions as compared to the original dataset. If the shrinking procedure stops at this level, the finial thresholding is applied. It revalues those coefficients of nonzero and non-128 value. If the absolute value of this kind of coefficient is larger than a pre-set threshold **T2**, it will be revalued as 128; otherwise, it is revalued as 0. If further shrinking is needed, the same thresholding algorithm is applied with the threshold **T1**. Further shrinking proceeds as previously described, but is applied to the dataset shrunk at the last previous level. The decomposition procedure can be recursively applied until the resulting volume meets the desired reduced data volume. In virtual endoscopy, the slice images are of 512X512 pixel size. The maximum decomposition level is usually three, resulting in a 64x64 reduced pixel size.

The volume is isotropically shrank in all directions with the presented method. The two pre-set thresholds, **T1** and **T2**, are used to control the degree of shrinking. If the volume is significantly over shrunk, connectivity may be lost in the reduced volume. If it is over shrunk to a lesser degree, two separate branches may merge into one branch in the reduced volume dataset. The larger the two threshold values, the thinner the reduced volume is. The range of those two thresholds is [0, r x 128], where $0<r<1$. Preferably, the range for virtual endoscopy is r∈ (0.08, 0.28) for **T1** and r∈ (0.7, 0.98) for **T2**. The exact determination is dependant on the feature size of the particular application and is selected to achieve reduction while retaining the fidelity of the structure information in the shrunk volume.

After shrinking the original volume, the tree branch searching procedure can be applied to the smaller volume (steps 3420-3440). The resultant skeleton can be mapped back into the original scale space. When scaled to the original space, the image of the smaller scale skeleton no longer remain a connected path in the original scale space. These voxels in the image act as control points for the final skeleton. The control points are centralized using the algorithm as described previously, and then, they are interpolated to form the final skeleton of the object.

Computer Assisted Diagnosis

The virtual examination techniques described herein lend themselves to applications for the computer assisted diagnosis (CAD) of various conditions. For example, as described above, by examining the geometry of an organs tissue for local Gaussian curvatures, regions with abnormal geometry, such as polyps inside a colon lumen, can automatically be identified. This technique can be generalized and used in conjunction with texture features to provide CAD functionality for a number of applications.

For example, using the multi-scan imaging of the bladder described above, automated detection or tumors in the bladder wall can be performed. In this case, the degree of tumor invasion within the bladder wall is generally used to define the stage of bladder cancer. Using the multi-scan imaging and image segmentation techniques described above, the region of the bladder wall can be readily delineated. Regions of normal bladder tissue generally exhibit a substantially uniform texture feature. However, if a tumor is present in the region, the uniform texture feature will be interrupted. Thus, using texture analysis to evaluate the wall of the bladder, a region which may exhibit a tumor will present itself as a disturbance, or "noisy region" within the uniform texture.

The texture of a region can be represented by a probability distribution function (PDF) which characterizes the intensity correlation between voxels within a defined range. A two-dimensional PDF can be used to represent a texture feature. Such a PDF characterizes the correlation between two closest voxels along all directions. To estimate the PDF, the intensities of any two closest neighbor voxels in a region of interest can be recorded as a sample vector for the region of interest (e.g., context). Using a number of such sample vectors, a cumulating distribution function (CDF) can be generated which estimates the PDF for that context. For each voxel, sample vectors within a range of its neighbor can also be used to generate a local CDF.

A statistical test, such as a Kolmogorov-Smirnov test, can be applied to the CDF to determine whether the CDF of the context and the local CDF are statistically equivalent, e.g., within a predefined confidence level. If so, the local texture feature around the current voxel is regarded as identical to the context. Otherwise, the current voxel exhibits a different texture feature from that of the

context and may be regarded as a potential abnormality, such as a tumor. The level of confidence used to determine whether a voxel is statistically equivalent to the context can be varied to increase or decrease the sensitivity of detection.

In an alternative method of applying the PDF or CDF for texture analyis, each CDF or PDF can be regarded as a point in a functional linear space. The distance between two CDF's or PDF's in that space can be measured, such as in terms of the Skorohold metric. This distance provides a measure of the degree of similarity of PDF's. For example, the distance between a local CDF and the context CDF can be calculated and the resulting distance can be compared to one or more distancing thresholds. If the distance is large, the local texture may be considered different from the context, which can indicate that such a voxel belongs to a region with a potential abnormality or tumor. Preferably, the distancing thresholds are determined based on evaluation of a statistically sufficient known data sets.

The distance calculated above can be used with visualization techniques and volume rendering techniques, such as those described herein. For example, a feature volume dataset having a size comparable to the original dataset can be created. The intensity for each voxel in the new dataset can then be assigned based upon the distance between the local CDF and the CDF of the context. When this three dimensional volume dataset is viewed through volume rendering techniques, the regions which contain suspected tumors will exhibit a higher image intensity than the surrounding area.

As was discussed above in connection with automatic detection of polyps, the surface of a lumen can be represented as a continuously second differentiable surface in three dimensional Euclidean space, such as by using a C-2 smoothness surface model. In such a model, each voxel on the surface of the colon has an associated geometrical feature which has a Gauss curvature, referred to as Gauss curvature fields. For various organs, certain expected local features can be characterized by distinct curvature templates. For example, in the context of the colon, the expected local features include smooth curve surfaces, ring folds, convex hills from a smooth surface and plateaus from a smooth surface. These last two local features may be indicative of a polyp or tumor. Accordingly, by searching the Gauss curvature

fields for specific predetermined local feature templates, polyps, tumors and other abnormalities of interest can be automatically detected. This use of surface geometry to perform computer assisted diagnosis can be used alone, or in conjunction with the texture-based CAD techniques described above.

As an alternative to rendering and viewing the entire organ or region of interest, the surface under observation can be partitioned into small areas, or patches, which are defined by the local curvature templates. Each patch should contain voxels which have a common geometry feature, or curvature template. A single viewing point is then determined for the patch which allows all voxels of the patch to be observed. The patches are then assigned a priority score indicating the probability that the patch represents a polyp or other abnormality. The patches can then be observed individually, in priority order, rather than requiring the operator to navigate the entire organ volume to search out suspect areas. Of course, a preferred diagnostic system includes the ability to toggle between views such that an operator can readily change from viewing a patch to viewing the patch in the context of the organ. Alternatively, these two views can be presented simultaneously. Again, the texture based approaches can be used to supplement this approach. By mapping the results of texture analysis onto the patches being observed, the texture information can also be observed and used in diagnoses.

The foregoing merely illustrates the principles of the present imaging and examination systems and methods. It will thus be appreciated that those skilled in the art will be able to devise numerous systems, apparatus and methods which, although not explicitly shown or described herein, embody the principles of the invention and are thus within the spirit and scope of the invention as defined by its claims.

For example, the methods and systems described herein could be applied to virtually examine an animal, fish or inanimate object. Besides the stated uses in the medical field, applications of the technique could be used to detect the contents of sealed objects which cannot be opened. The techniques can also be used inside an architectural structure such as a building or cavern and enable the operator to navigate through the structure.

CLAIMS

1. A method for performing virtual examination of an object comprising:

performing at least one scan of an object with the object distended by the presence of a contrast agent;

performing at least one scan of the object with the object relieved of the contrast agent;

converting the scans to corresponding volume datasets comprising a plurality of voxels;

performing image segmentation to classify the voxels of each scan into a plurality of categories;

registering the volume datasets of each scan to a common coordinate system;

displaying at least two of the volume datasets in a substantially simultaneous manner; and

performing virtual navigation operations in one of the volume datasets and having the corresponding navigation operations take place in at least one other volume dataset.

2. The method for performing virtual examination according to claim 1, wherein the at least one scan of the distended object includes a transverse scan and a coronal scan of the object.

3. The method for performing virtual examination according to claim 2, wherein the at least one scan of the relieved object includes a transverse scan and a coronal scan of the object.

4. The method for performing virtual examination according to claim 3, wherein the object is a bladder.

5. The method of performing virtual examination according to claim 4, wherein the scans are computed tomography scans.

6. The method of performing virtual examination according to claim 4, wherein the scans are ultrasound imaging scans.

7. The method of performing virtual examination according to claim 4, wherein the scans are magnetic resonance imaging scans.

8 The method of performing virtual examination according to claim 7, wherein the contrast agent is urine.

9. The method for performing virtual examination according to claim 1, wherein the at least one scan of the relieved object includes a transverse scan and a coronal scan of the object.

10. The method for performing virtual examination according to claim 1, wherein the object is a bladder.

11. The method of performing virtual examination according to claim 10, wherein the scans are computed tomography scans.

12. The method of performing virtual examination according to claim 10, wherein the scans are ultrasound imaging scans.

13. The method of performing virtual examination according to claim 10, wherein the scans are magnetic resonance imaging scans

14. The method of performing virtual examination according to claim 13, wherein the contrast agent is urine.

15. The method of performing virtual examination according to claim 1, further comprising evaluating the at least one scan with the object distended and the at least one scan with the object relieved to identify regions where contrast is more visible in one of said scans and evaluating the scan with more contrast in a region of interest to determine physiological characteristics of the object.

16. The method of performing virtual examination according to claim 15, wherein said step of image segmentation includes classifying voxels based on local intensity vectors of the voxels.

17. The method of performing virtual examination according to claim 16, wherein the step of image segmentation further includes using a region growing algorithm to identify regions of the object based on the classified voxels.

18. The method of performing virtual examination according to claim 1, further comprising partitioning the volume image datasets into a plurality of regions related to the coordinate system.

19. The method of performing virtual examination according to claim 18, wherein the plurality of regions include eight regions defined in a three dimensional coordinate system.

20. A method for performing virtual examination of an object comprising:

performing an imaging scan of the object to acquire image scan data;

converting the acquired image scan data to a plurality of voxels;

interpolating between the voxels to generate an expanded dataset;

performing image segmentation to classify the voxels into a plurality of categories;

extracting a volume of the object interior from the expanded dataset;

generating a reduced resolution dataset from the expanded dataset;

storing the expanded dataset in a tree data structure;

rendering images for the expanded dataset and reduced resolution dataset; and

selecting at least one of the reduced resolution dataset or expanded dataset renderings for display.

21. The method for performing virtual examination of an object of claim 20, wherein the selecting step comprises:

selecting the reduced resolution dataset during image interaction; and

selecting the expanded dataset rendering if no image interaction has occurred in a predetermined time period.

22. The method for performing virtual examination of an object of claim 20, wherein the imaging scan is a computed tomography scan.

23. The method for performing virtual examination of an object of claim 20, wherein the imaging scan is a magnetic resonance imaging scan.

24. The method for performing virtual examination of an object of claim 20, wherein the imaging scan is an ultrasound imaging scan.

25. The method for performing virtual examination of an object of claim 20, wherein the object is the larynx.

26. The method for performing virtual examination of an object of claim 20, wherein the tree structure is a binary space partition tree structure.

27. A method of performing virtual angiography comprising:

acquiring imaging scan data including at least a portion of the aorta;

converting the imaging scan data to a volume representation including a plurality of voxels;

segmenting the volume representation to classify the voxels into one of a plurality of categories;

analyzing the segmented volume representation to identify voxels indicative of at least a portion of an aneurysm in the aortic wall; and

generating at least one closing surface around the voxels indicative of at least a portion of an aneurysm to estimate the contour of the aneurysm.

28. The method of performing virtual angiography of claim 27, wherein the imaging scan is a computed tomography scan.

29. The method of performing virtual angiography of claim 27, wherein the imaging scan is a magnetic resonance imaging scan.

30. The method of performing virtual angiography of claim 27, wherein the segmenting operation classifies voxels in at least the categories of blood, tissue, and calcium deposits.

31. The method of performing virtual angiography of claim 27, further comprising estimating the volume of the aneurysm using the generated closing surfaces.

32. The method of performing virtual angiography of claim 27, further comprising generating a navigation path through the aortic lumen.

33. The method of performing virtual angiography of claim 32, further comprising estimating the length of the aneurysm based on the navigation path.

34. A method of performing virtual endoscopy of a blood vessel comprising:

acquiring imaging scan data including at least a portion of the vessel;

converting the imaging scan data to a volume representation including a plurality of voxels;

segmenting the volume representation to classify the voxels into one of a plurality of categories including the categories of blood, tissue, and calcium deposits; and

generating a navigation path through the vessel.

35. The method of performing virtual endoscopy of claim 34, wherein the vessel is a carotid artery.

36. The method of performing virtual endoscopy of claim 34, further comprising the step of determining the diameter of the carotid artery along the navigation path to identify regions of narrowing.

37. The method of performing virtual angiography of claim 34, wherein the imaging scan is a computed tomography scan.

38. The method of performing virtual angiography of claim 34, wherein the imaging scan is a magnetic resonance imaging scan.

39. A method of determining the characteristics of a stent graft using virtual angioscopy, comprising:

acquiring imaging scan data including at least a portion of the aorta;

converting the imaging scan data to a volume representation including a plurality of voxels;

segmenting the volume representation to classify the voxels into one of a plurality of categories;

analyzing the segmented volume representation to identify voxels indicative of at least a portion of an aneurysm in the aortic wall;

generating at least one closing surface around the voxels indicative of at least a portion of an aneurysm to estimate the contour of the aneurysm;

identifying the location of the endpoints of the aneurysm contour;

calculating the length between the endpoints of the aneurysm contour to determine the length of the stent graft; and

calculating the diameter of the aortic lumen at the endpoints of the aneurysm contour to determine the required outside diameters of the stent graft.

40. The method of determining the characteristics of a stent graft of claim 39, further comprising determining the angle of interface of the aneurysm and normal aortic lumen to determine an angular direction of a corresponding end of the stent graft.

41. The method of determining the characteristics of a stent graft of claim 39, further comprising locating arterial branches proximate the aneurysm to determine a maximum length of the stent graft.

42. The method of determining the characteristics of a stent graft of claim 41, wherein the arterial branches proximate the aneurysm include at least one of the renal and femoral arterial branches.

43. The method of determining the characteristics of a stent graft of claim 39, further comprising conducting a virtual biopsy of the aortic region proximate the ends of the aneurysm to determine the nature of the tissue at the anticipated graft interface locations.

44. A method of defining a skeleton for a three dimensional image representation of a hollow object formed with a plurality of voxels comprising:

identifying a root voxel within the hollow object;

generating a distance map for all voxels within the hollow object, the distance map being formed using a 26-connected cubic plate of neighboring voxels having Euclidian weighted distances;

identifying voxels having a local maxima in the distance map as endpoints of branches in the hollow object; and

for each local maxima voxel, determining a shortest connected path to one of the root voxel or a previously defined shortest path.

45. The method of defining a skeleton for a three dimensional image representation of claim 44 further comprising performing multi-resolution data reduction to the three dimensional image representation to generate a reduced data set for the generating and identifying operations.

46. The method of defining a skeleton for a three dimensional image representation of claim 44 further comprising centralizing the shortest paths within the respective branches of the object.

47. The method of defining a skeleton for a three dimensional image representation of claim 44, wherein the object includes at least one blood vessel.

48. The method of defining a skeleton for a three dimensional image representation of claim 44, wherein the object includes the airways of a lung.

49. The method of defining a skeleton for a three dimensional image representation of claim 44, wherein the object includes the bladder.

50. The method of defining a skeleton for a three dimensional image representation of claim 44, wherein the object includes the spinal cord of a vertebrate animal.

51. A method of performing computed assisted diagnosis of a region of interest, comprising:

acquiring imaging scan data including at least a portion of the region of interest;

converting the imaging scan data to a volume representation including a plurality of voxels, at least a portion of the voxels representing a surface of the region of interest; and

analyzing said portion of voxels representing a surface for at least one of a geometric feature and a textural feature indicative of an abnormality.

52. The method of performing computed assisted diagnosis according to claim 51, wherein the textural feature is included in a probability density function characterizing a correlation between two voxels of the portion of voxels.

53 The method of performing computed assisted diagnosis according to claim 52, wherein the two voxels are adjacent voxels.

54. The method of performing computer assisted diagnosis according to claim 52, wherein intensities of said portion of voxels are used to generate an estimate of the probability density function.

55. The method of performing computer assisted diagnosis according to claim 54, wherein a plurality of voxel intensities are used to generate a cumulating distribution function of the region of interest and a local cumulating distribution function, and wherein the local cumulating distribution function is compared against the context cumulating distribution function to identify regions of abnormality.

56. The method of performing computer assisted diagnosis according to claim 55, wherein a distance is determined between said local cumulating distribution function and said context cumulating distribution function, the distance providing a measure of abnormality.

57. The method of performing computer assisted diagnosis according to claim 56, wherein the distance is used to assign intensity values to the voxels representing a

surface of the region of interest and wherein said method further comprises displaying said voxels such that variations in intensity represent regions of abnormality.

58. The method of performing computer assisted diagnosis according to claim 57, wherein the region of interest includes the colon and wherein the abnormality includes polyps.

59. The method of performing computer assisted diagnosis according to claim 51, wherein the region of interest includes the aorta and wherein the abnormality includes abdominal aortic aneurysms.

60. The method of performing computer assisted diagnosis according to claim 51 wherein the surface is represented as a second differentiable surface where each surface volume unit has an associate Gauss curvature and wherein said Gauss curvatures combine to form said geometric features.

61. The method of performing computer assisted diagnosis according to claim 59 wherein a plurality of predetermined geometrical feature templates are defined and wherein the geometric features of said surface are compared to said templates to determine a geometric feature classification.

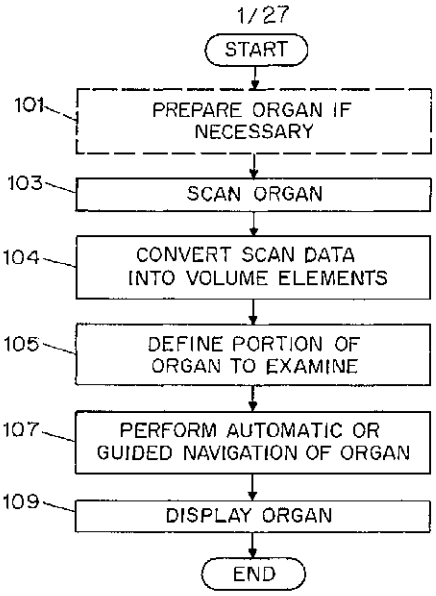
START
101
PREPARE ORGAN IF NECESSARY
103
SCAN ORGAN
104
CONVERT SCAN DATA INTO VOLUME ELEMENTS
105
DEFINE PORTION OF ORGAN TO EXAMINE
107
PERFORM AUTOMATIC OR GUIDED NAVIGATION OF ORGAN
109
DISPLAY ORGAN
END

FIG. 1

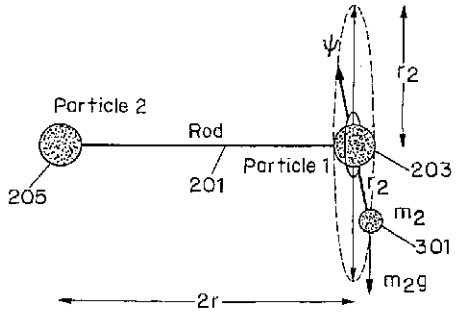
Particle 2
Rod
Particle 1
205
201
203
r2
r2
m2
301
m2g
2r

FIG 3

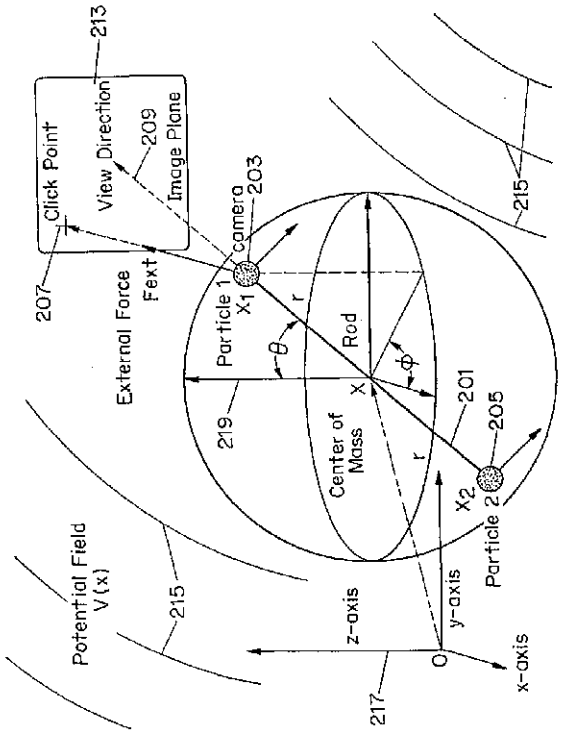
213
Click Point
View Direction
209
Image Plane
207
External Force
Fext
Particle 1
X1
Camera
203
r
θ
Rod
φ
219
X
Center of
Mass
201
205
r
X2
Particle 2
215
215
Potential Field
V(x)
z-axis
y-axis
x-axis
0
217

FIG. 2

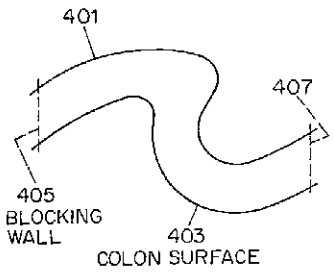

FIG. 4

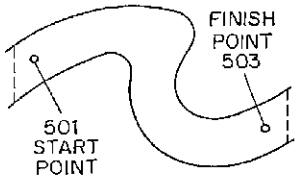

FIG. 5

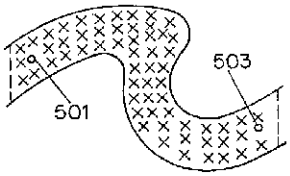

FIG. 6

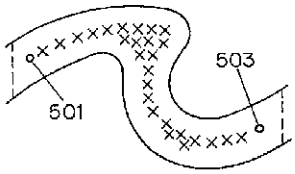

FIG. 7

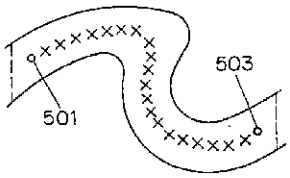

FIG. 8

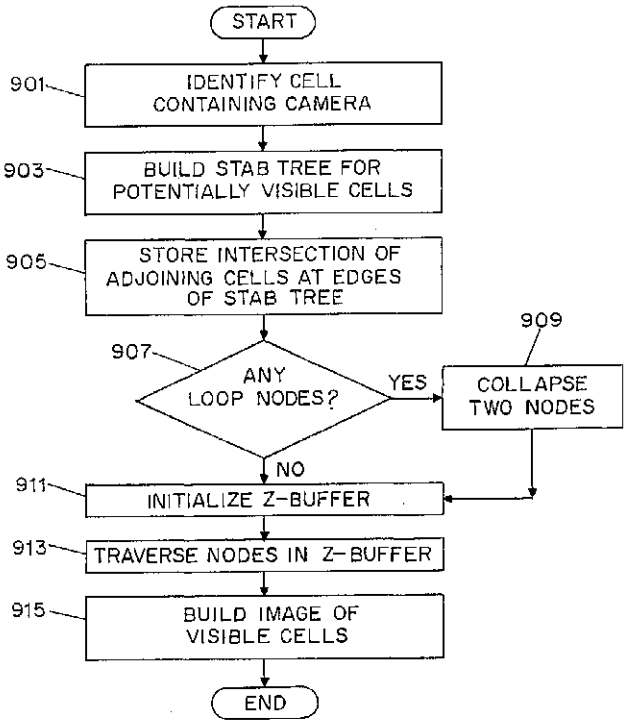
START
901
IDENTIFY CELL CONTAINING CAMERA
903
BUILD STAB TREE FOR POTENTIALLY VISIBLE CELLS
905
STORE INTERSECTION OF ADJOINING CELLS AT EDGES OF STAB TREE
907
ANY LOOP NODES?
YES
909
COLLAPSE TWO NODES
NO
911
INITIALIZE Z-BUFFER
913
TRAVERSE NODES IN Z-BUFFER
915
BUILD IMAGE OF VISIBLE CELLS
END

FIG. 9

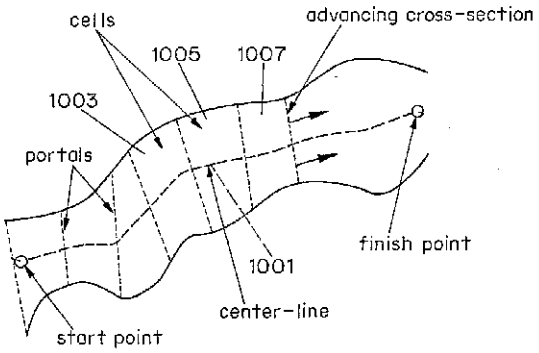

FIG. 10

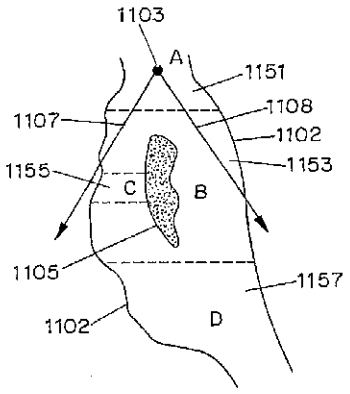

FIG. 11(a)

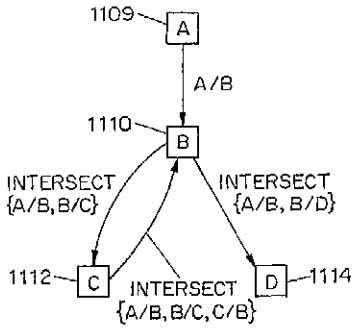

FIG. 11(b)

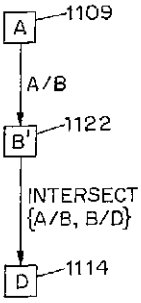

FIG. 11(c)

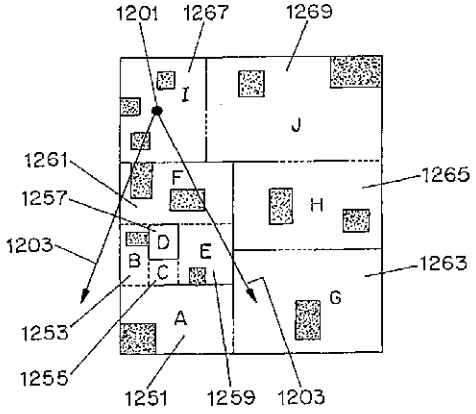

FIG. 12(a)

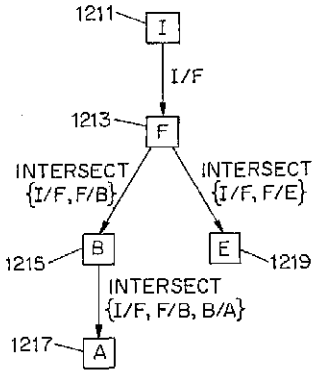

FIG. 12(b)

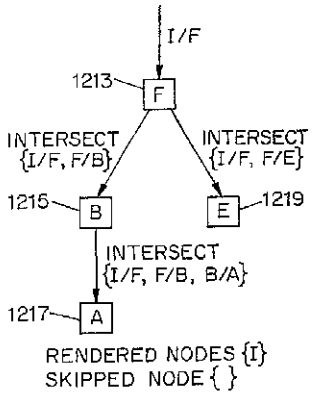

FIG. 12(c)

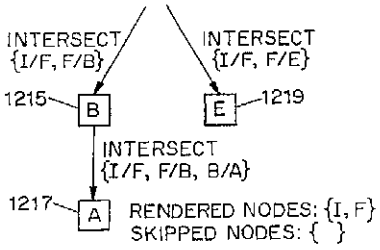

FIG. 12(d)

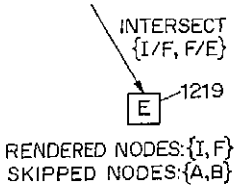

FIG. 12(e)

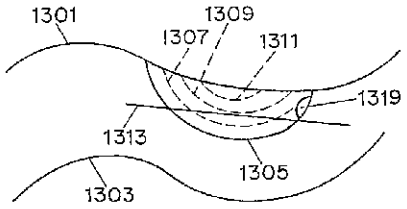

FIG. 13

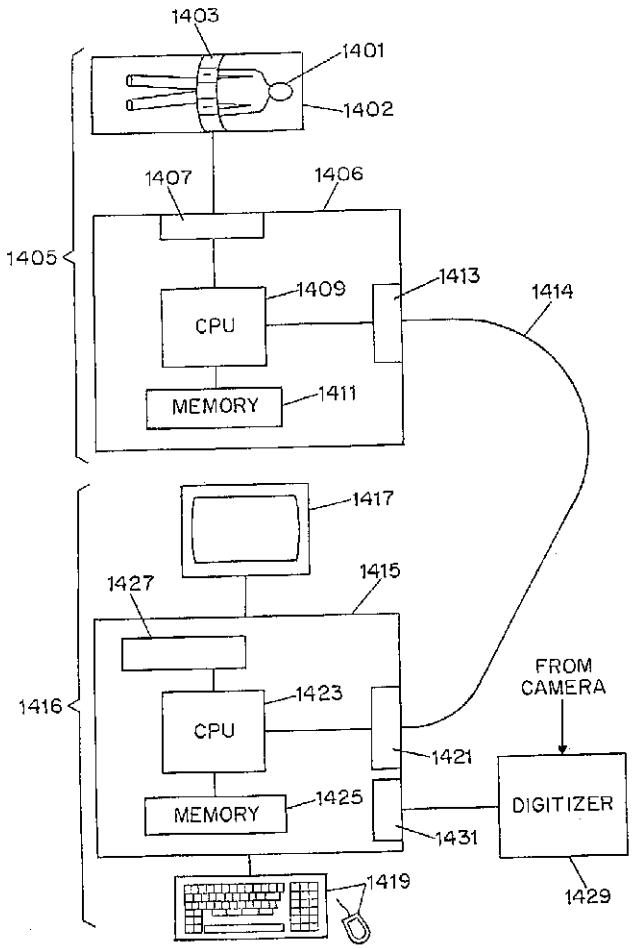

FIG 14

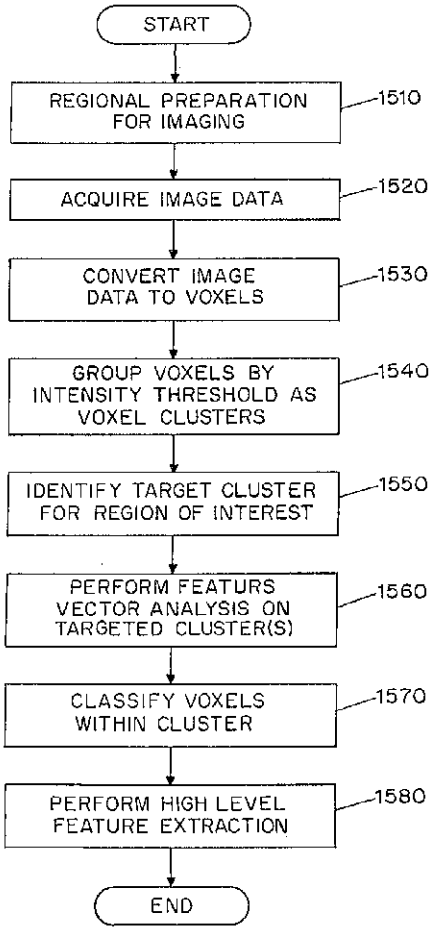
START
REGIONAL PREPARATION FOR IMAGING
1510
ACQUIRE IMAGE DATA
1520
CONVERT IMAGE DATA TO VOXELS
1530
GROUP VOXELS BY INTENSITY THRESHOLD AS VOXEL CLUSTERS
1540
IDENTIFY TARGET CLUSTER FOR REGION OF INTEREST
1550
PERFORM FEATURS VECTOR ANALYSIS ON TARGETED CLUSTER(S)
1560
CLASSIFY VOXELS WITHIN CLUSTER
1570
PERFORM HIGH LEVEL FEATURE EXTRACTION
1580
END

FIG 15

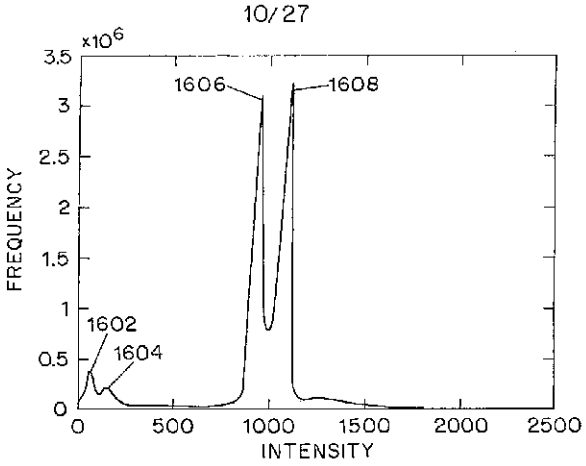
x10^6
3.5
3
2.5
2
1.5
1
0.5
0
FREQUENCY
1606
1608
1602
1604
0
500
1000
1500
2000
2500
INTENSITY

FIG. 16

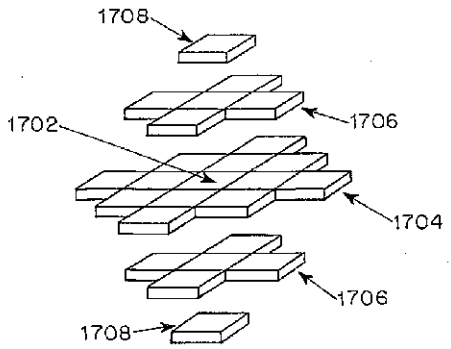
1708
1706
1702
1704
1706
1708

FIG. 17

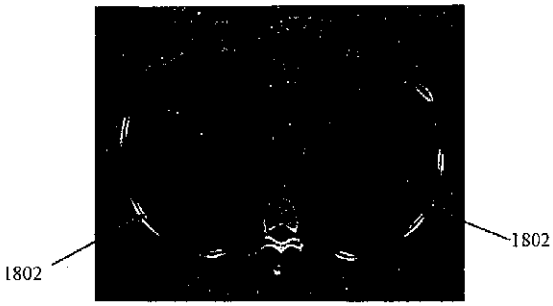

FIG. 18A

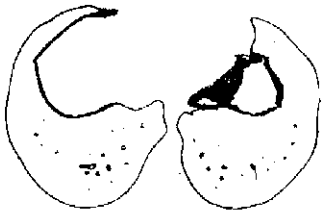

FIG. 18B

FIG. 18C

FIG. 19A

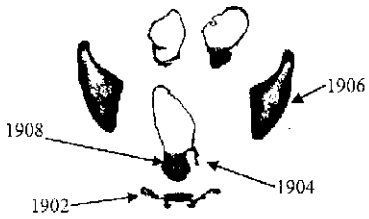

FIG. 19B

FIG. 19C

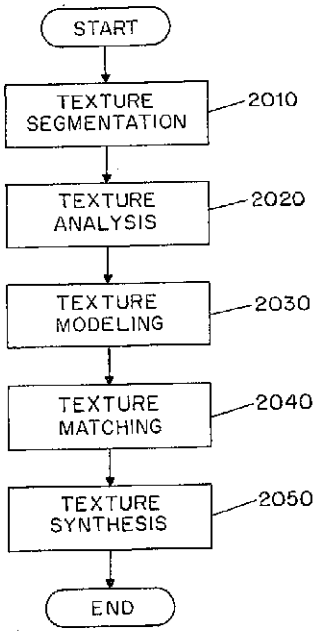
START
TEXTURE SEGMENTATION
2010
TEXTURE ANALYSIS
2020
TEXTURE MODELING
2030
TEXTURE MATCHING
2040
TEXTURE SYNTHESIS
2050
END

FIG. 20

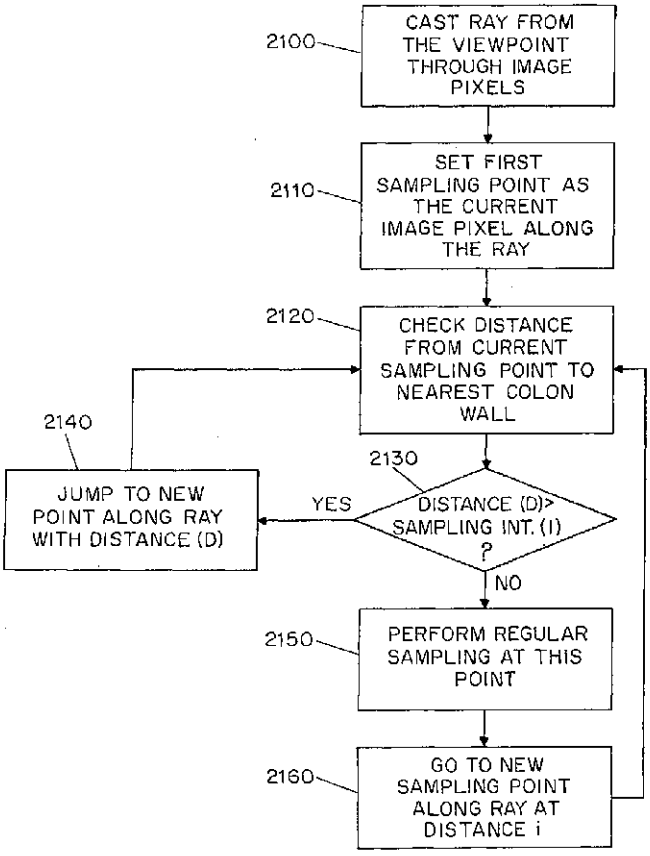
2100
CAST RAY FROM THE VIEWPOINT THROUGH IMAGE PIXELS
2110
SET FIRST SAMPLING POINT AS THE CURRENT IMAGE PIXEL ALONG THE RAY
2120
CHECK DISTANCE FROM CURRENT SAMPLING POINT TO NEAREST COLON WALL
2130
DISTANCE (D)> SAMPLING INT. (I) ?
YES
NO
2140
JUMP TO NEW POINT ALONG RAY WITH DISTANCE (D)
2150
PERFORM REGULAR SAMPLING AT THIS POINT
2160
GO TO NEW SAMPLING POINT ALONG RAY AT DISTANCE i

FIG. 21

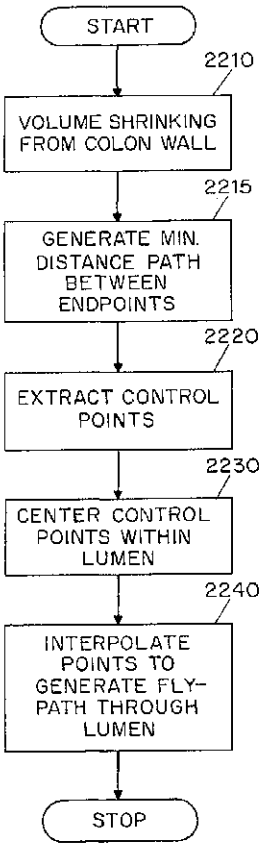
START
2210
VOLUME SHRINKING FROM COLON WALL
2215
GENERATE MIN. DISTANCE PATH BETWEEN ENDPOINTS
2220
EXTRACT CONTROL POINTS
2230
CENTER CONTROL POINTS WITHIN LUMEN
2240
INTERPOLATE POINTS TO GENERATE FLY-PATH THROUGH LUMEN
STOP

FIG. 22

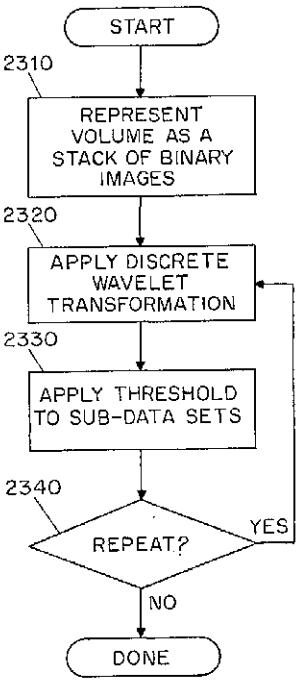
START
2310
REPRESENT VOLUME AS A STACK OF BINARY IMAGES
2320
APPLY DISCRETE WAVELET TRANSFORMATION
2330
APPLY THRESHOLD TO SUB-DATA SETS
2340
REPEAT?
YES
NO
DONE

FIG. 23

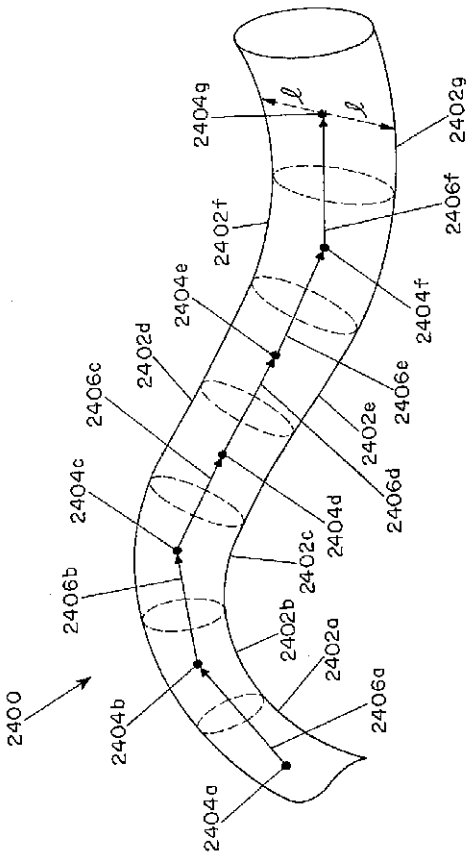
2400
2402a
2402b
2402c
2402d
2402e
2402f
2402g
2404a
2404b
2404c
2404d
2404e
2404f
2404g
2406a
2406b
2406c
2406d
2406e
2406f
ℓ
ℓ

FIG. 24

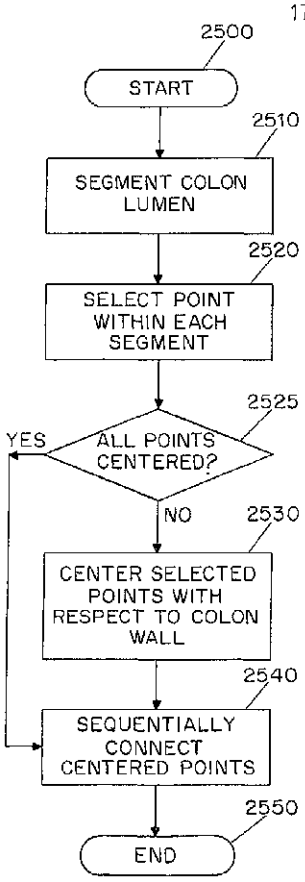
2500
START
2510
SEGMENT COLON LUMEN
2520
SELECT POINT WITHIN EACH SEGMENT
2525
ALL POINTS CENTERED?
YES
NO
2530
CENTER SELECTED POINTS WITH RESPECT TO COLON WALL
2540
SEQUENTIALLY CONNECT CENTERED POINTS
2550
END

FIG. 25

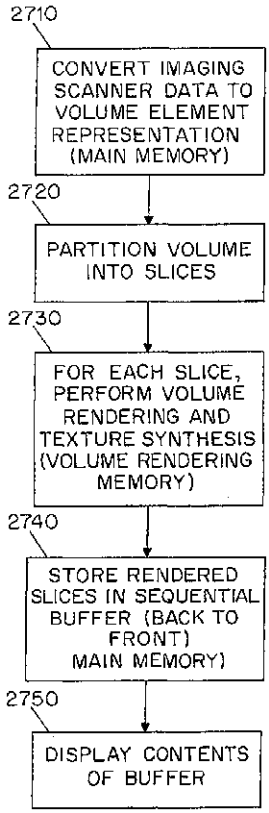
2710
CONVERT IMAGING SCANNER DATA TO VOLUME ELEMENT REPRESENTATION (MAIN MEMORY)
2720
PARTITION VOLUME INTO SLICES
2730
FOR EACH SLICE, PERFORM VOLUME RENDERING AND TEXTURE SYNTHESIS (VOLUME RENDERING MEMORY)
2740
STORE RENDERED SLICES IN SEQUENTIAL BUFFER (BACK TO FRONT) MAIN MEMORY)
2750
DISPLAY CONTENTS OF BUFFER

FIG. 27

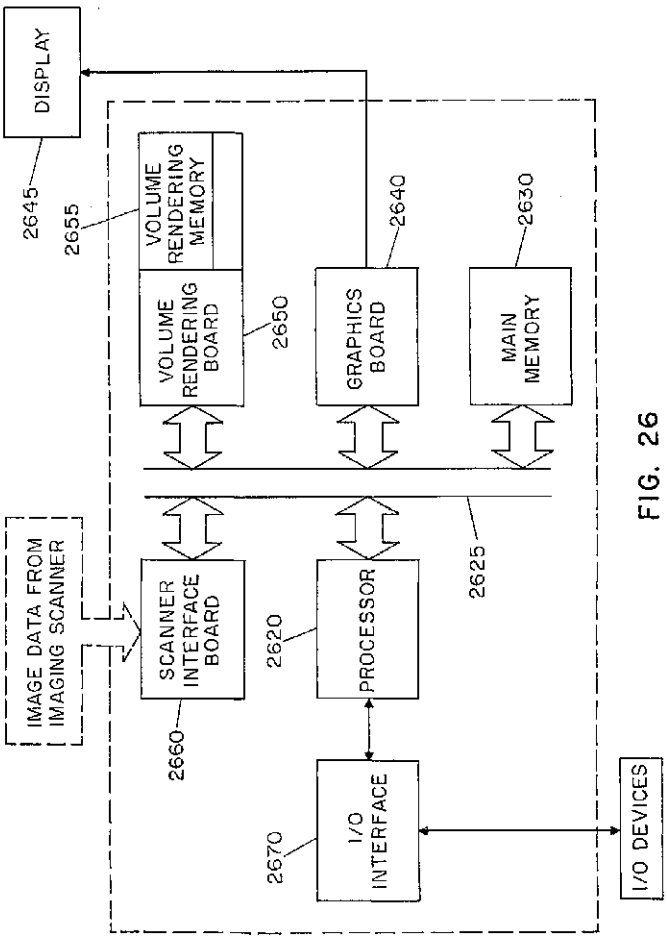
DISPLAY
2645
2655
VOLUME RENDERING MEMORY
VOLUME RENDERING BOARD
2650
2640
GRAPHICS BOARD
2630
MAIN MEMORY
2625
IMAGE DATA FROM IMAGING SCANNER
SCANNER INTERFACE BOARD
2660
2620
PROCESSOR
2670
I/O INTERFACE
I/O DEVICES

FIG. 26

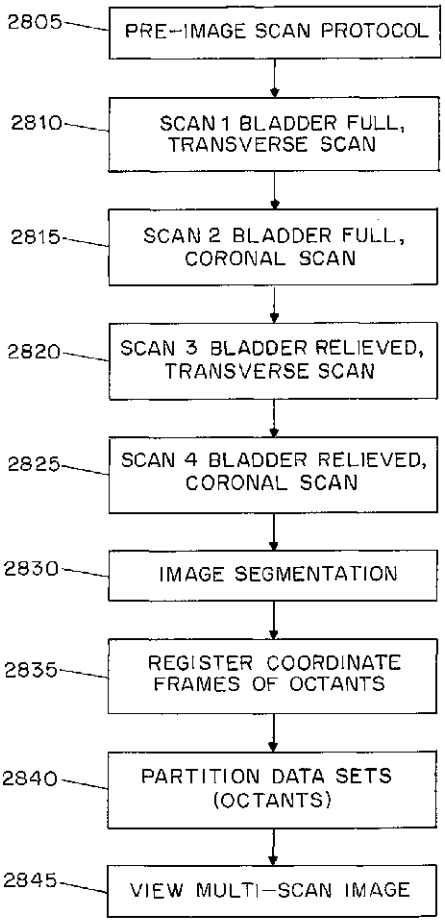
2805
PRE-IMAGE SCAN PROTOCOL
2810
SCAN 1 BLADDER FULL, TRANSVERSE SCAN
2815
SCAN 2 BLADDER FULL, CORONAL SCAN
2820
SCAN 3 BLADDER RELIEVED, TRANSVERSE SCAN
2825
SCAN 4 BLADDER RELIEVED, CORONAL SCAN
2830
IMAGE SEGMENTATION
2835
REGISTER COORDINATE FRAMES OF OCTANTS
2840
PARTITION DATA SETS (OCTANTS)
2845
VIEW MULTI-SCAN IMAGE

FIG. 28

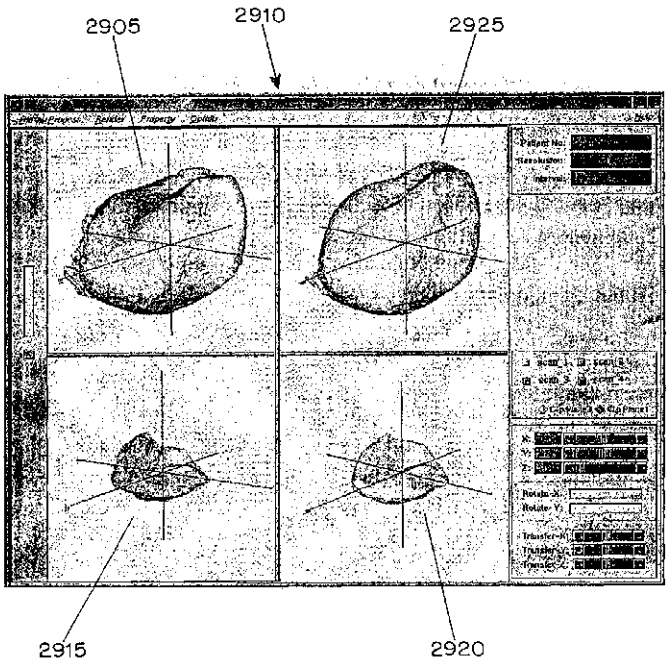

FIG. 29

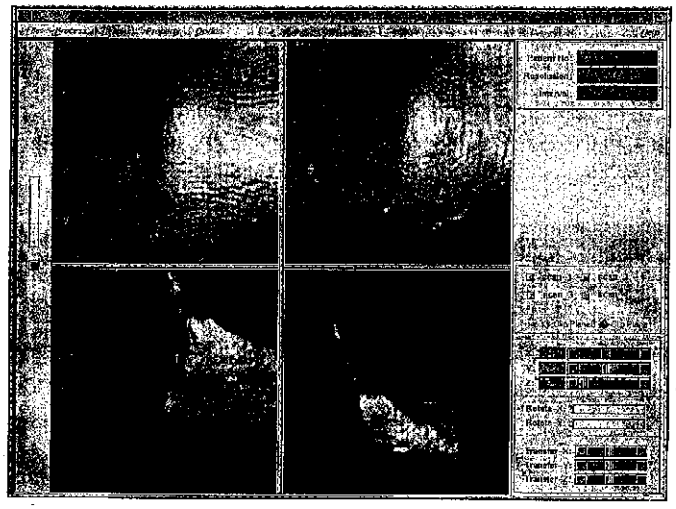

FIG. 30

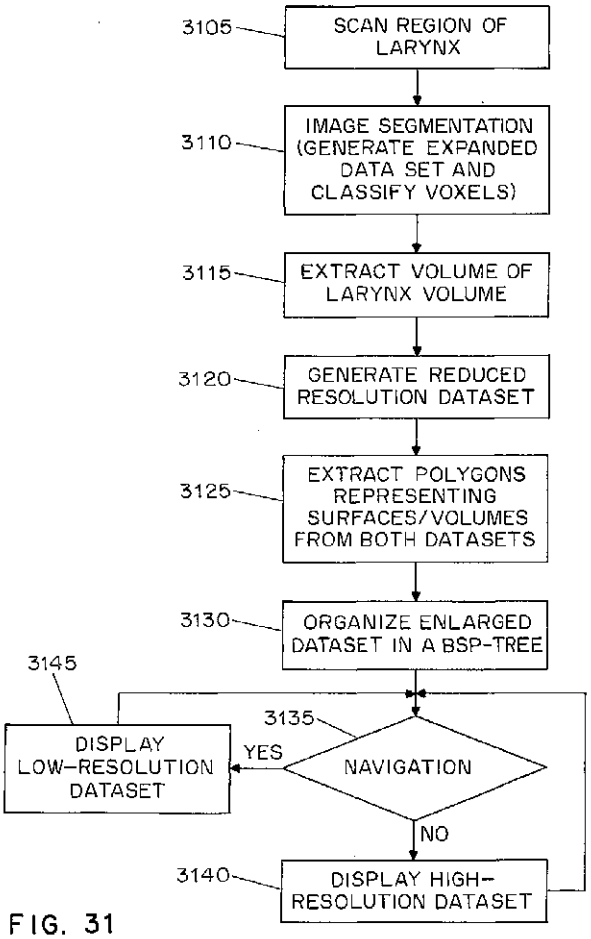
3105
SCAN REGION OF LARYNX
3110
IMAGE SEGMENTATION (GENERATE EXPANDED DATA SET AND CLASSIFY VOXELS)
3115
EXTRACT VOLUME OF LARYNX VOLUME
3120
GENERATE REDUCED RESOLUTION DATASET
3125
EXTRACT POLYGONS REPRESENTING SURFACES/VOLUMES FROM BOTH DATASETS
3130
ORGANIZE ENLARGED DATASET IN A BSP-TREE
3145
3135
DISPLAY LOW-RESOLUTION DATASET
YES
NAVIGATION
NO
3140
DISPLAY HIGH-RESOLUTION DATASET

FIG. 31

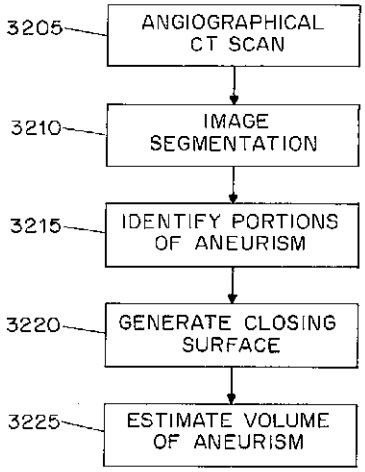
3205
ANGIOGRAPHICAL CT SCAN
3210
IMAGE SEGMENTATION
3215
IDENTIFY PORTIONS OF ANEURISM
3220
GENERATE CLOSING SURFACE
3225
ESTIMATE VOLUME OF ANEURISM

FIG. 32

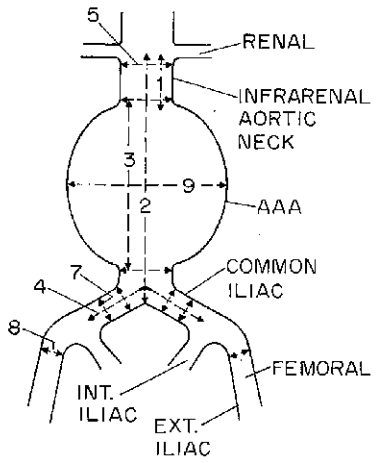

FIG. 33A

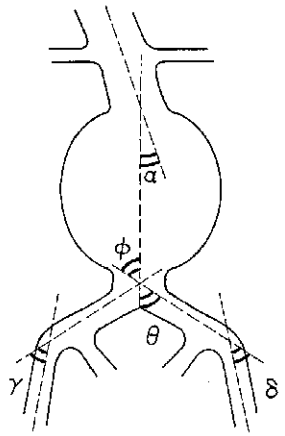

FIG. 33B

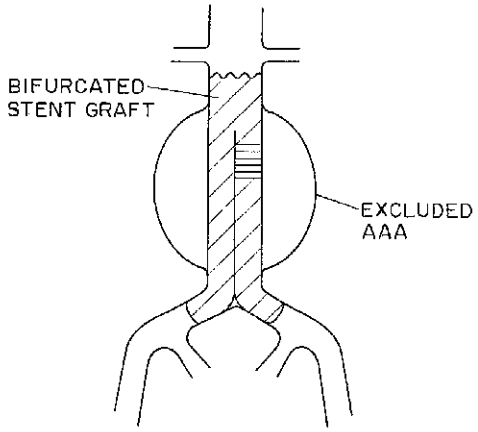

FIG. 33C

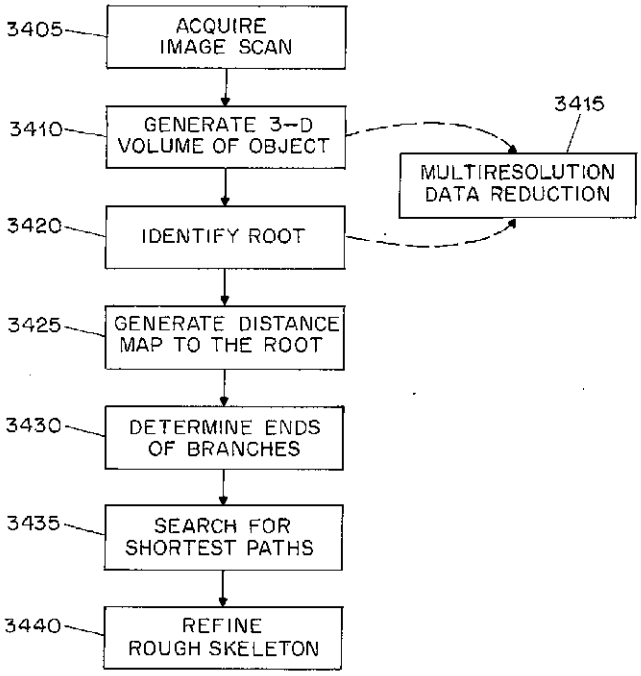
3405
ACQUIRE IMAGE SCAN
3410
GENERATE 3-D VOLUME OF OBJECT
3415
MULTIRESOLUTION DATA REDUCTION
3420
IDENTIFY ROOT
3425
GENERATE DISTANCE MAP TO THE ROOT
3430
DETERMINE ENDS OF BRANCHES
3435
SEARCH FOR SHORTEST PATHS
3440
REFINE ROUGH SKELETON

FIG. 34

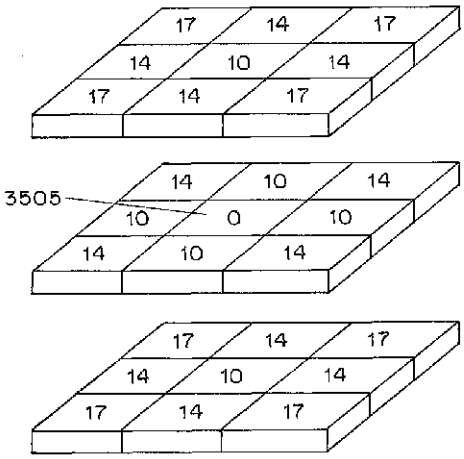
17
14
17
14
10
14
17
14
17
3505
14
10
14
10
0
10
14
10
14
17
14
17
14
10
14
17
14
17

FIG. 35

```
1) Label root voxel with integer 0;
2) Construct a queue and line up the root in the queue;
3) If (There is at least one voxel in the queue)
     Serve the voxel x on the top of the queue:
     For (each of x's 26-connected neighbor voxel y) {
      If (y in the volume and has not been labeled yet) {
        Line up the y in the queue;

        /* label the voxel y */
        Set dist = 999999;
        For (each of y's 26-connected neighbor voxel z) {
         If (z in the volume and has been already labeled with an
          integer of n_z ) {

            d_z ≡ n_z + d (y, z);
            where d (y,z) is 10, 14 or 17 if the Euclidean distance
             between y and z is
            1, √2, or √3, respectively;
         }
         If (dist > d_z ) {
            label y with integer dist;
            dist = d_z ;
         }
        }
      }
    }
    x leaves the quere;
  }
  Else {
     end of calculating the distance map.
  }
```

FIG. 36

【国際調査報告】

INTERNATIONAL SEARCH REPORT

International application No.
PCT/US01/30704

A. CLASSIFICATION OF SUBJECT MATTER
IPC(7) : G06B 23/28; G06F 17/00; G06T 1/00, 13/00, 15/00, 15/50, 17/00
US CL : (Please See Extra Sheet.
According to International Patent Classification (IPC) or to both national classification and IPC

B. FIELDS SEARCHED
Minimum documentation searched (classification system followed by classification symbols)
U.S. : 434/262, 267, 278; 345/418, 419, 420, 424, 426, 473, 474, 952, 959

Documentation searched other than minimum documentation to the extent that such documents are included in the fields searched

Electronic data base consulted during the international search (name of data base and, where practicable, search terms used)
EAST
search terms: three-dimensional, image, object, internal, organ, volume, visualization

C. DOCUMENTS CONSIDERED TO BE RELEVANT

Category*	Citation of document, with indication, where appropriate, of the relevant passages	Relevant to claim No.
&	US 5,971,767 A (Kaufman et al) 26 October 1999, See The Whole document.	NONE
&, E	US 6,331,116 B1 (Kaufman et al) 18 December 2001, See The Whole Document	NONE
&, E	US 2001/0031920 A1 (Kaufman et al) 18 October 2001, See The Whole Document.	NONE

☐ Further documents are listed in the continuation of Box C. ☐ See patent family annex.

* Special categories of cited documents:
"A" document defining the general state of the art which is not considered to be of particular relevance
"E" earlier document published on or after the international filing date
"L" document which may throw doubts on priority claim(s) or which is cited to establish the publication date of another citation or other special reason (as specified)
"O" document referring to an oral disclosure, use, exhibition or other means
"P" document published prior to the international filing date but later than the priority date claimed
"T" later document published after the international filing date or priority date and not in conflict with the application but cited to understand the principle or theory underlying the invention
"X" document of particular relevance; the claimed invention cannot be considered novel or cannot be considered to involve an inventive step when the document is taken alone
"Y" document of particular relevance; the claimed invention cannot be considered to involve an inventive step when the document is combined with one or more other such documents, such combination being obvious to a person skilled in the art
"&" document member of the same patent family

Date of the actual completion of the international search	Date of mailing of the international search report
19 DECEMBER 2001	23 JAN 2002

Name and mailing address of the ISA/US	Authorized officer
Commissioner of Patents and Trademarks Box PCT Washington, D.C. 20231	JOHN ROVNAK Sheila Veney Paralegal Specialist Technology Center 3700
Facsimile No. (703) 305-3230	Telephone No. (703) 308-[illegible]

Form PCT/ISA/210 (second sheet) (July 1998)*

INTERNATIONAL SEARCH REPORT

International application No.
PCT/US01/30704

A. CLASSIFICATION OF SUBJECT MATTER:
US CL :

[illegible]

Form PCT/ISA/210 (extra sheet) (July 1998)*

フロントページの続き

(51)Int.Cl.[7]	F I	テーマコード（参考）
Ｇ０６Ｔ 17/40	Ｇ０１Ｎ 24/02 ５３０Ｙ	

(81)指定国 AP(GH,GM,KE,LS,MW,MZ,SD,SL,SZ,TZ,UG,ZW),EA(AM,AZ,BY,KG,KZ,MD,RU,TJ,TM),EP(AT,BE,CH,CY,DE,DK,ES,FI,FR,GB,GR,IE,IT,LU,MC,NL,PT,SE,TR),OA(BF,BJ,CF,CG,CI,CM,GA,GN,GQ,GW,ML,MR,NE,SN,TD,TG),AE,AG,AL,AM,AT,AU,AZ,BA,BB,BG,BR,BY,BZ,CA,CH,CN,CO,CR,CU,CZ,DE,DK,DM,DZ,EC,EE,ES,FI,GB,GD,GE,GH,GM,HR,HU,ID,IL,IN,IS,JP,KE,KG,KP,KR,KZ,LC,LK,LR,LS,LT,LU,LV,MA,MD,MG,MK,MN,MW,MX,MZ,NO,NZ,PH,PL,PT,RO,RU,SD,SE,SG,SI,SK,SL,TJ,TM,TR,TT,TZ,UA,UG,UZ,VN,YU,ZA,ZW

(72)発明者 ザングロング リアン
アメリカ合衆国 ニューヨーク州 １１７９０ ストーニー ブルック ハクトン ブールヴァード ２８
(72)発明者 マーク アール ワックス
アメリカ合衆国 ニューヨーク州 １１７４０ グリーンローン イースト サンダース ストリート ６
(72)発明者 ミン ワン
アメリカ合衆国 ニューヨーク州 １１７９０ ストーニー ブルック チャピン コンプレックス ４５９
(72)発明者 ドンキン チェン
アメリカ合衆国 ニューヨーク州 １１７７９ レイク ロンコンコマ ロンコンコマ アヴェニュー １００ イー１
(72)発明者 ビン リ
アメリカ合衆国 ニューヨーク州 １１７５５ レイク グローヴ ウィリアムズ ブールヴァード １ アパートメント ２階

Ｆターム(参考) 4C093 AA22 CA23 DA01 DA02 EE20 FF22 FF23 FF42 FF47
4C096 AA20 AB41 AB50 AC04 AC05 AC10 AD14 AD15 AD25 BA18
DA03 DA14 DB08 DB13 DC09 DC11 DC14 DC19 DC21 DC22
DC28 DC33 DC36 DC37 DD20
4C167 AA41 BB11 BB12 CC08 CC10 DD01 FF05 HH30
5B050 AA02 BA08 BA09 DA02 EA27 FA02 FA12 FA13
5B080 AA17 BA02 GA00

专利名称(译)	用于对诸如器官的对象进行三维虚拟检查的系统和方法		
公开(公告)号	JP2004510515A	公开(公告)日	2004-04-08
申请号	JP2002533259	申请日	2001-10-01
申请(专利权)人(译)	国家盐湖城纽约的研究基金会		
[标]发明人	アリーイーコーフマン ザングロングリアン マークアールワックス ミンワン ドンキンチェン ビンリ		
发明人	アリー イー コーフマン ザングロング リアン マーク アール ワックス ミン ワン ドンキン チェン ビン リ		
IPC分类号	G01R33/54 A61B5/055 A61B6/03 A61F2/82 G06T15/00 G06T15/08 G06T17/00 G09B23/28 A61M29/00 G06T17/40		
CPC分类号	A61B5/055 A61B5/726 A61B6/032 A61B8/483 G06T7/11 G06T15/08 G06T19/00 G06T2207/10072 G06T2207/30028 G06T2207/30084 G06T2207/30172 G06T2210/41 G06T2219/028 G06T2219/2004 G09B23/28		
FI分类号	A61B6/03.360.G A61M29/00 G06T15/00.200 G06T17/40.E A61B5/05.380 G01N24/02.530.Y		
F-TERM分类号	4C093/AA22 4C093/CA23 4C093/DA01 4C093/DA02 4C093/EE20 4C093/FF22 4C093/FF23 4C093/FF42 4C093/FF47 4C096/AA20 4C096/AB41 4C096/AB50 4C096/AC04 4C096/AC05 4C096/AC10 4C096/AD14 4C096/AD15 4C096/AD25 4C096/BA18 4C096/DA03 4C096/DA14 4C096/DB08 4C096/DB13 4C096/DC09 4C096/DC11 4C096/DC14 4C096/DC19 4C096/DC21 4C096/DC22 4C096/DC28 4C096/DC33 4C096/DC36 4C096/DC37 4C096/DD20 4C167/AA41 4C167/BB11 4C167/BB12 4C167/CC08 4C167/CC10 4C167/DD01 4C167/FF05 4C167/HH30 5B050/AA02 5B050/BA08 5B050/BA09 5B050/DA02 5B050/EA27 5B050/FA02 5B050/FA12 5B050/FA13 5B080/AA17 5B080/BA02 5B080/GA00		
优先权	60/237665 2000-10-03 US 09/777120 2001-02-05 US		
外部链接	Espacenet		

摘要(译)

提供了使用体积可视化技术生成诸如内部器官的对象的三维可视图像的方法。该技术包括多扫描成像方法;多分辨率成像方法;以及用于生成复杂三维对象的骨架的方法。应用包括虚拟膀胱镜检查，虚拟喉镜检查，虚拟血管造影等。

$$\frac{\partial v(x)}{\partial x}, \frac{\partial v(x)}{\partial y}, \frac{\partial v(x)}{\partial z}$$